Rajan Kumar Thapa

Optimization of Flow Behavior in Biomass Gasification Reactor

Thesis for the degree of Doctor Philosophiae
Porsgrunn, Norway
May 2015

Telemark University College
Faculty of Technology

Telemark University College

Telemark University College
Faculty of Technology
Department of Process, Energy and Environmental Technology
Post Box 203
N-3901, Porsgrunn, Norway

www.hit.no
Doctoral Dissertation at TUC 2015: 2
© Rajan Kumar Thapa
ISBN 978-82-7206-394-7
ISSN 1893-3068
Printed by the Copy Center at TUC - Bø

Optimization of Flow Behavior in Biomass Gasification Reactor

Rajan Kumar Thapa

Thesis submitted to the Telemark University College for
the degree of philosophiae doctor (PhD)

Dedicated to all those who have brought me to this stage

Preface

I would like to thank my father who never gave up pushing me forward and being proud of me in my every small success. I am happier for my mother than myself knowing that she will be one of the happiest persons for this success even though she does not know exactly what it means to finish a PhD project. She never had a chance to go to school.

Only a luckiest PhD candidate can have an opportunity to work under the supervision of Professor Britt Halvorsen. She has an amazing capability to be a strict, systematic supervisor with profound ability to guide and explain the things patiently and persistently. At the same time, she had been a guardian for me all time during thesis. As a result, I never lost my motivation to work even for a single day. It is not possible to describe all my gratitude towards my supervisor in these few pages.

Enormous thanks go to my co-supervisor Professor Christoph Pfeifer. I have been many times to Vienna during this project. His explanation about the lab scale hot model and cold model in Vienna University of Technology, technical excursion to biomass gasification plant in Güssing Austria are valuable help for me to understand the technology, its challenges and possibilities of improvements. Special thanks for arrangement of experimental works in University of Natural and Life Sciences (BOKU), Vienna to my Co-supervisor , Gregor and Andreas.

I feel myself grateful to have brother and sisters who are even ready to sacrifice a lot to push me ahead. Enormous thanks go to my wife Ekaterina and daughter Irina who have been going through all these exciting days. Even they have a surface knowledge about many of the papers I wrote within this project. Thanks for helping to prepare geometries of reactors for Barracuda simulation tool.

During my PhD period, many friends and colleagues were there for help and/or valuable suggestions and they are too many to name all here. My sincere gratitude to all of them.

Porsgrunn, May 2015

Abstract

Dual fluidized bed reactor for steam gasification of biomass is a promising technology and can be used in Combined Heat and Power (CHP) production. The producer gas from the reactor can have a calorific value up to 14 MJ/Nm^3. The technology is well known for the comparative high efficiency and is neutral to CO_2 emission. Although the dual fluidized bed reactor has gained advantages compared to corresponding reactors, the technology has to be improved to become competitive in the world energy market.

The current project is focused on optimization of flow behavior and reaction kinetics in the gasification reactor to improve the reactor performance. The study of fluid dynamics and thermo-chemical behavior is performed using experimental and computational methods. Computational Fluid Dynamic (CFD) and Computational Particle Fluid Dynamic (CPFD) models are used in the study.

The dual fluidized bed gasification technology consists of a bubbling fluidized bed reactor and circulating fluidized bed reactor. The experimental and computational studies are carried out for both types of reactors. A CFD model is validated against the experimental measurements in a cold flow model of bubbling fluidized bed reactor. Good agreements were obtained between computational and experimental minimum fluidization velocities and pressure drops. The gasification reactor at high temperature conditions is simulated using the validated CFD model. The CFD model is also used for verification of Glicksman’s full set and simplified set of dimensionless parameters for scaling of biomass gasification reactors. In addition, the model is used to study Glicksman’s viscous limit set of dimensionless scaling parameters. The computational results show that Glicksman’s viscous limit set of dimensionless parameters is applicable for scaling of fluidized beds operating at particle Reynold’s number up to 15.

The CPFD model is used to simulate reaction and reaction kinetics in the gasification reactor. The computational results of composition of the producer gas agree well with the measured gas compositions reported from the biomass gasification plant in Güssing, Austria.

Circulation rate of bed material, steam to biomass ratio, bed material to biomass ratio and the corresponding temperatures are important for optimization of the gasification reactor. The CPFD model is used to study these parameters. The results show that the optimum bed material circulation rate is about 26 times of the biomass feed, the steam to biomass ratio is 0.2 on mass basis and the optimal reaction temperature is 1173 K. The results make a contribution to meet a challenge of increasing the steam conversion rate.

Steam production for the biomass gasification reactor requires significant amount of energy. Various gasification data show the steam conversion rate is lower than 10 vol.% [1, 2]. The rest of the 90 vol. % of steam is used only as fluidizing gas. The reduction of particle size of biomass and bed material significantly reduces the amount of steam required for the fluidization. The computational results based on the CPFD model show that decreasing particle size of bed material and the wood increases the producer gas quantity.

Experiments have been performed in a lab-scale cold model of a Circulating Fluidized Bed (CFB) reactor. Pressure data and bed material circulation rates show good agreements with the computational results. The CPFD model is used for optimization of gas feed positon in the CFB reactor in order to obtain maximum bed material circulation rate. The results of the CPFD simulations show that the optimum ratio of the heights of the feed position for the primary and secondary gas to the total height of the reactor are 0.125 and 0.375 respectively.

The optimization of the flow in the CFB needs identification of all flow regimes occurring in the reactor. The flow regimes have been identified along with the minimum fluidization, transport and fast fluidization velocities for glass particles with mean particle size of 156 µm. The CPFD model prediction shows that the gas velocity range of $10u_{mf}$ to $35u_{mf}$ should be avoided to maintain constant bed material circulation rate in CFB.

Contents

Preface ... vii

Abstract ... ix

List of Figures ... xii

List of Tables ... xv

Nomenclature ... xvii

Abbreviations ... xviii

I Overview ... 1

1 Introductions ... 1

- 1.1 Background ... 3
- 1.2 Objectives ... 5
- 1.3 Thesis layout ... 6
- 1.4 Main Contribution ... 7

2 Fluidization ... 9

- 2.1 Bubbling fluidized bed ... 11
- 2.2 Geldart classification of particles ... 12
- 2.3 Circulating fluidized bed ... 13
- 2.4 Scaling of fluidized bed reactors ... 16

3 Overview of biomass gasification ... 21

- 3.1 Types of biomass Gasification reactors ... 22
- 3.2 Dual fluidized bed gasification technology ... 22
- 3.3 Challenges related to the technology ... 29

4 Experimental work on bubbling and circulating fluidized bed reactors ... 31

- 4.1 Cold model of bubbling fluidized bed reactor ... 31
- 4.2 Cold model of circulating fluidized bed reactor ... 33

5 Mathematical model 39
  5.1 Euler-Euler method 39
  5.2 Eulerian-Lagrangian method 45
6 Biomass properties and reaction kinetics 51
7 Conclusion and recommendations 57
  7.1 Conclusions 57
  7.2 Recommendation for future work 62
Bibliography 64
II Published and submitted articles 69
Paper A
Study of flow behavior in bubbling fluidized bed biomass gasification reactor using CFD simulation 71
Paper B
Scaling of biomass gasification reactor using CFD simulation 83
Paper C
Scaling of bubbling fluidized bed reactors with Glickman’s viscous limit set and CFD simulations 95
Paper D
Modeling of reaction kinetics in bubbling fluidized bed biomass gasification reactor 107
Paper E
Influence of size and size distribution of biomass and bed material on performance of a dual fluidized bed gasification reactor 119
Paper F
Stepwise analysis of reaction and reacting flow in a dual fluidized bed gasification reactor 127
Paper G
Heat transfer optimization in a fluidized bed biomass gasification reactor 141
Paper H
Optimization of fluid dynamics in a circulating fluidized bed reactor 153
Paper I
Flow Regime Identification in the Riser of a Dual Fluidized Bed Gasification Reactor 169

List of Figures

1.1 Summery of the project work 4

2.1 Different Fluidization regimes 9

2.2 Pressure drop as a function of superficial gas velocity, olivine particle with air at ambient condition 10

2.3 Geldart classification of particles for air at ambient conditions [12] 12

2.4 Circulating Fluidized Bed 13

2.5 Zones of solid volume fractions and solid motion in a CFB [22] 14

2.6 U_c and U_k as defined by Yerushalmi and Cankurt [25] 15

2.7 Pressure vs dimensionless gas velocity at the dimensionless bed height of 0.5 19

3.1 Principal of dual fluidized bed gasification process 23

3.2 Flow sheet of CHP plant Gusing 24

3.3 Overview of main process occurring in a FB gasifier 27

4.1 (a) Fluidized bed setup: 1) Fluidized bed used in the experiment 2) Pressure reduction valve 3) Digital flow meter 4) Pressure sensors 5) Computer program. (b) Dimensions of the bed and pressure sensors locations 32

4.2 Experimental vs computational pressure drop at ambient and high temperature conditions 33

4.3 (a) CFB cold model with airflow regulation and pressure measurement arrangements (b) pressure tapping points 34

4.4 Rotameters for primary and secondary fluidization 36

4.5 Experimental and computational solid circulation rate 37

4.6 Solid circulation rate vs Primary air feed position 38

5.1 Contours of solid volume fractions of two beds 45

5.2 Solid out flux vs gas velocity 50

6.1 Mole fraction of producer gas at the top of the reactor 55

6.2 Volume percent of major gas composition 56

6.3 Increase in producer gas total energy as a function of steam to biomass ratio 57

6.4 Volume fraction of wood particle at simulation time of 300s. 57

6.5 HHV of producer gas leaving the reactor 58

List of Tables

3.1 Ranges of producer gas components in the Güssing plant [50] 25

3.2 Characteristic data from the CHP plant, Güssing [51] 26

3.3 Parameters of the riser at Güssing plant [59] 28

4.1 Height of the pressure tapping points 35

4.2 Flow range of rotameters 36

6.1 Elemental analysis of wood [73] 53

6.2 Composition of volatiles [73] 53

6.3 Major gasification reactions 54

6.4 Reaction kinetics used in the model 55

6.5 Comparison between predicted producer gas composition and plant data 55

Nomenclature

A	Particle acceleration [m/s^2]
A_0	Pre exponential constant [-]
Ar	Archimedes number [-]
C	Sub grid eddy coefficient [-]
$\bar{c}$	Cross sectional average volume fraction [-]
C_D	Drag coefficient [-]
C_p	Specific heat capacity [J/kg·k]
C_s	Fluctuating velocity of particle [m/s]
D	Mass diffusivity [m^2/s]
d_s	Particle diameter [m]
E	Activation energy [J/mol]
E_0	Activation energy constant [J/mol]
e_s	Coefficient of restitution [-]
F	Rate of momentum exchange per volume [$kg \cdot m/s^2$]
g	Acceleration due to gravity [m/s^2]
g_{os}	Radial distribution function [-]
h_g	Gas enthalpy [J]
K_{ls}	Drag between particles [N]
k_{gs}	Drag between fluid and solid [N]
L	Bed dimension [m]
$\dot{m}_{gs}$	Mass transfer rate [kg/s]
$\dot{m}_p$	Gas mass production rate per volume [$kg/(m^3 \cdot s)$]
MW	Molecular weight [g]
Nu	Nusselt number [-]
P_g	Fluid pressure [N/m^2]
Pr	Prandtl number [-]
P_s	Solid pressure [N/m^2]
$\dot{Q}$	Energy source per unit volume [J/m^3]
q	Gas heat flux [w/m^2]
R	Universal gas constant [J/(mol·K)]
Re_{mf}	Reynolds number at minimum fluidization [-]
T	Temperature [K]

u_o	Gas velocity [m/s^2]
u_{mf}	Minimum fluidization velocity [m/s^2]
u_{mb}	Minimum bubbling velocity [m/s^2]
Φ	Shape factor or sphericity [-]
S	Strain rate [1/s]
Sc	Schmidt number [-]
$\vec{u}_s$	Particle velocity [m/s^2]
$\vec{V}_s$	Average particle velocity [m/s^2]
U_{tr}	Transport velocity [m/s^2]
α_s	Particle volume fraction [-]
α_g	Gas volume fraction [-]
β	Stoichiometric coefficient [-]
λ_g	Gas thermal conductivity [w/(m·k)]
λ_s	Solid bulk viscosity [Pa·s]
λ_t	Turbulent eddy conductivity [w/(m·k)]
μ_s	Solid shear viscosity [Pa·s]
μ_{fr}	Frictional viscosity [Pa·s]
$\mu_{s,coll}$	Collisional shear viscosity [Pa·s]
$\mu_{s,kin}$	Kinetic shear viscosity [Pa·s]
ε_{mf}	Void fraction at minimum fluidization [-]
μ_g	Gas viscosity [Pa·s]
$\mu_{s,coll}$	Collisional part of shear viscosity [Pa·s]
$\mu_{s,kin}$	Kinetic part of collisional viscosity [Pa·s]
ρ_s	Particle density [kg/m^3]
ρ_g	Fluid density [kg/m^3]
τ_s	Solid stress [Pa]
τ_{gs}	Particle relaxation time [s]
θ_s	Granular temperature [J]
γ_s	Collisional dissipation of energy [J]

Abbreviations

BOKU	University of Natural and Life Sciences
CFB	Circulating Fluidized Bed
CFD	Computational Fluid Dynamics
CHP	Combine Heat and Power
CPFD	Computational Particle Fluid Dynamics

DFB	Dual Fluidized Bed
FB	Fluidized Bed
HHV	Higher Heating Value
KTGF	Kinetic Theory of Granular Flow
MP-PIC	Multiphase Particle in Cell
PDF	Particle Distribution Function

Part I

Overview

Chapter 1

Introduction

1.1 Background

There have been many discussions about the global warming and climate change due to the greenhouse gas emission by the use of fossil fuel. Many researchers and scientist believe on the need to reduce the emission in order to maintain global climate balance. The surge in the fossil fuel price has been observed from time to time leading to the instability on the world energy market. Other source of energy such as nuclear power plant also shows its instability towards the safety and environmental concerns. Accidents in nuclear power plants in Chernobyl and Fukushima are the prominent examples [3, 4]. Despite this, the energy demand in the world has been increasing continuously and the largest part of the demand is covered by fossil fuel [5, 6]. The fossil fuel sources have also their limits and will come to the end in the near future. The fact indicates the need of alternative energy sources. It is desirable that the alternative source can solve both the problem of energy crisis and greenhouse gas emission. One of the alternatives is biomass as a source of renewable energy neutral to CO_2 emission. Biomass insures long term and continuous supply. Biomass exists in many places in the world and can therefore be processed locally.

The conventional way of using biomass as energy source is burring it directly to produce heat energy. Alternatively, it is combusted to produce steam that is used in steam cycle for heat and power production.

During the past few decades, researchers have focused on gasification of biomass. The process of biomass gasification gives a mixture of combustible gases. The mixture is called syngas or producer gas depending on its composition. The gas is then combusted or co-combusted in power plants or the gas is further used in synthesis processes leading to liquid biofuels [7]. Alternatively, the producer gas is burned in gas engine or gas turbine to produce electricity and heat. This technology is known as Combined Heat and Power (CHP) production. The reason for gasification of biomass for CHP is the higher conversion efficiency compared to direct combustion or steam cycle [8] .

Among the different types of biomass gasification technology, the dual fluidized bed steam gasification has gained increased application throughout Europe during the past two decades. The technology produces comparatively high calorific value producer gas. The gasification technology has been successfully demonstrated as 8 and 10 MW CHP plants in Güssing and Oberwart, Austria respectively [9, 10]. The technology is described in more detail in Chapter 3.

Despite the novelty of the technology, there are still some challenges in making the products of gasification competitive in the fossil fuel dominated energy market. One of the major challenges is to increase the efficiency of the technology. The efficiency of the gasification system depends on the thermo-chemical and fluid dynamic behavior in the reactor. The thermo-chemical and fluid dynamic behaviors in the gasification reactor are still not well understood. It is necessary to understand the phenomenon in the reactor in order to figure out the possibilities of increasing the reactor efficiency. The series of experimental and simulation work carried out for studying fluid dynamic and thermo-chemical behaviors in gasification reactors are summarized in Figure 1.1.

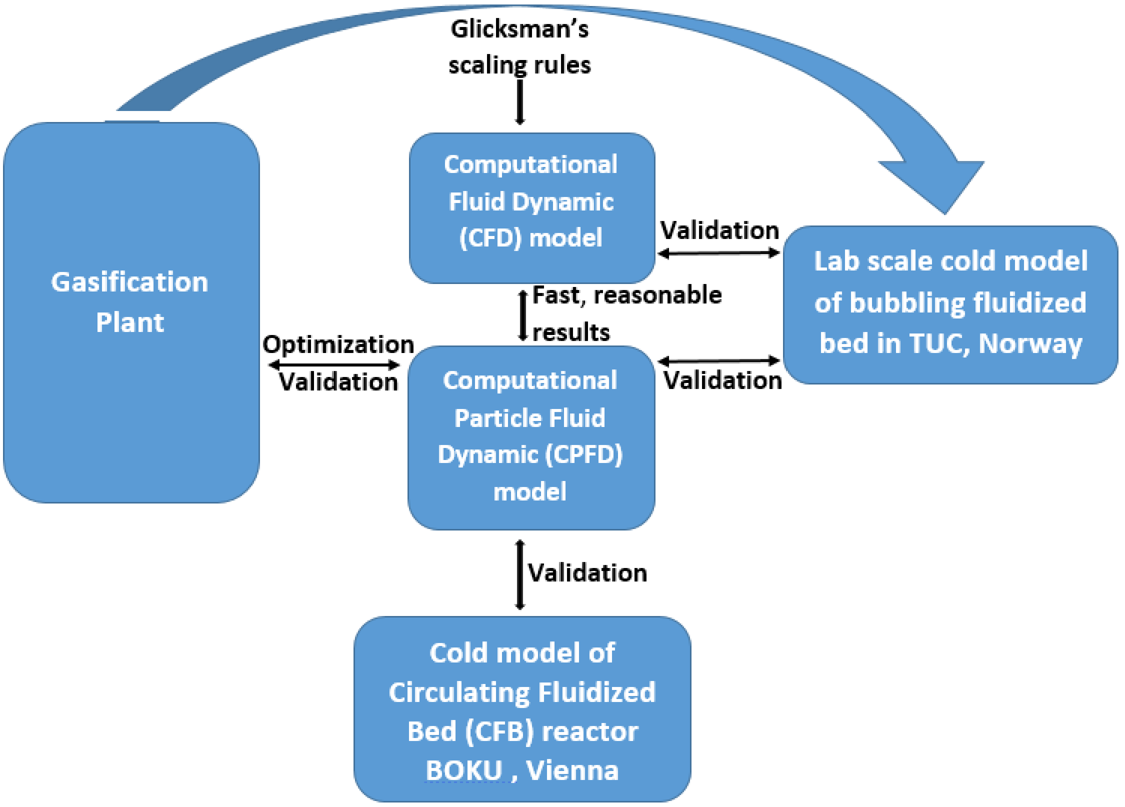
Glicksman's scaling rules
Computational Fluid Dynamic (CFD) model
Validation
Lab scale cold model of bubbling fluidized bed in TUC, Norway
Gasification Plant
Fast, reasonable results
Optimization
Validation
Computational Particle Fluid Dynamic (CPFD) model
Validation
Validation
Cold model of Circulating Fluidized Bed (CFB) reactor BOKU , Vienna

Figure 1.1: Summery of the project work

The bubbling fluidized bed gasification reactor based on a dual fluidized bed gasification system is scaled down to a lab-scale cold model using Glicksman's dimensionless scaling rules. Experiments were carried out in the lab-scale cold model to validate the Computational Fluid Dynamic (CFD) model and Computational particle Fluid Dynamic (CPFD) model. The validated CFD model is used to verify Glicksman's scaling rules.

The CPFD model is also validated against the reported plant data from the biomass gasification plant in Güssing Austria. The CPFD model is used for optimizing some operating parameters in the gasification reactor. The CPFD model is also validated against lab-scale cold model of circulating fluidized bed reactor located in University of Natural and Life Sciences (BOKU), Vienna. The model is used to optimize operating parameters in the combustion reactor of the gasification system.

1.2 Objectives

The dual fluidized bed biomass gasification system consists of two reactors. One reactor is a bubbling fluidized bed gasification reactor and the other is a circulating fluidized bed combustion reactor. The major process occurring inside both of the reactors is gas-solid reacting flow. The performance of the reactor is defined by the reactions and their kinetics and the fluid dynamic and fluidization properties in the reactor. Therefore, it is very important to understand the thermo-chemical and fluid dynamic behaviors in the reactor. Study and investigate the parameters effecting on the reactions kinetics and fluid dynamics in the reactor in an operating plant is difficult due to various technical challenges. The measurement of the parameters such as pressure, velocity, particle circulation rates is difficult due to high operating temperature. Moreover, it is not feasible to break continuous operation of the plant in order to take measurements. The task can be accomplished by downscaling the plant using the established scaling laws for gas-solid flow. Another way to perform the study can be the use of computational tools such as Computational Fluid Dynamic (CFD) and Computational Particle Fluid Dynamic (CPFD) models and simulations. The objective of this project is to investigate and optimize the flow and thermo-chemical behavior and fluidization properties in a dual fluidized bed gasification reactor in order to improve producer gas composition and production rate which increase the efficiency of the reactor. In order to achieve the main objective, the following investigation are set as objectives:

1. Verification of CFD and CPFD models for the study of bubbling and circulating fluidized bed biomass gasification reactors.
2. Down-scaling the gasification reactors to lab-scale cold flow models using the established scaling rules. Verify the applicability of scaling rules using the CFD models.
3. Validation of CPFD model for reactions in the gasification reactor against reported plant data.
4. Study of individual reaction kinetics in order to study their individual contribution on the producer gas composition.

5. Study of operating parameters such as fluidization velocity, pressure drop , temperature, particle and gas density and viscosity on the performance of gasification reactor using CPFD model.
6. Study the effect of bed material and wood/char particle size on the performance of the gasification reactor using CPFD model.
7. Study of bed material circulation rate, reaction temperature, steam to biomass feed ratio, steam feed temperature on the performance of gasification reactor.
8. Study of primary and secondary air feed positions for CFB in order to optimize the bed material circulation rate.
9. Study of flow regimes in the CFB for optimization of bed material circulation rate

1.3 Thesis layout

The thesis is divided into two major parts. In part one, the theoretical backgrounds are presented in seven chapters. Chapter 1 introduces the biomass gasification technology and explains the need for improvement of the technology. The gasification reactors studied in this work are related to bubbling and circulating fluidized beds. Chapter 2 describes briefly about the different gas-solid fluidization regimes, Geldart classification of particles, bubbling fluidized bed and circulating fluidized bed. One of the objectives of the project is to downscale the gasification reactors using the scaling rules and computational models. The chapter also includes a section for scaling of fluidized bed reactors. The commonly used scaling rule is Glickman's dimensionless scaling parameters, which is explained in the section. The gasification technology investigated in this project is based on the dual fluidized bed reactors. The dual fluidized bed gasification technology investigated in this work is designed by Vienna University of Technology and demonstrated as a successful story in eight megawatt biomass gasification plant for combined heat and power production. The plant is located in Güssing, Austria. Chapter 3 gives an overview of biomass gasification technology with the main focus on the dual fluidized bed gasification system. The biomass gasification plant in Güssing, Austria is described briefly with separate sections of the bubbling fluidized bed gasifier and circulating fluidized bed combustion reactor or riser. Chapter 4 describes the experimental set up and procedures. Experimental set up for the cold model of bubbling and circulating fluidized bed reactors are described in the chapter. A short description of the experimental procedures are given with corresponding figures.

Modeling and simulations are one of the major part of the work. A brief description of mathematical models used in the work are presented in Chapter 5. The Euler-Euler model for CFD and Euler-Lagrange model for CPFD are described. Chapter 6 gives the basic properties of biomass used in the simulations.

Some of the important properties of biomass used in this work are presented in the chapter. The major reactions representing the steam gasification of biomass are presented together with their corresponding reaction kinetics. The last Chapter of the part I of this work presents the conclusions and recommendation for future work. The conclusions are described in the sequences of papers included in this work.

Part II includes nine scientific papers. Seven of them are published in international journals and proceedings of the international conferences and two of them are submitted for publications in international journals and are under review.

1.4 Main Contribution

As stated in the objective of the current work, the major focus is on the flow behavior and fluidization properties in a dual fluidized bed biomass gasification reactor. The contribution of the present studies is divided into three major categories. The first part is related to the process of studying flow behaviors in the fluidized bed gasification reactors. This part gives down scaling solution to the existing difficulties related to study of fluid dynamics of the reactor. The second part is related to the investigation of the effect of various parameters on the fluid dynamic and thermo-chemical behavior in the reactors. The third part is identification and optimization of the flow regime in the fluidized bed reactors in order to avoid undesired flow regimes and achieve optimal bed material circulation rate. The contributions are briefly summarized as:

1. A Computational Fluid Dynamic (CFD) model is validated for gas-solid flow in a bubbling fluidized bed gasification reactor. The advantage of the validation is that the model can further be used to study the fluid dynamics of the reactors at high temperature operating conditions. Reactors with any particle size and density can be simulated which are not always possible in experimental investigations. The reason is that the particles of desired density and particle size are not always available on the market.
2. Applicability of Glicksman's set of dimensionless parameters for scaling the biomass gasification reactors have been verified. It has been shown that Glicksman's full set and simplified set of dimensionless parameters are applicable for the scaling of biomass gasification reactors. Exact experimental verification of the parameters is difficult for gasification reactors because the scaling rules require the particle with very high density (about 12000 kg/m^3) which is not easily available on the market. Alternatively, it requires a fluidizing gas with very low density which is very expensive to use. In addition, the applicability of Glicksman's viscous limit set of dimensionless scaling parameters has

also been shown. For the reactors with lower particle Reynold’s number, the viscous limit set is more flexible and easy to apply.

3. A Computational Particle Fluid Dynamic (CPFD) model is validated against experimental measurements in bubbling and circulating fluidized bed reactors. The model is also validated against the composition of the producer gas from the biomass gasification plant in Güssing, Austria. The models can be used to study the fluid dynamics and thermo-chemical behaviors in the dual fluidized bed gasification reactors.
4. The major parameters effecting the fluid dynamics and thermo-chemical properties of the reactor have been investigated. It has been shown that the larger bed material and fuel particle size have adverse effect on thermo-chemical performance of the gasification reactor. Reduced particle sizes give better performance of the reactor.
5. Simulations using the CPFD model have shown that the optimum steam to biomass feed ratio is 0.2 on mass basis. Actual use of the amount of steam in the reactor is much higher than that is required for gasification reaction. This is because steam is passed through the bed to fluidize bed material and biomass particles. If the particle size in the bed is reduced, the steam required for fluidization also reduces significantly. The highest optimum biomass steam gasification temperature is 1173 K and the optimum biomass to bed material ratio is 25-30 on mass basis.
6. When ratio of the gas velocity to minimum fluidization velocity (u/u_{mf}) in the riser of circulating fluidized bed is in the range from 10 to 35, the bed material circulation rate is unsteady. This range of velocity in the riser should be avoided for the constant circulation of the bed materials.
7. The fluid dynamics at ambient conditions are different from the high temperature conditions and reacting flow. The primary and secondary air flow rate and feed positions have significant effect on the performance of the combustion reactor. The optimum ratio of the height of the feed position to total height of the reactor for primary and secondary air are 0.125 and 0.375 respectively. Bed material circulation rate and pressure drops are less at high temperature conditions than at ambient condition.

Chapter 2

Fluidization

Many industrial processes including biomass gasification need a good contact between fluid and solids. The fluid can be liquid as well as gas but the current study is particularly focused on gas-solid contact. The gas-solid contact is achieved by passing the gas through a bed of particles [11]. If the superficial velocity of the passing gas is gradually increased, the gas transforms the solid particles into a fluid like state through a suspension. This state is known as fluidization and the bed at this condition is fluidized bed. The fluidized bed has an advantage of good mixing of fluid and particles which gives higher heat and mass transfer, lower pressure drop and low temperature gradient in bed [12]. Solid particles can be added or removed from the bed continuously. This is the advantage for many processes which require constant solid circulation [13].

Different fluidization regimes occur depending upon the superficial gas velocity, as shown in Figure 2.1.

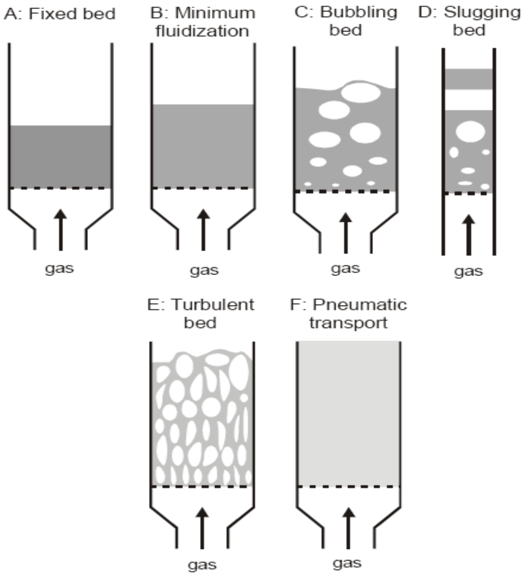

Figure 2.1: Different fluidization regimes

At low gas velocity, the fluid passes through the voids of the stationary bed and the state is defined as fixed bed.

The gas passing through the bed of solid particles develops pressure drop due to the drag forces. The pressure drop increases with gas velocity. At the condition when the pressure drop equals to the bed weight, the particles separate from each other. This is the starting point of fluidization. The gas velocity at this condition is known as minimum fluidization velocity (u_{mf}) and the bed is at minimum fluidization condition. The minimum fluidization velocity depends primarily on the particle size and density. With further increase of the gas superficial velocity, the pressure drop does not increase and remains approximately equal to the bed weight. Figure 2.2 presents the maximum pressure drop at fluidized bed conditions for olivine particles fluidized by ambient air.

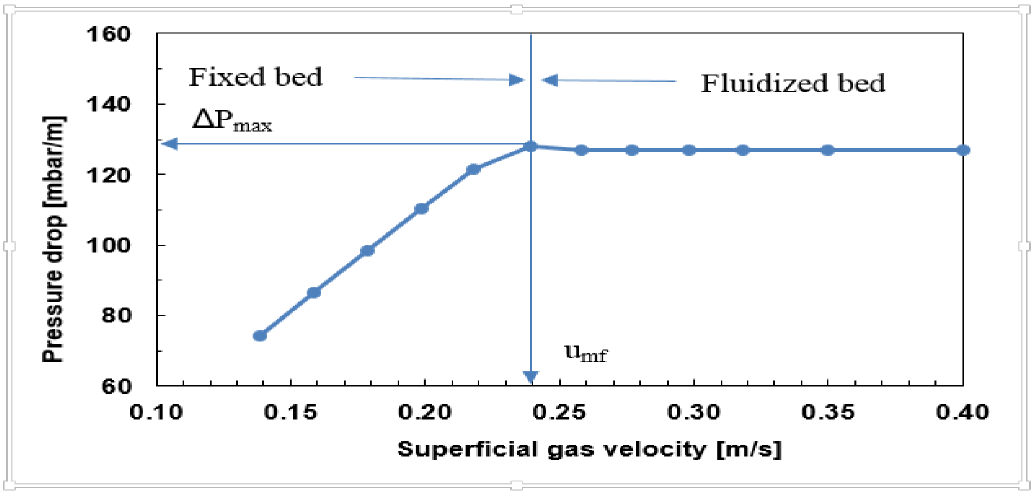

Figure 2.2: Pressure drop as a function of superficial gas velocity, olivine particles with air at ambient condition

When the gas velocity is increased above the minimum fluidization velocity, bubble formation is observed and the bed changes to bubbling fluidized bed. For the deep narrow beds, the bubbles can grow as big as the diameter of the bed and the bed is then a slugging bed. A fluidized bed is classified as a dense fluidized bed if the upper surface of the bed is clearly distinguishable. At gas velocity higher than terminal velocity of the particles, the upper surface of the bed disappears and a significant entrainment of the particles is observed. Turbulent motion of solid clusters and voids occurs and the bed is then in the turbulent flow regime. By further increasing the gas velocity, the particles are transferred out of the bed together with the gas. This state of bed is fast fluidization or pneumatic transport. Dual fluidized bed gasification reactor is operated at most of the these fluidization regimes. Although the dual fluidized bed reactor can be a combination of different reactors, this work deals with the combination of bubbling and circulating fluidized beds. The two beds are of main interest in this work and are described in Chapter 2.1 and 2.3 respectively.

2.1 Bubbling fluidized bed

Bubbling fluidized bed is one part of a dual fluidized bed reactor used in steam gasification of biomass. Bubbling beds are very important particularly in applications where gas solid mixing is essential. A dense bubbling fluidized bed has regions of low solid density called voids or simply bubbles. These voids or bubbles control the gross movement of the particles and the mixing of the gas and particles [14]. The region of higher particle density is called emulsion or dense phase. A bubbling bed behaves like a bubbling liquid of low viscosity. The gas velocity at which bubbles are first observed is called the minimum bubbling velocity u_{mb}. The u_{mb} strongly depends on the particle size and densities which is discussed in Section 2.2 [12]. Small bubbles are formed at the bottom of the bed and are more desirable for bubbling fluidized beds. The uniform bubbles make gas to move more uniformly through the bed and particles are distributed well in the fluid stream [15]. However not all the bubbling beds has small and uniform bubbles. The bubbles coalesce and grow as they rise along the height of the bed.

The minimum fluidization velocity is one of the important parameters that characterizes the fluidized bed. Different models for theoretical calculation of minimum fluidization velocity are developed. One of the commonly used models to predict u_{mf} is derived from the buoyancy-equals-drag balance including Ergun Equation [16].

$$u_{mf} = \frac{(\Phi.d_s)^2 \Delta\rho.g}{150\mu_g} \cdot \frac{\alpha_{g,mf}^3}{1-\alpha_{g,mf}} \tag{2.1}$$

where Φ is shape factor; $\alpha_{g,mf}$ is void fraction at minimum fluidization condition; d_s is particle diameter; $\Delta\rho$ is particle and gas density difference and μ_g is the gas viscosity. Wen and Yu [17] has derived an approximation for the term given by equation 2.2. The relation is valid for Reynolds number (based on the particle diameter) at minimum fluidization conditions less than 20.

$$\frac{\Phi_s^2 \alpha_{g,mf}^3}{1-\alpha_{g,mf}} \cong 11, \quad Re_{mf} < 20 \tag{2.2}$$

With the application of Equation 2.2 in the Equation 2.1, the minimum fluidization velocity becomes

$$u_{mf} = \frac{d_s^2 (\rho_s - \rho_f) g}{1650\mu_g} \tag{2.3}$$

The equation shows that the minimum fluidization velocity is a function of particle size, gas and particle density and gas viscosity.

In the basis of size and density Geldart [16] has classified particles in different groups. The classification is given in Section 2.2.

2.2 Geldart classification of particles

The mean particle size and its density defines the behavior of the particle in fluidized bed [18]. Geldart has classified the particles into four groups: A, B, C and D as shown in Figure 2.3. The Figure is valid for uniformly sized particles at ambient conditions [16].

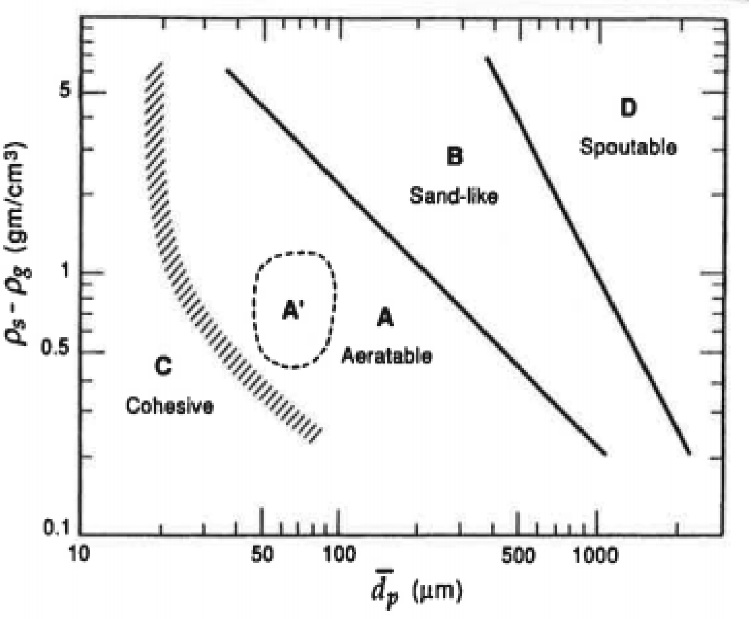

Figure 2.3: Geldart classification of particles for air at ambient conditions [12]

The bed of group A particles expands significantly after minimum fluidization condition before the appearance of bubbles. The group of particles has distinct minimum fluidization and minimum bubbling velocities. The minimum bubbling velocity is always greater than minimum fluidization velocity $(u_{mf} < u_{mb})$. For group B particles bubble formation starts at minimum fluidization velocity. Therefore, the minimum fluidization and minimum bubbling velocities are equal $(u_{mf} = u_{mb})$. Olivine and sand particles used in this work are examples of group B particles. The particles are widely used as bed materials in dual fluidized bed biomass gasification reactors. Group C are cohesive powders that are difficult to fluidize. Group D particles tend to create slugging and spouting conditions. Biomass and char particles may belong to this group depending on their size [19].

2.3 Circulating fluidized bed

The industrial application of circulating fluidized bed have been increased dramatically during the last two decades [20]. The advantage of circulating fluidized bed can be summarized as the bed with limited back mixing, controllable residence time of particles, uniform temperature without hot spots, flexibility in handling particles of wide size distribution, densities and shapes [21]. The circulating fluidized bed is a part of a dual fluidized gasification reactor. The reactor is used to heat the bed materials and transfer them to the gasification reactor. Circulating fluidized bed (CFB) consists of a riser, cyclone separator, siphon and a downcomer as shown in Figure 2.4.

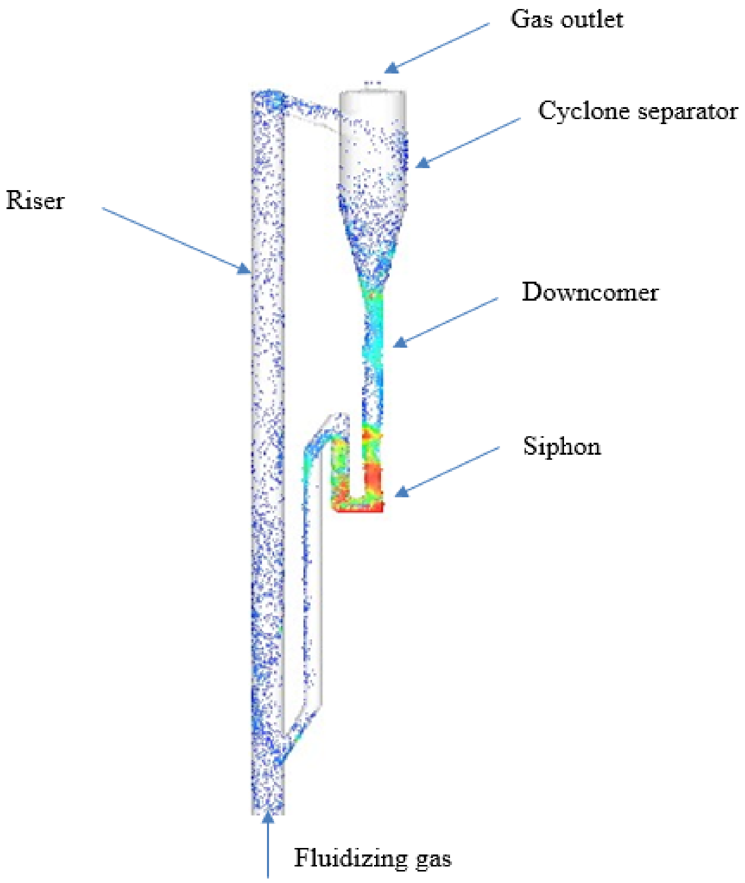

Figure 2.4: Circulating fluidized bed

The particles are transported through the riser by a high velocity fluid stream. At the top of the riser, the particles are separated from the gas and then the particles are returned to the bottom via the downcomer. The particle volume fraction throughout the riser and downcomer depends on the particle circulation rate. At low feed rate, all particles in the riser are transported to the top. When the solid feed rate is increased gradually the upward transport flow collapses and the dense region of the particles is formed at the bottom of the riser [11].

In this case, the particle volume fraction along the height of the riser varies from dense to dilute. The distribution of particles in a CFB is of fundamental interest for many industrial applications. The particle distribution influences many factors such as temperature distribution in the bed, chemical reactions and reaction rates.

Werther and Hirschberg [22] divided the riser into four sections depending on the solid concentration as shown in Figure 2.5. In the dense bottom zone, the solids volume fraction is typically 10 to 20% and particles are accelerating. The fluid dynamic properties in the zone are similar to a bubbling fluidized bed. Above the dense zone, there is a transition zone. The dilute zone starts above the transition zone and occupies the main part of the riser. The volume fraction in this zone is about 1%. At the top of the bed, there is an exit zone. In the Figure 2.5, the arrows in the bed indicate the flow directions. The cross sectional average volume concentration is denoted by $\bar{C}$. However, the concentration and the particle volume fractions are also strongly dependent on the particle circulation rate.

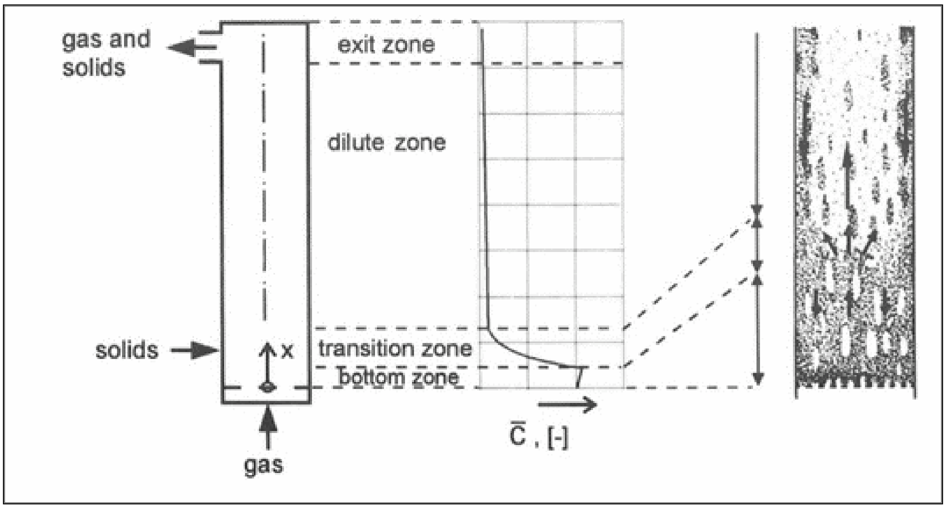

Figure 2.5: Zones of solid volume fractions and solid motion in a CFB [22]

The fluidization regimes are specified by a range of fluidization velocities. Circulating fluidized beds of high solid flux (about 120 kg/ $m^2 \cdot s$) are usually operated at fast fluidization regime. A detailed study of the fluidization velocities from minimum fluidization to pneumatic transport is necessary to establish an overview of the flow regimes in a CFB reactor. In the fluidized beds of large diameter with Geldart B particles, the transfer of regimes occurs from bubbling to turbulent [23] not slugging. In the turbulent fluidization regime, the pressure and solid volume fraction fluctuate with low amplitude [24].

Yerushalmi and Cankurt [25] developed a fluidization diagram over a full range of operating gas velocities. They characterized turbulent fluidization regime by two velocities U_c and U_k.

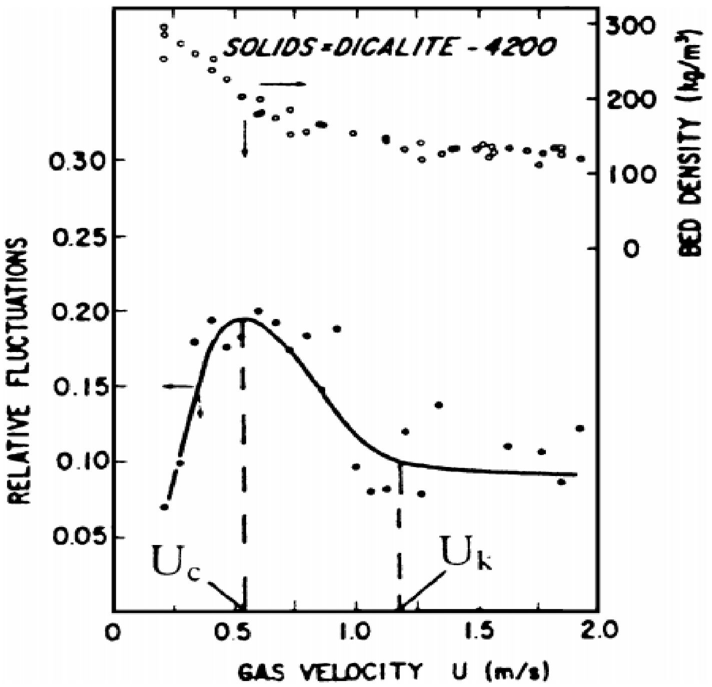

Figure 2.6: U_c and U_k as defined by Yerushalmi and Cankurt [25]

U_c corresponds to the bed operating condition when the bubbles or slugs reach their maximum, resulting maximum amplitude of pressure fluctuation across the bed [24]. Continuous increase in the gas velocity breaks up the bubbles resulting in smaller amplitude of pressure fluctuation. The velocity in this state is U_k.. The velocities are calculated using the correlations given by Equations 2.4 and 2.5 proposed by Horio [26]. The lower pressure fluctuation in the bed, the more uniform is the rate of particle transport.

$$(Re)_c = \frac{d_p \rho_g U_c}{\mu} = 0.936 Ar^{0.472} \qquad (2.4)$$

$$(Re)_k = \frac{d_p \rho_g U_k}{\mu} = 1.46 Ar^{0.472} \qquad (2.5)$$

When superficial gas velocity in the bed is increasing, there is a sharp change in pressure drop along the height of the riser. As the superficial gas velocity is increased beyond a certain point, the sharp increase of pressure drop disappears. The gas velocity at this point is known as transport velocity and is the onset of fast fluidization. Below the velocity there is a distinct interface between top-dilute and bottom dense phase regions. Beyond the velocity, the interface becomes relatively diffuse. The theoretical transport velocity is calculated by Equation 2.6 [27].

$$U_{tr} = 1.53 Ar^{0.5}\ for\ 2 < Ar < 4.10^5 \qquad (2.6)$$

The final transition is from fast fluidization to pneumatic transport. The transition velocity from fast fluidization to pneumatic transfer is known as chocking velocity.

The bubbling beds is characterized by solid concentration of about 0.45 - 0.25 whereas the turbulent bed is characterized by the solid concentration from 0.25 and lower [28]. The pneumatic transport regime occurs at solid volume fraction less than 1%. Fast fluidization regime occurs when the solid volume fraction is 5 - 15% at the lower part and 1-5% at the upper part of the bed [12].

Many fluidization regimes in circulating fluidized beds that are widely investigated so far by the various researchers are based on a single feed of gas at the bottom part of the bed. The CFB related to this project has three different gas feed positons. The gas is fed at the bottom and at two different positions along the height of the reactor as primary and secondary gas [29, 30]. The flow regime and fluid dynamics in the bed are different when the gas feed is located at multiple positions. The change in fluid dynamics effects the pressure and solid circulation rate. The fluid dynamics is also changing for different feed ratio of bottom, primary and secondary gas. The gas density and viscosity change significantly with increasing temperature. The gas feed data from the experimental investigations in a cold flow model is not always the same under high temperature conditions. The reactions in the bed make the flow even more complex. During the reactions, some gases are consumed and others are produced making the volume of the gas varying from the bottom to top.

2.4 Scaling of fluidized bed reactors

The fluidized bed reactors for gasification of biomass operate at high temperature and/or pressure. Due to the operating conditions, it can be difficult to investigate fluid dynamic behavior in the operating reactor. It is not convenient to take measurements for research purpose in an operating plant requiring continuous operation. The new design of reactors is easy to investigate in small lab-scale models and then up-scale to pilot and demonstration plants. In order to achieve the fluid dynamic similarity between two fluidized bed reactors, they should be scaled with properly developed scaling rules. The rules should consider all scale dependent parameters.

There are various scaling rules proposed for scaling of fluidized bed reactors [31-33] . The most commonly used is the one purposed by Glickman et.al. [34, 35].

Glickman [34] has derived a set of dimensionless parameters. The dimensionless parameters are derived based on the governing conservation equation of particles and fluid. Glickman’s full set of independent dimensionless parameters are given in Equation 2.7 [36].

$$\frac{u_0^2}{gL}, \frac{\rho_s}{\rho_g}, \frac{\rho_g u_o d_p}{\mu_g}, \frac{L_1}{L_2}, \frac{L}{d_p}, \Phi, particle\ size\ distribution \tag{2.7}$$

If all sets of dimensionless parameters given by Equation 2.7 are matching, then according to Glickman, the beds have fluid dynamic similarity. However, all the full set of parameters can be difficult to match in practice. Taking this fact into consideration, Glickman et. al. simplified the set of dimensionless parameters resulting another set known as Glicksman's simplified set of dimensionless parameters given by Equation 2.8. In the simplified set, the Reynolds number is replaced by the ratio of excess gas velocity to minimum fluidization velocity [35].

$$\frac{u_0^2}{gL}, \frac{\rho_s}{\rho_g}, \frac{u_o}{u_{mf}}, \frac{L_1}{L_2}, \frac{L}{d_p}, \Phi, particle\ size\ distribution \tag{2.8}$$

The simplified set is applied for two flow conditions. When fluid-particle drag is dominated by inertial forces, it is inertia dominated flow. The flow condition is represented by the higher particle Reynolds number. For the flow representing the inertial limit, all the dimensionless parameters presented by Equation 2.8 should be matched for fluid dynamic similarities. When the drag is dominated by viscous forces it is the viscous limit flow. For the flow dominated by viscous forces, the gas particle density ratio is not significant. Therefore, the gas particle density ratio is omitted when the particle Reynold's numbers is less than 4. In this case, the dimensionless parameters become less and more flexible for scaling the fluidized bed. The set is known as Glickman's viscous limit set of dimensionless parameters which is given by Equation 2.9 with the condition for Reynolds number presented in Equation 2.10.

$$\frac{u_0^2}{gL}, \frac{u_o}{u_{mf}}, \frac{L_1}{L_2}, \emptyset, particle\ size\ distribution \tag{2.9}$$

$$Re = \frac{\rho_g u_o d_p}{\mu} < 4 \tag{2.10}$$

Although, the viscous limit set is more flexible for scaling the fluidized bed reactors, it can only be used when the condition given by Equation 2.10 is fulfilled.

The applicability of Glicksman's scaling set of dimensionless parameters for gas solid fluidized bed has been confirmed by experimental investigations. Some of the experimental results are reported by Nicastro and Glicksman [37], Glicksman et al.[35, 38]. However, there are no verification found for the gas-solid flow at the operating conditions used for biomass gasification process.

The dual fluidized bed steam gasification reactor has olivine or quartz sand particles of density about 2960 kg/m^3 and mean particle diameter of 500 µm as bed materials. The fluidizing gas for the gasification reactor is steam at high temperature. Design, modification and improvement of the reactor requires various investigations of fluid dynamics and thermo-chemical properties as well as the geometry of the reactor. This is possible to accomplish in a laboratory using ambient air as a fluidizing gas when the reactor is scaled down using proper scaling rules. The high temperature steam used in the reactor has density about four time less than ambient air used in the lab scale cold model. The steam at high temperature has viscosity two and a half time less than that of the air. The density and viscosity ratio has to be handled properly while scaling down the reactor. For example, scaling down the gasification reactor to lab-scale cold model using Glickman's scaling rules can be started matching the particle gas density according to relation given by Equation 2.11.

$$\frac{\rho_{p1}}{\rho_{g1}} = \frac{\rho_{p2}}{\rho_{g2}} \tag{2.11}$$

where ρ_{p1} and ρ_{g1} is particle and gas density in gasification reactor; ρ_{p2} and ρ_{g2} is particle and gas densities in cold flow model. The particle and gas density in the gasification reactor are fixed as required by the gasification technology. As long as ambient air is used as fluidizing gas in the cold model, the gas is also fixed. The only one parameter that has flexibility to change is particle density in the cold model. The particle density can be calculated using the relation given by the Equation 2.11. The calculation gives that the particles required for the cold model should have a density of about 12000 kg/m^3. The required particles with very high density are not easily found on the markets. Therefore, the experimental verification of the scaling rules for fluidized bed biomass gasification reactors has some challenges. Kreuzeder et al. used bronze particles with density about 8730 kg/m^3 and they had to rely on approximate results [39].

To overcome this problem, a validated CFD model can be used to investigate if the Glicksman's scaling rules are applicable to biomass gasification reactors.

There are some technical difficulties in matching particle sphericity and particle size distribution in experimental investigations. It is difficult, for example, to match the particle sphericity and size distribution between two beds with different particles. However, in the CFD simulations the problems can easily be solved by assigning required particle sphericity and size distribution.

The bubbling fluidized biomass gasification reactor as a 'reference' bed, is scaled down to the lab-scale cold model as 'scaled' bed applying the Glicksman's full set and simplified set of dimensionless parameters. Both the reference bed and scaled bed are then simulated to investigate fluid dynamic similarities. The fluid dynamic properties such as pressure, solid volume fractions are monitored at 25 equally distributed locations of the beds. One of the sets of pressure data monitored at the dimensionless height of 0.5 is shown in Figure 2.7. The dimensionless height is the ratio of height of the monitor to the total height of the bed.

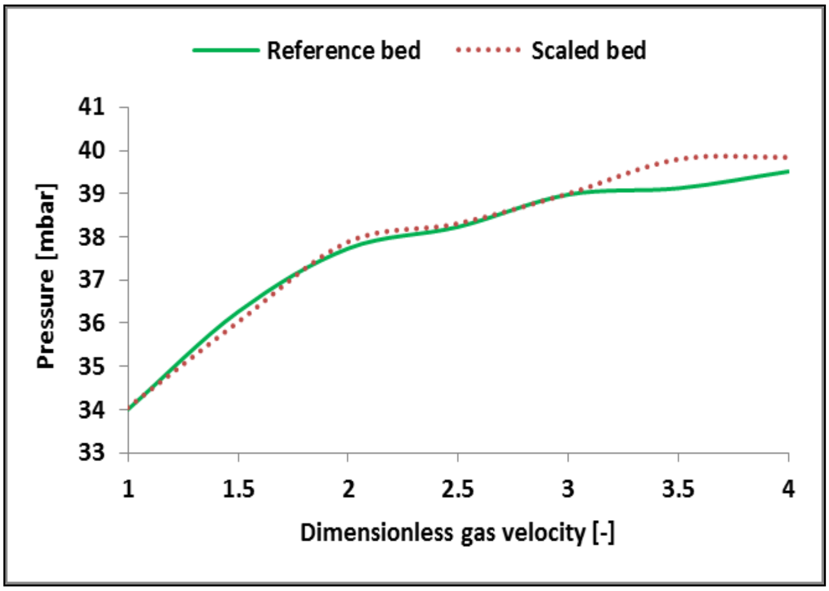

Figure 2.7: Pressure vs dimensionless gas velocity at the dimensionless bed height of 0.5.

The plot of pressure as a function of dimensionless velocities in two beds show that the fluid dynamic similarity between the beds exists. The dimensionless gas velocity is the ratio of gas velocity to the minimum fluidization velocity. The pressure for both of the beds increases with the increase in dimensionless gas velocities. The similarities of the pressure is maintained for all ranges of the gas velocities. The details of the simulations and results are presented in Paper B in Part II of this thesis.

Chapter 3

Overview of biomass gasification

Thermo-chemical processes for energy recovery from biomass consists of three major processes: pyrolysis, combustion and gasification. Pyrolysis is a thermal decomposition of biomass that takes place in the absence of oxygen. The process converts biomass into solid charcoal, liquid (such as tar) and gaseous products at temperature about 100 °C - 600 °C. High temperature and longer residence time favors production of gases while moderate temperature and short residence time is optimal for production of liquids [40]. Pyrolysis is also the intermediate step in a gasification and combustion process. The technology has already become a state-of art in thermal conversion of biomass [41]. Combustion is a method for conversion of biomass to heat energy under excess supply of oxygen at the temperature range of 700 °C to 1200 °C and is used today in conventional power plants. Biomass combustion is a major energy source in developing countries for cooking and heating houses. Combustion is used not only for heat but also for the power production. The overall efficiency of power production via combustion is about 15% for small power plant and up to 30% for larger and newer power plants [40]. Gasification is a process that converts biomass into a mixture of combustible and non-combustible gases (e.g. CO, CO_2, N_2, H_2, CH_4, and H_2O) which is known as a producer gas. The producer gas composition mainly depends on the gasification agent and gasification temperature. When air is used as gasification agent, the high amount of nitrogen content in the air makes the producer gas diluted and its calorific value reduces. Steam gasification, on the other hand, leads to a producer gas without nitrogen and with high hydrogen content. The gasification process is carried out generally at the temperatures ranging from 700 °C to 1200 °C and with the fuel to oxygen ratio less than stoichiometric. However the temperature can be as high as 1500 °C for entrained flow gasifier and even higher in plasma gasification. The efficiency of conversion for a gasification plant ranges from 35% to 50% for smaller to larger scale plants respectively [40]. The main difference between the pyrolysis, combustion and gasification processes lies on the amount of oxygen supplied to the process and the operating temperature. The producer gas from the gasification is widely used in gas engines or gas turbines to produce electricity and heat.

Alternatively, the producer gas is used in synthesis processes for production of biofuels. Liquid biofuel can be produced through Fischer-Tropsch synthesis process whereas the methanation process gives Bio SNG.

3.1 Types of biomass Gasification reactors

While combustion is an exothermic process, gasification is an endothermic process and needs a source of heat supply. The method of heat supply to the endothermic reaction divides the gasification process into autothermal and allothermal. If the heat required is provided by a partial oxidation of the gaseous products, the process is autothermal gasification. The reactors used for the autothermal gasification process are fixed bed, fluidized bed and entrained flow reactors. Generally, air is used as the gasifying agent in the autothermic gasification process. If the heat required for the gasification process is added indirectly by heat exchanger or heat carrier, then the process is allothermal. Dual fluidized bed steam gasification process is an example of allothermic gasification [42].

The fixed bed reactors are further divided into downdraft-fixed bed and updraft fixed bed reactors. The difference between them is the direction of gas flow. In updraft-fixed bed gasifier, the gas flows from bottom to top and the fuel is fed from the top of the reactor [43]. In downdraft-fixed bed, the gas and fuel move in the same direction from the top to bottom [44]. Entrained flow reactors are used in large scale gasification plants. The gasification temperature in the entrained flow reactors is comparatively high which results in low amount of tar in the producer gas. Fluidized bed reactors are well known for the good mixing, heat and mass transfer. The operating temperature of the reactor can be maintained more uniform over the reaction area which gives high reaction rate. The fluidized bed reactors are easy to scale up and scale down. They have a good gas solid contact and possibility for using catalytic bed material for tar reduction. Bubbling fluidized bed and circulating fluidized beds are widely used in biomass gasification applications [40]. The fluidizing gas used in the gasifier is oxygen, air and steam. Use of oxygen as fluidizing gas produces high quality gas. However, the operating cost is very high. Use of air as fluidizing gas dilutes the producer gas due to the nitrogen content in the air. The dual fluidized bed steam gasification has more concentrated producer gas due to use of steam instead of air. The heat required for the endothermic gasification reactor is supplied from the separate reactor.

3.2 Dual fluidized bed gasification technology

The dual fluidized bed (DFB) gasification reactor can be a combination of bubbling and circulating fluidized beds. The gasification system was developed by Vienna University of Technology [9, 45].

The technology has been successfully demonstrated in 8MW and 10 MW gasification plant in Güssing and Oberwart, Austria respectively.

The principal of the dual fluidized bed gasification process is shown in Figure 3. 1. The dual fluidized bed gasification system is divided into two parts: gasification reactor and combustion reactor.

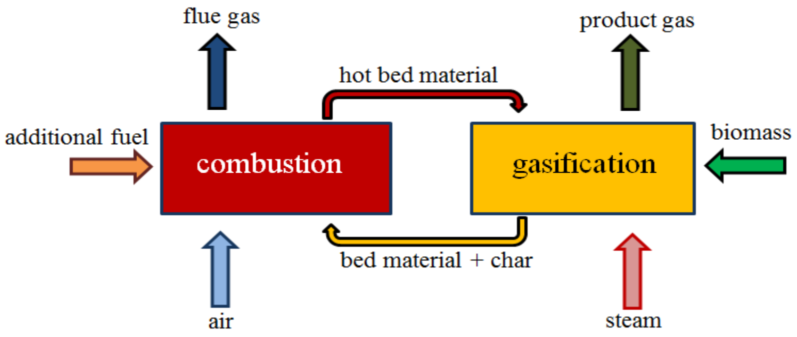

Figure 3.1: Principal of dual fluidized bed gasification process

The gasification reactor is a bubbling fluidized bed reactor where bed materials such as sand or olivine are fluidized by high temperature steam. The olivine particles act as heat carrier to the gasification rector. At the same time, the particles act as catalyst for reduction of tar in product gas. Biomass fed to the reactor is mixed with the bed materials and the steam. The biomass undergoes an endothermic gasification reaction to produce a mixture of combustible (CO, CH_4, H_2) and non-combustible (CO_2 and H_2O) gases. The hot bed materials transported from the combustion part supplies the heat required for the endothermic gasification reaction.

As a result of steam gasification of biomass, there are some unreacted char particles remaining as residual fuel. The particles are transported to the combustion reactor along with bed materials via an inclined connecting chute. The connecting chute is fluidized by steam in order to prevent the leakage of flue gas from the combustion reactor to the gasifier. The combustion part is a circulating fluidized bed which is fluidized by ambient air. The purpose of the combustion reactor is to heat bed material and circulate it back to the gasification reactor [46, 47].

3.2.1 Biomass gasification plant in Güssing, Austria

One of the biomass gasification plants for combined heat and power production is located in a small town, Güssing in Austria. At present Güssing is supplied with 100% renewable energy based on biomass [48].

The basic concept of this plant lies on the development dual fluidized bed gasification technology. The gasification and combustion reactions are separated into two zones in order to produce nitrogen free producer gas [49]. The flow sheet of the CHP plant in Güssing is shown in Figure 3.2.

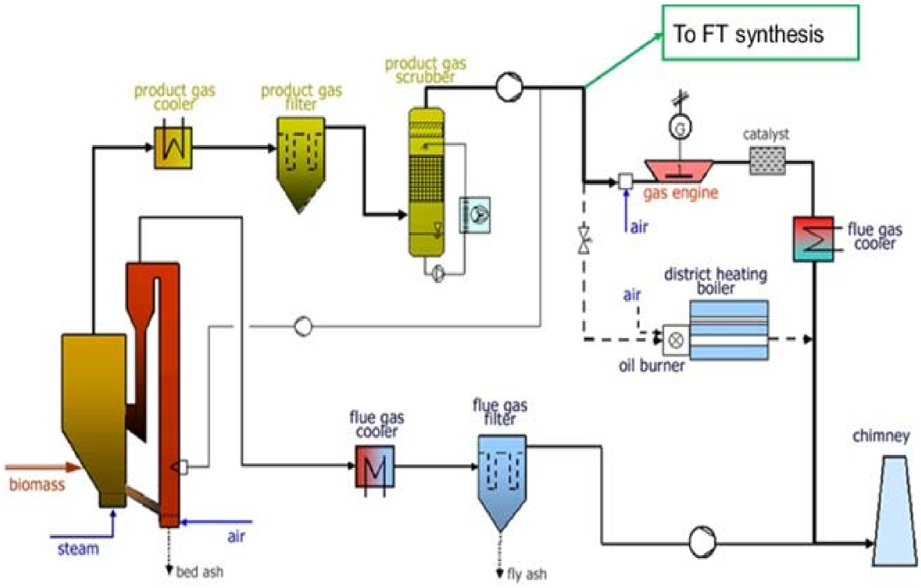
To FT synthesis
product gas cooler
product gas filter
product gas scrubber
G
catalyst
gas engine
air
flue gas cooler
district heating boiler
air
oil burner
flue gas cooler
flue gas filter
chimney
biomass
steam
air
bed ash
fly ash

Figure 3.2: Flow sheet of CHP plant Gussing [49]

Biomass is injected via a screw feeder to the bubbling fluidized bed gasifier. Biomass is mixed with hot bed material and high temperature steam. As a result the biomass devolatilzes forming char and volatiles. The char particles further undergo the heterogeneous char gasification at a temperature of 800°C – 850°C. After gasification, some of remaining char particles are transported to the combustion reactor to burn them and heat the bed materials. The combution reactor is a circulating fluidized bed. Air is used as fluidizing agent in the reactor. A small amount of producer gas is recirculated to the reactor to heat the bed materials at the start up of the reactor.The hot bed materials are seperated from the flue gas in a cyclone separator via a loop seal. The loop seal is fluidized with steam to prevent gas leakage between the combustion and gasification reactors. Then the hot bed materials are circulated to the gasifier to supply required heat for endothermic reaction in the gasifier [50].

The temperature difference between the gasification and combustion reactors depends on the heat required for the endothermic reaction and the circulation rate of the bed material.The system is self stabilizing. Decrease in the temperature of the gasification reactor increases unreacted char particles transported to the combustion reactor. When more char is transported to the combustion reactor, the temperature of the bed materials will increase and the heat transfer to the gasifier increases. More heat transfer to the gasification reactor increases the reaction rate. The increase in the gasification reaction rate again decreases the the amount of char particles tranported to the combusiton reactor. The process continues until the steady operation of the reactor is established.

In this way the gasfication process and reaction temperature is auto stabilized. Both the gasification and combustion reactors are operated at atmosphereic pressure.

As a result of the gasification and combustion process, the dual fluidized bed reactor gives two separate gas streams: high quality producer gas from gasification process and flue gas at a high temperature from the combustion reactor. The producer gas is characterized by a relatively low concentration of higher hydrocarbones such as tars, low concentration of N_2 and high concentration of H_2 [50]. The typical composition of the producer gas is given in Table 3.1.

Table3.1: Ranges of producer gas compnonts in the Gussing plant [51]

Gas components	Units	Range
Hydrogen (H_2)	Vol-%	35 -45
Carbon monoxide (CO)	Vol-%	20 -30
Carbon dioxide (CO_2)	Vol-%	15 -25
Methane (CH_4)	Vol-%	8 -12
Nitrogen (N_2)	Vol-%	3 -5

The hot flue gas from the combustion reactor is sent to the energy recovery heat exchangers. The gas is cooled down to a temperature of about 120°C. The fly ash is filtered in a flue gas filter and then the flue gas is sent to the atmoshphere. The heat recovered from process is partially used for steam generation and the biomass preheating process and rest are connected to the district heating grid. The producer gas is cooled in two stages. In the first stage, the gas is cooled by water cooling heat exchanger. It is cooled from the temperature of 850°C -900°C to about 150°C. The gas is cleaned in fabric filter separating dust particles and some of the tar from the product gas.

The second stage of cooling is in the wet scrubber where the producer gas is cooled to the temperature of 40°C. This is the requirement for the feed temperature of gas engines or gas turbines. In the scrubber, the gas is simultaneously cleaned from tar. The heat from the gas cooling is recovered and used for district heating. The particles separated from fabric filter and the tar separated by scrubber are recycled to the combustion reactor and the combustible part of them are burned together with the char particles [49]. The cleaned and cooled gas is then burned in a gas engine to produce electric energy. The produced electricity is connected to the transmission lines. There are a lot of process heat from the gas engine cooling system. All the excess process heat is used for district heating.

The heat is used for heating residential buildings as well as in the industries that need heat. The major characteristic data from the plant are presented in Table 3.2.

Table 3.2: Characteristic data from the CHP plant,Gussing [52]

Start up of gasifier	November 2001
Strat up of gas engine	April 2002
Fuel	Wood chips
Fuel power [MW]	8
Electrical output [MW]	2
Thermal output [MW]	4.5
Electrical efficiency [%]	25
Thermal efficiency [%]	56.3
Total efficiency [%]	81.3

The efficiency of the gasification reactor can be further improved by improving the fluid dynamic and thermo-chemical properties in the reactor. Modification and improvement of the gasifier can increase the hydrogen content in product gas. Biomass gasification with pure steam in a fluidized bed reactor can achieve up to 60 vol % of hydrogen production on dry basis and 70-75 vol% can be reached if a circulating fluidized bed gasification reactor is used [53].

3.2.2 The gasifier

Biomass is fed into the bubbling fluidized bed gasification reactor in the form of wood particles. In the reactor, biomass first undergoes a drying process where the moisture content in the biomass is removed. The second process is volatilization of biomass. This is a process of decomposition of biomass in the absence of oxygen. The biomass is decomposed to char particles and volatiles. The components from the process of drying and volatilization are shown in Equation 3.1. The composition of the products depends on the wood composition and operating condition of the reactor [54].

$$wood \rightarrow H_2, CO, CO_2, CH_4, HC, H_2O, tars, char(s) \tag{3.1}$$

The volatiles undergoes secondary reaction with other volatiles as well as char particles. The remaining char particles are gasified by steam and carbon dioxide. Some of the unreacted char particles are transported from the gasifier to the combustion reactor with the bed materials.

The major reactions occurring in the gasification reactor are summarized in Equations 3.2 – 3.6 [55-58]. The reactions are steam gasification, carbon dioxide gasification, methanation, water gas shift reactions and methane reforming respectively.7

$$C + H_2O \rightleftharpoons H_2 + CO \tag{3.2}$$

$$C + CO_2 \rightleftharpoons 2CO \tag{3.3}$$

$$0.5\,C + H_2 \rightleftharpoons 0.5CH_4 \tag{3.4}$$

$$CO + H_2O \rightleftharpoons CO_2 + H_2 \tag{3.5}$$

$$CH_4 + H_2O \rightleftharpoons CO + H_2 \tag{3.6}$$

Figure 3.3 gives an overview of the main process occurring in a fluidized bed gasifier [57].

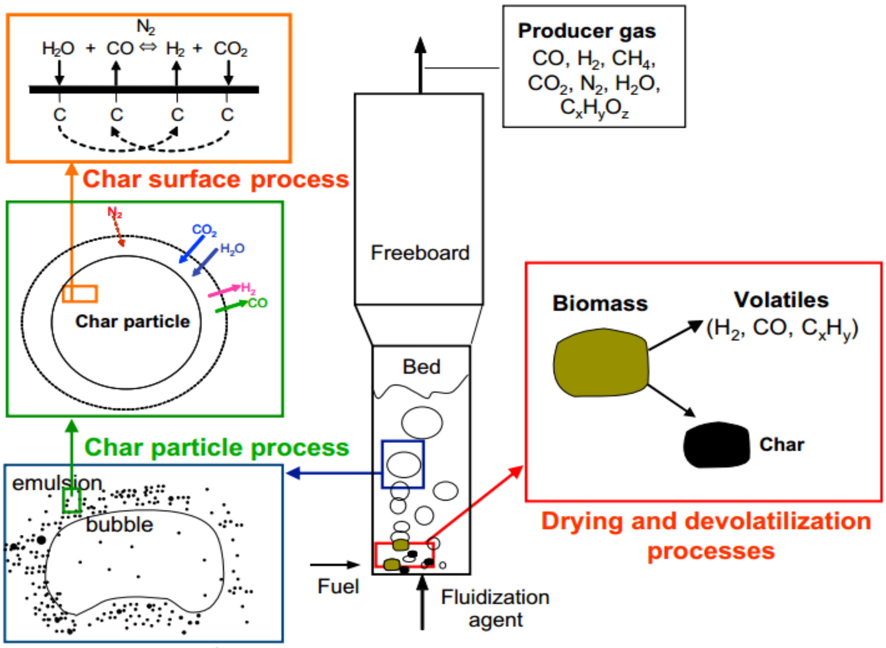
N_2
H_2O + CO ⇔ H_2 + CO_2
C
C
C
C
Char surface process
N_2
CO_2
H_2O
H_2
CO
Char particle
Char particle process
emulsion
bubble
Producer gas
CO, H_2, CH_4, CO_2, N_2, H_2O, $C_xH_yO_z$
Freeboard
Bed
Fuel
Fluidization agent
Biomass
Volatiles
(H_2, CO, C_xH_y)
Char
Drying and devolatilization processes

Figure 3.3: Overview of main process occurring in a FB gasifier [57]

Most of the conversion processes take place within the bed and some conversion processes take place in the freeboard region. The composition of the producer gas highly depends on the gasification agent used. As long as high temperature steam is used as gasifying agent, the nitrogen content in the producer gas is insignificant. However, a small amount of nitrogen is present due to the leakage from the combustion reactor as well as the nitrogen content in biomass.

3.2.3 The riser

The riser or circulating fluidized bed combustion reactor is a part of the dual fluidized bed gasification system responsible for energy supply to the gasification reactor. The dual fluidized bed gasification system can be regarded as a circulating fluidized bed with a bubbling fluidized bed gasification reactor in the return loop of the system [59]. The feed is residual char particles and bed materials. At the top of the riser, there is cyclone separator that separates the hot bed material from flue gas.

Some of the important parameters of the combustion reactor in the biomass gasification plant in Güssing, Austria is given in Table 3.3.

Table 3.3: Parameters of the riser at Güssing plant [60]

Parameters	Unit	Value
Diameter of the riser	m	0.61-0.66
Height of riser	m	12
Diameter of bed material	m	500.10^{-6}
Density of bed material	kg/m^3	2960
Diameter of char	m	0.008
Density of char	kg/m^3	200
Volume flow of bottom, primary, secondary air	Nm^3/h	720,2880,860
Temperature of bottom, primary and secondary air	°C	60,400,460
Temperature of bed material	°C	850
Bed material circulation rate	Kg/s	37

The combustion reactor is operated with two zones. Each of the zones have different fluid dynamics. The bottom part is dense zone and has bubbling fluidization regime. The upper part of the reactors operates in fast fluidization regime and this regime covers the main part of the reactor. Preheated air is used as fluidizing gas and is introduced at three feed locations as bottom, primary and secondary air. A part of the preheated producer gas is also introduced to the reactor and burned in order to heat the bed material when the reactor is just started.

With the bottom air as fluidizing gas the bottom part of the bed works at bubbling fluidization regime. When the primary air is introduced, the upper part of the bed above the primary air feed position is operated at fast fluidization regime. The particle volume fraction has significant radial gradient at fast-fluidized regime. At the center the particles are transported upwards whereas near the wall there is downward movement of particles and the particle concentration is higher [59].

3.3 Challenges related to the technology

After the short description of the technology, it seems valuable to discuss some of the challenges in the technology. The riser is operated at circulating fluidization condition in order to transport the bed materials to the gasification reactor. The gasification reactor is operated as a bubbling fluidized bed reactor in order to avoid leakage of steam. If the gasification reactor is operated in a regime with higher gas velocity, possibility for significant amount of steam leakage through the connecting chute to the combustion reactor increases. The steam loss reduces overall efficiency of the system. However, fluidization regime with higher gas velocity gives better mixing and heat and mass transfer. The design of the system should be changed to have more efficient fluidization regime. Otherwise, the lower part of the bed should remain in bubbling fluidization regime.

According to the various gasification test in the Güssing plant, the conversion rate of steam is only about 10 vol%., which indicates significant energy loss during the process. Increasing steam velocity leads to further decrease in this conversion rate. This is the another reason for keeping the gasification rector in bubbling fluidization regime. The steam conversion rate is still a challenge for the gasification reactor. Only change in existing gas-solid flow behavior or gas and particle properties can contribute to meet this challenge. The current work have addressed some of the challenges.

It is still an open question whether it is possible to improve the thermo-chemical properties in the reactor. Fluid dynamic and thermo-chemical behavior of the gasification system is not well enough understood yet. Therefore, the current project attempts to figure out some of them.

The reactor in a gasification plant is operating at high temperature conditions. It is not convenient to take measurements or make continuous investigation of fluid dynamics and thermochemistry in an operating plant. It makes disturbance of the production, it is very costly, the high temperature measurements are not safe and not all measurements can be accomplished at that conditions. For example, it is still challenging to measure bed material circulation rate in an operating hot reactor. These facts indicate the need of lab-scale cold model for investigating fluid dynamics and other properties in the reactors.

The lab scale cold flow model should have fluid dynamic similarity with the reactor in the gasification plant.

In order to have fluid dynamic similarity, the plant should be scaled following the established scaling rules. The applicability of the scaling rules needs to be verified. Current project offers the solution using validated CFD and CPFD models for investigating fluid dynamic similarities between the scaled beds. The validated models for bubbling and circulating fluidized bed reactors are also used to study fluid dynamic and thermo-chemical properties of the reactors.

The major focus of the current project is to optimize the flow behavior and the thermo-chemical properties in the rectors. The flow in the bubbling fluidized bed and the circulating fluidized bed reactors are reacting flow. That means there are fluid dynamics in the bed along with chemical reaction. The chemical reactions also contribute to the fluid dynamic properties. The aim is to study the flow with and without chemical reaction step by step. The study is therefore, divided into two parts. The first part is studying of fluid dynamics in the reactors without the chemical reactions. As discussed in Chapter 2, the fluid dynamic properties in fluidized beds are significantly affected by the particle and gas density and particle size distribution. These effects have to be studied thoroughly. The fluid dynamics are also effected by the operating fluidization regime in the bed and the gas feeding points. Changing the gas feed location along the reactor are difficult in the experimental studies. This fact highlights the importance of molding and simulation approach in the study of fluid dynamics. The second part is the study of thermo-chemical behavior in the reactor.

There are different chemical processes in the bubbling and circulating fluidized bed reactors. The reactions in bubbling fluidized bed gasifier are effected by steam feed rate and temperature, bed material feed rate and temperature, biomass and bed material size distribution and the fluidization regimes. The parameters effecting the reactions in circulating fluidized bed combustor are bottom, primary and secondary airflow rates, feed positons and preheat temperatures. The reactions are also effected by bed material and residual char particle size distribution and the fluidization regime of the reactor. These challenges are addressed in the current project.

Chapter 4

Experimental work on bubbling and circulating fluidized bed reactors

The major part of the project is based on simulation of dual fluidized bed biomass gasification reactors. However, the computational models have to be verified against experimental data. There are still many technical challenges that make it difficult to perform experimental test in each and every study. Actually, this is the main reason for developing computational methods. The experimental and computational studies are interdependent. The focus on experiments is given to validate the computational models against experimental data before using the model in the study of the gasification reactors. As the gasification reactor consist of two different fluidized bed reactors, the experimental validations have been performed separately in the cold models of bubbling and circulating fluidized bed reactors.

4.1 Cold model of bubbling fluidized bed reactor

The cold model of bubbling fluidized bed reactor is located at Telemark University College. The model consists of a transparent cylindrical fluidized bed rig with height 1.4 m and diameter 0.084 m. The experimental set up is presented in Figure 4.1.

A set of pressure tapping points are located along the height of the rig and the pressure sensors are connected to the lab-view program to log and store the pressure readings. The program saves pressure reading every second. The rig with required equipment is presented in Figure 4.1(left). The location of the pressure taping points along the height of the rig is shown in Figure 4.1(right). The distance between pressure measuring points is 10 cm. The bed of particles in the rig is fluidized with ambient air which is supplied from an air compressor. Air is supplied to the bed through a uniform air distributor at the bottom of the reactor. The flow is regulated by valves and measured by the flow measurement system. The flow is controlled by the lab-view program.

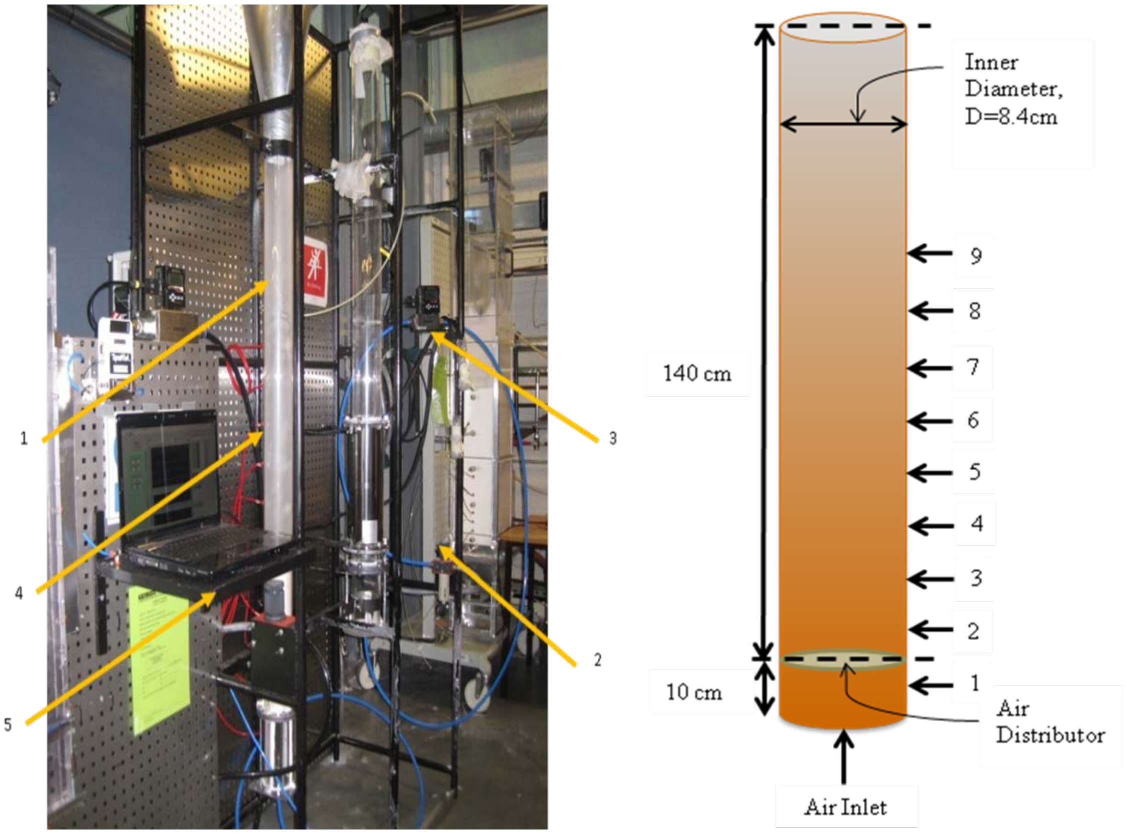

Figure 4.1: Left - Fluidized bed setup: 1) Fluidized bed used in the experiment 2) Pressure reduction valve 3) Digital flow meter 4) Pressure taping points 5) Computer program.
Right – Dimensions of the bed and pressure point locations

The cold flow experimental set up is used to validate the CFD model. Experimental pressure drop along the height of the bed and minimum fluidization velocity are compared with the model predictions. The model predictions have good agreements with the experimental data. Figure 4.2 presents the comparison of experimental and computational pressure drops for glass particles fluidized with ambient air.

The model is then used to investigate the flow behaviors and fluidization properties in the bubbling fluidized biomass gasification reactor including high temperature operating conditions. The simulation results of the pressure drop for olivine particles fluidized by steam at a temperature of 850℃ is also presented in Figure 4.2.

In the experimental work, the pressure drop is measured for fixed and fluidized bed gradually. The pressure drop along the height of the bed starts at the fixed bed conditions. In the simulations, the pressure drops are monitored only at fluidized conditions. The fixed bed was not simulated.

This was because the main interest of comparison was minimum fluidization conditions and not the fixed bed conditions. The results confirms good agreement between experimental and computational pressure drops at the ambient condition. The pressure data of olivine particles at high temperature conditions show that the pressure drop at high temperature conditions is similar to glass particles with lower particle size at ambient condition. More details of the experimental and computational procedures and results can be found in Paper A.

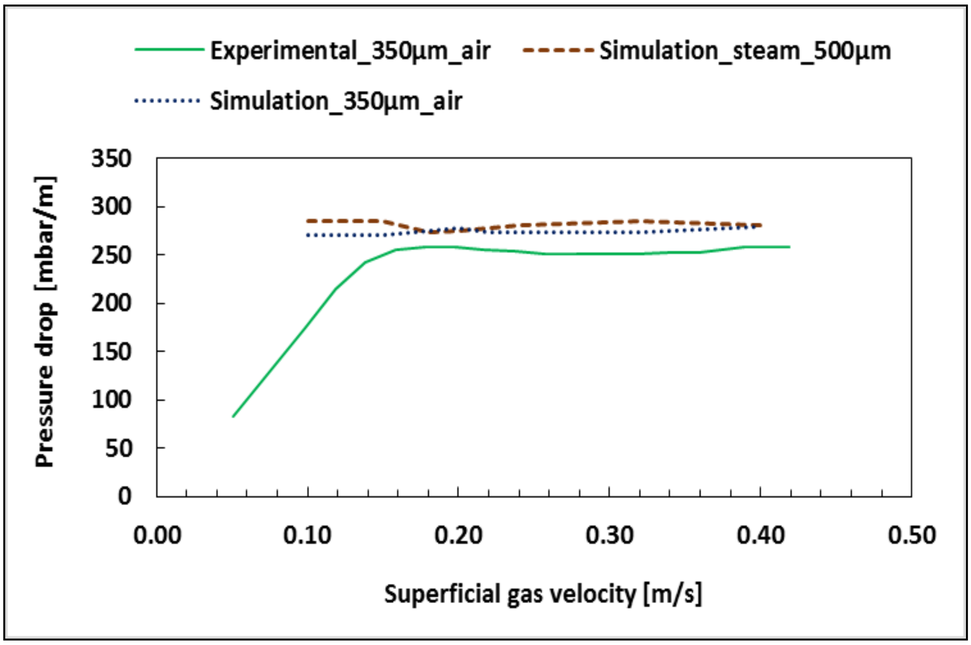

Figure: 4.2: Experimental vs computational pressure drop at ambient and high temperature conditions

The CFD model is also used to investigate the applicability of Glickman's full, simplified and viscous limit sets of scaling parameters. The results of the investigation are presented in Paper B and Paper C. Experiments were performed in the cold model of the bubbling fluidized bed reactor to validate the CPFD models as well. The paper containing the validation results is not included in this work [61]. The validated CFD and CPFD models are further used in the computational study of bubbling fluidized gasification reactor.

4.2 Cold model of circulating fluidized bed reactor

The experimental set up of the cold model circulating fluidized bed is located in University of Natural and Life sciences (BOKU) in Vienna, Austria. The set up consists of a circulating fluidized bed of height of 1.6 m and diameter 0.05 m as shown in Figure 4.3. The cold model includes a riser, cyclone separator, down comer and siphon.

The cold flow model is made of plexiglas which makes it easy to visualize the fluidization inside the riser, cyclone and downcomer. Pressure tapping points are connected to 15 points throughout the reactor as shown in Figure 4.3(a). The pressure tapping points are connected to the pressure acquisition system with pressure sensors which are connected to the computer program to record pressure readings.

The cold model is wrapped with copper wire to avoid electrostatic effects that make the particles stick to the wall. The bed and the siphon is fluidized by compressed air.

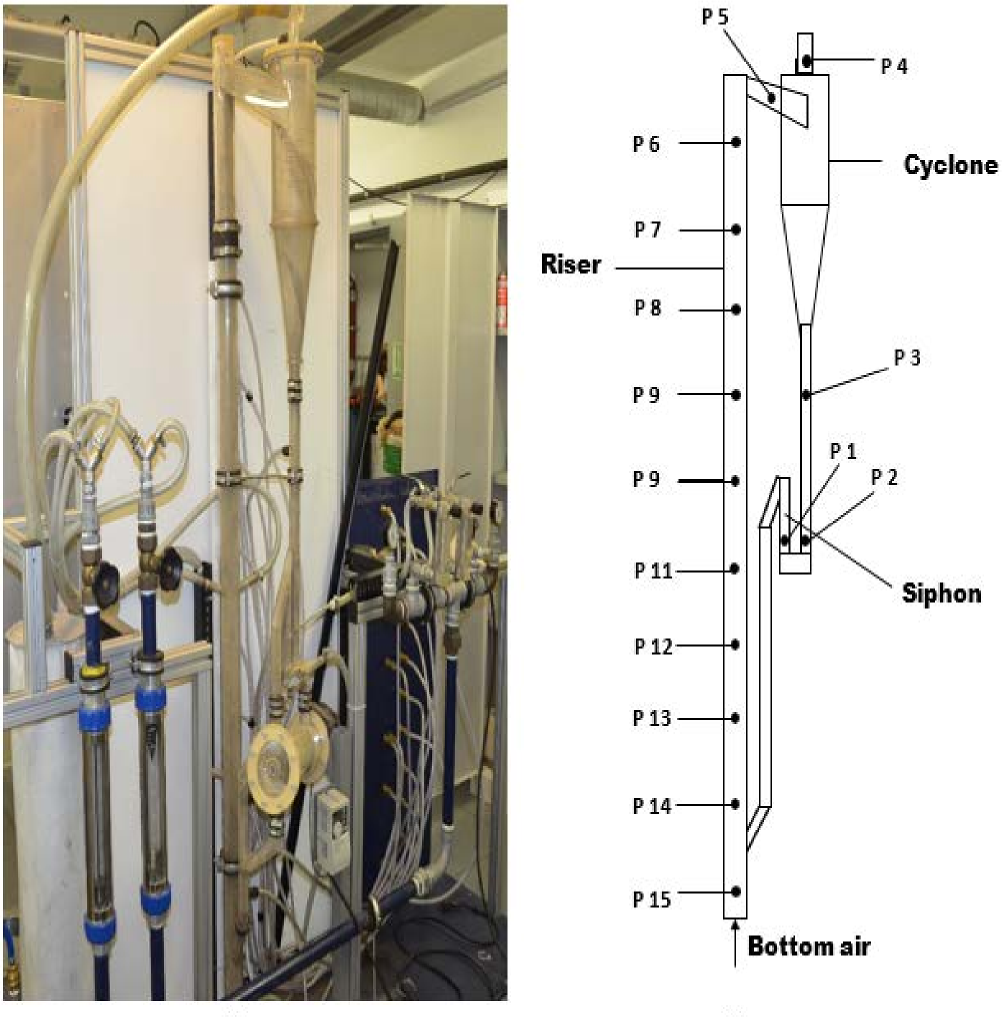

(a) (b)

Figure 4.3: (a) CFB cold model with airflow regulation and pressure measurement arrangements (b) pressure tapping points

The location of the pressure tapping points are shown in Figure 4.3 (b) and their corresponding heights are shown in Table 4.1.

The pressure measurements are performed via hoses connecting all the tapping points to a pressure gauge. The device can take readings of 24 pressure tapping points to measure absolute or differential pressure. The pressure sensors are grouped according to their capacity of pressure measurement range. 14 sensors measure in the range of 0-100 mbar, 6 in the range of 0-250 mbar and 4 of them in the range of 0-500 mbar. The tapping points with possible higher pressure are connected to the high-pressure range sensors.

The pressure measurements are recorded as a function of various airflow rates. For each of the air flow rate, the pressure data are registered for 2-3 minutes and averaged.

Table 4.1: Height of the pressure tapping points

Labelling	Position	Height [mm]
P1	Siphon top	665
P2	Siphon top	665
P3	Down comer	1010
P4	Exit Filter	1685
P5	Intersection Precipator	1595
P6	Reactor	1535
P7	Reactor	1330
P8	Reactor	1170
P9	Reactor	1005
P10	Reactor	850
P11	Reactor	610
P12	Reactor	525
P13	Reactor	365
P14	Reactor	205
P15	Reactor	40
P16	Siphon bottom	425
P17	Siphon bottom	205

Pressure reduction valves regulate the ambient airflow and the flow is measured by rotameters shown in Figure 4.4. The characteristics of the rotameters used in the experiments are presented in Table 4.2.

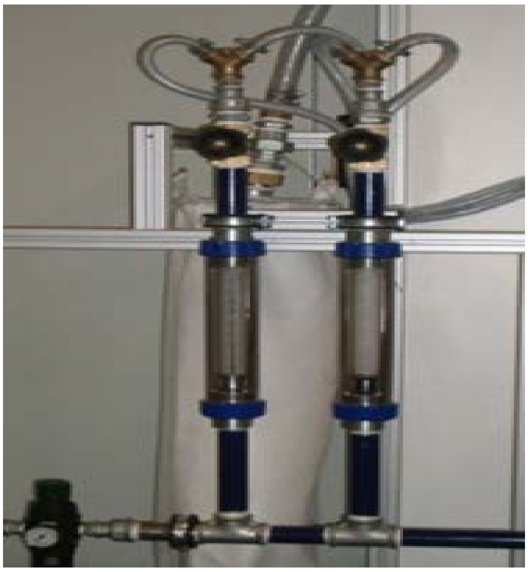

Figure 4.4: Rotameters for primary and secondary fluidization

Table 4.2: Flow range of rotameters

Air feed	Range of volume flow [Nm^3/h]
Primary fluidization	5.5 - 55
Secondary fluidization	2.9 – 29
Siphon fluidization	0.2 - 2

The bed is fluidized with constant rate of airflow and the steady state circulation of bed materials is achieved. The particle height in the down comer is measured. Then the fluidization of the siphon is suddenly interrupted. The particle level at the downcomer increases over a given interval of time. The particle height is measured again. The difference of initial and final height gives the height of the accumulated particles. Knowing the cross sectional area, the amount of solid circulation during the given time interval is determined.

The experimental results of pressure drops and solid circulation rates are used to validate a CPFD model. The experimental and computational solid circulation rates as a function of air flow are presented in Figure 4.5.

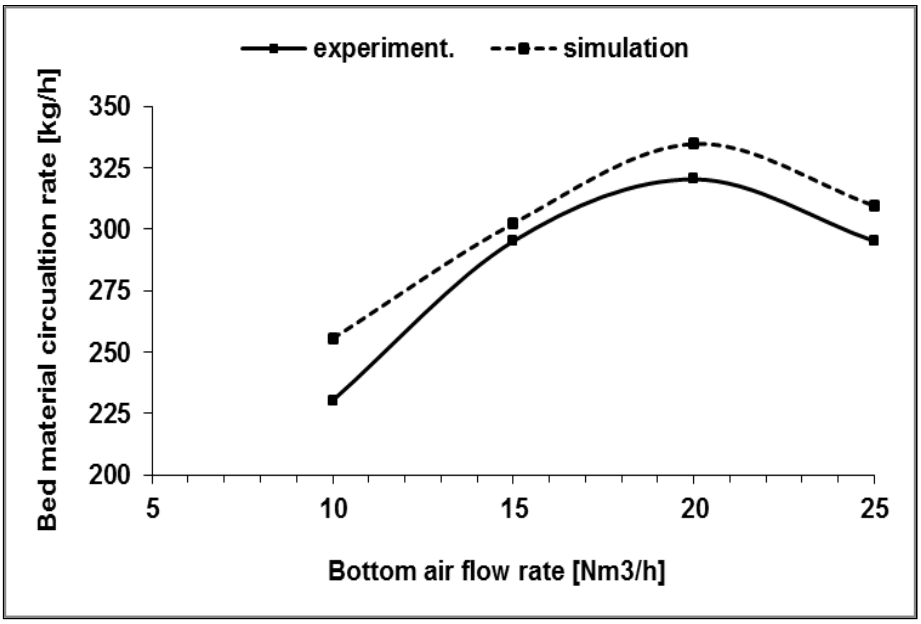

Figure 4.5: Experimental and computational solid circulation rate

The solid circulation rate is highest at gas flow rate of 20 Nm^3/h. The computational and experimental results agree well to each other. The deviation between the results are 2% to 10%. The CPFD model is then used to investigate various fluid dynamic properties of the bed.

The primary airflow is introduced while maintaining a constant bottom air feed rate of 15 Nm^3/h. The primary air feed rate is 5 Nm^3/h. The primary air feed position is varied from the height of 200 mm to 1200 mm from the bottom of the riser with an interval of 200 mm. For every primary air feed position, the total air feed rate in the simulation is constant and 20 Nm^3/h which is the sum of bottom and primary air flow. The total air feed of 20 Nm^3/h is used because the highest circulation rate is achieved at this flow rate as presented in Figure 4.5. Solid circulation rate as a function of the primary air feed position is shown in Figure 4.6. The solid circulation rate is decreasing with increase in the height of primary air feed position.

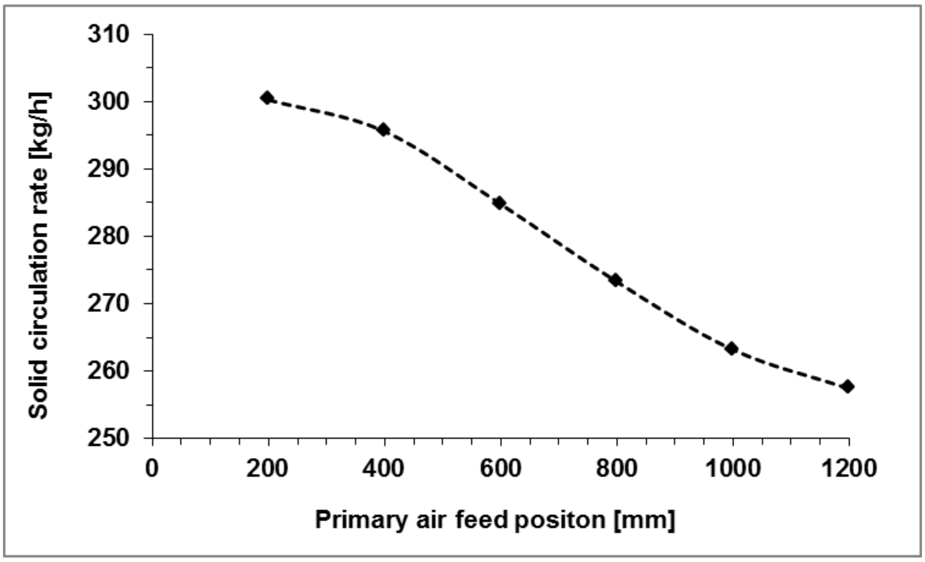

Figure 4.6: Solid circulation rate vs Primary air feed position

The highest solid circulation rate is achieved when the ratio of primary air feed position to the total height of the reactor is 0.125.

Chapter 5

Mathematical Model

There are generally two directions in Computational Fluid Dynamics (CFD) modeling of two-phase gas-particle flow. One of them uses Eulerian continuum governing equations for both gas and particle phases [62]. The second one uses Lagrangian description for the particle phase and an Eulerian continuum description for the gas phase [16]. Sections 5.1 and 5.2 give a short description of each of the modeling approaches.

5.1 Euler-Euler method

The Euler-Euler method treats the continuous fluid and dispersed solid as interpenetrating continua. The fluid and solid are treated as primary and secondary phases respectively. The two phases interact with each other by momentum exchange. The model solves a set of conservation equations (e.g. continuity and momentum) for the primary and secondary phases. The secondary phase is differentiated by the solid particle diameter. Each group of particles with a unique diameter is regarded as a separate phase. A single pressure is shared by all the phases. A short description of the method is given in this chapter [63]. The continuity equation for the secondary phase is given by Equation 5.1.

$$\frac{\partial}{\partial t}(\alpha_s\rho_s) + \nabla\cdot(\alpha_s\rho_s\vec{u}_{\boldsymbol{s}}) = \dot{m}_{gs} \tag{5.1}$$

Where $\dot{m}_{gs}$ is the mass transfer rate, for example due to chemical reaction or evaporation. The granular phase momentum equation is expressed by:

$$\begin{aligned}\frac{\partial}{\partial t}(\alpha_s\rho_s\vec{u}_s) &+ \nabla\cdot(\alpha_s\rho_s\vec{u}_s\vec{u}_s)\\ &= -\alpha_s\nabla P_g + \nabla\tau_s + \sum_{s=1}^{n}\left(\vec{R}_{gs} + \dot{m}_{gs}\vec{u}_{gs}\right) + \vec{F}_s\end{aligned} \tag{5.2}$$

In the equation, P_g is the fluid pressure, τ_s is solid stress and $\vec{R}_{gs}$ is the phase interaction term. Since a volume occupied by one phase can not be occupied by another phase, the concept of volume fraction is introduced. The sum of volume fraction of phases equals to one.

$$\alpha_s + \alpha_g = 1 \tag{5.3}$$

where, α_s in this equation represents the sum of the volume fraction of all possible solid phases whereas α_g is gas phase volume fraction.

The effects of particle-particle interactions are counted for using Kinetic Theory of Granular Flow (KTGF). The KTGF approach was widely accepted as an essential constitutive model for particle flow [64]. The KTGF approach introduces the concept of granular temperature (solid fluctuating energy) of particles. Solid pressure and viscosity are determined by considering the energy dissipation due to particle-particle collision and introducing the concept of the coefficient of restitution [65, 66]. The kinetic energy of particles due to their fluctuating velocity is measured as granular temperature. The granular temperature is proportional to the kinetic energy of the random motion of the particles and is defined as:

$$\theta_s = \frac{1}{3}\langle \vec{C}_s \vec{C}_s \rangle \tag{5.4}$$

where $\vec{C}_s = \vec{u}_s - \vec{v}_s$ is fluctuating velocity of particle and $\vec{v}_s$ is average particle velocity.

The granular temperature is determined by solving the transport equation, which describes the variation of particle velocity fluctuations. The transport equation is given by:

$$\begin{aligned}\frac{3}{2}\left[\frac{\partial(\alpha_s\rho_s\theta_s)}{\partial t} + \nabla\cdot(\alpha_s\rho_s\vec{u}_s\theta_s)\right] \\ = \bar{\tau}_s : \nabla\vec{u}_s + \nabla\cdot(K_{\theta s}\nabla\theta_s) - \gamma_s + \Phi_{lm} + \Phi_{gs}\end{aligned} \tag{5.5}$$

In the equation above $\bar{\tau}_s : \nabla\vec{u}_s$ is the production of granular temperature by the solid stress,$\nabla\cdot(K_{\theta s}\nabla\theta_s)$is diffusion of granular temperature, $K_{\theta s}$ is granulartemperature conductivity, γ_s is dissipation due to particle-particle collision and $\Phi_{lm} + \Phi_{gs}$ is the exchange term.

More constitutive equations are needed to account for interphase interaction presented in the moment conservation equation for granular flow (Equation 5.2). Solid stress $\nabla\tau_s$ accounts for interactions within the particle phase. The solid stress term is derived from the kinetic theory of granular flow and is expressed as:

$$\tau_s = -P_s\bar{I} + 2\alpha_s\mu_s\bar{S} + \alpha_s\left(\lambda_s - \frac{2}{3}\mu_s\right)\nabla\cdot\vec{u}_s\bar{I} \tag{5.6}$$

where

$\vec{S} = \frac{1}{2}(\nabla\vec{u}_s + (\nabla\vec{u}_s)^T)$ = Strain rate

P_s = Solid pressure

λ_s, μ_s = Solid bulk and shear viscosity

Solid pressure is the pressure exerted on the containing wall due to the presence of particles. This is the measure of the momentum transfer due to motion of the particles and collisions. Different models for the solid pressure proposed by different authors are summarized below:

Lun et al.:

$$P_s = \alpha_s\rho_s\theta_s + 2\rho_s\theta_s(1+e_s)\alpha_s^2 g_{os} \tag{5.7}$$

where $\alpha_s\rho_s\theta_s$is kinetic contribution and $2\rho_s\theta_s(1+e_s)\alpha_s^2 g_{os}$ is collisional contribution.

Syamlal et al.:

$$P_s = 2\rho_s\theta_s(1+e_s)\alpha_s^2 g_{os} \tag{5.8}$$

The equation contains only collisional contributions.

Ma and Ahmadi:

$$P_s = \alpha_s\rho_s\theta_s[(1+\alpha_s g_{os})] + \frac{1}{2}(1+e_s)(1-e_s+2\mu_{fr})] \tag{5.9}$$

μ_{fr} is frictional viscosity and e_s is coefficient of restitution. In the models, $g_{0s}(\alpha_s)$ is radial distribution function described as a correction factor that modifies the probability of collision close to packing limit. The expression for the radial distribution function in the Syamlal model is:

$$g_{0s}(\alpha_s) = \frac{1}{1-\alpha_s} + \frac{3\alpha_s}{2(1-\alpha_s)^2} \tag{5.10}$$

Solid shear viscosity arises due to translational (kinetic) motion and collisional interaction of particles

$$\mu_s = \mu_{s,coll} + \mu_{s,kin} \tag{5.11}$$

The collisional contribution to the shear viscosity is given by Lun et al. and adopted by all the other models:

$$\mu_{s,coll} = \frac{8}{5}\alpha_s^2\rho_s d_s g_{os}\eta\left(\frac{\theta_s}{\pi}\right)^{1/2} \tag{5.12}$$

The kinetic term of the shear viscosity is given by the models developed by Syamlal and Gidaspow :

Syamlal:

$$\mu_{s,coll} = \frac{\alpha_s\rho_s d_s(\theta_s\pi)^{1/2}}{12(2-\eta)}\left[1+\frac{8}{5}\eta(3\eta-2)\alpha_s g_{os}\right] \tag{5.13}$$

Gidaspow:

$$\mu_{s,coll} = \frac{5\rho_s d_s(\theta_s\pi)^{1/2}}{96\eta g_{os}}\left[1+\frac{8}{5}\eta\alpha_s g_{os}\right] \tag{5.14}$$

The bulk viscosity accounts for particle resistance to expansion and compression, which is given by Lun et al.:

$$\lambda_s = \frac{8}{3}\alpha_s^2\rho_s d_s g_{os}\eta\left(\frac{\theta_s}{\pi}\right)^{1/2} \tag{5.15}$$

where d_s particle diameter.

In the regime of maximum packing (0.63 in ANSYS Fluent) which is also known as frictional packing, the frictional stresses become important. The particles at this stage do not collide but rub against each other. Therefore, the momentum transfer occurs through friction. The granular flow becomes incompressible. The packing limit is the maximum limit of granular volume fraction in a bed. The frictional stresses are determined from soil mechanics [67]:

$$\mu_{s,frict} = \frac{P_s\, sin\varphi}{2\sqrt{I_2}} \tag{5.16}$$

The effective frictional viscosity in the granular phase is determined from the maximum of the frictional and shear viscosities.

$$\mu_s = max\left[\mu_{s,coll} + \mu_{s,kin}, \mu_{frict}\right] \tag{5.17}$$

Interaction between phases is based on forces on a single particle corrected for effects such as concentration, clustering particles shape and mass transfer effects. The sum of all forces vanishes:

$$\sum_{s=1}^{n}\left(\vec{R}_{gs}+\dot{m}_{gs}\vec{u}_{gs}\right)=0 \tag{5.18}$$

Drag is a force caused by relative motion between phases.

$$\sum_{l=1}^{n}\Big(K_{ls}(\vec{u}_{l}-\vec{u}_{s}))+K_{gs}\left(\vec{u}_{g}-\vec{u}_{s}\right)\Big)=0 \tag{5.19}$$

Where $K_{gs}$is the drag between fluid and particles and K_{ls} is drag between particles. The general form of drag term is given by:

$$K_{gs}=\alpha_{s}\rho_{s}\frac{f_{drag}}{\tau_{gs}} \tag{5.20}$$

With particle relaxation time

$$\tau_{gs}=\frac{\rho_{s}d_{s}^{2}}{18\mu_{g}} \tag{5.21}$$

The Syamlal & O’Brien drag model is used in granular flows to compute the drag forces between fluid and solid phases.

$$k_{gs}=\frac{4}{3}C_{D}\left(\frac{\alpha_{s}\alpha_{g}\rho_{g|v_{slip}|}}{d_{s}}\right)\frac{Re_{s}}{v_{r}^{3}} \tag{5.22}$$

$$C_{D}=\left(0.63+\frac{4.8}{\sqrt{Re/v_{r}}}\right)^{2} \tag{5.23}$$

$$v_{r}=0.5\Big(A-0.06Re+\sqrt{(0.006Re)^{2}+0.12Re(2B-A)+A^{2}}\Big) \tag{5.24}$$

$$A=\alpha_{g}^{4.41}$$
$$B=\begin{cases}0.8\alpha_{g}^{1.28}\ for\ \alpha_{g}\leq 0.85\\ 0.8\alpha_{g}^{2.65}\ for\ \alpha_{g}\geq 0.85\end{cases} \tag{5.25}$$

Experiments were performed with glass particles and air as fluidizing gas in the cold model of bubbling fluidized bed. The glass particles have about the same size and density as the bed materials used in the dual fluidized biomass gasification reactor. A series of simulations were run using different drag models to find which model gives the best results. The drag and granular viscosity is calculated using Syamlal-O'Brien model. Frictional viscosity is calculated using Schaeffer model whereas granular bulk viscosity is kept constant. Radial distribution function and solid pressure are calculated using the Ma-Ahmadi model. The validated CFD model is used to study the flow behavior in the cold model of bubbling fluidized bed gasification reactor.

The model is used to investigate Glicksman's dimensionless scaling parameters. A 'reference' bed and a 'scaled' bed are simulated using Glicksman's full set and simplified sets of dimensionless scaling parameters. In the bubbling fluidized bed gasification reactor, olivine or silica sand particles are used as bed materials with the high temperature steam as fluidizing gas. Down scaling, the reactor using Glicksman's rule to use ambient air needs particles with density of about 12000 kg/m^3. Consequently, it is difficult to verify Glicksman's scaling rule experimentally for the biomass gasification reactor. This difficulties are easy to overcome with the CFD model and simulated results in this work.

The CFD model is also used to verify Glicksman's viscous limit set of dimensionless parameters. The viscous limit set is more flexible for scaling of gasification reactors.

A reference bed with lower particle Reynold's number is scaled down applying Glicksman's viscous limit sets of dimensionless parameters. The fluid dynamic properties such as pressure fluctuations and solid volume fraction fluctuations are monitored at a number of equally distributed locations in the beds. The pressure fluctuation and the solid volume fraction fluctuations are similar for the reference and scaled beds at particle Reynolds number up to 15. The solid volume fraction fluctuation of the two beds as a function of time is presented in Figure 5.1. The figure shows the similarity in particle flow between the two beds.

The results confirm that fluidized beds with smaller particle size and operating at low gas velocities can be scaled by using the viscous limit set of dimensionless parameters.

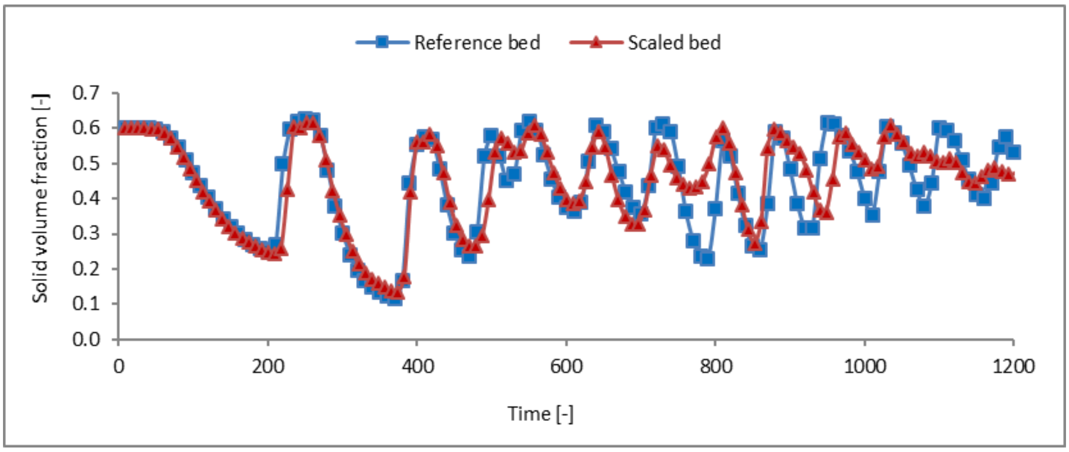

Figure 5.1: Solid volume fraction fluctuation with time. Dimensionless bed height = 0.5, dimensionless bed width = 0.75, dimensionless gas velocity = 2.

5.2 Eulerian-Lagrangian method

CPFD (Computational Particle Fluid Dynamic) model is one of the latest developments using Eulerian-Lagrangian method. The method blends discrete Lagrangian and continuum Eulerian method [68]. The CPFD method solves fluid and particle conservation equations in three dimensions treating the fluid field as Eulerian and the particles as Lagrangian. There is a strong coupling between the fluid and the particles.

Thermal and chemistry calculations are available for the fluid and particle phases coupled for energy and reaction purposes. The CPFD is incorporated with Multiphase-Particle in cell (MP-PIC). In the MP-PIC method, conservation equations are solved for the continuous phase. For solid phase a transport equation is solved for the particle distribution function [16, 69]. The short description of gas and particle equations are given in this chapter referring the literature references [56, 70, 71] and more details are found in th.

Gas phase mass conservation is given by Equation 5.26 [70]:

$$\frac{\partial(\alpha_g \rho_g)}{\partial t} + \nabla \cdot (\alpha_g \rho_g \vec{u}_g) = \delta \dot{m}_p \tag{5.26}$$

where α_g is gas volume fraction (void fraction), ρ_g is gas density, $\vec{u}_g$ is the gas velocity, $\delta \dot{m}_p$ is the gas mass production rate per volume from the particle-gas chemistry . The momentum conservation equation for the gas phase is given as:

$$\frac{\partial(\alpha_g \rho_g \vec{u}_g)}{\partial t} + \nabla \cdot (\alpha_g \rho_g \vec{u}_g \vec{u}_g) = -\alpha_g \nabla p_g + \vec{F} + \alpha_g \rho_g \vec{g} + \nabla \cdot (\alpha_g \tau_g) \tag{5.27}$$

where p_g is gas pressure, $\vec{g}$ is acceleration due to gravity, $\vec{F}$ is the rate of interphase momentum transfer per unit volume and τ_g is gas stress tensor. The constitutive equation for the gas stress is given in index notation as:

$$\tau_{g,ij} = \mu\left(\frac{\partial u_i}{\partial x_j} + \frac{\partial u_j}{\partial x_i}\right) - \frac{2}{3}\mu\delta_{ij}\frac{\partial u_k}{\partial x_k} \tag{5.28}$$

where μ is shear viscosity. The shear viscosity is the sum of laminar shear viscosity and turbulence viscosity based on the Smagorinsky turbulence model. In the model, large eddies are directly calculated. The unresolved sub grid turbulence is modeled by using eddy viscosity. The turbulence viscosity is given as:

$$\mu_t = C\rho_g\Delta^2\sqrt{\left(\frac{\partial u_i}{\partial x_j} + \frac{\partial u_j}{\partial x_i}\right)^2} \tag{5.29}$$

where C is sub grid eddy coefficient and known as Smagorinsky coefficient. In the simulation of bubbling fluidized bed gasification reactor the coefficient is used with a constant value of 0.01. The sub grid length is given by the relation, $\Delta = (\Delta x\Delta y\Delta z)^{1/3}$. The energy equation for the gas phase is given by:

$$\begin{aligned}\frac{\partial(\alpha_g\rho_g h_g)}{\partial t} &+ \nabla\cdot(\alpha_g\rho_g h_g\vec{u}_g) \\ &= -\alpha_g\left(\frac{\partial p}{\partial t} + \vec{u}_g\cdot\nabla p_g\right) + \emptyset - \nabla\cdot(\alpha_g\vec{q}) + \dot{Q} \\ &+ S_h + \dot{q_D}\end{aligned} \tag{5.30}$$

where h_g is the gas enthalpy, $\emptyset$ is viscous dissipation, $\dot{Q}$ is energy source per unit volume, S_h is conservative energy exchange from solid phase to the gas phase, $\vec{q}$ is gas heat flux and $\dot{q_D}$ is enthalpy diffusion term. The gas heat flux $\vec{q}$ is calculated as:

$$\vec{q} = -\lambda_g\nabla T_g \tag{5.31}$$

where λ_g is gas thermal conductivity. The thermal conductivity is the sum of molecular conductivity and eddy conductivity. The eddy conductivity is determined from Prandtl number as:

$$Pr_t = \frac{C_p\mu_t}{\lambda_t} \tag{5.32}$$

The standard value of Prandtl number used in the model is 0.9.

The enthalpy diffusion term is given by:

$$\dot{q}_D = \sum_{i=1}^{N_i} \nabla\left(h_i \alpha_g \rho_g D \nabla Y_{g,i}\right) \tag{5.33}$$

The mixture enthalpy is related to the species enthalpy by:

$$h_g = \sum_{i=1}^{N_i} Y_{g,i}\, h_i \tag{5.34}$$

where the summation is all gas species N_i. The species enthalpy depends on the gas temperature and expressed by:

$$h_i = \int_{T_0}^{T_1} C_{p,i} dT\, \Delta h_{f,i} \tag{5.35}$$

where $\Delta h_{f,i}$ is the heat of formation at reference temperature T_0 and $C_{p,i}$ is the specific heat at constant pressure for species i. The equation of state for an ideal gas is used to determine the pressure:

$$p = \rho_g R T_g \sum_{i}^{N_i} \frac{Y_{g,i}}{MW_i} \tag{5.36}$$

where R is universal gas constant and MW_i is the molecular weight of the species i.

A gas can be a mixture of different species. A transport equation is solved for each of the gas species and the total fluid phase properties are calculated from the species mass fraction. The transport equation for the individual species in the gas phase is given by:

$$\begin{aligned} \frac{\partial\left(\alpha_g \rho_g Y_{g,i}\right)}{\partial t} &+ \boldsymbol{\nabla}\left(D \alpha_g \rho_g Y_{g,i} \vec{u}_g\right) \\ &= -\nabla \cdot \left(\rho_g D \alpha_g \nabla Y_{g,i}\right) + \delta \dot{m}_{\,i,chem} \end{aligned} \tag{5.37}$$

$Y_{g,i}$ is the mass fraction of each gas species and $\delta \dot{m}_{\,i,chem}$ is the net production rate of species due to gas phase chemical reactions. D is the turbulent mass diffusion rate which is related to viscosity by Schmidt number. The default value of Schmidt number is 0.9 in this work.

$$\frac{\mu_g}{\rho_g D} = Sc \tag{5.38}$$

MP-PIC method calculates the particle phase dynamics using the particle distribution function (PDF), f_s. A transport equation is solved for the PDF. The transport equation for f_s is given by [72]:

$$\frac{df_s}{dt} + \frac{\partial(f_s\vec{u}_s)}{dx} + \frac{\partial\left(f_s\vec{A}_s\right)}{du} = \frac{f_D - f}{\tau_D} \tag{5.39}$$

where $\vec{A}_s$ is the particle acceleration and is given by:

$$\vec{A}_s = \frac{d\vec{u}_s}{dt} = D_s\left(\vec{u}_g - \vec{u}_s\right) - \frac{1}{\rho_s}\nabla p_g + \vec{g} - \frac{1}{\alpha_s\rho_s}\nabla\tau_s + \vec{g} + \vec{F}_s \tag{5.40}$$

In the equation above, $\vec{F}_s$ is the particle friction per unit mass whereas D_s is the drag function. The drag function depends on the particle size, velocity, position and time as shown in Equation 5.41. The particle size is expressed as particle radius instead of diameter. Wen-Yu drag model is used in the CPFD model. Although, the Syamlal & O'Brien model is used in the CFD model in this work, there was no possibility of using the same drag model in CPFD simulation due to the restrictions in the CPFD solver Barracuda VR 14.1. The Syamlal & O'Brien model is not included in Barracuda and the solver does not allow the users to define the model.

$$D_s = C_D\frac{3}{8}\frac{\rho_g}{\rho_s}\frac{\left|\vec{u}_g - \vec{u}_s\right|\alpha_g^{-2.65}}{r_s} \tag{5.41}$$

where

$$C_D = \begin{cases} \frac{24}{Re}(1 + 0.15Re^{0.687})Re < 1000 \\ 0.44 \quad Re \geq 1000 \end{cases} \tag{5.42}$$

$$Re = \frac{\rho_g\left|\vec{u}_g - \vec{u}_s\right|r_s}{\mu_g} \quad and\ r_s = \left(\frac{m}{\frac{4}{3}\pi\rho_s}\right)^{1/3} \tag{5.43}$$

The particle movement equation is:

$$\frac{d\vec{x}_s}{dt} = \vec{u}_s \tag{5.44}$$

The particle volume fraction is defined by f_s is:

$$\alpha_s = \iiint f_s \frac{m_s}{\rho_s} dm_s d\vec{u}_s dT_s \tag{5.45}$$

The sum of volume fraction of the gas and solid phase is unity:

$$\alpha_g + \alpha_s = 1.0 \tag{5.46}$$

The interphase momentum transfer included in the Equation 5.27 is:

$$\vec{F} = \iiint f_s \left\{ m_s \left[D_s\left(\vec{u}_g - \vec{u}_s\right) - \frac{\nabla \mathrm{p}}{\rho_s} \right] + \vec{u}_s \frac{dm_s}{dt} \right\} dm_s d\vec{u}_s dT_s \tag{5.47}$$

It is assumed that no heat is released inside the particles during the chemical reaction. This means that the temperature is constant inside the particles when they undergo chemical reaction. Moreover, it is assumed that the heat released at the particle surface does not affect the surface energy balance significantly.

The relation for the particle to gas phase conservative energy exchange equation is:

$$\begin{aligned} S_h = \iiint f_s \Bigg\{ & m_s \left[D_s\left(\vec{u}_g - \vec{u}_s\right)^2 - C_v \frac{dT_s}{dt} \right] \\ & - \frac{dm_s}{dt} \left[h_s + \frac{1}{2}\left(\vec{u}_s - \vec{u}_g\right)^2 \right] \Bigg\} dm_s d\vec{u}_s dT_s \end{aligned} \tag{5.48}$$

where h_s is particle enthalpy. The lumped heat equation for the particle is:

$$C_v \frac{dT_s}{dt} = \frac{1}{m_s} \frac{\lambda_g Nu_{g,s}}{2r_s} A_s\left(T_g - T_s\right) \tag{5.49}$$

where C_v is specific heat of the particle, $Nu_{g,s}$ is Nusselt number for heat transfer from gas to the particle. T_s and T_g is the particle and gas temperature respectively.

The chemistry in the CPFD model is specified as mass action kinetics. The chemical reactions are described by stoichiometric equations including the corresponding reaction kinetics. The reaction kinetics is expressed as:

$$k = A_0 m_s^{c_1} T^{c2} \exp\left(-\frac{E}{RT} + E_0 \right) \tag{5.50}$$

where A_0 is the pre-exponential factor, E is activation energy, E_0 is activation energy constant, R is universal gas constant, c is a constant. T is the temperature of a particle gas film.

The film temperature is an average of the particle temperature and the bulk gas temperature. The particle concentration is given by mass per volume and $m_s = \rho_s \alpha_s$.

The CPFD model is validated against experimental data obtained from bubbling and circulating fluidized bed reactors. The model is used to simulate bubbling and circulating fluidized bed reactors. One of the studies in CFB includes the effect of gas velocity on the bed material outflow at varying bed material feed rates.

The particle out-flow rate vs gas velocity is shown in Figure 5.2. At a given feed rate of particles, the particle outflow rate increases with the gas velocity up to the dimensionless gas velocity about 35. The dimensionless velocity is the ratio of gas velocity to minimum fluidization velocity and when exceeding 35, the solid outflow rate is constant.

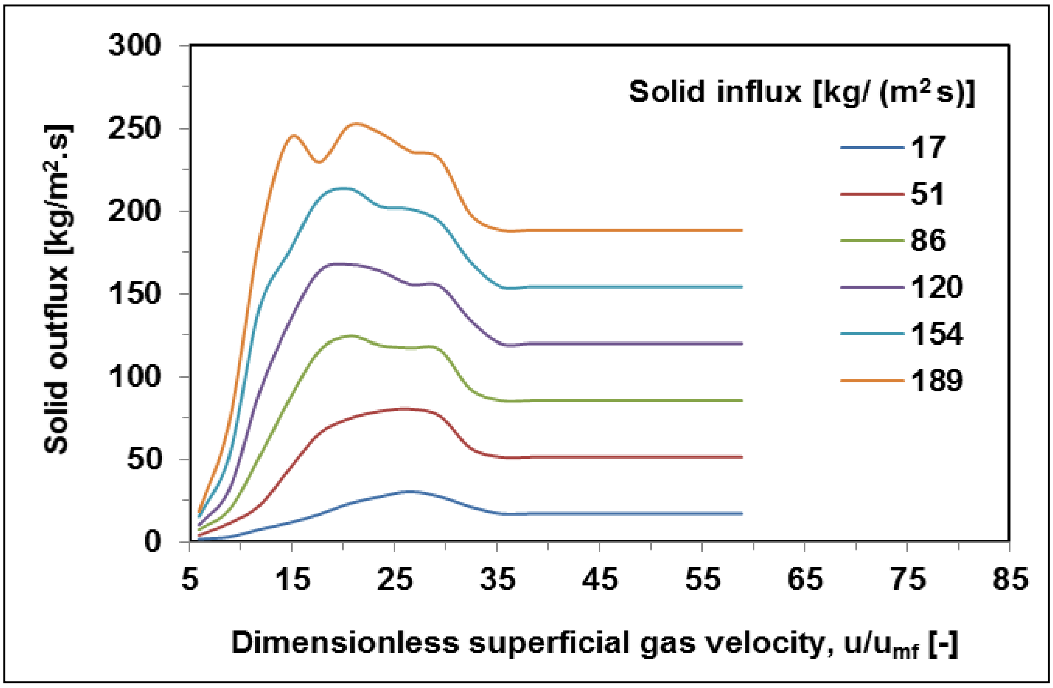

Figure 5.2: Solid out-flux vs gas velocity

The velocity range that corresponds to the unsteady outflow rate of the particles should be avoided in order to have a steady state circulation of bed materials. The fluctuation of the bed material outflow is related to the variation of average pressure drop along the height of the riser at that range of gas velocities. The details of the simulation results regarding the flow regime in the CFB combustion reactor and the parameters effected by the flow regimes are discussed in Paper I.

Chapter 6

Biomass properties and reaction kinetics

Characterization of biomass and experimental determination of gasification reaction kinetics are beyond the scope of the present work. The data used in this study are from published literature. The biomass is wood (birch). The wood is considered as a virtual element with the elemental analysis given in Table 6.1 [73].

Table 6.1: Elemental analysis of wood

Elements	Wt.%
Carbon, C	48.6
Hydrogen, H	5.6
Oxygen, O	45.6
Nitrogen, N	0.2

The table includes only the major components of the wood and the rest of the components are neglected in order to simplify the reactions in the model. Volatilization of biomass is the first step of the gasification process and it is an important step in the conversion process. In this process most of the wood particles (91 wt.%) are converted to volatiles and tars and the rest is char particles. The composition of the volatiles is presented in Table 6.2. The composition of volatiles given here is in dry basis.

Table 6.2: Composition of volatiles [73]

Components	Wt. fraction
Methane (CH_4)	0.1213
Carbon monoxide (CO)	0.6856
Carbon-dioxide (CO_2)	0.1764
Hydrogen (H_2)	0.0167

The gasifier in the dual fluidized bed gasification system is operated at a temperature between 800 °C and 900 °C using pure steam as the gasifying agent.

The conversion reactions in the gasification process are heterogeneous and homogeneous.

The heterogeneous reactions are the reactions of char particles with gasifying agents and the homogeneous reactions are the reactions in gas phase changing the composition of product gas. The major of the heterogeneous and homogeneous reactions occurring between char particles and gases are shown in Table 6.3.

Table 6.3: Major gasification reaction and heat of reaction [73]

Reactions	Chemical equations	$\Delta H_{R,\,850}$ [kJ/mol]
Steam gasification	$C + H_2O \leftrightarrow CO + H_2$	+118.5
Boudouard	$C + CO_2 \leftrightarrow 2CO$	+159.5
Methanation	$C + 2H_2 \leftrightarrow CH_4$	-87.5
Water gas shift	$CO + H_2O \leftrightarrow CO_2 + H_2$	-33.6
Methane reforming	$CH_4 + H_2O \leftrightarrow CO + 3H_2$	+225.5

The heat of reactions shows that the overall gasification process is endothermic and requires external heat supply.

The reactions with the corresponding reaction kinetics are presented in Table 6.4. The higher heating value of the wood is 17.07 MJ/kg [73]. The model evaluates the reaction kinetics with changing particle size of the biomass and bed material.

Table 6.4: Reaction kinetic used in the model

Reactions	Reaction rate	Reference
Steam gasification 1.C(s) + H_2O → CO + H_2 2.CO + H_2 → C(s) + H_2O	$r_1 = 1.272 m_s T \exp\left(\frac{-22645}{T}\right) [H_2O]$ $r_2 = 1.04410^{-4} m_s T^2 \exp\left(\frac{-6319}{T} - 17{,}29\right) [H_2][CO]$	[74]
Carbon dioxide gasification 3. C(s) + CO_2 → 2 CO 4. 2CO → C(s)+ CO_2	$r_3 = 1.272 m_s T \exp\left(\frac{-22645}{T}\right) [CO_2]$ $r_4 = 1.04410^{-4} m_s T^2 \exp\left(\frac{-2363}{T} - 20{,}92\right) [CO]^2$	[74]
Methanation 5. 0.5C(s) + H_2 → 0.5 CH_4 6. 0.5 CH_4 → 0.5C(s) + H_2	$r_5 = 1.36810^{-3} m_s T \exp\left(\frac{-8078}{T} - 7{,}087\right) [H_2]$ $r_6 = 0.151 m_s T^{0{,}5} \exp\left(\frac{-13578}{T} - 0{,}372\right) [CH_4]^{0{,}5}$	[71]
Water gas shift reaction 7. CO + H_2O → CO_2 + H_2 8. CO_2 + H_2 → CO + H_2O	$r_7 = 7.6810^{10} T \exp\left(\frac{-36640}{T}\right) [CO]^{0{,}5}[H_2O]$ $r_8 = 6.410^{9} T \exp\left(\frac{-39260}{T}\right) [H_2]^{0{,}5}[CO_2]$	[71]
Methane-reforming 9. CH_4 + H_2O → CO + $3H_2$ 10. CO + $3H_2$ → CH_4 + H_2O	$r_9 = 3.1005 \exp\left(\frac{-15000}{T}\right) [CH_4][H_2O]$ $r_{10} = 3.55610^{-3} T \exp\left(\frac{-15000}{T}\right) [CO][H_2]^2$	[57]

The CPFD model is used to simulate the reactions and reaction kinetics in a bubbling fluidized biomass gasification reactor. The model prediction of the producer gas composition have good agreements with the corresponding composition in the biomass gasification plant in Güssing, Austria. The comparison of predicted producer gas components is given in Table 6.5.

Table 6.5. Comparison between predicted producer gas composition and plant data

Components	Predicted vol%	Plant data vol%
Hydrogen (H_2)	34	32
Carbon monoxide (CO)	25	25
Carbon dioxide (CO_2)	22	22
Methane	10	12

The simulated results of the producer gas composition is presented in Figure 6.1. The reactions in the gasifier are unsteady at the first 20 seconds of the simulation. The change in mole fraction of methane with time is insignificant.

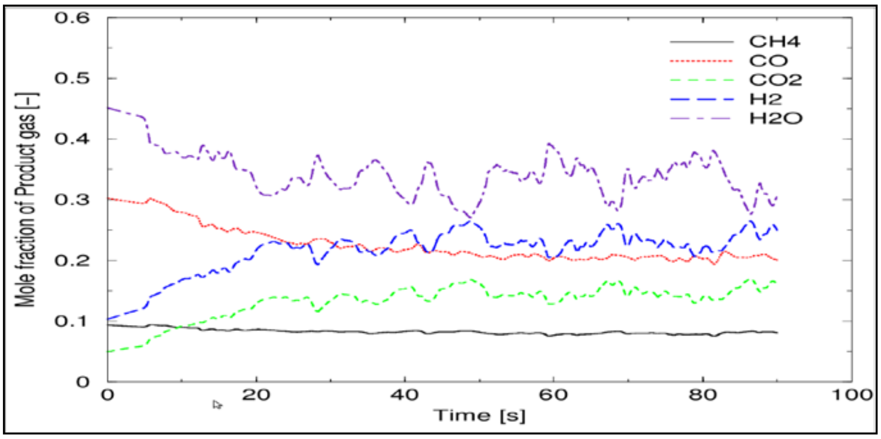

Figure 6.1: Mole fraction of producer gas at the top of the reactor

This indicates the slow reaction kinetics of methanation and methane reforming. Initially the fraction of CO is high and is decreasing with time whereas the fraction of CO_2 is increasing with time. More and more CO undergoes the water- gas shift reaction. The high percent of water indicates the low conversion rate of the steam. Increase in steam conversion rate is one of the major challenges in the steam gasification process in the dual fluidized gasification reactors.

In order to investigate the contribution of each of the reactions presented in Table 6.4, the reactions are simulated separately. The volume% of producer gases representing sequence 1 is the product of the volatilization and steam gasification reactions. The reaction sequence 2 presents the volume% of the producer gases when only volatilization and carbon dioxide gasification are considered. The volume fraction of tar remains unchanged because the tar conversion is not considered in this work.

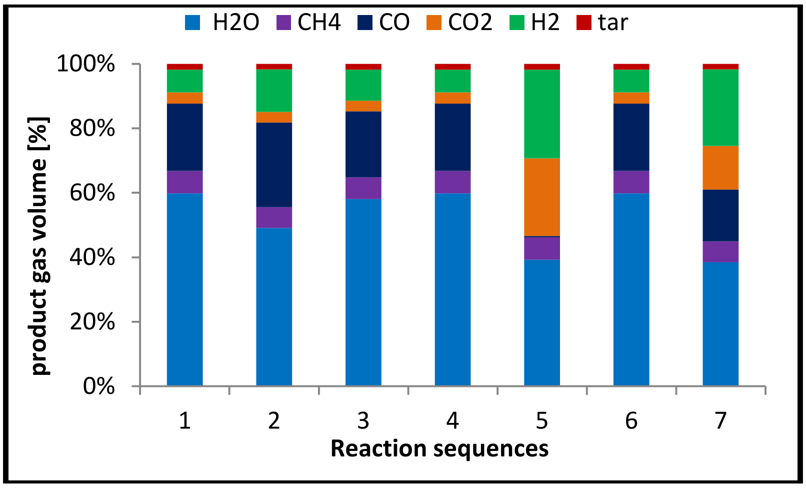

Figure 6.2: volume percent of major gas composition

The water volume fraction is highest for all the cases. This shows that non of the reactions have high steam conversion rate.

The feed of steam is much higher than necessary for the gasification reaction. The high amount of steam is used as the fluidizing agent. The lowest steam to biomass ratio that is tested is 0.2. Lower ratios will not give sufficient fluidization velocities. Based on this, the simulation results show that the steam to biomass ratio of 0.2 is optimal for the performance of the reactor. The producer gas energy as a function of steam to biomass ratio is presented in Figure 6.3.

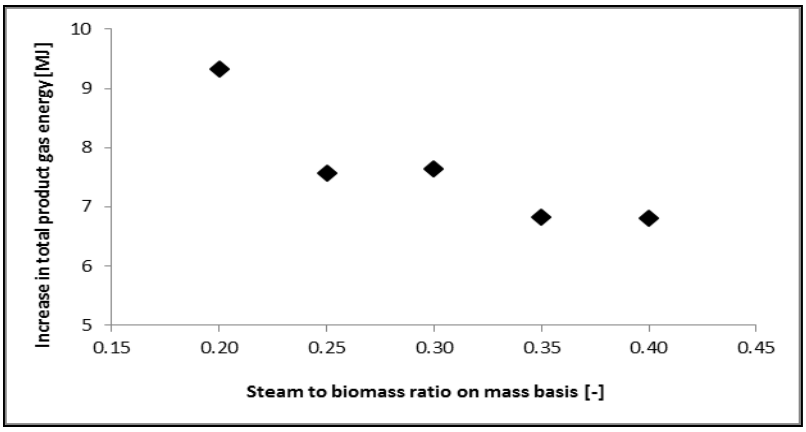

Figure 6.3: Increase in producer gas total energy as a function of steam to biomass ratio

Another important parameter effecting the performance of the gasification reactor is the particle size of biomass and bed material. Increasing particle size of biomass and bed material effect negatively on the performance of the gasification reactor. Figure 6.4 presents the volume fraction of wood particles. The volume fractions are presented from the left to right in order of increasing particle sizes. The particle size distribution is presented in Table 6.5.The wood particles are concentrated at the middle of the reactor above the surface of the dense bed.

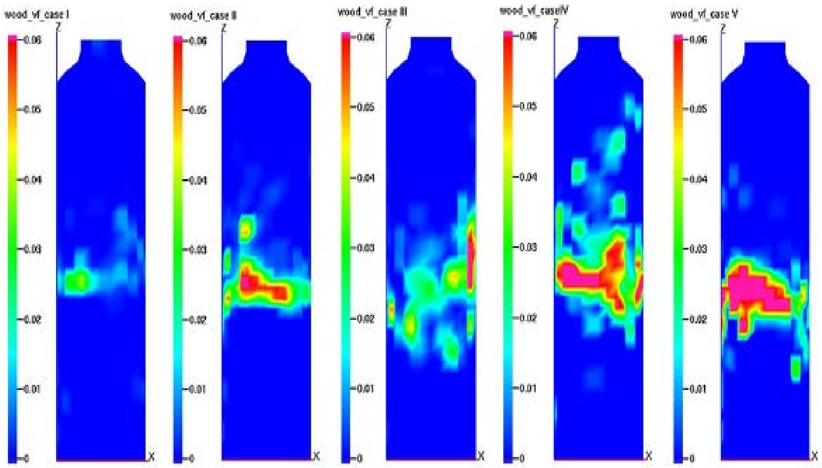

Figure 6.4: Volume faction of wood particle at simulation time of 300s. Simulation cases 1 to 5 from left to right

The larger the biomass particles are, the more is the biomass accumulated in the reactor which indicates lower conversion rate. The performance of the reactor with increasing particle sizes of biomass feed is investigated using the total HHV of producer gas coming out of the reactor. The producer gas HHV for the corresponding simulation cases are presented in Figure 6.6.

Table 6.6: Biomass particle size

Case	Biomass size [mm]
1	1-5
2	6-10
3	11-15
4	16-20
5	21-25

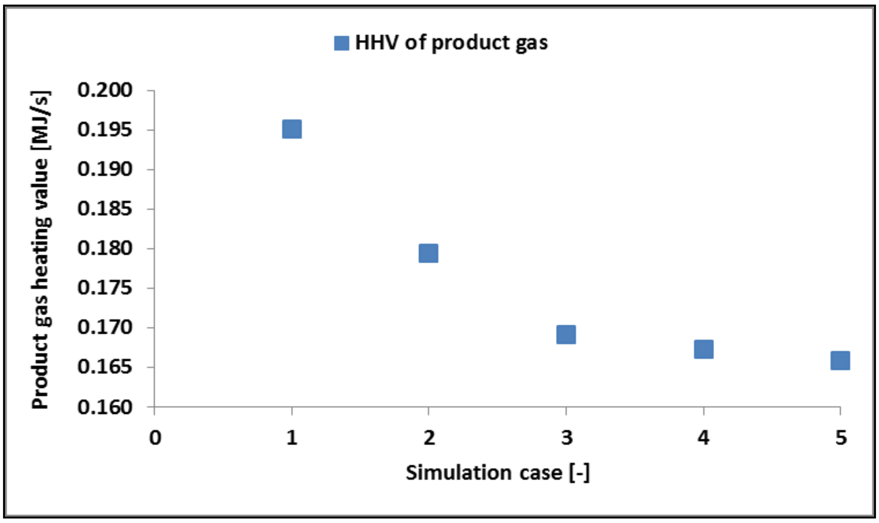

Figure 6.5: HHV of producer gas leaving the reactor

The HHV of the producer gas is decreasing with increasing particle size of biomass.

Chapter 7

Conclusion and future recommendations

The current work represents a set of experimental and computational results on optimization of fluid dynamics and thermo-chemical behavior in the dual fluidized gasification reactor. The results are divided into three parts. The first part is validation of the CFD and CPFD models. The models are validated against experimental data obtained by using lab-scale cold models of bubbling and circulating fluidized bed reactors. The CPFD model with gasification reactions is validated against the published data about the producer gas composition from the biomass gasification plant in Güssing, Austria. The second part is scaling of the fluidized bed gasification reactor and the computational verification of the applicability of the scaling rules. The third part of this work is computational study of parameters effecting the performance of the gasification and combustion reactors. The purpose of the study is to identify optimal parameters and flow regimes that can contribute to increase the efficiency of the gasification reactor. The details of the study and the results are explained in Chapter 7.1. In Chapter 7.2, recommended future works are summarized.

7.1 Conclusions

(Paper A) 2D computational model for the lab-scale bubbling fluidized bed reactor is developed and simulated using a commercial CFD software ANSYS Fluent. Experiments were performed in a lab-scale cold flow model of a bubbling fluidized bed reactor. Experimental results for minimum fluidization velocity and pressure drops across the bed height are compared with computational results. The results show good agreements. Experimental and computational minimum fluidization velocities are also compared with theoretical calculation and the results are close to each other. The validation gives the possibility of using the CFD model for simulating the bubbling fluidized bed reactors. The model is then used to simulate gas-solid flow in the reactor using high temperature steam as the fluidizing gas. The flow behavior of particles at ambient condition with air as fluidizing gas somewhat differs from the flow at high temperature conditions with steam as fluidizing gas. The minimum fluidization velocity, pressure drop and bubble behavior of 350-µm sand particles fluidized with ambient air are similar to the 500-µm olivine particles fluidized with high temperature steam.

Paper A presents the more details of the experimental and simulation procedure and results. The different flow behaviors at the ambient and the high temperature conditions indicate the need of scaling down the gasification reactors to lab-scale cold model.

(Paper B) A bubbling fluidized gasification reactor operating with high temperature steam as fluidizing gas is scaled down to a lab scale cold model operating with ambient air. The gas and particle properties and the reactor geometry are calculated using Glicksman's full and simplified sets of dimensionless scaling parameters. The calculation show that particles with density about 12000 kg/m^3 are required in the downscaled cold model. These types of particles are difficult to find on the market. To overcome this challenge, the validated CFD model is used to investigate if Glicksman's set of dimensionless scaling parameters are applicable for scaling down the bubbling fluidized bed gasification reactor. The reference reactor and down scaled reactor are simulated using ANSYS Fluent. Pressure fluctuations and solid volume fraction fluctuations are investigated. The comparison of results between the reference reactor and the downscaled reactor show good agreements. The maximum deviation of relative pressure, pressure standard deviation and average pressure drop across the bed are 2%, 8% and 1% respectively. The results indicate that the fluid dynamic similarity between two different beds can be achieved using Glicksman's full set and simplified set of scaling parameters. The details of the scaling and simulation procedures and the results are presented in Paper B.

(Paper C) Glickman's viscous limit set of dimensionless scaling parameters has a significant importance because of its flexibility with respect to particle density. The possibilities and limitation of the viscous limit set have been investigated by scaling down a bubbling fluidized bed reactor. The reference reactor and scaled reactor are simulated to compare the fluid dynamic similarities. Dimensionless pressure standard deviation, relative pressure and average pressure drop across the bed height were investigated as a function of dimensionless superficial gas velocities. The dimensionless superficial gas velocities are the ratio of gas velocity to the minimum fluidization velocity. The results indicate that the fluid dynamic similarity of the bed can be achieved for beds with particle Reynolds number up to 15. This Reynolds number is much higher than the particle Reynolds number of 4 which is the recommended limit for using the Glickman's viscous limit set of dimensionless parameters. All details of the simulations and results are presented in Paper C. The summary of the results of Paper B and Paper C are valuable for scaling any fluidized bed reactors including biomass gasification reactor for the purpose of investigating and improving the fluid dynamic properties.

(Paper D) In the next step of the project work, the CPFD model is used to simulate the reactions in the gasifier. The properties and composition of wood particles, the reaction and reaction kinetics are the data found in literature. The heterogeneous gasification reactions are steam gasification, carbon-dioxide gasification and methanation. The homogeneous gas phase reactions are water-gas shift and methane reforming. The commercial software Barracuda is used in the 3D Computational Particle Fluid Dynamic (CPFD) simulations. The results show that most of the reactions occur at the dense zone of the bed and the vicinity of the dense region of the freeboard. As the gas flows up through the freeboard region, the gas compositions becomes more and more constant. The composition of the producer gas are monitored at the top of the reactor. The volume fraction of carbon-monoxide, carbon-dioxide, hydrogen and methane are 25%, 22%, 34% and 10% respectively on dry basis. The volume fraction of CO, CO_2, H_2 and CH_4 in the producer gas in the biomass gasification plant in Güssing are 25%, 22%, 32% and 12% respectively. The good agreements between the computational and measured producer gas composition confirms that the model can be used in studies and optimization of the gasification reactor. The details of the simulations and the results of the gasification reactions are given in Paper D.

(Paper E) The work is continued by studying the influence of particle size of wood chips and bed material on the performance of the reactor. Simulations were performed increasing the particle size of the biomass while keeping the particle size of bed material constant and then increasing the particle size of bed material and keeping the size of biomass constant. The biomass particle sizes used in the reactor range from 1 mm to 25 mm and the bed material particle size range from 200 µm to 1200 µm. The mass flow rate of producer gas is monitored at different heights in the reactor. For each case, the gas leaving the top of the reactor is monitored and the volume flow and higher heating value (HHV) of the producer gases are calculated. The result shows that the volume and the HHV of producer gas decrease linearly with increasing the wood particle size up to 15 mm. The HHV of producer gas decreases from 0.195 MJ/s to 0.170MJ/s when wood particle size is increased from 1 to 15 mm. The contours of wood/char particle volume fraction shows accumulation of more wood/char particles on the top of bed confirming lower conversion rate with increasing particle size. Further increase of particle feed size above 15 mm results in a more moderate decrease in gas volume flow and HHV. Particle size of 25 mm gives HHV of about 0.166 MJ/s. When the wood particle size distribution is 6-10 mm and the bed martial size is increased gradually from 300 µm to 1200 µm, the HHV of producer gas decreases about 0.2 MJ/s to 0.125 MJ/s. The decrease is linear and more significant than the decrease observed with increasing particle size of biomass. This indicates the importance of fluid dynamics on the performance of the reactor. More details of the simulation procedures and results can be found in Paper E.

(Paper F) The gasification reactions occurring in the gasifier are studied individually in order to predict the contribution of each of the reactions and reaction kinetics on the producer gas composition. Case 1 is the volatilization of wood particles and is modeled and simulated to figure out the composition of volatiles and char particles.

Each of the gasification reaction are added one by one to investigate their contribution to producer gas composition.

The gasification reaction added are steam gasification (Case2), carbon-dioxide gasification (Case3), methanation (Case 4), water gas shift reaction (Case 5) and methane reforming (Case 6). Simulation parameters such as biomass and bed material feed rate and temperature, bottom steam feed rate and temperature, fluidization velocity and reaction temperatures are kept constant. The volume fraction of methane does not change significantly when more reactions are added and remains the same as in simulation case 1 (i.e. volatilization of wood). This shows that the methanation reaction is very slow and does not contribute significantly to the change in the composition of producer gas. Steam gasification is the main reaction contributing to formation of CO and H_2. The fraction of CO and H_2 increased significantly when simulation Case 2 is added to Case 1. The water gas shift reaction adds more H_2 and is consuming CO. These results gives the conclusion that the steam gasification and water gas shift reactions contribute more to the producer gas composition than the other three reactions. More details about the results can be found in the in paper F.

(Paper G) Heat transfer optimization is one of the major focus in the current work. The CPFD model is used to investigate the effect of various parameters on the heat transfer. The parameters used in optimization is bed material feed rate, bed material temperature, bottom steam feed rate and bottom steam feed temperature. The bed material circulation rate is increased gradually keeping other parameters constant. The optimum output is the maximum energy output from the reactor. The total energy output from the reactor as a function of increasing bed material circulation rate is monitored. Analysis of the results show that the optimum heat transfer in the gasification reactor occurs at bed material to biomass feed ratio of 25–30. A series of simulations were run by increasing the bed material feed temperature from 847℃ – 967℃. The output of the total energy from the reactor is maximum at the bed material feed temperature of about 900℃. Another series of simulations were run to investigate the effect of steam feed rate on the total energy output from the reactor. The steam feed rate is measured as steam to biomass feed ratio on mass basis. The maximum energy output occurs at low steam to biomass ratio. The results show that the higher the temperature of bottom steam the better heat transfer is obtained in the reactor. Paper G gives an overview of the investigations and analysis of the results.

(Paper H) The CFB used in dual fluidized bed gasification reactors has three air feed positions: bottom air, primary air and secondary air. Experiments were performed to validate the CPFD model and the validated model is then used for optimizing the bed material circulation rate depending on air feed positions, temperature and reaction conditions. Experiments were performed in a lab scale cold model of circulating fluidized bed. Pressure along the height of the riser and the bed material circulation rates are measured for different airflow rates at ambient conditions. A 3D CPFD model is used to simulate the CFB at the same conditions. The model predictions and the experimental measurements agree well.

The deviations are 0% to 20% for pressure data and 2% to 10% for bed material circulation. The CPFD model is used to investigate the air feed positions on bed material circulation rate.

The bed material circulation rate is maximum when the ratio of primary air feed position to the total height of the reactor is 0.125. The corresponding ratio for the secondary air feed position is 0.375. At a given feed rate the bed material circulation rate is decreasing when the air feed is split into bottom primary and secondary air. The bed material circulation rate decreases with increasing temperature and if there is reactions in the bed.

(Paper I) The CPFD model is used to identify the flow regimes in the CFB at high temperature isothermal conditions. The temperature is 1000℃. The particles used in the reactor are olivine and char particles. The combustion reaction is however not included in this study. A series of simulation have been performed to identify the various flow regimes in the reactor. Bubbling, turbulent and fast fluidization regime in the reactor and their corresponding velocities are identified. The bed inventory emptying method is used to find transport velocity. The minimum fluidization velocities, u_{mf} for olivine, char particles and a mixture of olivine and char particles are 0.06 m/s, 0.06 m/s and 0.07 m/s respectively. This indicates that u_{mf} increases when the olivine and char particles are mixed. The mixture contains 1 vol% of char particles. The void fraction of olivine, char and the mixture at minimum fluidization condition are 0.44, 0.45 and 0.52 respectively. The transport velocities of olivine, char and the mixture are 2.6 m/s, 2.6 m/s and 2.8 m/s. The transport velocity for all particles are about forty times of minimum fluidization velocity indicating that the transport velocity is dependent on minimum fluidization velocity. The average pressure drop and bed material influx and outflux are monitored for a wide range bottom feed gas velocities. The investigations are performed for the mixture of olivine and char particles. Simulations were run to investigate the average pressure drop along the height of the bed at increasing dimensionless superficial gas velocities. The dimensionless superficial gas velocity is the ratio of gas velocity to minimum fluidization velocity. The simulations were run for the solid flux rate of 17, 51, 86, 120, 154 and 189 kg/ ($m^2 \cdot s$).The average pressure drop along the bed height is monitored at dimensionless gas velocities from 9 to 58. The dimensionless gas velocity is the ratio of gas velocity to minimum fluidization velocity. The result shows that the pressure drop is fluctuating with increasing dimensionless velocity up to 35 and remains constant at the higher velocities. The solid outflux monitored at the same condition shows that the solid flux is fluctuating at the dimensionless gas velocities from 9 to 35 and becomes constant at higher velocities. The result indicates that the dimensionless velocities from 9 to 35 should be avoided in order to maintain constant supply rate of bed materials.

The bottom part of the reactor is kept in bubbling fluidization regime at the air feed rate of 10 u_{mf}. The bed material influx is also kept constant at 120 kg/($m^2 \cdot s$) which is the influx to the riser of the biomass gasification plant in Güssing.

The bed material outflow rate is increasing with increasing primary air flow rate up to 48 u_{mf} and remains constant for higher flow rates. The result shows that the total gas flow rate should be increased when the gas is fed as bottom and primary air. The bed inventory decreases with increase in primary gas flow rate. The result also show that there is not a significant effect of secondary air feed on the bed material transportation rate.

7.2 Recommendation for future work

Research and development is a continuous process. The current work is able to meet some important challenges and to answer many questions regarding improvement of the flow behavior and thermo-chemical activities in dual fluidized bed biomass gasification reactor. Although the objective of the work have been fulfilled, many other research question and challenges arose during the work.

7.2.1 Verification of the results of this work in the Güssing plant

The optimization of gasification reactor in this work is conducted using computational methods and needs verification in a real plant. Therefore, one of the most important future work could be verification of these improvements in the Güssing plant. This verification could bring the research project into the next level of improvements.

7.2.2 Simulate the whole dual fluidized bed gasification reactor

During the PhD project, the bubbling fluidized bed gasification reactor and circulating fluidized bed combustion reactors are separated and focus is given only to the gasification reactor. The flow regimes of combustion reactor has been studied and simulation of combustion reactor is started but not finished due to lack of time.

The simulation of whole reactor including gasification and combustion part could be the another important part of the future work which gives more accurate results towards the optimization process.

7.2.3 Scaling of reacting flow in fluidized bed gasification reactor

Many parameters in fluidized bed gasification reactors are not dependent on geometry factors. Some of them are bed density, gas velocity at minimum fluidization and minimum bubbling conditions [74]. The scaling of a cold flow model is well established and can be performed with more confidence using Glicksman’s dimensionless sets of scaling parameters. The chemical conversation of biomass, steam and other gas-solid components should also be considered while scaling the reactions. A scale change may influence on the mass transfer, reaction kinetics and fluid dynamics [75]. Further studies of scale dependence of the gasification reaction could be valuable for the scaling of gasification reactors from demonstration or pilot plant to the lab-scale hot models.

7.2.4 Biomass characterization and gasification reaction kinetics

All properties of biomass including proximate and ultimate analysis, used in the present work are found in literature. The reaction kinetics of the five major gasification reactions are also taken from the existing literature. In order to get more accuracy, the biomass properties and the reaction kinetics should be determined at the fluidized bed steam gasification conditions.

7.2.5 Experimental measurements in lab-scale hot model of gasification reactor and model verification

The major part of the results of current work includes the cold flow model and experimental work. The results of the work the CPFD models can be used for investigation of fluid dynamics. The only validation of the hot model is volume fraction of producer gas compositions. The future work should focus on the validation of the CFD and/or CPFD models against various thermo-chemical results from the experimental measurements in lab-scale hot model.

7.2.6 Investigate the gas composition with respect to further utilization

One of the option of utilizing the producer gas is to use it in CHP plants. One of the reason for creating this PhD project work was to investigate the way of utilizing the wood and wood waste in Telemark , Norway. The increasing rate of growth of wood have been problematic in the region because the cultivated land is occupied by trees more and more every year. The CHP production is turned out to be not fully feasible for the region due to lack of projects that can consume the produced heat. Therefore, the future work should focus on production of syngas for further synthesis processes that leads to the bio fuel for vehicles.

Bibliography

[1]. Hofbauer, H. and R. Rauch, Stoichiometric water consumption of steam gasification by the FICFB-gasification process, in Progress in Thermochemical Biomas Conversion, A.V. Bridgewater, Editor. 200, Blackwell Science Ltd. London: Innsbruck, Austria.

[2]. Feorenza, G., J. Canonaco, and G. Braccio, An advanced model for biomass steam gasification process, in 15th Europian Conference on Biomass for Energy Industry and Climate Protection. 2007: Berlin, Germany.

[3]. Aquilina, L., J.M. Matray, and J. Lancelot, 25 years after the Chernobyl power plant explosion: Management of nuclear wastes and radionuclide transfer in the environment Foreword. Applied Geochemistry, 2012. **27**(7): p. 1291-1296.

[4]. Homma, T. and K. Akimoto, Analysis of Japan's energy and environment strategy after the Fukushima nuclear plant accident. Energy Policy, 2013. **62**: p. 1216-1225.

[5]. IEA: World energy demand to grow briskly to 2030. Oil & Gas Journal, 2002. **100**(42): p. 36-38.

[6]. Agency, I.E., World Energy Outlook. 2012: Paris, France.

[7]. Bakovsky, D., et al., Status of Advanced Biofuels Demonstration Facilities in 2012, in A REPORT TO IEA BIOENERGY TASK 39. 2013, IEA.

[8]. Bridgwater, A.V., The technical and economic feasibility of biomass gasification for power generation. Fuel, 1995. **74**(5): p. 631-653.

[9]. Hofbauer, H., et al., eds. Six Year Experience with the FICB- Gasification Process. 12th European Biomass Conference ed. W. Plaz, et al. 2002: ETA Florence, Italy. 982-985.

[10]. Kirnbauer, F., J. Kotik, and H. Hofbauer. Investigations on inorganic matter in DFB biomass steam gasification plants in Gussing/Austria and Oberwart/Austria. in 19th Europian Biomass Conference and Exhibistion. 2011. Berlin, Germany.

[11]. Kehlenbeck, R., et al., Novel scaling parameter for circulating fluidized beds. AIChE Journal, 2001. **47**(3): p. 582-589.

[12]. Kunnii, D. and O. Levenspiel, Fluidization Engineering. 2 ed. 1991, USA: Butterworth-Heinemann.

[13]. Rhodes, M.J., Principles of Powder Technology. 1990, London: John Wiley & Sons Ltd.

[14]. Croxford, A.J. and M.A. Gilbertson, Pressure fluctuations in bubbling gas-fluidized beds. Chemical Engineering Science, 2011. **66**(16): p. 3569-3578.

[15]. Lin, C.-L. and M.-Y. Wey, Statistical and power spectral analysis of quality of fluidization for different particle size distributions at high temperature. Advanced Powder Technology, 2004. **15**(1): p. 79-96.

[16]. Gidaspow, D., Multiphase Flow and Fluidization Continuum and Kinetic Theory Description. 1994, Boston: Academic Press.

[17]. Wen, C. and Y. Yu, Mechanics of fluidization. Chemical Engineering Progress Symposium Series, 1966. **62**: p. 100-111.

[18]. Geldart, D., Types of gas fluidization. Powder Technology, 1973. **7**(5): p. 285-292.

[19]. Gidaspow, D., ed. Multiphase Flow and Fluidization. 1994, ACADEMIC PRESS,INC.: California.

[20]. Grace, J.R., Circulating fluidized beds. 1997, London [u.a.]: Blackie Acad. & Professional.

[21]. Golriz, M., J.R. Grace, and H.T. Bi, Circulating Fluidized Beds, in Handbook of Fluidization and Fluid-Particle System, W.C. Yang, Editor. 2003, CRC Press.

[22]. Werther, J. and B. Hirchberg, Solid Motion and Mixing, in Circulating Fluidized Beds, J.R. Grace, A.A. Avidan, and T.M. Knowlton, Editors. 1997, Blackie Academic & Professionals: London. p. 119-148.

[23]. Yang, W.C., ed. A Hand Book of Fluidization and Fluid-Particle System. 2003, MARCEL DEKKER, INC: New York.

[24]. Bi, H.T. and J.R. Grace, Effect of measurement method on the velocities used to demarcate the onset of turbulent fluidization. The Chemical Engineering Journal and the Biochemical Engineering Journal, 1995. **57**(3): p. 261-271.

[25]. Yerushalmi, J. and N.T. Cankurt, Further studies of the regimes of fluidization. Powder Technology, 1979. **24**(2): p. 187-205.

[26]. Yerushalmi, H. and C. N.T., Further studies of the regimes of fluidization Powder Technol., 1979. **24**: p. 187-205.

[27]. Bi, H.T. and J.R. Grace, Flow regime diagrams for gas-solid fluidization and upward transport. International Journal of Multiphase Flow, 1995. **21**(6): p. 1229-1236.

[28]. Smolders, K. and J. Baeyens, Gas fluidized beds operating at high velocities: a critical review of occurring regimes. Powder Technology, 2001. **119**(2–3): p. 269-291.

[29]. Kaushal, P., T. Pröll, and H. Hofbauer, Model for biomass char combustion in the riser of a dual fluidized bed gasification unit: Part II — Model validation and parameter variation. Fuel Processing Technology, 2008. **89**(7): p. 660-666.

[30]. Kaushal, P., T. Pröll, and H. Hofbauer, Model for biomass char combustion in the riser of a dual fluidized bed gasification unit: Part 1 — Model development and sensitivity analysis. Fuel Processing Technology, 2008. **89**(7): p. 651-659.

[31]. Horio, M., et al., A new similarity rule for fluidized bed scale-up. AIChE Journal, 1986. **32**(9): p. 1466-1482.

[32]. Zhang, J., et al., Adaptability verification of scaling law to solid mixing and segregation behavior in bubbling fluidized bed. Powder Technology, 2012. **228**(0): p. 206-209.

[33]. Foscolo, P.U., et al., Scaling relationships for fluidisation: the generalised particle bed model. Chemical Engineering Science, 1990. **45**(6): p. 1647-1651.

[34]. Glicksman, L.R., Scaling Relationships for Fluidized beds. Chemical Engineering Science, 1984. **39**(9): p. 1373-1379.

[35]. Glicksman, L.R., M. Hyre, and K. Woloshun, Simplified scaling relationships for fluidized beds. Powder Technology, 1993. **77**(2): p. 177-199.

[36]. van Ommen, J.R., et al., Computational validation of the scaling rules for fluidized beds. Powder Technology, 2006. **163**(1–2): p. 32-40.

[37]. Nicastro, N. and L.R. Glicksman, Experimental Verification of Scaling Relationships for Fluidized beds. Chemical Engineering Science, 1984. **39**: p. 1381-1391.

[38]. Glicksman, L.R., M. Hyre, and P.A. Farell, Dynamic Similarity in Fluidization. International Journal of Multiphase Flow, 1994. **20**: p. 331-386.

[39]. Kreuzeder, A., C. Pfeifer, and H. Hofbauer, Fluid-Dynamic Investigations in a Scaled Cold Model for a Dual Fluidized bed Biomass Steam Gasification Process: Solid Flux Measurements and Optimization of Cyclone. International Journal of Chemical Reactor Engineering, 2007. **5**.

[40]. Bridgwater, A.V., Renewable fuels and chemicals by thermal processing of biomass. Chemical Engineering Journal, 2003. **91**(2–3): p. 87-102.

[41]. Maschio, G., C. Koufopanos, and A. Lucchesi, Pyrolysis, a promising route for biomass utilization. Bioresource Technology, 1992. **42**(3): p. 219-231.

[42]. Pfeifer, C., S. Koppatz, and H. Hofbauer, Steam gasification of various feedstocks at a dual fluidised bed gasifier: Impacts of operation conditions and bed materials. Biomass Conversion and Biorefinery, 2011. **1**(1): p. 39-53.

[43]. Beenackers, A.A.C.M., Biomass gasification in moving beds, a review of European technologies. Renewable Energy, 1999. **16**(1–4): p. 1180-1186.

[44. Zainal, Z.A., et al., Experimental investigation of a downdraft biomass gasifier. Biomass and Bioenergy, 2002. **23**(4): p. 283-289.

[45]. Fercher, E., et al. Two Years Experience with the FICB-Gasification Process. in 10th European Conference and Technology Exhibition. 1998. Wurzburg.

[46]. Hofbauer, H., R. Rauch, and K. Bosch. Biomass CHP Plant Gussing - A Success Story. in Expert Meeting on Pyrolysis and Gasification of Biomass and Waste. 2002. Strasbourg, France.

[47]. Marquard-Mollenstedt, T., et al. NEW APPROACH FOR BIOMASS GASIFICATION TO HYDROGEN. in 2nd World Conference and Technology Exhibition on Biomass for Energy, Industry and Climate Protection. 2004. Rome, Italy.

[48]. Hermann, H., R. Reinhard, and B. Klaus, Biomass CHP Plant Gussing - A Success Story. International Slovak Biomass Forum, Bratislava, 2004.

[49]. Bolhàr, M. and H. Hofbauer, GASIFICATION DEMONSTRATION PLANTS IN AUSTRIA. International Slovak Biomass Forum, Bratislava, 2004.

[50]. Kreuzeder, A., C. Pfeifer, and H. Hofbauer, Fluid-Dynamic Investigations in a Scaled Cold Model for a Dual Fluidized Bed Biomass Steam Gasification Process: Solid Flux Measurements and Optimization of the Cyclone. INTERNATIONAL JOURNAL OF CHEMICAL REACTOR ENGINEERING, 2007. **5**.

[51]. Bolhàr, M. and H. Hofbauer, GASIFICATION DEMONSTRATION PLANTS IN AUSTRIA. IV. International Slovak Biomass Forum, Bratislava, 2004.

[52]. Hofbauer H., B.K., Siefer I.,Aichernig C. ,Tremmel H.,Voigtlaende K., Seam Gasification of Biomass at CHP Plant Gusing – Status of The Demonstration Plant.

[53]. Corella, J., J.M. Toledo, and G. Molina, A Review on Dual Fluidized-Bed Biomass Gasifiers. Industrial & Engineering Chemistry Research, 2007. **46**(21): p. 6831-6839.

[54]. Authier, O. and J. Lédé, The image furnace for studying thermal reactions involving solids. Application to wood pyrolysis and gasification, and vapours catalytic cracking. Fuel, (0).

[55]. Kaushal, P., T. Proll, and H. Hofbauer. Modelling and simulation of biomass fired duel fluidized bed gasifier at Gussing/Austria. in International Conference on Renewable Energies and Power Quality. 2007. Sevilla.

[56]. Snider, D.M., S.M. Clark, and P.J. O'Rourke, Eulerian–Lagrangian method for three-dimensional thermal reacting flow with application to coal gasifiers. Chemical Engineering Science, 2011. **66**(6): p. 1285-1295.

[57]. Gómez-Barea, A. and B. Leckner, Modeling of biomass gasification in fluidized bed. Progress in Energy and Combustion Science, 2010. **36**(4): p. 444-509.

[58]. Umeki, K., et al., High temperature steam-only gasification of woody biomass. Applied Energy, 2010. **87**(3): p. 791-798.

[59]. Kaushal, P., T. Pröll, and H. Hofbauer, Model development and validation: Co-combustion of residual char, gases and volatile fuels in the fast fluidized combustion chamber of a dual fluidized bed biomass gasifier. Fuel, 2007. **86**(17–18): p. 2687-2695.

[60]. Kaushal, P., T. Proll, and H. Hofbauer, Model for biomass char combustion in the riser of a dual fluidized bed gasification unit: Part II - Model validation and parameter variation. Fuel Processing Technology, 2008. **89**(7): p. 660-666.

[61]. Perera, K.K., R.K. Thapa, and B.M. Halvorsen. Simulation and optimization of steam gasification process using CPFD in Energy Production and Management in the 21st Century – The Quest for Sustainable Energy. 2014. Ekaterinburg, Russia: Wessex Institute of Technology, UK.

[62]. Batchelor, G.K., A new theory of instability of a uniform fluidized bed. Journal of fluid mechanics, 1988. **193**: p. 75-110.

[63]. Andre, B. Lecture 17 - Eulerian - Granular Model. Applied Computational Fluid Dynamics 2002-2006 [cited 2015 11.01.2015]; Available from: http://www.bakker.org

[64]. Benyahia, S., et al., Simulation of particles and gas flow behavior in the riser section of a circulating fluidized bed using the kinetic theory approach for the particulate phase. Powder Technology, 2000. **112**(1–2): p. 24-33.

[65]. Lun, C., et al., Kinetic Theories for Granular Flow:Inelasetic Particles in Coutte Flow and Slightly Inelastic Particles in a General Flow Field. Journal of fluid mechanics, 1984. **140**: p. 223.

[66]. Jenkins, J.T. and S.B. Savage, A Theory for the rapid flow of identical, smooth, nearly elastic, spherical particles. Journal of fluid mechanics, 1983. **130**: p. 187-202.

[67]. Schaeffer, D.G., Instability in the evolution equations describing incompressible granular flow. Journal of Differential Equations, 1987. **66**(1): p. 19-50.

[68]. Andrews, M.J. and P.J. O'Rourke, The multiphase particle-in-cell (MP-PIC) method for dense particulate flows. International Journal of Multiphase Flow, 1996. **22**(2): p. 379-402.

[69]. Crighton, D.G., Nonlinear waves in fluidized beds. , in Nonlinear Waves in Real Fluids, A. Kluwick, Editor. 1991, Springer. p. 83-90.

[70]. Xie, J., et al., Simulation on gasification of forestry residues in fluidized beds by Eulerian–Lagrangian approach. Bioresource Technology, 2012. **121**(0): p. 36-46.

[71]. Xie, J., et al., Eulerian–Lagrangian method for three-dimensional simulation of fluidized bed coal gasification. Advanced Powder Technology, 2013. **24**(1): p. 382-392.

[72]. Andrews, M.J. and P.J. O'Rourke, The multiphase particle-in-cell (MP-PIC) method for dense particle flow. International Journal of Multiphase Flow, 1996. **22**: p. 379-402.

[73]. Zanzi, R., K. Sjostrom, and E. Bjornbom, Rapid pyrolysis of agriculatural residues at high temperature. Biomass and Bioenergy, 2002. **23**: p. 357-366.

[74]. Matsen, J.M., Scale-up of fluidized bed processes: Principle and practice. Powder Technology, 1996. **88**(3): p. 237-244.

[75]. Rüdisüli, M., et al., Scale-up of bubbling fluidized bed reactors — A review. Powder Technology, 2012. **217**(0): p. 21-38.

Part II

Published and submitted papers

Paper A

Study of flow behavior in bubbling fluidized bed biomass gasification reactor using CFD simulation

This paper was presented in an international conference on ‘Fluidization XIV From Fundamentals to Products’. The conference was held on May 26-31, 2013 in NH Conference Center Leeuwenhorst, Noordwijkerhout, the Netherlands.

The paper is published in the conference proceedings, Fluidization XIV, pp 541-548 edited by J.A.M. Kuipers, R.F. Mudde, J.R. van Ommen and N.G. Deen and published by Engineering Conference International, Inc, New York, USA.

Engineering Conferences International

ECI Digital Archives

The 14th International Conference on Fluidization – From Fundamentals to Products

Refereed Proceedings

1-1-2013

Study of Flow Behavior in Bubbling Fluidized Bed Biomass Gasification Reactor Using CFD Simulation

Rajan Kumar Thapa
Telemark University College, Norway

Britt Margrethe Halvorsen
Telemark University College, Norway

Follow this and additional works at: http://dc.engconfintl.org/fluidization_xiv

Part of the Chemical Engineering Commons

Recommended Citation

Rajan Kumar Thapa and Britt Margrethe Halvorsen, "Study of Flow Behavior in Bubbling Fluidized Bed Biomass Gasification Reactor Using CFD Simulation" in "The 14th International Conference on Fluidization – From Fundamentals to Products", Eds, ECI Symposium Series, Volume (2013). http://dc.engconfintl.org/fluidization_xiv/69

This Article is brought to you for free and open access by the Refereed Proceedings at ECI Digital Archives. It has been accepted for inclusion in The 14th International Conference on Fluidization – From Fundamentals to Products by an authorized administrator of ECI Digital Archives. For more information, please contact franco@bepress.com.

Study of flow behavior in bubbling fluidized bed biomass gasification reactor using CFD simulation

Rajan Kumar Thapa[a], Britt Margrethe Halvorsen[a]
[a] Institute for Process, Energy and Environmental Technology
Telemark University College
Kjølnes ring 56, P.O.Box 203 , N-3901, Porsgrunn, Norway
T*: 47-99485965;F: 47-35575001; E: rajan.k.thapa@hit.no

ABSTRACT

Experiments and simulations are performed to study flow behavior in biomass gasification reactor. Glass beads of particle size 350 µm and density 2500 kg/m^3 are used for experiments and simulations. A validated CFD model is established. Using the same CFD model, simulation is performed for quartz sand of particle size 500 µm fluidized with high temperature steam which is used as bed material in the gasification reactor.

INTRODUCTION

Bubbling fluidized bed is widely used in industrial processes. It has gained increasing application due to good mixing, heat and mass transfer. Biomass gasification reactor for combined heat and power (CHP) production is one of them.

Flow behavior and fluidization properties in the gasifier are studied by considering the operating parameters such as pressure drop, minimum fluidization velocity and bubble behavior. These parameters significantly affect the efficiency of the gasifier. It is essential to study the flow behavior in the reactor in order to choose correct parameters for a given flow regime. Experimental study of the parameters in a plant operating at high temperature is difficult.

Down-scaled models are used to simplify the task. In the gasifiers, high temperature steam is used as a fluidizing gas. In the down-scaled model ambient air is used instead of the high temperature steam (1-3).

High temperature steam and ambient air has different density and viscosity. In order to consider these factors with existing scaling laws (4), the cold model requires particles with very high density and very small particle size. This kind of particles is not easily available in the market. Particles used for the experiments in downscaled cold models do not have the physical properties required by the existing downscaling laws. Therefore, computational fluid dynamics (CFD) could be a suitable solution for the study of flow behavior in the biomass gasification reactor. In order to make CFD a suitable tool for the study of flow behavior in fluidized bed gasification reactors, an established model is required. The model is established with validation against the experimental measurements.

Wach em *et al* (5) has compared simulated results for Geldart B particles with experimental data in literature. Taghpour *et al* (6) have compared modeling prediction with experimental measurements. Hamzehi *at al* (7) studied the effect of gas velocity and particle size using CFD model. Azadi (8) has used the CFD model to simulate elutriation of limestone from binary mixture of particles and compared the results with experimental measurements. Sahoo *et al* (9) has studied hydrodynamics of semi-cylindrical gas-solid fluidized bed. Reasonable agreements between computational and experimental results have been reported.

Prior to this work, CFD simulation and experimental work is performed by the authors for glass beads of mean particle size of 500 µm (10). The model prediction has good agreements with experimental measurements.

The bed material in a typical gasification reactor is quartz sand of mean particle size 500 µm and density 2500 kg/m^3 fluidized with high temperature steam (11).Theoretical minimum fluidization velocity (12) calculated for these particles is the same as the minimum fluidization velocity of glass beads of density 2500 kg/m^3 and particle size 350 µm fluidized with ambient air. Therefore, the glass particles of size 350 µm are used in the experiments in order to investigate whether the flow behaviors are similar to steam fluidized quartz sand.

Experiments are performed in a cold model of bubbling fluidized bed. The fluidizing gas is ambient air. Commercial CFD software package ANSYS/ Fluent 12.1 has been used for computational study. The computational and experimental results are in good agreements to each other. A validated CFD model is established for the particles.

Using the same CFD model, further computational study is performed for the 500µm quartz sand fluidized with a high temperature steam.

THEORETICAL CALCULATION

The mean particle size and density of the bed material are 500 µm and 2500 kg/m^3. Fluidizing gas is steam at 800^{0}C. The steam has density and viscosity about 0.29 kg/m^3 and 4.1x10^{-5} Pa·s respectively (2). A theoretical minimum fluidization velocity of the particles is calculated using equation (1) derived from Erguns equation with gravity- equals - drag balance (12). Based on this equation the minimum fluidization velocity is calculated to be 0.12 m/s.

$$u_{mf} = \frac{(\Phi \cdot d_s)^2 (\rho_s - \rho_g) \cdot g}{150 \cdot \mu} \cdot \frac{\varepsilon_{mf}^3}{1 - \varepsilon_{mf}} \tag{1}$$

The maximum gas velocity in the gasification reactor is 5u_{mf}. With this velocity, particle Reynolds's number does not exceed the value of 3. According to Glicksman's viscous limit set of dimensionless parameters, only Froude number and the ratio of minimum fluidization velocity to superficial gas velocity are important for this limit [4].

Glass beads of particle size 350 μm fluidized with ambient air give the same theoretical minimum fluidization velocity of 0.12 m/s. The objective of the preliminary theoretical calculation is to study whether the flow behavior of the gasifier fluidized with high temperature steam can be simulated in a cold flow model using 350 μm particles and air at ambient conditions.

EXPERIMENTAL SET-UP

Experiments are performed in a cold cylindrical fluidized bed with height 1.4 m and diameter 0.084 m. The pressure sensors are located along the height of the cylinder and connected to a lab-view program for data storage as shown in Figure 1.

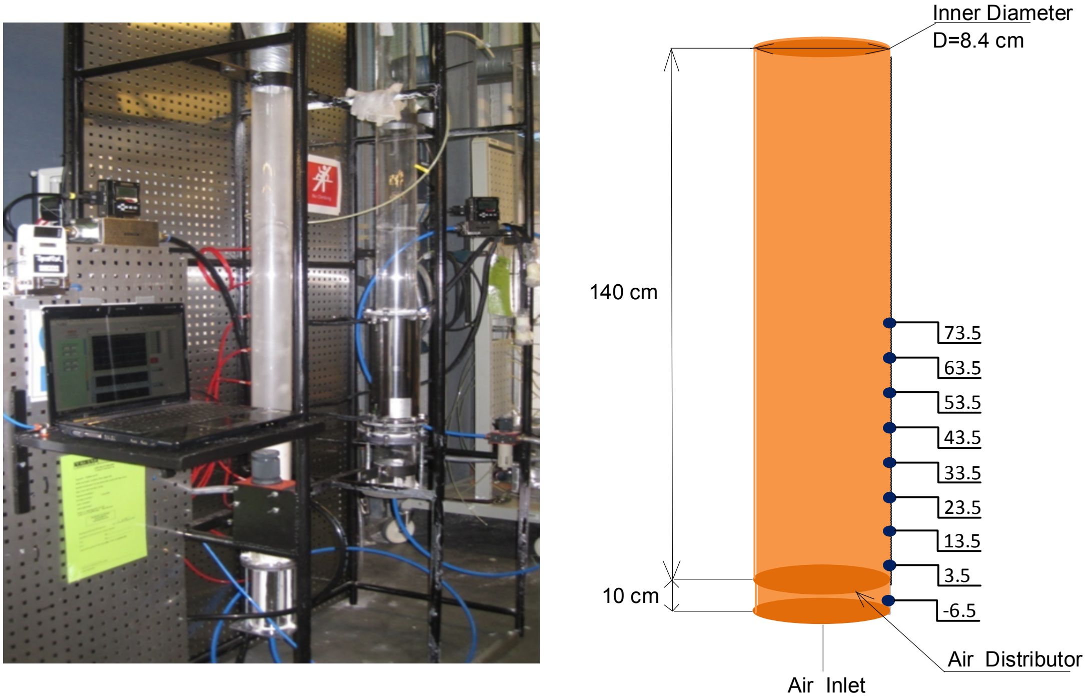

Figure 1: Experimental set-up: fluidized bed with pressure reduction valve, digital flow controller, pressure sensors.

The air flowing through an air distributor is controlled using the lab view program in order to maintain a steady flow of gas. The properties of gas and particles used in the experiments are presented in Table 1.

Table 1: Properties of gas and particles

Parameters	Value	Remarks
Particle density [kg/m^3]	2500	Glass
Gas density [kg/m^3]	1.225	Air
Gas viscosity [pa.s]	1.78x10^{-5}	Air
Particle diameter [μm]	350	Mean

COMPUTATIONAL MODEL

A multiphase Eulerian model describes the gas-solid fluidized bed consisting of two interpenetrating fluids. A non-steady state model is applied in order to consider the transient nature of a gas-solid bubbling fluidized bed system (13). Mass and momentum balance equations are solved for both the solid and gas. The kinetic theory of granular flow has been applied. The theory considers the conservation of solid fluctuation energy. Other constitutive equations for the model are applied in accordance to the models suggest by Jayarathna, S.A.(13). The parameters used in the simulations are presented in Table 3.

Table 3: Simulation parameters

Parameters	Value	Remarks
Particle density [kg/m^3]	2500	Glass
Gas density [kg/m^3]	1.225	Air
Gas density [kg/m^3]	0.29	Steam
Gas viscosity [Ps.s]	1.78x10^{-5}	Air
Gas viscosity [Ps.s]	4.1x10^{-5}	Steam
Particle diameter [µm]	350; 500	Mean
Restitution coefficient	0.9	Specified
Initial solid packing	0.6	
Maximum solid volume fraction [-]	0.63	
Bed diameter [m]	0.084	
Static bed height [m]	0.32	
Time step	1x 10^{-5}	
Number of iterations per time step	40	

In the first case, the simulations are performed with 350 µm particles with air as fluidizing gas. The particles and the gas properties are similar to those used in the experiments. In the second case, the simulations are performed with 500 µm particles and steam as fluidizing gas

RESULTS AND DISCUSSION

A series of experiments are performed for the glass beads of mean particle size 350 µm at ambient conditions. Pressure standard deviations calculated for a series of superficial air velocities are shown in Figure 3. Below minimum fluidization velocity (u_{mf}), the solids are relatively quiescent and the pressure fluctuations in the bed are negligible. The fluctuations are significant as the bed starts fluidizing.

The figure shows significant pressure fluctuations at superficial gas velocity of 0.14 m/s in the experimental measurements and 0.15 m/s in the simulation results. This indicates fluidizing condition of the bed. The experimentally measured u_{mf} is higher than the theoretically calculated value. The deviation between the experimental and theoretical value is 17%. Theoretical calculation involves mono-sized particles, whereas particles with a range of particle sizes are used in the experiments. The u_{mf} is affected by the particle size distribution. Computational pressure standard deviation indicates that the values of u_{mf} for 350 µm glass particles fluidized with air and 500 µm quartz sand fluidized with steam are about the same. The values deviate from experimental measurements by 7%.

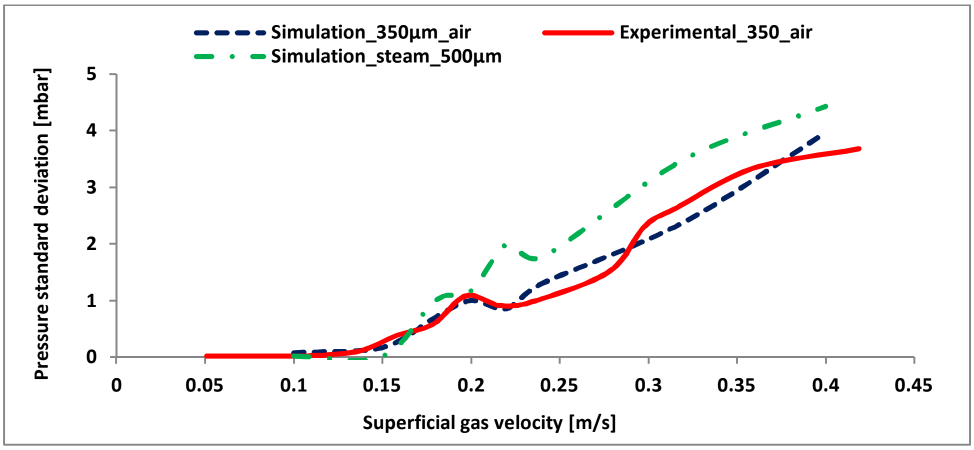

Figure 3: Comparison of pressure standard deviation as a function of superficial air velocity.

The experimental and computational pressure drops after minimum fluidizations agree well as can be seen from Figure 4. Below minimum fluidization the experimental and computational pressure drop seems to deviate significantly. This is because the model in Fluent does not consider the condition of the bed before fluidization.

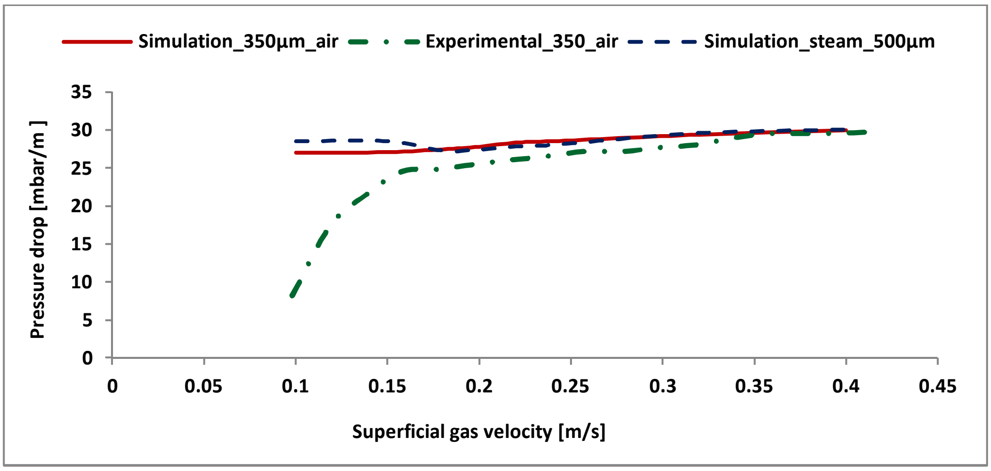

Fig.4. Comparison of experimental and computational pressure drop as a function of superficial air velocity.

Computational results of solid volume fraction fluctuations are used to study the minimum fluidization condition and the bubble behaviors. The solid volume fraction is monitored at different levels of the bed for a series of superficial gas velocities. Before the minimum fluidization condition, fluctuation of solid volume fraction is negligible as the particles do not have significant movements. At the superficial gas velocity of 0.15 m/s, the fluctuation of solid volume fraction is almost negligible for both the steam fluidized and air fluidized particles. This indicates the inception of fluidization condition. At the superficial air velocity of 0.18 m/s, significant fluctuation of the solid volume fraction indicates the bubble formation as shown in Figure 5.

The bubble activities are started at this velocity for the both air fluidized and steam fluidized particles.

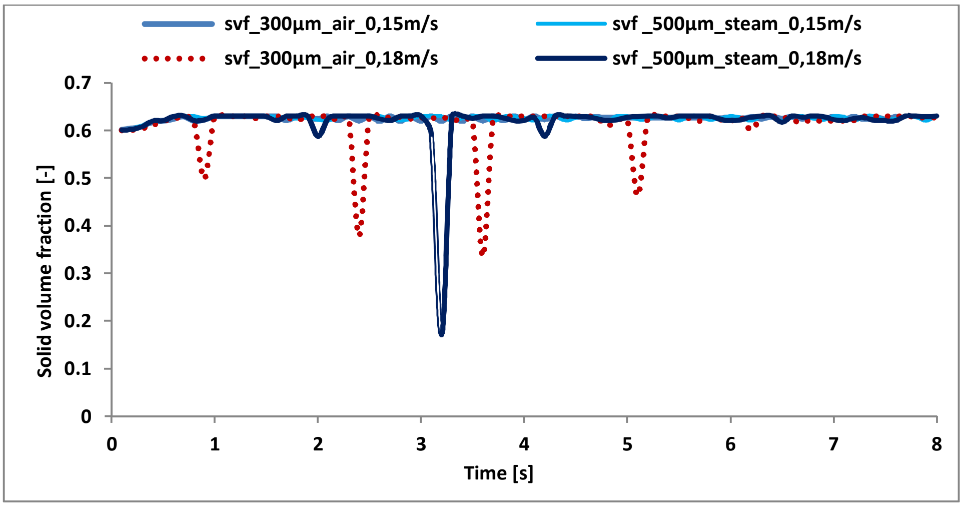

Figure 5. Comparison of simulated solid volume fraction as a function of time. Bed height 0.23m.

At the superficial gas velocity of 0.20 m/s, significant fluctuation of solid volume fraction indicates the increasing bubble frequency with superficial gas velocities as shown in Figure 6.

The figure shows the bubble frequencies for 350 µm particles fluidized with air and 500 µm particles fluidized with steam are 0.25 bubbles per second and 0.38 bubbles per second respectively.

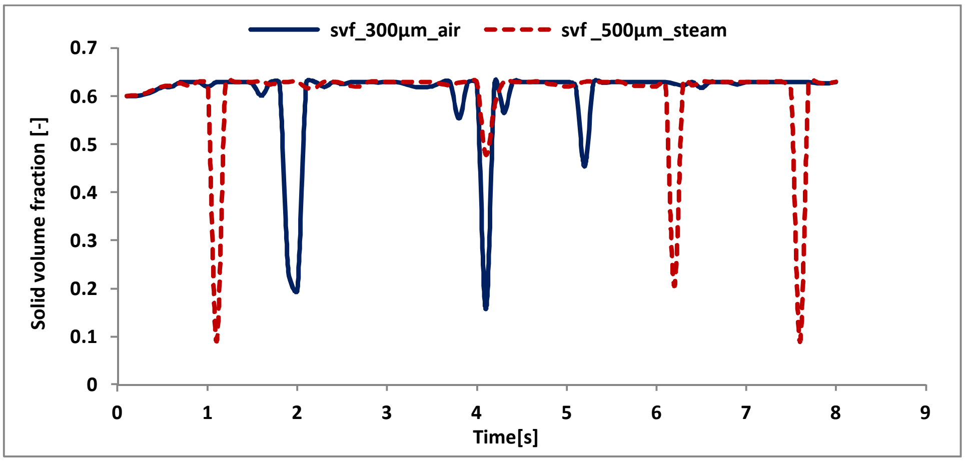

Figure 6: Comparison of solid volume fraction as a function of time.
Bed height 0.23m. Superficial gas velocity 0.20 m/s.

The bubble frequency and bubble size are compared in Figure 7 at the higher gas velocities. The contour of solid volume fraction indicates that the bubble behaviors for air fluidized and steam fluidized particles deviate at higher gas velocities.

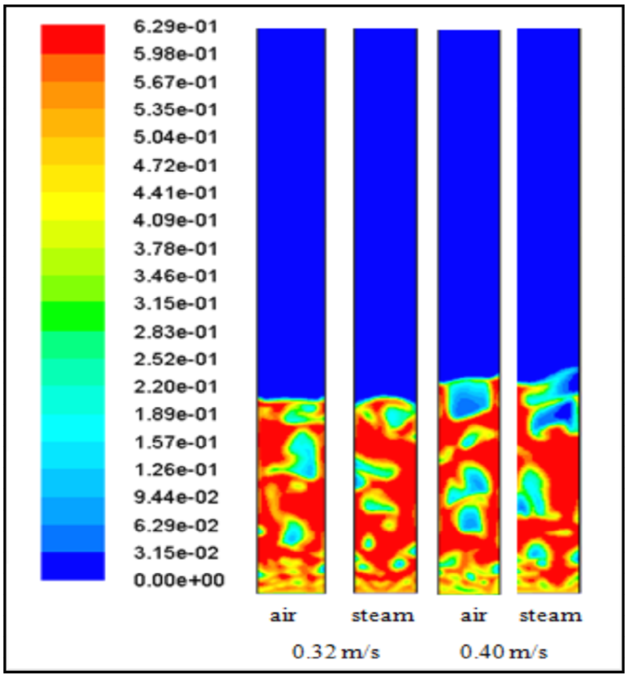

Figure 7: Comparison of contours of solid volume fraction.

CONCLUSION

A multi-phase Eulerian model is applied to predict the flow behaviors and fluidization properties of 500 µm steam fluidized quartz sand and air fluidized 350 µm glass beads. The results are compared. The minimum fluidization velocity is predicted using pressure standard deviation. Predicted u_{mf} for both the particles is the same, 0.15 m/s. Preliminary calculation of theoretical u_{mf} for the particles is 0.12 m/s. The experimental measurement of u_{mf} for air fluidized 350 µm glass beads is 0.14 m/s. The deviation of u_{mf} between experimental measurements and simulated results is 7%. The computational pressure drop across the bed height for 350 µm glass particles fluidized with air and 500 µm quartz sand fluidized with steam are about the same and the results deviate from the experimental measurements by 18% at minimum fluidization condition

Minimum bubbling velocity, bubble size and bubble frequency are studied using the fluctuation of solid volume fraction and the contours of solid volume fraction. Computational minimum bubbling velocity is 0.18 m/s for both quartz sand and glass particle. Bubble size and frequencies deviates for the two cases as the gas velocities increases from minimum fluidization velocity.

SYMBOLS AND ABBREVIATIONS

CFD	computational fluid dynamics
CHP	combined heat and power
d_s	particle diameter [m]
g	acceleration due to gravity [m/s^2]
u_{mf}	minimum fluidization velocity[m/s]
ρ_s	particle density [kg/m^3]
ρ_g	gas density [kg/m^3]

μ	gas viscosity [Pa·s]	ε_{mf}	void fraction at minimum fluidization [-]
ϕ	particle sphericity [-]		

REFERENCES

1. A. Kreuzeder et al. Fluid-dynamic investigations in a scaled cold model for a duel fluidized bed biomass gasification process: solid flux measurement and optimization of the cyclone. International Journal of Chemical Reactor Engineering, 2007. 5.
2. T. Proll et al. Cold flow model study on a dual circulating fluidized bed system for chemical looping process. Chem.Eng.Technol., 2009. 32: p. 418-424.
3. M.K. Karmakar, A.B.Datta. Hydrodynamics of duel flluidized bed gasifier. Advance Powder Technology, 2010. 21: p. 521-528.
4. L.R. Glicksman et al. Simplified Scaling Relationships for Fluidized Beds. Powder Technology, 1993
5. B.G.M. van Wachem et al. Validation of the Eulerian simulated dynamic behavior of gas-solid fluidized bed. Chemical Engineering Science, 1999. 54: p. 2141-2149.
6. F.Taghipour et al. Experimental and computational study of gas-solid fluidized bed hydrodynamics. Chemical Engineering Science, 2005. 60: p. 6857-6867.
7. M.Hamzehei et al. Studies of gas velocity and particle size effects on fluidized bed hydrodynamics with CFD modeling and experimental investigations. Journal of Mechanics, 2010. 26.
8. M. Azadi. Multifluid Eulerian modeling of limestone particles' elutriation from a binary mixture in a gas-solid fluidized bed. Journal of Industrial and Engineering Chemistry, 2011. 17: p. 229-236.
9. A.Sahoo et al. Experimental and computational study of the bed dynamics of semi-cylindrical gas-solid fluidized bed. Canadian Journal of Chemical Engineering, 2009. 87: p. 11-18.
10. R.K. Thapa and B.M. Halvorsen. Validation of the CFD model for prediction of flow behaviour in fluidized bed reactors, Advances in Fluid Mechanics IX, 2012.pp 231-239
11. M. Bolhàr-Nordenkampf et al. Scale-up of a 100kWth pilot FICFB-gasifier to a 8 MWth FICFB-gasifier demonstration plant in Güssing (Austria). 1st International Ukrainian Conference on BIOMASS FOR ENERGY, September 23-27, 2002 Kyiv, Ukraine.
12. D. Kunii and O. Levenspiel. Fluidization Engineering. Butterworth-Heinemann. second ed. 1991
13. S.Cooper, C. J. Coronella. CFD simulations of particle mixing in a binary fluidized bed. Power Technology, 2005. 151: p. 27-36.
14. S.A Jayarathna. Recommendation of a model for simulating & analysis of the influence of particle size distribution on the simulation of bubbling fluidized bed, in Department of Process, Energy and Environment. 2008, Telemark University College.Norway. p. 22-46.

Paper B

Scaling of biomass gasification reactor using CFD simulation

This paper was presented on ‘International Conference on Polygeneration strategies (IPCS)’ held on September 3rd to 5th 2013 in Vienna, Austria.

The paper is published in Proceedings of the IPCS; pp 237-246, edited by Hermann Hofbauer and Michael Fuchs and published by Vienne University of Technology. ISBN: 978-3-9502754-8-3.

Scaling of biomass gasification reactor using CFD simulation

R.K. Thapa1, C. Pfeifer[2] and B.M. Halvorsen[3]

1, 3. Department of Process Energy and Environmental Technology, Telemark University College, Norway
2. Institute of Chemical Engineering, Vienna University of Technology, Austria

Abstract

Proper scaling of fluidized bed biomass gasification reactors from laboratory scale to full scale is still a major challenge. Scaling rules based on the dimensionless group are used to accomplish the task. Glicksman's scaling rules with a set of dimensionless parameters is one of them.

Olivine of average particle size 530µm and density 2960 kg/m^3 can be used as a bed material in the gasification reactor. The particles are fluidized by steam with density about 0.29 kg/m^3. In order to get the correct density ratio in a cold model, the fluidizing gas such as helium should be used. Requirement of the enormous amount of helium gas makes it infeasible. Alternatively, heavy particles with density about 12248 kg/m^3 are required with air as a fluidizing gas. These types of particles are not available in market. Such types of difficulties make it reasonable to use Computational Fluid Dynamic (CFD) simulation.

Scaling rules based on the set of dimensionless groups are studied using CFD simulations. Glicksman's full set as well as simplified set of dimensionless groups are used. Commercial CFD software has been used in simulations. The simulations are performed for olivine particles fluidized with steam. Further simulations are performed for the scaled particles with density of 12248 kg/m^3 fluidized with air. Pressure drop, pressure standard deviation and fluctuation of solid volume fractions have been studied at different points of the bed. The results are compared and discussed.

1. Introduction:

The interest of using biomass as a primary source of energy has been increasing continuously [1]. Biomass gasification is an attractive technology for combined heat and power (CHP) production [2]. The use of fluidized bed gasification reactors in the technology is becoming more and more popular due to its increased efficiency in comparison to other conventional gasifiers. However, it is believed that the efficiency of the technology needs to be increased more in order to make the technology economically competitive in the world energy market. The efficiency of technology primarily depends on the fluid dynamic behavior inside the gasification reactor. The measurement of primary data in an operating plant is complex due to its high temperature and pressure. Therefore, the study of fluid dynamic behavior in the gasifier needs possibility of measurements in ambient conditions.

The commonly used method to study fluid dynamic behavior of an operational gasification reactor is scaling it down to lab-scale cold model. This makes it possible to take measurements in ambient pressure and temperature. The procedure of scaling requires properly developed scaling rules that can consider all scale dependent parameters. However, at the present time there are no general rules for the scaling of biomass gasification reactors found in publications. Due to the complicated phenomenon encountered in gas-solid flow, scaling of fluidized bed reactors is extremely difficult to this date[3]. Several attempts on scaling of fluidized bed reactors have been reported in literatures [4-6]. A set of non-dimensional parameters have been purposed. In order fluid dynamic behavior of the reactors to be similar, the set of dimensionless parameters should be matched. Among the purposed sets of non-dimensional parameters, most commonly used is the one purposed by Glicksman [7]. Experimental verification of Glicksman's set of dimensionless parameters for biomass gasification reactor needs particles with very high density which is not easily available. To overcome the problem, CFD simulation seems to be an appropriate solution.

The interest in this work is gasification technology based on dual fluidized bed reactors. The basic concept of the technology is to divide the reactors in two zones – gasification zone and combustion zone. The combustion zone is fluidized with air and serves as supplier of necessary heat required for the endothermic gasification reaction in the gasification zone. The gasification zone is fluidized with high temperature steam. Biomass such as wood chips is mixed with the hot bed materials. Biomass undergoes endothermic gasification reaction to produces a mixture of combustible gases. In order to increase efficiency of the technology, good mixing between biomass, bed material and fluidizing steam in the gasification zone should be ensured. This work is focused only on the study of fluid dynamics in the gasification zone. Thus, the gasification zone or bubbling fluidized bed reactor is scaled down to lab scale cold model using Glicksman scaling set of dimensionless parameters.

2. Glicksman Scaling Rules:

Glicksman derived sets of dimensionless parameters for scaling of fluidized bed reactors [7]. The set of parameters are derived non-dimensionalizing the governing equation of solid and fluid flow. The governing equations are mass and momentum balance with their boundary conditions. A number of assumptions are made while deriving the set of parameters. The fluidizing gas is assumed as an incompressible. Inter-particle forces other than mechanical forces due to collision are neglected. The inter-particle forces include forces due to particle-particle collision and electrostatic forces. The set of dimensionless parameters are given in Equation 1. They are Glicksman's full set of independent dimensionless parameters.

$$\frac{u_0^2}{gL}, \frac{\rho_s}{\rho_g}, \frac{\rho_g u_0 d_p}{\mu}, \frac{L_1}{L_2}, \frac{L}{d_p}, \phi, \textit{particle size distribution} \quad (1)$$

Two beds with identical values of the independent dimensionless parameters should have the same dimensionless dependent variables at every location of the bed. This is the requirement for the similarity between two beds. The dependent variables are dimensionless velocity, pressure, bubble size and bubble distribution. The dimensionless gas velocity is the ratio of particle velocity to superficial gas velocity throughout the bed. The dimensionless pressure is the ratio of pressure between the same dimensionless bed heights. The dimensionless bubble size is the ratio of bubble diameter to the bed length or particle size.

The two beds should have same geometrical configuration. The particle sphericity and particle size distribution also should be the same. The time and frequency should be scaled properly.

All parameter given by the full set is sometimes difficult to match in practice. Because of this reason, Glicksman et al

[8] derived a simplified set of the parameter. The set is presented in Equation 2.

$$\frac{u_0^2}{gL},\frac{\rho_s}{\rho_g},\frac{u_0}{u_{mf}},\frac{L_1}{L_2},\phi,\ particle\ \ size\ \ distribution \qquad (2)$$

As a result of simplification, the Reynolds number in the full set is changed to the ratio of excess gas velocity to minimum fluidization velocity. The ratio of bed diameter to particle diameter is omitted.

If the beds have different fluid properties, the particle diameter of the scaled bed is determined using Archimedes number. The superficial gas velocity is determined by Froude number.

The full set and inertial part of simplified sets are used in this work to scale down biomass gasification reactor. The particle and fluidizing gas properties used in scaling are presented in Tab.1. The scaling factor is 0.224.

Set	d_p [µm]	ρ_p [kg/m^3]	ρ_g [kg/m^3]	μ_g [Pa·s]
Reference bed	530	2960	0.29	$3.66\cdot10^{-5}$
Scaled bed	128	12248	1.20	$1.80\cdot10^{-5}$

Tab. 1: Properties of particles and fluidizing gases

The fluidizing gas in the gasification reactor and the lab-scale model is high temperature steam and ambient air respectively. Both of the gas has fixed density and viscosity. Since the gas density and viscosity are fixed and the particle density ratio has to be maintained, the full set and simplified set for inertial limit become similar. The viscous limit set has not been studied in this work.

The bed geometries of the gasification reactor and cold model with the scaling factor 0.224 are presented in Tab.2. The size of the gasification reactor is reduced to some extent in order to avoid very long simulation time.

Set	h [m]	H [m]	D [m]
Reference bed	3.00	0.414	0.348
Scaled bed	0.73	0.100	0.084

Tab. 2: Geometries of reactor and cold model

3. Computational model

Two approaches in modeling of gas-solid multiphase flow have been applied currently. Eulerian-Lagrangian and Eulerian-Eulerian. Eulerian-Lagrangian model tracks the motion of each particle and solve the dynamics of the fluid at the length scale smaller than the particle diameter. The modeling approach requires large computer memory and time for simulation but better computational accuracy can be expected. Eulerian-Eulerian model treats both the fluid and solid phases as interpenetrating continua and solve the dynamics averaging their equation of motion. The modeling approach is computationally less demanding [9].The Eulerian-Eulerian approach is implemented in modeling the fluid dynamics of gasification reactor in this work. The model was validated with experimental measurements in previous work of the authors [10].

In order to treat the particles as continuum, kinetic theory of granular flow is applied. The kinetic theory of granular flow considers the conservation of solid fluctuation energy [11]. 2D simulations are performed using commercial CFD software ANSYS/ Fluent 13.0.The coefficient of restitution is set to 0.9. The coefficient represents the elasticity of collision between the particles. The simulation is initialized with solid volume fraction of 0.6. In the simulations, the particles in both beds are assumed as spherical mono-sized particles. The simulation time for reference and scaled bed are 10 s and 4.9s respectively. The simulation time is different for two beds in order to adjust the scaling factor with time. It should be noted that the dimensionless time should be used for the comparison of scale dependent parameters of two beds.

The locations of the data monitors for the two beds are presented in Figure 1. In each bed, 25 equally distributed point monitors are set to record the pressure fluctuations and solid volume fraction fluctuations. The monitors are located at 0%, 25%, 75% and 100% along both the bed height and the bed width. In addition to this, line monitors are set at the bed height of 25%, 50% and 75% for the solid volume fraction fluctuation.

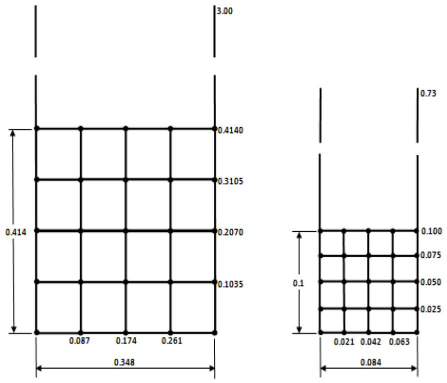

Fig.1: Location of monitors along the bed height and width.

The dimensionless groups used in simulation for reference bed and scaled bed are presented in Tab.3.

Set	u_0	$\frac{u_0^2}{gd_p}$	$\frac{u_0}{u_{mf}}$	Re_p	Re_D
Reference bed	0.258	12.82	1.0	1.08	711
	0.387	28.84	1.5	1.63	1067
	0.516	51.26	2.0	2.17	1423
	0.645	80.10	2.5	2.71	1779
	0.774	115.34	3.0	3.25	2134
	0.903	156.99	3.5	3.79	2490
	1.032	205.05	4.0	4.33	2486
Scaled bed	0.127	12.86	1.0	1.08	711
	0.1905	28.93	1.5	1.63	1067
	0.254	51.43	2.0	2.17	1422
	0.3175	80.36	2.5	2.71	1778
	0.381	115.72	3.0	3.25	2134
	0.4445	157.51	3.5	3.79	2489
	0.508	205.73	4.0	4.34	2845

Tab. 3: Gas velocities and dimensionless groups used in simulations.

3. Results and discussion

Pressure fluctuation is most commonly used in the studies of fluid dynamic behaviors in fluidized beds. In bubbling fluidized bed, the pressure fluctuations are related to the bubble motion in the bed. A single pressure point contains the global information about the bed. Many researchers has attempted to validate fluid dynamic similarity between the bubbling fluidized beds from the analysis of time series pressure data[12].

The pressure fluctuations in the bed are monitored at the equally distributed 25 points and 3 lines within the beds. The data are recorded at the dimensionless gas velocities from 1 to 4.The dimensionless gas velocity is the ratio of superficial gas velocity to minimum fluidization velocity.

The analysis of relative pressure drop at all monitoring points show similar results for the reference as well as the scaled bed. The deviations of results at various monitoring points are from 0% to 2%. The line monitors along the dimensionless bed height of 0.25, 0.5 and 0.75 also give the similar result. The relative pressure drop as a function of dimensionless gas velocities at the dimensionless bed height of 0.5 is presented in Fig.2. At the given dimensionless bed height, the deviation on relative pressure drop between two beds are almost zero at the dimensionless superficial gas velocities from 1 to 3. The result deviates slightly at the dimensionless gas velocity of 3.5 and 4.

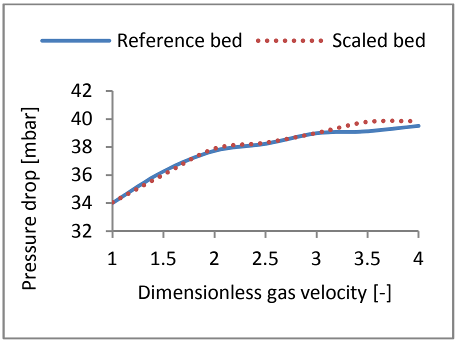

Fig.2: Pressure drop as a function of dimensionless gas velocity at the dimensionless bed height of 0.5.

The standard deviation of pressure fluctuation is indirect method to identify the fluid dynamic behavior in fluidized beds[13]. The pressure standard deviation as a function of dimensionless superficial gas velocity at the different points of the bed shows deviation between the two beds from 0% to 8%. It should be noted that the deviation of pressure fluctuation is higher than the deviation in relative pressure drop. The deviation of pressure standard deviation mainly occurs when the dimensionless superficial gas velocities become much higher. The result indicates that the pressure drop of the two beds at all locations agrees well but the pressure fluctuations deviate in some of the locations. The pressure standard deviation as a function of dimensionless gas velocity at the dimensionless bed height of 0.75 is presented in Fig.3. The deviation starts from the dimensionless gas velocity equal of 2.5.

Comparison of the results in Fig.2 and Fig.3 indicates that the deviation of pressure fluctuation is higher at dimensionless bed height of 0.75 than 0.5. Data from other monitors also indicate the deviations are almost zero at the center of the bed.

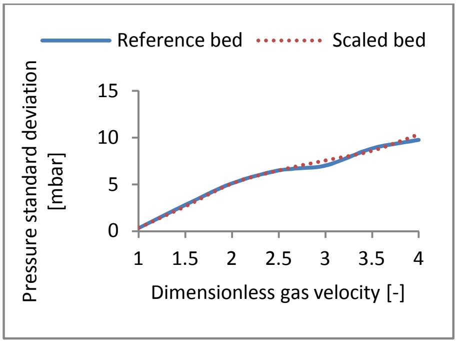

Fig. 3: Pressure standard deviation as a function of dimensionless gas velocity at the dimensionless bed height of 0.75.

The dimensionless average pressure drop as a function of dimensionless superficial gas velocities are presented in Fig.4. Dimensionless average pressure drop is the ratio of average pressure drop along the total bed height. The dimensionless pressure drop is about the same as the scaling factor of the beds and equals to 0.224.

The figure shows that the dimensionless average pressure drop is similar for the two beds. The maximum deviation of the results between two beds is about 1%. As can be seen from the figure, the dimensionless average pressure drop does not change significantly with the increasing dimensionless gas velocity.

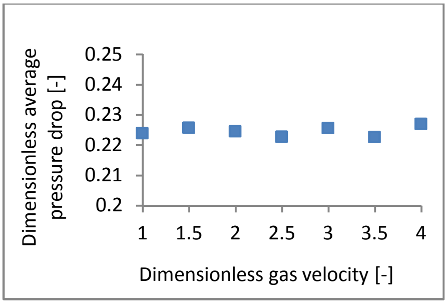

Fig.4: Dimensionless average pressure drop across the bed as a function of dimensionless gas velocity.

The pressure data taken in all monitoring points and lines shows that the pressure fluctuation between the two beds has good agreements with Glicksman's full set and simplified (inertial limit) sets of dimensionless parameters. However, agreements in pressure fluctuation between two beds are not sufficient in order to scale the reference bed to lab-scale model. Interest on the study of fluid dynamics of biomass gasification reactor is to study bubble behaviors inside the bed as well. Heat, mass transfer and mixing of the particles in the bed mainly depend on the bubble activities.

Similar to pressure fluctuations, the fluctuations of solid volume factions also studied in the same locations within the beds. The solid volume fraction fluctuation in a given point of observations gives an indication of bubble behavior only at that point[14].

The standard deviations of solid volume fraction fluctuations between two beds are recorded by all monitors. The deviations between the results of two beds are higher than that of the pressure fluctuations. In some locations of the beds the values are reached up to 30% whereas in some of the other locations the deviation is 0%. Fig.5 and Fig.6 show the fluctuation of solid volume fraction at the dimensionless bed height of 0.25 and 0.5 respectively. The deviations are higher at the lower part of the bed than upper part. The deviations show opposite tendency than that of pressure fluctuation.

The deviation of the solid volume fraction fluctuations are further investigated changing coefficient of particle restitution to 0.85 and 0.95 instead of 0.9 and series of simulations are performed. In the both case the deviations are further increased.

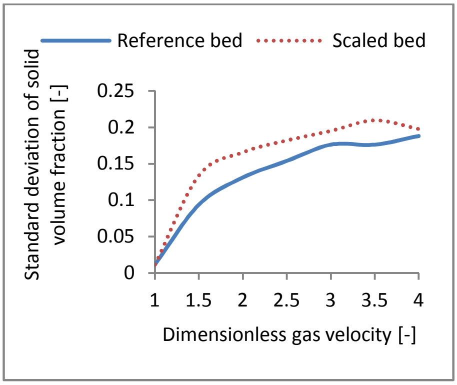

Fig.5: Standard deviation of solid volume fraction as a function of dimensionless gas velocity at the dimensionless bed height of 0.25.

A number of simulations have been performed using Gidaspow drag model instead of Syamlal O'Brien. The deviation in solid volume fraction fluctuation remains the same.

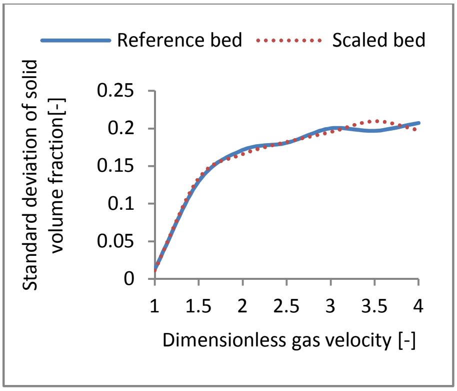

Fig.6: Standard deviation of solid volume fraction as a function of dimensionless gas velocity at the dimensionless bed height of 0.5.

The contours of solid volume fraction of the beds represent the bubble activities inside the bed. The contours of solid volume fractions are recorded at every 0.1 of dimensionless time for both of the beds. The dimensionless simulation time is the ratio of simulation time between two beds. The contours show the bubble behaviors of the two beds are similar at the beginning of the fluidization. As the dimensionless simulation time increases up to 3-4, the counters of the solid volume fractions start to deviate. Fig.7 and Fig.8 show the contours of solid volume fraction at the dimensionless simulation time 2-3 and 4-5 respectively. The dimensionless superficial gas velocity is same and equals to 2 for both of the beds.

Fig.7 shows the contour of solid volume fraction of two beds at the simulation time 2 and 3. As indicted by figure the contours show almost exact similarity between the beds. But the contours deviate as the dimensionless simulation time increased. Fig.8 shows the variation in contours at dimensionless simulation time of 4 and 5.

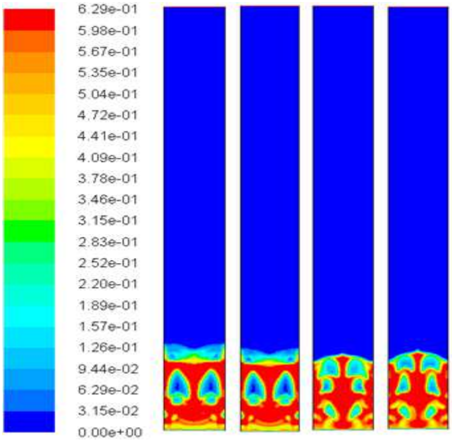

Fig.7: Contours of solid volume fraction of the bed at dimensionless gas velocities of 2. Dimensionless time =2and 3. Left reference bed right, scaled bed.

The contours of solid volume fraction show similar results for the all dimensionless gas velocities from 1 to 4.

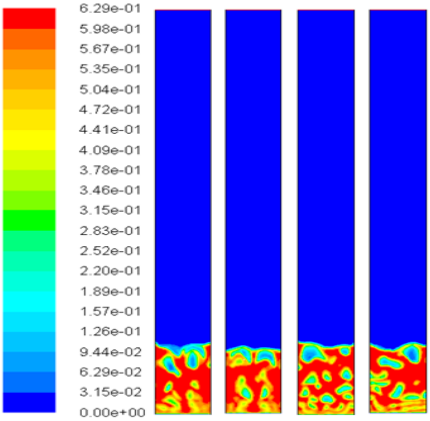

Fig.7: Contours of solid volume fraction of the bed at dimensionless gas velocities of 2. Dimensionless time =4and 5. Left reference bed right, scaled bed.

The results of the simulations indicate that the similarities in pressure fluctuation between two scaled beds do not lead to complete similarities in bubble behavior.

The pressure fluctuations give global information of the bed. There exists local factor influencing the bubble activities at a given point of the bed.

The large variation of solid volume fraction fluctuation in some of the location of two beds gives a question whether there are sufficient dimensionless parameters in Glicksman's full set in order to ensure fluid dynamic similarities between two scaled beds.

Inter-particle forces except mechanical forces due to collision are omitted while deriving the dimensionless parameters. Similarly, particle coefficient of restitution and inter-particle friction coefficient are not included. The effect of these parameters on fluid dynamic behavior of the bed should be investigated further.

4. Conclusion and Outlook

Scaling of bubbling fluidized bed biomass gasification reactor has been performed to study applicability of Glicksman’s full set and simplified (inertial limit) set of dimensionless parameters. 2D simulation has been carried out using commercial CFD software ANSYS/fluent 13.0. The scaling factor between two beds is 0.224.

Pressure fluctuations data are monitored at 25 equally distributed points along the height and width of the beds. The data are also monitored at 3 equally distributed lines along the bed height. Data from the all points and lines of the beds show good agreements. The maximum deviations of relative pressure, pressure standard deviation, and average pressure drop across the beds are 2%, 8% and 1% respectively. At some of the point in bed, the deviations are zero. The pressure fluctuation show sufficiently good agreement between the beds.

The data for solid volume fraction fluctuations are also monitored using the same monitors as in pressure fluctuation. Standard deviation of solid volume fraction fluctuation at the different points in the beds varies from 0% to 30%. The large variation of the solid volume fraction at some of the points in bed has to be investigated further. However, it should be noted that the large variation is only some of the points in the bed. Most of the location of the bed show good agreements.

The contour of solid volume fractions is similar for the beds up to dimensionless time of 3. After that, the contours deviate slightly. The tendency of variation is similar for all dimensionless gas velocities.

5. Symbols

CFD	Computational fluid dynamics
D	Bed diameter [m]
d_p	Particle diameter [m]
g	Acceleration due to gravity [m/s^2]
H	Static height of bed [m]
h	Height of reactor
L_1, L_2	Bed geometry [m]
Re	Reynolds number [-]
u_0	Excess gas velocity [m/s]
u_{mf}	Minimum fluidization velocity [m/s]
ρ_s	Particle density [kg/m^3]
ρ_g	Gas density [kg/m^3]
μ_g	Gas viscosity [Pa·s]
ϕ	Particle sphericity [-]
ε_{mf}	Void fraction at minimum fluidization [-]

6. References

[1] Kehlenbeck R, Yates J, Di Felice R, Hofbauer H and Rauch R. *Novel scaling parameter for circulating fluidized beds.* AIChE Journal, 2001. **47**(3): p. 582-589.

[2] Kreuzeder A, Pfeifer C and Hofbauer H. *Fluid-Dynamic Investigations in a Scaled Cold Model for a Dual Fluidized Bed Biomass Steam Gasification Process: Solid Flux Measurements and Optimization of the Cyclone.* International Journal of Chemical Reactor Engineering, 2007. **5**.

[3] Didwania AK and Catolica RJ. *CFD Simulation Scale-up of a Dual-Fluidized Bed Gasifier for Biomass*. in *Seventh International Conference on CFD in Minerals and Process Industries*. 2009. Melbourne, Australia.

[4] Horio M, Nonaka A, Sawa Y and Muchi I. *A new similarity rule for fluidized bed scale-up.* AIChE Journal, 1986. **32**(9): p. 1466-1482.

[5] Zhang J,Gao W,Zhao Z, Liu Z, Narukawa M, Suda T et al., *Adaptability verification of scaling law to solid mixing and segregation behavior in bubbling fluidized bed.* Powder Technology, 2012. **228**(0): p. 206-209.

[6] Foscolo PU, Di Felice R, Gibilaro LG, Pistone L and Piccolo V. *Scaling relationships for fluidisation: the generalised particle bed model.* Chemical Engineering Science, 1990. **45**(6): p. 1647-1651.

[7] Glicksman LR. *Scaling Relationships for Fluidized beds.* Chemical Engineering Science, 1984. **39**(9): p. 1373-1379.

[8] Glicksman LR, Hyre M, and Woloshun K. *Simplified scaling relationships for fluidized beds.* Powder Technology, 1993. **77**(2): p. 177-199.

[9] Mazzei L. *Eulerian modelling and computational fluid dynamics simulation of mono and polydisperse fluidized suspensions*, in *Department of Chemical Engineering* 2008, University College London: UK.

[10] Thapa RK and Halvorsen BM. *Validation of CFD model for prediction of flow behaviour in fluidized bed reactors*. in *Advances in Fluid Mechanics IX*. 2012. Split, Croatia: WIT PRESS.

[11] Gidaspow D. *Multiphase Flow and Fluidization*. 1994, California: Academic Press Inc.

[12] Brown RC and Brue E. *Resolving dynamical features of fluidized beds from pressure fluctuations.* Powder Technology, 2001. **119**(2–3): p. 68-80.

[13] Van Ommen JR, Sasic S, Van der Schaaf J, Gheorghiu S, Johnsson F and Coppens, M. *Time-series analysis of pressure fluctuations in gas–solid fluidized beds – A review.* International Journal of Multiphase Flow, 2011. **37**(5): p. 403-428.

[14] Van Ommen, JR, Teuling M, Nijenhuis J and Van Wachem BGM. *Computational validation of the scaling rules for fluidized beds.* Powder Technology, 2006. **163**(1–2): p. 32-40.

Paper C

Scaling of bubbling fluidized bed reactors with Glicksman's viscous limit set and CFD simulations

The paper is published in the International Journal of Computational Methods and Experimental Measurements.V2 (2), 2014 pp 135-144. ISSN: 2046-0546 (paper format), ISSN: 2046-0554 (online),http://journals.witpress.com. DOI: 10.2495/CMEM-V2-N2-135-144.

R. K. Thapa & B. M. Halvorsen, Int. J. Comp. Meth. and Exp. Meas., Vol. 2, No. 2 (2014) 135–144

SCALING OF BUBBLING FLUIDIZED BED REACTORS WITH GLICKSMAN'S VISCOUS LIMIT SET AND CFD SIMULATION

R. K. THAPA & B. M. HALVORSEN
Institute for Process, Energy and Environmental Technology, Telemark University College, Norway.

ABSTRACT

Glicksman's viscous limit set of dimensionless parameters have been investigated using experimentally verified computational fluid dynamics model. Simulations have been performed for the two bubbling fluidized beds with different particle sizes and densities. Dimensionless average pressure drops across the bed height, dimensionless pressure standard deviations and dimensionless relative pressures have been investigated as a function of dimensionless superficial gas velocities for the two beds. Fluctuation of solid volume fraction and contours of solid volume fraction have also been investigated at different dimensionless gas velocities. Time series data of the pressure fluctuation and solid volume fraction are compared. The results indicate that the fluid dynamic similarity between two beds holds up to particle Reynolds number of 15. After this, the bubble activities in the two beds start to deviate significantly. The results of the work show that the analysis of solid volume fraction fluctuation gives higher accuracy than time-series pressure fluctuation when scaling the bubbling fluidized bed within the viscous limit.

Keywords: Fluidized bed, scaling, viscous limit, Glicksman, CFD.

1 INTRODUCTION

Scaling of fluidized bed reactors in a proper way remains a major challenge in process industries. Scaling of fluidized beds is still an inexact science rather than a mix of mathematics, witchcraft, history and common sense as indicated by Matsen [1]. The scaling law for fluidized bed reactors has been developed by Glicksman. The law is derived by non-dimensionalizing the governing fluid dynamic equations for gas–solid flow [2]. This gives a set of dimensionless parameters. For two fluidized bed reactors to be fluid dynamically similar, the set of dimensionless parameters should be matched. The set of the dimensionless parameters is used to developed lab-scale cold models that simulate the flow behavior of an operating plant. This enables to improve the flow behavior of an existing plant when it is required. In addition, scaling is useful for the modification of the existing plants.

Glicksman has derived two sets of dimensionless parameter for scaling of fluidized beds: full set and simplified set. In the full set, dimensionless parameters such as Froude number, Reynolds number, density ratio, bed to particle size ratio, bed geometry ratio, particle sphericity and particle size distribution should be matched. van Ommen *et al.* studied the simplified set, full set and extended full set with additional dimensionless pressure group and found reasonable agreements [3]. In the particular application such as biomass gasification reactors, it is difficult to match all the parameters of the set. Sometimes exotic particles (very high density and very low particle size) are required when it comes to scaling down a very large operating plant to a lab-scale cold model [4]. To overcome this problem, Glicksman has simplified the full set. In the simplified set, Reynolds number has been replaced by the ratio of excess gas velocity to minimum fluidization velocity and the ratio of particle diameter to bed diameter has been omitted [5]. The simplified set gives more flexibility in selecting dimensions for the small-scale reactors.

© 2014 WIT Press, www.witpress.com
ISSN: 2046-0546 (paper format), ISSN: 2046-0554 (online), http://journals.witpress.com
DOI: 10.2495/CMEM-V2-N2-135-144

The simplified set is divided into two flow conditions. When the fluid–particle drag is dominated by inertial forces, it is the inertial limit. When the drag is dominated by viscous forces, it is the viscous limit. This division allows to consider the viscous dominated and inertial dominated flow separately [6]. In the viscous limit, the gas–particle density ratio is omitted for lower particle Reynolds numbers. For the particles with particle Reynolds number up to 4, the particle to gas density ratio can be omitted in the dimensionless set of parameters. This makes the viscous limit set of dimensionless parameters more flexible for scaling of fluidized bed. Bubbling fluidized bed reactors operate comparatively at lower gas velocities. Geldart A and B particles with lower gas velocities have low particle Reynolds numbers. Therefore, the viscous limit set is particularly suitable for scaling of bubbling fluidized bed reactors. In the literature, some authors have claimed that the viscous limit of the particle Reynolds numbers is higher than that given by Glicksman. The range of particle Reynolds numbers is not consistent. Stein *et al.* [7] have claimed that the density ratio can be neglected up to particle Reynolds number 100. Farrel [8] has shown that the viscous limit set does not hold for the particle Reynolds number between 10 and 25. Various reasons are responsible for the deviations.

The scaling of bubbling fluidized bed should be guided by the well understanding of particle properties and flow regimes in the bed. The scaling laws are derived from the set of independent dimensionless parameter. The dependent variables such as pressure and void fraction should also be compared in their non-dimensional form.

Downscaling of a large reactor to small lab-scale model sometimes requires significant reduction of particle size to maintain the dimensionless parameters. Particles with very different particle sizes belong to different Geldart groups. Different Geldart group particles have different flow regimes and this may result in different bubble behaviors in the scaled bed [9]. The selection of particle size and densities for scaled bed should be within the same Geldart group of particles. Scaling from very large commercial scale to small lab-scale cold model may also change the operating velocities between the two beds significantly. This may result in changing flow regime and consequently the bubble behavior of the two beds. In addition to this, the bed geometry also needs scaling. In practice, experimental investigation of all these conditions is not possible.

Computational fluid dynamic (CFD) models are valuable tools for this situation. The CFD tools have a significant potential in predicting the effect of scaling in hydrodynamics of fluidized beds [10]. Any particle density and size can be selected for the simulation of the model. The result of the simulations can serve as proper guidelines on selection of particle size, density and scaled bed geometry. This helps to avoid many intermediate errors in constructing lab-scaled cold model of an operating plant.

2 VISCOUS LIMIT SET OF SCALING RULES

The viscous limit set is derived by Glicksman for dense fluidized bed with low gas velocities [5]. In the dense region of the bed, the viscous forces are dominant compared with the inertial forces. Due to insignificant effect of inertial forces, requirements of dimensionless parameters to be matched are less. Equation (1) shows the viscous limit set of dimensionless parameters. Application of the set requires similarity of Froude number, the ratio of excess gas velocity to minimum fluidization velocity, bed geometry ratio, particle sphericity and particle size distribution. In addition to this, the particle Reynolds number should not exceed the value of 4. This criterion is shown in eqn (2). In practice, the viscous limit set of dimensionless parameters can be applied for scaling of bubbling fluidized beds. The particles of the large bed as well as scaled bed should have lower particle size.

$$\frac{u_0^2}{gL}, \frac{u_0}{u_{mf}}, \frac{L_1}{L_2}, \phi, \textit{particle size distribution} \tag{1}$$

$$\mathrm{Re} = \frac{\rho_g u_0 d_p}{\mu} < 4 \tag{2}$$

3 COMPUTATIONAL MODELS

Two approaches in modeling of gas–solid multiphase flow have been applied currently: Eulerian–Lagrangian and Eulerian–Eulerian. Eulerian–Lagrangian model tracks the motion of each particle and solves the dynamics of the fluid at the length scale smaller than the particle diameter. The modeling approach requires large computer memory and time for simulation. Eulerian–Eulerian model treats both the fluid and solid phases as interpenetrating continua and solves the dynamics averaging their equation of motion. The modeling approach is computationally less demanding [11]. The Eulerian–Eulerian approach is implemented in modeling the fluid dynamics of fluidized bed. To treat the particles as continuum, kinetic theory of granular flow is applied. The kinetic theory of granular flow considers the conservation of solid fluctuation energy [12]. The simulations have been performed using commercial CFD software ANSYS/Fluent 13.0.

The CFD model used in this work was validated against the experimental data. The experimental measurements were performed in a cold model with pressure sensors. Experimental data such as pressure drop across the bed height, pressure standard deviation and bubble behavior were compared with computational prediction of the model. A good agreement between the experimental measurements and the model predictions were established. The details of the validation work performed by the authors can be found in WIT Transactions on Engineering Series 2012 [13].

Two-dimensional simulations have been performed with air as fluidizing gas. The coefficient of restitution is set to 0.9. The coefficient represents the elasticity of collision between the particle–particle and particle–wall. Variation in the coefficient of restitution affects on fluid dynamic similarities between two beds [14,15]. The simulation is initialized with solid volume fraction of 0.6. In the simulations, the particles in both beds are assumed as spherical monosized particles. The simulation time for reference and scaled bed are 9.2 and 8 s, respectively. The simulation time is different for two beds to adjust the scaling factor with time.

The locations of the surface monitors for the two beds are presented in Fig. 1. In each bed, 25 surface monitors are set to record the pressure fluctuations and solid volume fraction fluctuations. The monitors are located at 0%, 25%, 75% and 100% along both the bed height and the bed width. In addition to this, line monitors are set at the bed height of 25%, 50% and 75% for the solid volume fraction fluctuation.

The properties of particles and gases used in the model for the two beds are presented in Table 1.

To start the simulation, theoretical minimum fluidization velocities for the particles are calculated using the following equation:

$$\frac{(\phi \cdot d_p)^2 (\rho_p - \rho_g) \cdot g}{150 \mu_g} \cdot \frac{\varepsilon_{mf}^3}{1 - \varepsilon_{mf}} \tag{3}$$

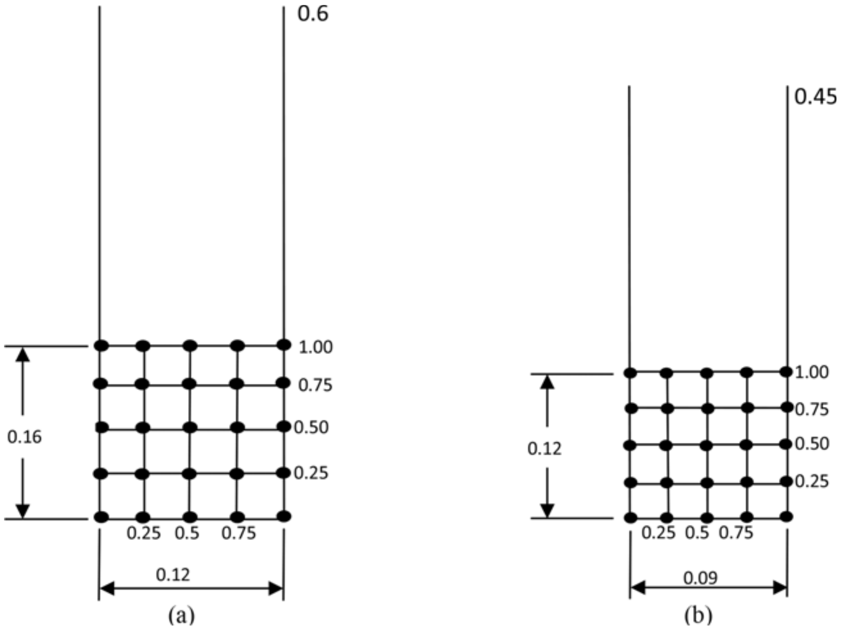

Figure 1: Bed dimensions and location of surface monitors: (a) reference bed and (b) scaled bed.

Table 1: Properties of particles and gases.

Set	d_p (μm)	ρ_p (kg/m^3)	ρ_g (kg/m^3)	μ_g (Pa·s)	u_{mf} (m/s)	H (m)	D (m)	Geldart group
Reference bed	320	2500	1.225	$1.78 \cdot 10^{-5}$	0.147	0.16	0.12	B
Scaled bed	240	3800	1.225	$1.78 \cdot 10^{-5}$	0.170	0.12	0.09	B

The gas velocities and the dimensionless parameters of the two beds used in the simulation are presented in Table 2.

4 RESULTS AND DISCUSSION

Pressure fluctuation is most commonly used in the studies of fluidized beds. In bubbling fluidized bed, the pressure fluctuation is related to the bubble motion in the bed. A single pressure point contains the global information about the bed. Many researchers have attempted to validate fluid dynamic similarity between the bubbling fluidized beds from time-series pressure data [16]. The standard deviation of pressure fluctuation is an indirect method to identify the fluid dynamics in fluidized beds [17].

The pressure fluctuations in the bed are monitored at the equally distributed 25 points within the bed. The dimensionless pressure standard deviation is the ratio of pressure standard deviation at identical points of the two beds with identical dimensionless gas velocity. The dimensionless gas velocity is the ratio of excess gas velocity to minimum fluidization velocities of the two beds. The dimensionless pressure standard deviation as a function of dimensionless gas velocity is presented in Fig. 2. For two beds to be fluid dynamically

Table 2: Gas velocities and dimensionless parameters used in the simulation.

Simulation	Set	u_0 (m/s)	u_0^2/gd_p (–)	u_0/u_{mf} (–)	Re (–)
1	Reference bed	0.170	9.19	1	2.43
	Scaled bed	0.147	9.24		3.73
2	Reference bed	0.340	36.75	2	4.86
	Scaled bed	0.294	36.98		7.46
3	Reference bed	0.510	82.69	3	7.28
	Scaled bed	0.441	83.20		11.20
4	Reference bed	0.680	147.00	4	9.71
	Scaled bed	0.588	147.9		14.93
5	Reference bed	0.850	229.69	5	12.14
	Scaled bed	0.735	231.10		18.66

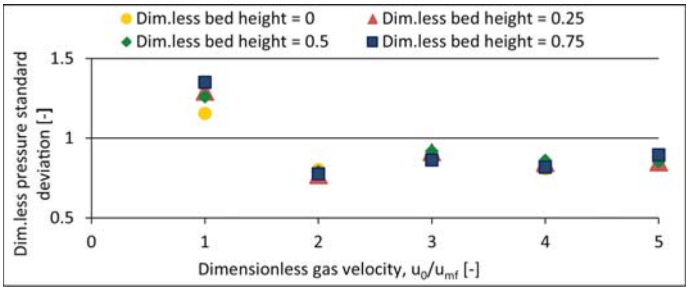

Figure 2: Dimensionless pressure standard deviation as a function of dimensionless gas velocity at different bed heights.

similar, the dimensionless pressure standard deviation should be similar for the same dimensionless gas velocity at any identical points of the beds. But the dimensionless pressure data need not to be equal to 1. This requirement applies only to Glickman's full sets and inertial limit sets of dimensionless parameters. In the viscous limit set, the density ratio between two beds does not need to be matched. This makes the set more attractive for scaling of fluidized bed reactors within the limited particle Reynolds number. The figure shows pressure standard deviations of the two beds at 0%, 25%, 50% and 75% of the bed heights at five different dimensionless gas velocities. The dimensionless pressure standard deviations are almost same for those points of the bed at the dimensionless gas velocities of 2–5. This shows the fluid dynamic similarity of the beds at gas velocities higher than minimum fluidization. The dimensionless pressure standard deviation at the dimensionless gas velocity of 1 has a slight deviation. Particularly, the dimensionless pressure standard deviation at the bottom of the bed has different value than other points along the height of the bed. The dimensionless velocity of 1 represents the transition of the beds from static condition to fluidizing condition. Slight difference in initial minimum fluidization velocity set in the simulation may result in such types of deviations. However, the deviation is within the acceptable error limit.

Table 3: Pressure standard deviation at dimensionless bed height of 0.5.

Dimensionless gas velocity (–)	Pressure standard deviations (Pa) Reference bed	Pressure standard deviations (Pa) Scaled bed	Dimensionless pressure standard deviation (–)
1	24.41	19.35	1.26
2	151.45	191.91	0.78
3	281.10	306.41	0.91
4	338.68	393.75	0.86
5	405.35	475.14	0.85

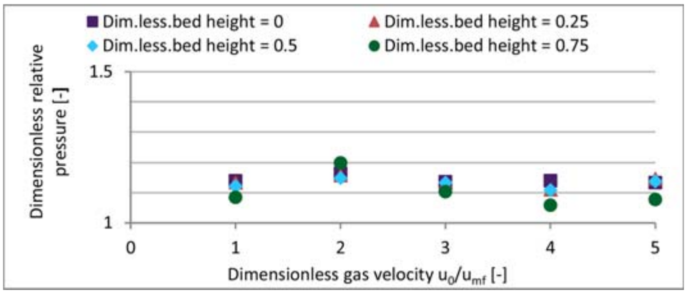

Figure 3: Dimensionless relative pressure as a function of dimensionless gas velocity at different bed heights.

The pressure standard deviation increases with gas velocity. The pressure standard deviations for both the beds taken separately have minimum values at the minimum fluidization velocity. The pressure standard deviation at the dimensionless bed height of 0.5 is presented in Table 3.

Dimensionless relative pressure as a function of dimensionless gas velocity is presented in Fig. 3. The dimensionless relative pressure is the ratio of the pressure along the same dimensionless bed height.

Dimensionless relative pressure does not show significant difference along the bed height with increasing dimensionless gas velocities. However, the dimensionless relative pressure is slightly decreased at dimensionless gas velocities of 4 and 5. This indicates the deviation of relative pressure at these dimensionless gas velocities in comparison to the others.

The dimensionless average pressure drop as a function of dimensionless gas velocity is shown in Fig. 4. The average pressure drop is the ratio of pressure drop across the bed height to the total height of the bed. In the viscous limit set, the density ratio of the particles is not maintained. The differences in the particle to gas density ratio result in different average pressure drop across the bed height. Therefore, the average pressure drop across the bed can only be compared in its dimensionless numbers. As indicated in the figure, the dimensionless values of average pressure drop are increased more at the dimensionless gas velocities of 4 and 5.

The increased dimensionless average pressure drop at dimensionless gas velocities 4 and 5 indicates the deviation of pressure fluctuation in the two beds for these dimensionless gas

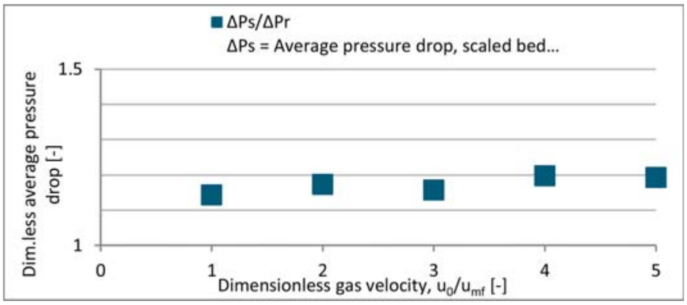

Figure 4: Dimensionless average pressure drop across the bed height as a function of dimensionless gas velocity.

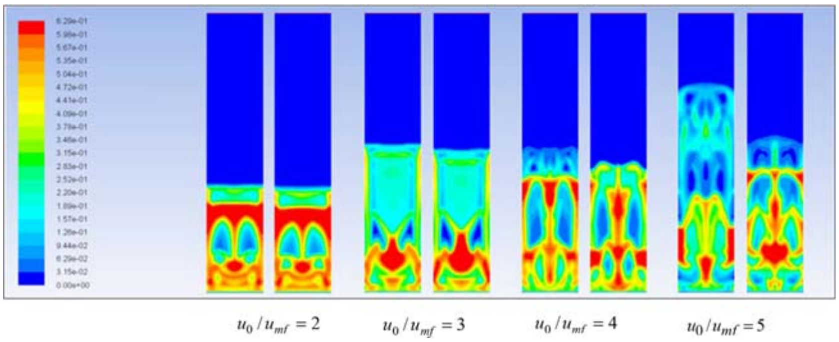

Figure 5: Contours of solid volume fraction at different dimensionless gas velocities at 9.2 and 8 s of simulation time for reference and scaled bed, respectively. Left: reference bed and right: scaled bed.

velocities. The deviation is significant as the particle Reynolds number numbers approaches about 15 and 19, respectively. The contours of solid volume fraction at these dimensionless gas velocities shown in Fig. 5 also confirm the significant deviation, suggesting the viscous limit set is valid up to the particle Reynolds number <15.

Analysis of time series of pressure fluctuation data in the two beds shows that the pressure fluctuations in the beds do not show significant deviation even the particle Reynolds number is significantly higher than the viscous limit. However, at the dimensionless gas velocities of 4 and 5, slight deviation of dimensionless pressure standard deviation, dimensionless relative pressure and dimensionless average pressure drop can be seen from the figures. It shows that the fluctuation of pressure between two beds at these velocities deviate significantly.

Detailed information about the bubble activities in the bed can be obtained from the data of solid volume fraction fluctuation. The fluctuation of solid volume fraction in a bubbling fluidized bed is due to the bubble activities. The contours of solid volume fraction for the two beds are presented in Fig. 5. The contours are presented from dimensionless gas velocity 2–5. The contours are snapshots taken at the simulation time of 9.2 and 8 s for reference and scaled bed, respectively. The simulation time is different because of the scaling factor. The ratio between the scaling times is 1.15, which is the scaling factor of the beds. As long as the

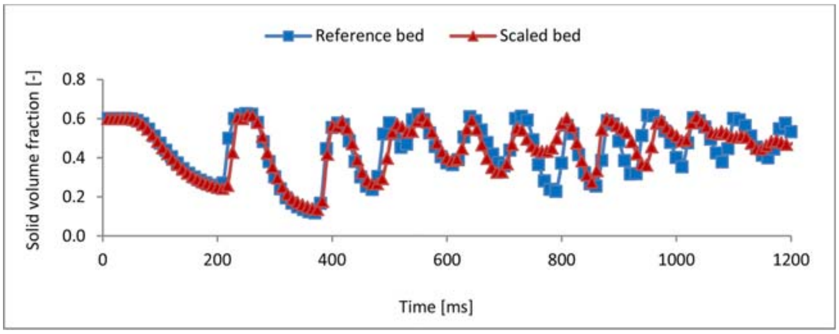

Figure 6: Solid volume fraction fluctuation with time. Dimensionless bed height = 0.5, dimensionless bed width = 0.75 and dimensionless gas velocity = 2.

time is also scaled, the solid volume fraction of the beds should be similar at a given time for two beds to have fluid dynamic similarity.

At the dimensionless gas velocity of 1, the beds are static and there are no bubbles in the bed. The contours of solid volume fraction for two beds at the dimensionless gas velocity of 2 and 3 are similar. This shows that the bubble formation and bubble activities in the bed are similar. The contours show negligible deviation between the two beds. The highest particle Reynolds number at these velocities is about 11. Up to this value of particle Reynolds number, the bubble behavior of the bed is similar. At the dimensionless gas velocity of 4, the contours show some deviation between the bubble activities in the beds. The particle Reynolds number for the dimensionless gas velocity is about 15. This is the Reynolds number at which the deviation of the bubble activities between the two beds starts. At the dimensionless gas velocity of 5, the contours deviate significantly. The particle Reynolds number at this velocity is about 18.

The time-series data of solid volume fraction fluctuations for the two beds are presented in Fig. 6. The time series of solid volume fraction fluctuation in the beds gives more precise information of bubble activities. The figure shows the solid volume fraction fluctuation at a single point. Similarity in the fluctuation of solid volume fraction between the two beds means the similar bubble behavior in the beds.

5 CONCLUSION

Glicksman's viscous limit set of dimensionless parameters are applied in scaling of bubbling fluidized beds with different particle sizes and densities. The beds are simulated using experimentally validated CFD model. The simulations are performed in commercial CFD software ANSYS/Fluent 13.0. Dimensionless pressure standard deviation, relative pressure and average pressure drop across the bed height are investigated as a function of dimensionless superficial gas velocities. Dimensionless pressure standard deviation is similar for the two beds at the dimensionless gas velocities 2–5. The dimensionless relative pressure and dimensionless average pressure drop deviate at dimensionless gas velocities of 4 and 5.

Fluctuation of solid volume fraction and contours are investigated as a function of dimensionless gas velocity. The contour of solid volume fraction is similar for the two beds at the dimensionless gas velocities of 2 and 3. The contour starts to deviate from the dimensionless gas velocity of 4 and deviates significantly at the velocity 5. The similarity of solid volume fraction fluctuation or the bubble activities in the bed holds for the particle Reynolds number up to 15.

NOMENCLATURE

CFD	computational fluid dynamics
D	bed diameter (m)
dp	particle diameter (m)
g	acceleration due to gravity (m/s^2)
H	static height of bed (m)
L_1, L_2	bed geometry (m)
Re	Reynolds number (–)
u_0	excess gas velocity (m/s)
u_{mf}	minimum fluidization velocity (m/s)
ρ_p	particle density (kg/m^3)
ρ_g	gas density (kg/m^3)
μ_g	gas viscosity (Pa·s)
ϕ	particle sphericity (–)
ε_{mf}	void fraction at minimum fluidization (–)

REFERENCES

[1] Matsen, J.M., Scale-up of fluidized bed processes: principle and practice. *Powder Technology*, **88(3)**, pp. 237–244, 1996. doi: http://dx.doi.org/10.1016/S0032-5910(96)03126-9

[2] Glicksman, L.R., Scaling relationships for fluidized beds. *Chemical Engineering Science*, **39(9)**, pp. 1373–1379, 1984. doi: http://dx.doi.org/10.1016/0009-2509(84)80070-6

[3] van Ommen, J.R., et al., Computational validation of the scaling rules for fluidized bed. *Powder Technology*, **163**, pp. 32–40, 2006. doi: http://dx.doi.org/10.1016/j.powtec.2006.01.010

[4] Rüdisüli, M., et al., Scale-up of bubbling fluidized bed reactors — a review. *Powder Technology*, **217(0)**, pp. 21–38, 2012. doi: http://dx.doi.org/10.1016/j.powtec.2011.10.004

[5] Glicksman, L.R., Hyre, M. & Woloshun, K., Simplified scaling relationships for fluidized beds. *Powder Technology*, **77(2)**, pp. 177–199, 1993. doi: http://dx.doi.org/10.1016/0032-5910(93)80055-F

[6] Sanderson, J. & Rhodes, M.J., Hydrodynamic similarity of solids motion and mixing in bubbling fluidized beds. *AIChE Journal*, **49(9)**, pp. 2317–2327, 2003. doi: http://dx.doi.org/10.1002/aic.690490908

[7] Stein, M., Ding, Y.L. & Seville, J.P.K., Experimental verification of the scaling relationships for bubbling gas-fluidised beds using the PEPT technique. *Chemical Engineering Science*, **57(17)**, pp. 3649–3658, 2002. doi: http://dx.doi.org/10.1016/S0009-2509(02)00264-6

[8] Farrel, P.A., *Hydrodynamic Scaling and Solid Mixing in Pressurized Bubbling Fluidized Bed Combustors*, Massachusetts Institute of Technology: Massachusetts, 1996.

[9] Kunnii, D. & Levenspiel, O., *Fluidization Engineering*. 2nd edn., Butterworth-Heinemann: USA, 1991.

[10] Knowlton, T.M., Karri, S.B.R. & Issangya, A., Scale-up of fluidized-bed hydrodynamics. *Powder Technology*, **150(2)**, pp. 72–77, 2005. doi: http://dx.doi.org/10.1016/j.powtec.2004.11.036

[11] Mazzei, L., *Eulerian Modelling and Computational Fluid Dynamics Simulation of Mono and Polydisperse Fluidized Suspensions*, University College London: UK, 2008.

[12] Gidaspow, D., *Multiphase Flow and Fluidization*, Academic Press Inc.: California, 1994.

[13] Thapa, R.K. & Halvorsen, B.M., Validation of CFD model for prediction of flow behaviour in fluidized bed reactors. *WIT Transactions on Engineering Sciences*, Vol. 74, WIT Press: Southampton, pp. 231–239, 2012.

[14] Detamore, M.S., et al., A kinetic theory analysis of the scale-up of circulating fluidized beds. *Powder Technology*, **115**, pp. 190–203, 2001. doi: http://dx.doi.org/10.1016/S0032-5910(00)00397-1

[15] Didwania, A.K. & Catolia, R.J., *CFD simulation scale-up of a dual fluidized bed gasifier for biomass*. *Seventh International Conference on CFD in the Minarals and Process Industries*, Melbourne, Australlia, 2009.

[16] Brown, R.C. & Brue, E., Resolving dynamical features of fluidized beds from pressure fluctuations. *Powder Technology*, **119(2–3)**, pp. 68–80, 2001. doi: http://dx.doi.org/10.1016/S0032-5910(00)00419-8

[17] van Ommen, J.R., et al., Time-series analysis of pressure fluctuations in gas–solid fluidized beds – a review. *International Journal of Multiphase Flow*, **37(5)**, pp. 403–428, 2011. doi: http://dx.doi.org/10.1016/j.ijmultiphaseflow.2010.12.007

Paper D

Modeling of reaction kinetics in bubbling fluidized bed biomass gasification reactor

This paper is publish in the International Journal of Energy and Environment, V5 (1), 2014 pp 35-45. ISSN 2076-2895 (Print), ISSN 2076-2909 (Online).

INTERNATIONAL JOURNAL OF
ENERGY AND ENVIRONMENT

Volume 5, Issue 1, 2014 pp.35-44
Journal homepage: www.IJEE.IEEFoundation.org

Modeling of reaction kinetics in bubbling fluidized bed biomass gasification reactor

R.K. Thapa[1], C. Pfeifer[2], B. M. Halvorsen[1]

[1] Telemark University College, Kjolnes ring 56, P.O. Box 203, 3901 Porsgrunn, Norway.
[2] University of Natural Resources and Life Sciences, Vienna, Austria.

Abstract

Bubbling fluidized beds are widely used as biomass gasification reactors as at the biomass gasification plant in Güssing, Austria. The reactor in the plant is a dual circulating bubbling fluidized bed gasification reactor. The plant produces 2MW electricity and 4.5MW heat from the gasification of biomass. Wood chips as biomass and olivine particles as hot bed materials are fluidized with high temperature steam in the reactor. As a result, biomass undergoes endothermic chemical reaction to produce a mixture of combustible gases in addition to some carbon-dioxide (CO_2). The combustible gases are mainly hydrogen (H_2), carbon monoxide (CO) and methane (CH_4). The gas is used to produce electricity and heat via utilization in a gas engine. Alternatively, the gas is further processed for gaseous or liquid fuels, but still on the process of development level. Composition and quality of the gas determine the efficiency of the reactor.

A computational model has been developed for the study of reaction kinetics in the gasification rector. The simulation is performed using commercial software Barracuda virtual reactor, VR15. Eulerian-Lagrangian approach in coupling of gas-solid flow has been implemented. Fluid phase is treated with an Eulerian formulation. Discrete phase is treated with a Lagrangian formulation. Particle-particle and particle-wall interactions and inter-phase heat and mass transfer have been taken into account.

Series of simulations have been performed to study model prediction of the gas composition. The composition is compared with data from the gasifier at the CHP plant in Güssing, Austria. The model prediction of the composition of gases has good agreements with the result of the operating plant.

Copyright © 2014 International Energy and Environment Foundation - All rights reserved.

Keywords: Biomass gasification; Fluidized bed; Computational Particle Fluid Dynamic CPFD; Eulerian-Lagrangian approach; Reaction kinetics; Dual fluidized bed; FICFB-gasification.

1. Introduction

Biomass is a source of renewable energy neutral to CO_2 emission. It is the oldest source of energy known to mankind. At present time it is the fourth largest source of energy after oil, coal and gas. Today, biomass contributes 14% world's energy consumption [1, 2]. Biomass is used in power plants to produce heat and power. In conventional power plants, biomass is combusted to produce steam. The steam is then used in steam cycles for power production. The overall efficiencies of those power plants are relatively low.

During the past two decades many researches are focused on the gasification of biomass. The technology allows producing a mixture of combustible gases in addition to some gases like CO_2 and water vapor.

The gas can further be utilized for heat and power production. One of those areas is dual fluidized bed gasification, formerly called Fast Internally Circulating Fluidized Bed (FICFB) gasification system. The technology was developed jointly by Vienna University of Technology and AE Energietechnik in Austria [3, 4]. The fundamental principal of the gasification process is shown in Figure 1. The basic concept behind the technology is to separate the gasification reactor from the combustion reactor. The gasification reactor is operated as a bubbling fluidized bed fluidized by high temperature steam. In the gasification reactor, biomass undergoes endothermic reaction to produce a mixture of combustible gases in addition to CO_2 and water vapor. The combustible gases are mainly hydrogen (H_2), methane (CH_4) and carbon-monoxide (CO). The mixture of gas is called producer gas. The combustion reactor is operated as a circulating fluidized bed reactor fluidized by air. The combustion reactor is used to heat the bed material. The heated bed material is then circulated to the gasification reactor in order to supply necessary heat for endothermic reactions in the gasification reactor.

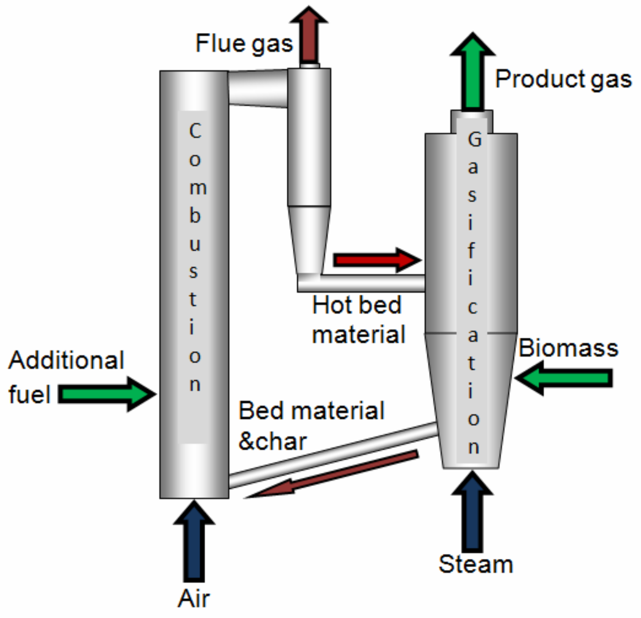

Figure 1. Principle of dual fluidized bed-gasification process

The producer gas can be used for several applications. It can be used in gas engines, gas turbines or fuel cells to produce electricity and heat. The gas can further processed through Fischer-Tropsch (FT) or dimethyl ether (DME) synthesis. The energy efficiency of the technology is higher than conventional technologies. The technology has less environmental impacts such as NO_x and particulate production [5]. The technology has been demonstrated as biomass gasification plant for combined heat and power (CHP) production. The $8MW_{fuel}$ plant is located in Güssing, Austria. The plant produces 2MW electricity and 4.5MW heat from the gasification of wood chips [6]. The technology produces almost nitrogen free, producer gas with high calorific value of about 12-14 MJ/Nm^3 [7].

Besides the novelty of the technology, the overall efficiency of the technology needs to be further increased. This makes the technology more competitive with other sources of energy in the world energy market. Gasification reactor is the heart of the technology and it is believed that the efficiency of the technology mainly depends on the thermo-chemical and fluid dynamic behavior in the reactor. Study of those parameters in an operating plant is almost impossible due to its high operating temperature. Down-scaled lab-models allow the study of fluid-dynamic behaviors [8, 9]. Nevertheless a detailed study of thermo-chemical behavior is still a major challenge. A validated computational model with CFD simulation could be the solution. The model prediction is helpful for improving efficiency of the technology. In addition, it can predict the optimized parameters in design for improvements and scaling of such plant.

2. The gasification reactor

The modeling in the present work is focused only on the gasification reactor excluding the combustion reactor. The gasification reactor is a bubbling fluidized bed. In the reactor, hot bed material, olivine particles are fluidized by high temperature steam. The geometry of the model reactor is shown in Figure 2. Biomass in the form of wood chips is fed to the reactor. The heated bed material of temperature about 900^0C is also fed to the gasification reactor from the combustion reactor. Biomass undergoes endothermic gasification reaction taking necessary heat from the hot bed material. The bed material with some amount of unreacted char particles leaves the gasification reactor to the combustion reactor. The producer gas leaves the reactor at the top.

Inside the reactor, biomass first undergoes a drying process and the moisture content of the biomass is removed in the form of water vapor. The second process is devolatilization. This is the process of thermal decomposition of biomass in the absence of oxygen where the biomass is decomposed to char particles and gases. The process can be shown as in Equation 1 [10]. The composition of the gases depends on the operating condition of the reactor.

$$wood \rightarrow H_2, CO, CO_2, CH_4, HC, H_2O, tars, char\,(s) \tag{1}$$

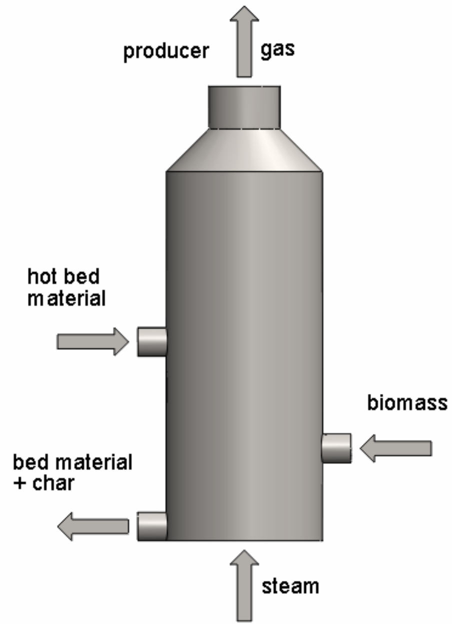

Figure 2. fModel of gasification reactor

The third step include sheterogeneous and homogeneous reactions. The reactions with the corresponding reaction kinetics are presented in Table 1 [11-14].

The process should be optimized in order to get the maximum fraction of H_2 and CO with reduced amounts of condensable water and organic vapor in the product gas. The reactions are depending on the heat and mass transfer as well as fluid dynamic behavior in the gasification reactor. Modeling and simulation of the reactor using Computational Particle Fluid Dynamics (CPFD) allows study of the reactor with varying parameters.

3. Computational model

There are mainly two approaches in modeling of gas-solid flow in fluidized bed reactors: Eulerian-Eulerian and Eulerian-Lagrangian. Eulerian-Eulerian approach assumes both the gas and solid phase as continuum and the two phase flow as interpenetrating continua. The major disadvantage encountered in this approach is that the model does not have the possibility to account for the particle size distribution in the bed. This is because separate momentum and continuity equation have to be solved for each size of particle [15]. However, the particle size distribution has significant influence on the performance of fluidized bed [16-18]. Eulerian-Lagrangian approach treats solid phase as discrete elements. The motions of individual particles are tracked using Newton’s law. The particle-particle, particle-wall and fluid-particle interaction forces are taken into account [19]. This approach simulates the gas solid flow with wide range of particle size distribution [20, 21].

Eulerian-Lagrangian approach is implemented for the modeling of gas-solid flow and chemical reactions in the biomass gasification reactor. Governing equations of the fluid phase are solved using continuum model. The particle phase is solved using Lagrangian model. The computational methods applied in this work is developed by D.M. Snider et al. and the details of the approach can be found in [22-24]. 3D simulations of gas-solid reacting flow are performed using commercial computational particle fluid dynamics (CPFD) software Barracuda VR 15.

One of the important advantages of CPFD software is that it allows simulating particles with different size and distribution. Figure 3 shows the particle size distribution of biomass and bed material feed to the reactor. It should be noted that the particle size are measured in their corresponding radius in Barracuda VR 15 instead of diameter.

Table 1. Reactions in the gasification reactor and their reaction kinetics

Reaction	Reaction kinetics
Steam gasification $C+H_2O \overset{r_{1f}}{\underset{r_{1r}}{\Longleftrightarrow}} H_2+CO$	$r_{1f} = 1.272\, m_s\, T \exp\left(\frac{-22645}{T}\right)[H_2O]$ $r_{1r} = 1.044\times10^{-4} m_s T^2 \exp\left(\frac{-6319}{T} - 17.29\right)[H_2][CO]$
Carbon-dioxide gasification $C+CO_2 \overset{r_{2f}}{\underset{r_{2r}}{\Longleftrightarrow}} 2CO$	$r_{2f} = 1.272 m_s T \exp\left(\frac{-22645}{T}\right)[CO_2]$ $r_{2r} = 1.044\times10^{-4} m_s T^2 \exp\left(\frac{-2363}{T} - 20.92\right)[CO]^2$
Methanation $0.5C+H_2 \overset{r_{3f}}{\underset{r_{3r}}{\Longleftrightarrow}} 0.5CH_4$	$r_{3f} = 1.368\times10^{-3} m_s T \exp\left(\frac{-8078}{T} - 7.087\right)[H_2]$ $r_{3r} = 0.151 m_s T^{0.5} \exp\left(\frac{-13578}{T} - 0.372\right)[CH_4]^{0.5}$
Water- gas shiftreaction $CO+H_2O \overset{r_{4f}}{\underset{r_{4r}}{\Longleftrightarrow}} CO_2+H_2$	$r_{4f} = 7.68\times10^{10} m_s T \exp\left(\frac{-36640}{T}\right)[CO]^{0.5}[H_2O]$ $r_{4r} = 6.4\times10^{9} m_s T \exp\left(\frac{-39260}{T}\right)[H_2]^{0.5}[CO_2]$
Methane reforming $CH_4+H_2O \overset{r_{5f}}{\underset{r_{5r}}{\Longleftrightarrow}} CO+3H_2$	$r_{5f} = 3.0\times10^{5} T \exp\left(\frac{-15042}{T}\right)[CH_4][H_2O]$ $r_{5r} = 0.0265\ T \exp\left(\frac{-32900}{T}\right)[CO][H_2]^2$

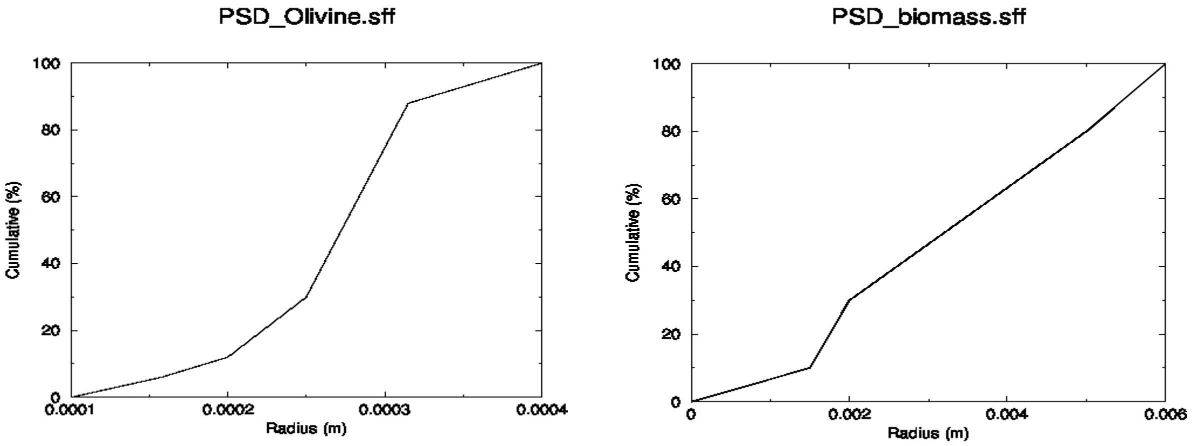

Figure 3. Particle size distribution of the bed material and biomass

Wood chips are fed to the hot bed material in the operating plant. The model assumes that the drying and devolatilization takes place immediately at the inlet of the reactor. The assumption makes sense because the temperature of the reactor is very high. The reaction temperature is about 1123 K. Feed of the reactor at biomass inlet is divided into char and volatile matters instead of wood chips [25]. The main products of wood pyrolysis are volatile matter, char, moisture, tar, higher hydrocarbons and some other components. As a simplification of the model, the tar, hydrocarbons and other compounds of the pyrolysis are neglected and the volatile matter is divided to91% of gases (CH_4,CO,CO_2 and H_2) and 9% of char particles on dry basis [26]. The wt% of the composition of gases is given in Table 2. The inlet of biomass is modeled as inlet of char particles and volatile matter.

Some of the physical properties of biomass and bed materials are presented in Table 3. Biomass feed rate as volatile matter and char is 28 kg/h. Bed material circulation is 40 times higher than biomass feed. The steam-fuel ratio is 0.6.

Initially the reactor is filled with hot bed material, char particles and superheated steam. The pressure and flow boundary conditions of the reactor are shown in Figure 4. The product gas outlet is pressure boundary. Biomass, bed materials and char particles inlet and outlets are flow boundaries as shown in the figure. The particles and gases passing through these boundaries are monitored by corresponding flux-planes. In addition to this, flow of the product gas is monitored by the flux planes located at 1.4m, 1.9m, 2.4m and 3m along the height of the reactor.

Table 2. Composition of volatile matters in wood

Components	Wt%
CH_4	0.1213
CO	0.6856
CO_2	0.1764
H_2	0.0167

Table 3. Properties of biomass and bed material

Material	Density [kg/m^3]	Flow rate [kg/h]
Olivine	2960	1120
Char	200	25.7
Volatile matter	1.200	2.3
Steam	0.204	16.8

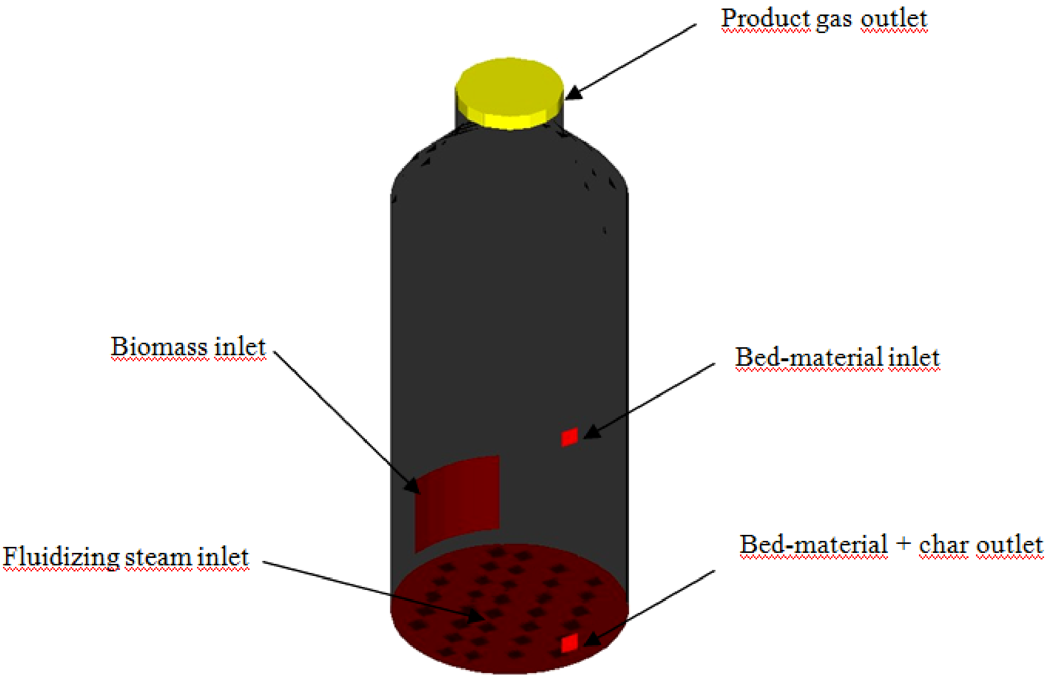

Figure 4. Pressure and flow boundary condition of the model

4. Results and discussion

The simulation was performed to gain 90 seconds of fluidizationas well as gasification reactions in the reactor. Average data was recorded after 10seconds of simulation in order to avoid the fluctuation of different parameter in starting of the reactor. The average data and transient data for different simulation parameters are assigned in different flux planes and transient data points respectively.

Analysis of the results is started from the flow parameters. During simulation, it is important that the flow of bed materialand biomass are consistent with the given feed rate. The in-flux and out-flux rates of bed material and biomass through corresponding flux planes are stored influx-data files. The cumulative rate of inflow and outflow of bed material is shown in Figure 5(a). The figure shows that circulation of bed material is maintained properly during the simulation period. Figure 5(b) shows cumulative mass flow rate of biomass feed. Biomass is divided to 91% volatiles and 9% of char. The figure shows consistent flow of biomass during the simulation period.

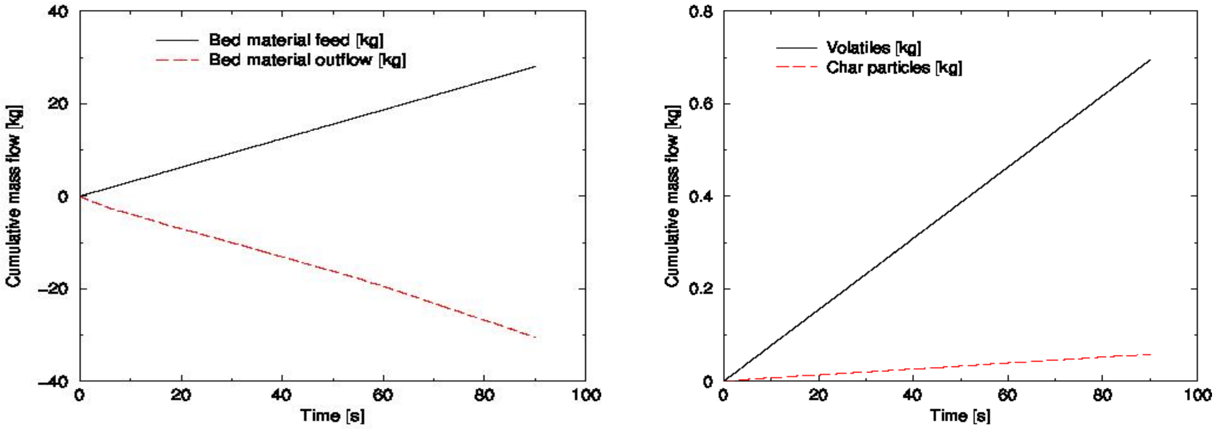

(a) (b)

Figure 5. (a) Cumulative flow of bed material; (b) Cumulative flow of biomass

Another significant parameter to be examined is temperature. Different transient points along the height of the reactor are assigned to record temperatures during the simulation. The contours of particle temperature and fluid temperature at 90s of simulation are shown in Figure 6.

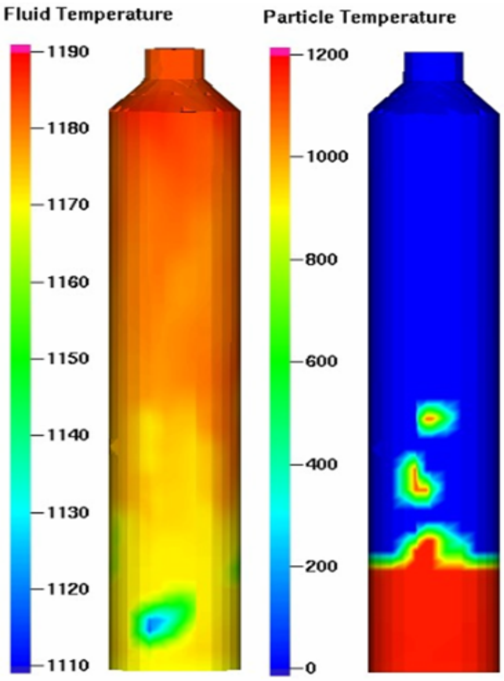

Figure 6. Variation of fluid temperature and particle temperature along the height of reactor

The particle feed temperature is 1173 K. The steam feed temperature is 1073 K. The average gasification temperature is 1073K-1123K. The figure shows both the particle temperature and fluid temperature is above 1073K. This means gasification reaction in the reactor is maintained constantly. The figure indicates that the average temperature of the fluid in freeboard is about 1110 K. The temperature distribution in the dense region as well as the freeboard region of the reactor is consistent with required reaction temperature.

Mass flow rate of the components of the product gas is recorded in different flux planes along the height of reactor. The flow rate through the flux plane located at the top of the reactor is presented in Figure7. Initially, the mass flow rate of CO and CH_4 is higher. This is the result of steam gasification and methanation. After some time, there is decrease in CO, CH_4 and water vapor with increase in H_2 and CO_2 indicating homogeneous water gas shift and methane reforming reactions. After few seconds of reaction the flow rate of gas does not vary significantly.

The mole flow rate of gas components are shown in Figure 8. The flow rate is transient data recorded in a point at the top of the reactor. The mole flow rate from transient data is similar to that of mass flow rate from the flux plane as shown in Figure 7. The more fluctuation of mole flow is due to transient nature of the data. Moreover it is the mole passing through a point monitor in the plane.

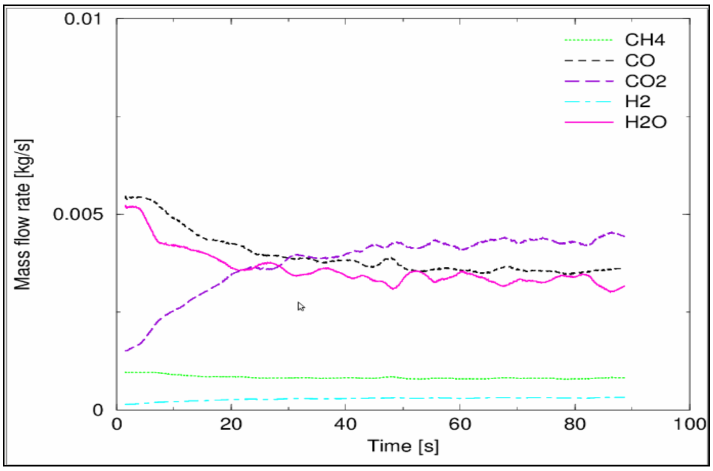

Figure 7. Mass flow rate of gas components through the top of reactor

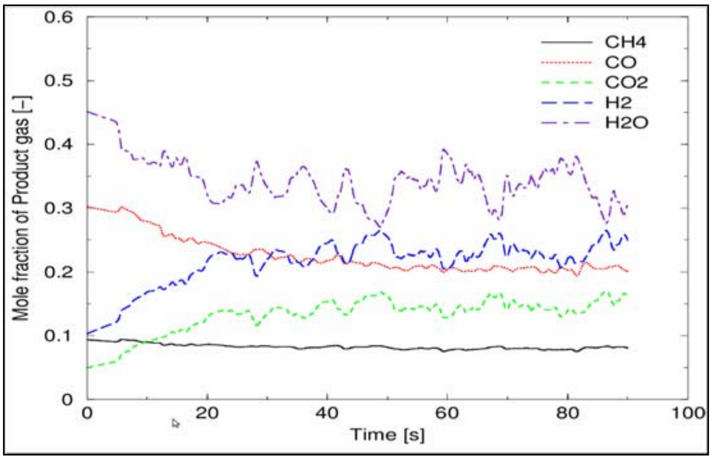

Figure 8. Mole fraction of product gas passing through a point on the top of the reactor

Figure 9 shows that the mass fraction of CO and H_2O is highest at the bottom of the reactor in the dense region of the bed. Steam gasification, CO_2 gasification and methanation reactions are responsible for the higher mass fraction of those components. Moreover, the pyrolysis of wood produces large mass fraction of CO.

The mass fraction of CO_2 and $H_2$is highest at the top of reactor. The fraction of CH_4 is decreasing slightly and continuously from the dense region to the freeboard. This indicates methane reforming reaction starts immediately at the freeboard region near to the dense region of the bed and continues along the height of the bed.

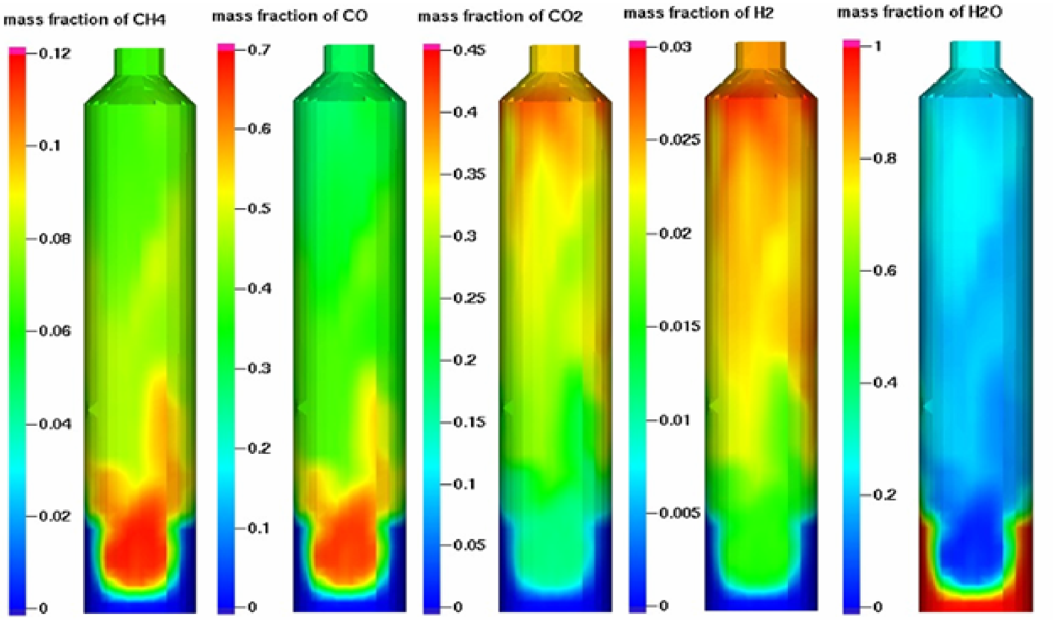

Figure 9. Mass fraction of the product gas components at simulation time of 90s

At the dense region of the reactor, chemical reactions occur to produce CH_4 and CO. At the freeboard region the mass fraction of CO and CH_4 is decreased forming more H_2 and CO_2. The fraction of steam is also decreased significantly at the freeboard region indicating the fact that more steam is consumed during homogeneous reactions in the freeboard.

The product gas compositions are recorded at the four different heights of the freeboard region of the reactor. The mass fractions are converted to volume fractions and presented in Figure 10. The product gas composition varies significantly at the dense region of the bed and its nearest freeboard region. As the product gas flows higher and higher along freeboard, the gas composition becomes more constant. This indicates less and less reactions as the gas moves along the height of the reactor.

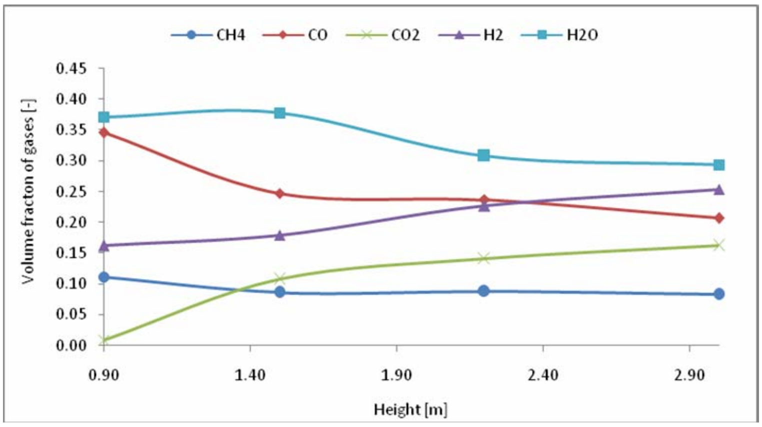

Figure 10. Gas volume fraction along the height of the reactor

The composition of producer gas in the Güssing plant can be found in many published literatures [3, 4, 27]. Simulated producer gas composition is compared with the measured composition of the CHP plant in Güssing. The data is presented in Table 4. The gasification temperature is about 800-850^{0}C at atmospheric pressure. The measured values are in dry basis. It should be noted that 9vol% of gases are assumed as tar and other hydrocarbons which are not included in the predicted results as well as in measured data from the CHP plant in Güssing.

Table 4. Comparison of simulated and measured product gas composition

Components	Predicted vol%	Measured vol%
Hydrogen (H_2)	34	32
Carbon monoxide (CO)	25	25
Carbon dioxide(CO_2)	22	22
Methane (CH_4)	10	12

5. Conclusion

A 3D gas solid reacting flow in the bubbling fluidized bed part of the dual fluidized bed biomass gasification reactor has been modeled. The model is simulated using computational particle fluid dynamic (CPFD) software Barracuda VR 15. Biomass is modeled as a 91wt% of volatile gases and 9wt% of char particles. The heterogeneous reactions considered are the steam gasification, CO_2 gasification, and methanation. Homogeneous reactions occurring in the gasification reactor are water-gas shift and methane reforming.

The results of the simulation shows most of the reactions occur at the dense region of the bed and the vicinity of the dense region in the freeboard. As the gases passes through the freeboard region, the composition of the gas becomes consistent. The predicted composition of the product gas is compared with measured data from the gasifier at the combined heat and power plant in Güssing, Austria. The compositions agree well.

A computational model of a wood gasification reactor has been established. The model can be used to study various parameters of the reactor such as influence of temperature, residence time and steam-fuel ratio as well as other parameters.

References

[1] Saxena, R.C., D.K. Adhikari, and H.B. Goyal, Biomass-based energy fuel through biochemical routes: A review. Renewable and Sustainable Energy Reviews, 2009. 13(1): p. 167-178.

[2] Bain, R.L., R.P. Overend, and K.R. Craig, Biomass-fired power generation. Fuel Processing Technology, 1998. 54(1–3): p. 1-16.

[3] Fercher, E., et al. TWO YEARS EXPERIENCE WITH THE FICFB-GASIFICATION PROCESS.

[4] Hofbauer, H., et al. SIX YEARS EXPERIENCE WITH THE FICFB-GASIFICATION PROCESS. in 12th European Conference and Technology Exhibition on Biomass, Energy, Industry and Climate Protection. 2002. Amsterdam

[5] Saw, W.L., I.A. Gilmour, and S.S. Pang. The influence of contact time on the perfermance of a 100kW dual fluidized bed gasifier in steam gasification of woody biomass intern ational Conference on Polygeneration Strategies 11. 2011. Vienna, Austria.

[6] Hofbauer, H., et al., The FICFB Gasification Process. Developments in thermochemical biomass conversion, 1997. 2: p. 1016-1025.

[7] Bolhar-Nordenkampf, M. and H. Hofbauer. GASIFICATION DEMONSTRATION PLANTS IN AUSTRIA. in IV. International Slovak Biomass Forum. 2004.Bratislava

[8] Rüdisüli, M et al., Scale-up of bubbling fluidized bed reactors - A review. Powder Technology, 2012. 217(0):p 21-38.

[9] Van Ommen, J.R., et al., Computational validation of the scaling rules for fluidized beds.Powder Technology, 2006.163(1-2):p.32-40

[10] Authier, O. and J. Lédé, The image furnace for studying thermal reactions involving solids. Application to wood pyrolysis and gasification, and vapours catalytic cracking. Fuel, (0)

[11] Kaushal, P., T. Proll, and H. Hofbauer. Modelling and simulation of biomass fired duel fluidized bed gasifier at Gussing/Austria. in International Conference on Renewable Energies and Power Quality. 2007. Sevilla.

[12] Snider, D.M., S.M. Clark, and P.J. O'Rourke, Eulerian–Lagrangian method for three-dimensional thermal reacting flow with application to coal gasifiers. Chemical Engineering Science, 2011. 66(6): p. 1285-1295.

[13] Gómez-Barea, A. and B. Leckner, Modeling of biomass gasification in fluidized bed. Progress in Energy and Combustion Science, 2010. 36(4): p. 444-50

[14] Umeki, K., et al., High temperature steam-only gasification of woody biomass. Applied Energy, 2010. 87(3): p. 791-798.

[15] Gidaspow, D., Multiphase Flow and Fluidization Continuum and Kinetic Theory Description. 1994, Boston: Academic Press.

[16] Thapa, R.K., C. Rautenbach, and B.M. Halvorsen. Investigation of flow behavior in biomass gasfier using Electrical Capacitance Tomography (ECT) and pressure sensors. in International Conference on Polygeneration Strategies (ICPS). 2011. Vienna.

[17] Rautenbach, C., M.C. Maelaaen, and B.M. Halvorsen. Investigation of the shifting-parameter as a function of particle size distribution in a fluidized bed traversing from a fixed to fluidized bed. in Fluidization XIII. 2010. South Koria: Engineering Conference International.

[18] Halvorsen, B.M., An experimental and computational study of flow behavior in bubbling fluidized beds, in Process, Energy and Environmental Technology2005, Telemark University College: Norway.

[19] Boyalakuntla, D.S., Simulation of Granular and Gas-Solid Flows Using Discrete Element in Department of Mechanical Engineering 2003, Carnegie Mellon University.p.74.

[20] Cundall, P.A. and O.D.L. Strack, The discrete numerical model for granular assemblies. Geotechnique, 1979. 29: p. 47-65.

[21] Amsden, A.A., P.J. O'Rourke, and T.D. Butler, A computer Program for Chemically Reactive Flows with Sprays, 1989, Los Alamos National Laboratory

[22] Snider, D.M., An Incompressible Three-Dimensional Multiphase Particle-in-Cell Model for Dense Particle Flows.Journal of Computational Physics, 2001. 170(2): p. 523-549.

[23] Snider, D.M., Three fundamental granular flow experiments and CPFD predictions. Powder Technology 2007,176 (1).p.36-46

[24] Snider, D. and S. Banerjee, Heterogeneous gas chemistry in the CPFD Eulerian–Lagrangian numerical scheme (ozone decomposition).Powder Technology 2010,199(1).p.100-106

[25] Xie, J., et al., Eulerian–Lagrangian method for three-dimensional simulation of fluidized bed coal gasification. Advanced Powder Technology, 2013. 24(1): p. 382-392.

[26] Zanzi, R., K. Sjöström, and E. Björnbom, Rapid pyrolysis of agricultural residues at high temperature.Biomass and Bioenergy.2002. 23(5).p.357-366.

[27] Hofbauer, H., R. Rauch, and K. Bosch. Biomass CHP Plant Gussing - A Success Story in Expert Meeting on Pyrolysis and Gasification of Biomass and Waste.2002.Strasbourg, France.

R.K. Thapa has completed master’s degree in Process Technology from Telemark University College Norway in 2011. He has worked as a Research Assistant in Telemark University College under supervision of Prof. Britt Halvorsen in the field of Biomass gasification. At present he is pursuing his PhD degree in Optimization of flow behavior in biomass gasification reactor. He has presented and published six papers in international conferences and journals.
E-mail address: rajan.k.thapa@hit.no

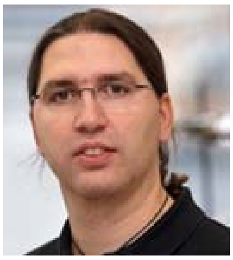

C. Pfeifer has got an education in Chemical Engineering from Vienna University of Technology and carried out his diploma as well his PhD thesis in the field of catalytic tar reforming by primary (in the dual fluidized bed gasification reactor) as well as by secondary measures (downstream fixed bed catalytic reactors).Starting 2005 he was responsible for the development of gasification technologies and the coordination of the pilot plants for gasification (pressurized bubbling fluidized bed gasifier, dual fluidized bed steam gasifier) as well as cold flow modeling of fluidized bed systems for gasification. Currently he is Professor at the University of Natural Resources and Life Sciences, Vienna in the field of Process Technology of Renewable Resources.
E-mail address: christoph.pfeifer@boku.ac.at

B.M. Halvorsen has her Master in Process Technology from Telemark University College. The PhD degree is from Norwegian University of Science and Technology and is in the field flow behavior in fluidized bed. Her research work includes both experimental and computational multiphase studies. She has worked within the field of fluidization since 2000. She is employed as Professor at Telemark University College in the field Process Technology.
E-mail address: britt.halvorsen@hit.no

Paper E

Influence of Size and Size Distribution of Biomass and Bed Material on Performance of a dual Fluidized Bed Gasification Reactor

The paper is presented in the 11th Internationl Conference on Fluidized Bed Technology, held on May 14-17, 2014 in Beijing China. The paper is published on proceedings of the conference edited by Jinghai Li, Fei Wei, Xiaojun Bao and Wei Wang.

INFLUENCE OF SIZE AND SIZE DISTRIBUTION OF BIOMASS AND BED MATERIAL ON PERFORMANCE OF A DUAL FLUIDIZED BED GASIFICATION REACTOR

R.K. Thapa[1], **C. Pfeifer**[2] **and B.M. Halvorsen**[1]

1. Institute for Process, Energy and Environmental Technology, Telemark University College, Norway

2. University of Natural Resources and Life Sciences, Vienna, Austria

Abstract – A computational fluid dynamic (CFD) model has been developed for the investigation of fluid dynamics and reaction kinetics in a dual fluidized bed biomass gasification reactor. Gas-solid flow and reaction kinetics are solved using Eulerian-Langrangian computational approach. Devolatilization of wood particles and chemical reactions: steam gasification, CO_2 gasification, methanation, water-gas shift and methane reforming are involved in the model. The effect of biomass and bed material size and size distribution on the performance of the reactor has been investigated. The efficiencies of the reactor as a result of different size distributions of fuel particles and bed materials are compared. The process parameters such as reaction temperature, steam/fuel ratio and fluidizing velocity are kept constant for all cases. It is observed that the efficiency of the reactor is higher with reduced particle size of biomass as well as of the bed material.

INTRODUCTION

Today, biomass has become the fourth largest source of energy after oil, coal and gas, contributing 14% of the demand in world energy market (Saxena et al.,2009). The neutral nature for CO_2 emission makes biomass even more attractive source in the context of greenhouse gas emission and global warming. However, the efficiency of the biomass-based energy technology has to be further increased in order to make the technology more sustainable. One of the promising technologies is gasification of biomass especially if using fluidized bed gasification reactors.

Dual fluidized bed gasification reactor is widely used in gasification of biomass for combined heat and power (CHP) production. The technology has also wide range of applications for synthesis processes leading to production of liquid and gaseous biofuels (Demirbas, 2008). The principle of the dual fluidized bed gasification process is shown in Figure 1. The basic idea behind the technology is to divide the reactor into two separate parts: combustion and gasification. Bed material is heated in combustion reactor and circulated to the gasification reactor. The bed materials are principally inert particles used for the heat transfer process from combustion reactor to gasification reactor. However it turned out that gas production is enhanced and reduced tar levels are achieved by proper selection of catalytically active bed materials such as olivine or calcite. Biomass fed to the gasification reactor is mixed with hot bed materials. As a result of the process, a mixture of combustible gases in addition to some CO_2 and water vapor are produced. The technology has been developed by Technical University of Vienna (TUV). The technology is demonstrated as a successful story in the example of the biomass CHP plant in Güssing, Austria (Fercher et al.,1998; Hofbauer et al.,2002) and is now duplicated several times throughout Europe.

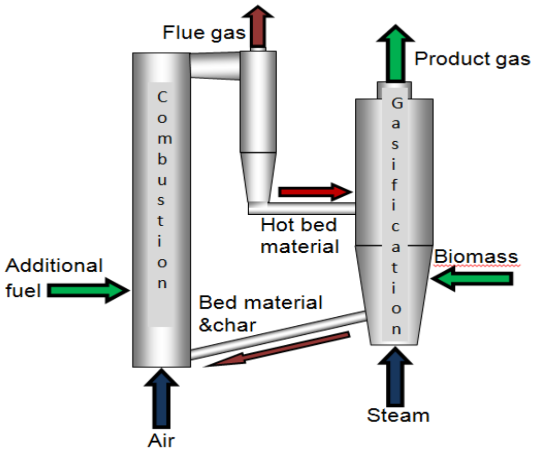

Fig.1. Principle of dual fluidized bed gasification process

In the dual fluidized bed gasification system, the gasification reactor is regarded as the heart of the technology. Fluid-dynamic properties and thermo-chemical processes in the reactor are responsible for the overall efficiency. There are a number of factors effecting on the fluid dynamics and reaction kinetics in the reactor. Study of these factors in an operating plant is difficult due to high temperature and other operating and economic reasons. A validated computational model could give an approximate answer to the many factors effecting on the efficiency of the plant. One of these factors is the size and size distribution of biomass (wood and char) particles and bed material. The current work is focused on investigation of the effect of biomass and bed material size on the performance of gasification reactor.

MODEL DESCRIPTION

In the model, the reactor is simplified to a single bubbling fluidized bed gasification reactor. The combustion part of the reactor is replaced by inlet and outlet of hot bed material as shown in Figure 2. The hot bed material is fluidized by high temperature steam. Biomass in the form of wood chips is fed to the reactor. The product gas leaves the reactor at the top. The model has the following major assumptions:

- Biomass (wood chips) feed to the reactor does not contain moisture. The biomass and char particles have uniform size distribution.
- All tars produced during the gasification process are modeled as higher hydrocarbons (C_3H_8). Sulphur, nitrogen and other minor components are neglected.
- Only global reactions and their kinetics are considered in the reactor.

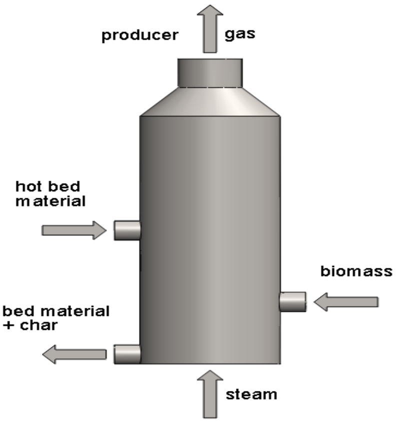

Fig.2. Model of gasification reactor

As the feed of biomass is assumed to be dry, it undergoes directly the process of devolatilization. This is the process of thermal decomposition of biomass in the absence of oxygen where the biomass is decomposed to char particles and gases. The process can be shown as in Equation 1 (Authier et.al.,2013). The composition of the gases depends on the operating condition of the reactor.

$$wood \xrightarrow{heat,gas agent} H_2, CO, CO_2, CH_4,\ tars,\ char(s) \qquad (1)$$

Table.1: Elemental analysis of wood

Elements	Wt.%
Carbon, C	48.6
Hydrogen, H	5.6
Oxygen, O	45.6
Nitrogen, N	0.2

The type of wood used in this work is birch. The wood is considered as a virtual compound with its elemental analysis given in Table 1 (Zanzi et.al.,2002). The next step includes heterogeneous and homogenous reactions. Steam gasification, the reaction of char particles with steam is the main reaction of gasification process. Along with the steam gasification, the char particles react with CO_2 and H_2. These reactions are known as carbon dioxide gasification and methanation respectively and they are much slower than the steam gasification. Homogenous reactions are water-gas shift and methane reforming. The latter is much slower than the former. The reactions with the corresponding reaction kinetics are presented in Table2. The higher heating value of the wood is 17.07 MJ/kg (Zanzi et.al.,2002). The model evaluates the reaction kinetics with changing particle size of the biomass and bed material. It is expected that the change in biomass size affects much in the thermo-chemical conversion while the change in particle size of bed material mainly effects on the fluid dynamic behavior in the bed. The fluid dynamics of the bed is responsible for heat transfer between biomass, bed material and fluidizing gas which consequently effect to the reaction kinetics in the reactor.

Table. 2: Reactions included in the reactor and their kinetic equations.

Reactions	Reaction kinetics	Reference
Steam gasification $C + H_2O = H_2 + CO$	$r_1 = 2.7\times10^7 m_s P^{0.73}\theta_f \exp\left(\frac{-26506}{T}\right)[H_2O]$	(Umeki et.al. 2010)
Carbon-dioxide gasification $C + CO_2 = 2CO$	$r_2 = 1.12\times10^8 m_s P^{0.31}\theta_f \exp\left(\frac{-29518}{T}\right)[CO_2]$	(Umeki et.al. 2010)
Methanation $0.5C + H_2 = 0.5CH_4$	$r_3 = 1.368\times10^{-3} m_s T \exp\left(\frac{-8078}{T} - 7.087\right)[H_2]$	(Xie et.al 2013)
Water- gas shift reaction $CO + H_2O = CO_2 + H_2$	$r_4 = 7.68\times10^{10} m_s T \exp\left(\frac{-36640}{T}\right)[CO]^{0.5}[H_2O]$	(Xie et.al 2013)
Methane reforming $CH_4 + H_2O = CO + 3H_2$	$r_5 = 3.0\times10^5 T \exp\left(\frac{-15042}{T}\right)[CH_4][H_2O]$	(Xie et.al 2012)

COMPUTATIONAL MODEL

Eulerian-Lagrangian approach is implemented for the modeling of gas-solid flow and chemical reactions in the gasification reactor. Governing equations of the fluid phase are solved using continuum model. The particle phase is solved using the Lagrangian model. More details of the computational approach can be found in (Snider,2001). The computational approach takes into account particle-particle, particle-wall and fluid-particle interaction forces (Boyalakuntla,2003). This approach solves the gas solid reacting flow with wide range of particle size distribution which makes the approach more accurate for gas-solid flow simulations. The fluid dynamic behavior in the bed changes significantly even with a small change in particle size and size distributions. Three dimensional simulations of gas-solid reacting flow are performed using commercial Computational Particle Fluid Dynamic (CPFD) software, Barracuda VR 15.

Some important operating parameters used in the simulation are presented in Table 3. The operating parameters effect the composition and heating value of product gas (Zainal,2010). All of the operating parameters presented in Table 3 are kept constant. The bed material is treated as inert particles and carrier of heat energy for endothermic gasification reaction. Catalytic effects of the bed materials are not considered. The aim is to study only the effect of particle size.

Table.3: Parameters used in simulation

Parameters	Units	Value	Parameters	Units	Value
Bottom steam feed rate	kg/h	112	Biomass feed rate	kg/h	112
Steam feed temperature	K	1073	Biomass inlet temperature	K	400
Fluidization velocity	m/s	0.64	Bed material circulation rate	kg/h	5980
Reaction temperature	K	1100 - 1130	Bed material inlet temperature	K	1150
Reactor diameter	m	0.55	Reactor height	m	2
Initial bed height	m	0.60	Wood feed position from the bottom of the reactor	m	0.15

The model is required to be validated against real data in order to be sure that the prediction of the model is acceptable. A simulation is performed with a range of size distribution of biomass and bed material in order to compare the result with the measured gas composition from the Güssing plant.

A series of simulations are performed with constantly increasing size of wood particle keeping the size of bed material constant. The biomass is divided into 6 different groups of size as shown in Table 4. The overall range of biomass is from 1 mm to 25 mm.

Similarly another series of simulation are performed with increasing size of bed material, keeping the size of wood particles constant. The bed materials are divided into 4 groups with a wide range of size distribution. The size of bed materials are ranging from 300µm to 1200 µm. In the all cases, the operating parameters given in Table 3 are kept constant.

Table. 4: Biomass and bed material sizes

Case	Biomass Size [mm]	Bed material size [µm]	Case	Biomass Size [mm]	Bed material size [µm]
0	1-12	200-800	6	6-10	300-600
1	1-5	200-800	7	6-10	450-750
2	6-10	200-800	8	6-10	600-900
3	11-15	200-800	9	6-10	900-1200
4	16-20	200-800			
5	21-25	200-800			

RESULTS AND DISCUSSION

Each set of simulation is performed for 300s of real time. The mass flow rate of the product gases are monitored at the different planes along the height of the reactor. The accumulated mass flow of the gas is also monitored at the same planes during 300s. The gases leaving the top of the reactor are monitored for each case and the volume flow rates and the higher heating value (HHV) of the product gases are calculated.

The volume flow rate of the simulation case 0 presented in Table 4 is compared with the measured volume percent of product gas from the gasification plant in Güssing, Austria. The results are shown in Table 5.

Table.5: Comparison of gas composition

Product gas components	Simulated vol%	Measured vol%
Hydrogen (H_2)	35	32
Carbon monoxide (CO)	25	25
Carbon dioxide(CO_2)	23	22
Methane (CH_4)	13	12

The results show good agreements between simulated gas compositions and the Güssing plant measurements. The deviation between the model prediction and measured data is from 0 to 9% for the individual component of the product gas. Simulation case 0 is only used to validate the model prediction with the plant data.

The effect of biomass size on the product gas outflow has been investigated using the results of the simulation cases from 1 to 5 as presented in Table 4. First, the effect of increasing biomass size on the heating value of the product gas has been analyzed. Figure 3 shows the higher heating value of product gas as a function of biomass particle feed size. The higher heating values (HHV) of the product gas are decreasing with the increasing biomass particle feed size. In the simulation cases 1, 2 and 3, decrease in HHV with biomass particle size is almost linear and significant. The particle size range is 1mm to 15mm. But in the simulation cases 4 and 5, the change in HHV of product gas is very small and insignificant. The biomass particle size is 16 mm to 25 mm.

Figure 4 shows the accumulative volume flow of the product gas components during 300s of simulations. The gas components studied here are only the product gases having heating values. The volume of product gas components also decreased with increasing particle size of biomass feed. This is obvious that the decrease in all product gas volume is the reason for the decreasing HHV of the gas. The volume flow of product gas in the simulation case 4 and 5 does not change significantly.

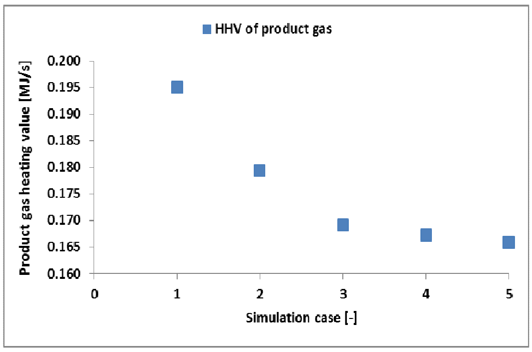

Fig.3. HHV of product gas leaving the reactor

What happening inside the reactor is devolatilization of the wood particle and simultaneous gasification of char particle in the presence of steam as a fluidizing gas. There are mainly two reasons behind the change in the gas flow rate. The first reason is increasing particle size of the wood requires more heat energy. Requirement of more energy increases the residence time of the wood particle, making the devolatilization process of wood particle slow. In addition to this, the larger particle requires more time to reach the bed temperature than the smaller particles. The contours of particle volume fraction of wood are presented in Figure 5. The contours show location and concentration of reacting wood particles in the reactor at a given time. In the first case of simulation , the particle size of wood is smallest (1mm-5mm) and the fraction of wood in the reactor is very small while in the case 5 of simulation, the particle feed size is largest (20mm-25mm) and the concentration of the wood particle is also highest. The concentration of wood particle increases with the increasing size of the wood particle. The contours also show that the accumulated wood particles are concentrated mainly near the top of the dense bed even though the particles are fed from the bottom of the reactor.

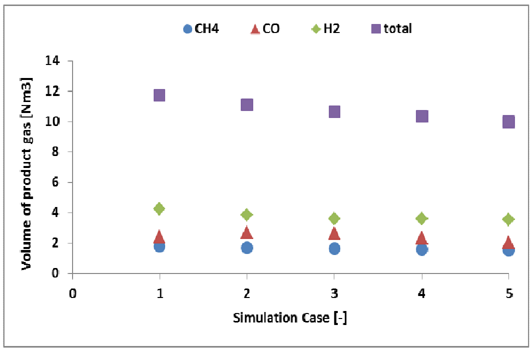

Fig.4. Accumulative volume of product gas during 300s of simulation

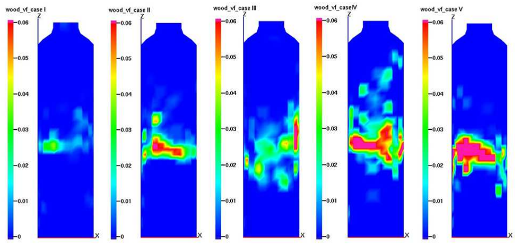

Fig. 5. Volume faction of wood particle at simulation time of 300s. Simulation cases 1 to 5 from left to right

Larger particle size of wood after devolatilization results in larger char particles as well. The larger char particles require more heat energy for gasification and thereby higher residence time for char gasification. The contours of char particle volume fraction in Figure 6 shows increasing char particle concentration in the bed with the simulation cases of increasing feed size of biomass particles. The concentration area of accumulating char particles is also near the top of dense bed.

The second reason is proper mixing of bed material, wood/char particle and fluidizing steam in the bed. The optimized supply of the energy required for devolatilization of wood particles and endothermic gasification reactions depends on the good mixing of the wood/char particles with bed material. The fluid dynamic properties are responsible for the mixing of the bed material, fuel particle and fluidizing steam. On the other hand, the fluid dynamic properties change significantly with the particle size and size distribution of particles in the bed.

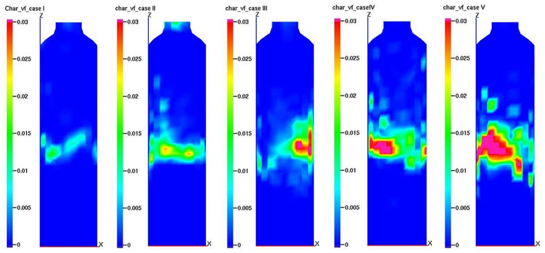

Fig.6. Volume fraction of char particle at simulation time 300s. Simulation case 1 to 5, from left to right

In the simulation cases 1 to 5, the particle size of bed material and velocity of fluidizing gas are fixed with constant circulation rate and temperature of the bed material. Even though the gas velocity is constant, the minimum fluidization velocity of the bed changes significantly with the change in particle size and size distribution.

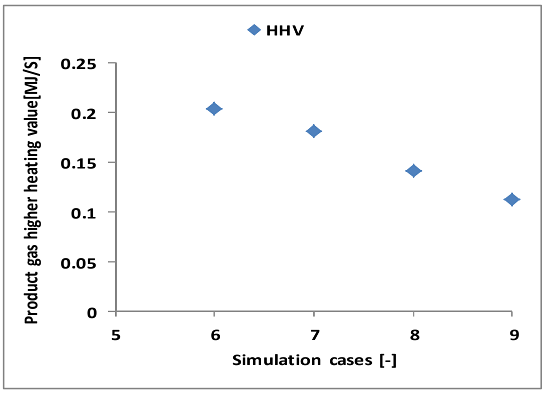

Fig. 7. HHV of the product gas as a function of the size of bed material

In the gasification reactor, there is a mixture of bed materials, wood particles and char particles. As the concentration of wood/char increases in the bed, the bed becomes a mixture of particles with three different densities with wide range of size distribution. The particle size and size distribution is different for each case of the simulation due to different concentration of wood/char particle in the bed as shown in Figures 5 and 6. The ratio of u_0/u_{mf} is about 4 for the first simulation case. As the concentration of wood/char particle increases in the bed, the ratio of u_0/u_{mf} also increases depending on the volume percent of lighter particles with larger particle size (Thapa, R.K. et al., 2011). This may enhance the particle mixing in the simulation cases 4 and 5. The effect of wood particle size on the gas flow rate and the reaction kinetics is nonlinear as shown by Figure 3 and 4. This fact tells that the size and size distribution of biomass particle should be taken into account along with the particle residence time in the reactor.

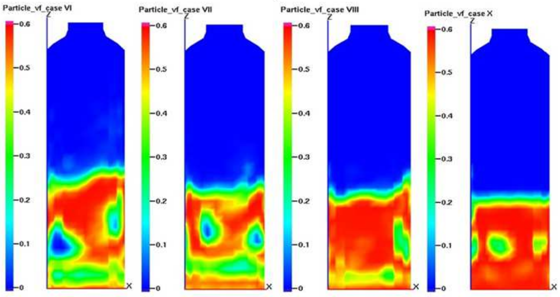

Fig. 8. Volume faction of bed material. Simulation cases 6 to 9 from left to right.

The large fraction of the bed is the bed material followed by wood particles and then char particles. Therefore, the particle size of the bed material has dominating effect on the flow behavior of the bed until the concentration of biomass particle in not increased significantly.

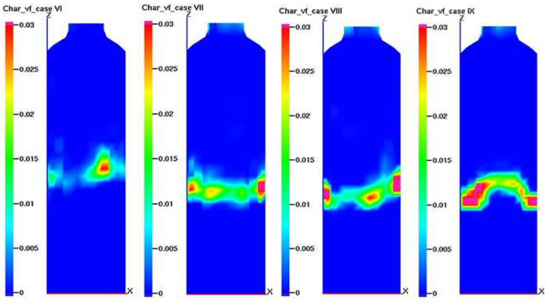

Fig. 9. Volume faction of char particle at simulation time of 300s. Case 6 to 9, from left to right

Simulation cases 6 to 9 presented in Table 4 are performed to check the effect of bed material size and size distribution on the product gas flow rate. Figure 7 shows a reduction of the heating value of the product gas with increasing size of bed material. The fluid dynamic properties in the bed changes significantly even with small changes of particle size. This is the reason for linear decrease of the product gas flow rate and consequently the corresponding HHV. The ratio u_0/u_{mf} decreases with increasing particle size of the bed material. Reduced the ratio of u_0/u_{mf} has a negative effect on the mixing of bed material, wood/char particles and fluidizing gas. Figure 8 shows the volume fraction of bed material with increasing particle size. The volume fraction increases continuously from the simulation case 6 to 9 causing less mixing of wood/char particles and fluidizing gas with the bed material. The increasing concentration of the char particle from simulation case 6 to 9 also shows the reduced mixing of the bed. This can be also seen from the concentrated location of char particles in the beds. The char particles are accumulating at the very narrow area in the bed. The fluidization velocity of the bed strongly varies with the particle size of the bed. In order to enhance mixing in the bed with large particle size, the fluidization velocity needs to be increased. Increase in fluidization velocity causes increase in fluidizing gas, steam. When the gas velocity is changed, the result may have totally different characteristics. However, the effect of gas velocity on the performance of the reactor is not studies in this work.

CONCLUSION

A series of simulations has been performed to investigate the effect of biomass and bed material particles size on the product gas composition and consequently corresponding heating value of a bubbling fluidized bed reactor for gasification. The simulated gas composition of the product gas is compared with the measured plant data from the biomass gasification plant in Güssing, Austria. The gas composition shows good agreements.

The simulation results show that the gas production rate and the HHV of product gas decreases with increasing fuel size and size distribution. The HHV of product gas does not change significantly when the feed size of biomass particles become much higher.

The product gas rate and HHV of the product gas decreases linearly with particle size of the bed material. The results show that the performance of the gasification reactor depends strongly on particle size of both biomass and bed material. It is necessary to account particle size and size distribution in designing the gasification reactor and defining its operating conditions.

REFERENCES

Authier, O., Lede, J. 2013.The image furnace for studying thermal reactions involving solids. Application to wood pyrolysis and gasification and Vapour catalytic cracking. Fuel.107.555-569.

Boyalakuntla, D.S., Simulation of Granular and Gas-Solid Flows Using Discrete Element.in Department of Mechnical Engineering 2003, Carnegie Mellon University.p.74.

Demirbas, A. 2008. Biofuel sources, biofuel policy, biofuel economy and global biofuel projections. Energy Conversion and Management.49.2106-16.

Fercher, E., Hofbauer, H., Flek, T., Rauch, R., Veronik, G. 1998. Two years' experience with The FICB-Gasification Process.10th European conference and Technology Exhibition.Wurzburg.

Hofbauer, H., Rauch, R., Loeffler, G., Kaiser, S, Fercher, E, Tremmel, H. 2002.Six Years' Experience With The FICB-Gasification Process. 12th European Conference and Technology Exhibition on Biomass for Energy, Industry and Climate Protection. Amstradam.

Saxena, R.C., Adhikari, D.K., Goyal, H.B.2009. Biomass-based energy fuel through biochemical routes.A review. Renewable and Sustainable Energy Reviews.13(1).167-178.

Snider, D.M. 2001. An Incompressible Three-Dimensional Multiphase Particle-in-Cell Model for Dense Particle Flows.Journal of Computational Physics. 170(2): p. 523-549.

Thapa, R.K., Rautenbach, C. , B.M. Halvorsen. 2011. Investigation of flow behavior in biomass gasfier using Electrical Capacitance Tomography (ECT) and pressure sensors. Proceedings of International Conference on Polygeneration Strategies (ICPS), Vienna.p.97-106.

Umeki, K., Yamamoto, K., Namioka, T., Yoshikawa, K.2010. High temperature steam only gasification of woody biomass. Applied Energy. 87.791-798.

Xie J., Zhong, W., Jin, B., Shao, Y., Huang, Y. 2013. Eulerian-Lagrangian method for three-dimensional simulation of fluidized bed coal gasification.Advanced Powder Technology.24.382-392.

Xie J., Zhong, W., Jin, B., Shao, Y.,Liu, H. 2012.Simulation on gasification of forestry residues in fluidized beds by Eulerian-Langrangian approach.Bioresource Technology.121.36-46.

Zainal, A., Lahijani, P. Mohammadi, M. 2010. Gasification of lignocellulosic biomass in fluidized beds for renewable energy development: A review.

Zanzi, R., Sjöström, K., Björnbom, E. 2002.Rapid pyrolysis of garicultural residues at high temperature. Biomass & Bioenergy. 23. 357-366.

Paper F

Stepwise analysis of reaction and reacting flow in a dual fluidized bed gasification reactor

The paper is published in WIT Transaction on Engineering Sciences, Vol. 82, pp 37-48, 2014, WIT press. ISSN 1743-3533 (online). Doi:10.2495/AFM 140041

Stepwise analysis of reactions and reacting flow in a dual fluidized bed gasification reactor

R. K. Thapa & B. M. Halvorsen
Institute for Process, Energy and Environmental Technology,
Telemark University College, Norway

Abstract

Dual fluidized bed gasification reactors are used in a wide range of biomass conversion processes. Some of the important processes are steam gasification of biomass for combined heat and power (CHP) production and synthesis processes leading to production of liquid and gaseous biofuels. Gas-solid multiphase flow and thermochemical processes are responsible for overall performance of the reactor. The multiphase flow involves reacting flow of solids (biomass and bed materials) with gases (steam and product gas components). The thermochemical process involves devolatilization of wood followed by steam gasification, CO_2 gasification, methanation, water gas shift and methane reforming. In order to optimize the performance of the reactor, it is important to study each of the global reaction and their reacting flow separately.

A computational model has been developed to study the reaction kinetics and the reacting flow in a dual fluidized bed gasification reactor. The model has been validated against the measurements of gas composition in an operating plant for biomass gasification. The reactions are simulated individually using commercial Computational Particle Fluid Dynamic (CPFD) software Barracuda VR 15. The results of simulations such as product gas compositions (CO, CO_2, CH_4, and H_2), wood particle volume fraction and char particle volume fractions are compared for each individual reaction. The results show each of the global reaction contributes to the product gas composition differently. The volume fractions of wood and char particles show that the residence time of wood and char particle in the reactor is different for different reactions. The contribution of devolatilization, steam gasification and water-gas shift in the product gas heating value is more significant than others.

Keywords: biomass gasification reactor, dual fluidized bed, CPFD, steam gasification, reaction kinetics, reacting flow.

WIT Transactions on Engineering Sciences, Vol 82, © 2014 WIT Press
www.witpress.com, ISSN 1743-3533 (on-line)
doi:10.2495/AFM140041

1 Introduction

Biomass is a renewable source of energy that does not contribute to greenhouse gas emission. Moreover, emission of sulphur and nitrogen compounds from the biomass is less in comparison to coal [1]. These factors make biomass an attractive source of energy. Wood is the largest representative among the biomass [2]. The energy recovery from the biomass is possible through the thermo-chemical conversion processes such as pyrolysis and gasification. Actually, pyrolysis is also a part of the gasification process. The gasification process mainly occurs in two stages: first devolatilization (pyrolysis) of biomass and then char conversion [3]. Char conversion can be achieved through the gasification of the char using gasification agents. The gasification agents can be air, oxygen, carbon-dioxide and steam. There are different types of gasification reactors such as fixed bed, moving bed and fluidized bed. Fluidized bed reactors are most popular among them due to their high heat and mass transfer rates that result in high rate of product gas. Among the different fluidized bed gasification reactors, steam gasification of wood in dual fluidized bed is one of the promising technologies for biomass conversion.

Dual fluidized bed gasification reactors are used in wide range of biomass conversion processes. Some of the important processes are gasification of biomass for combined heat and power (CHP) production and synthesis processes leading to production of liquid and gaseous biofuels [4, 5]. The principle of dual fluidized bed gasification process is shown in Figure 1.

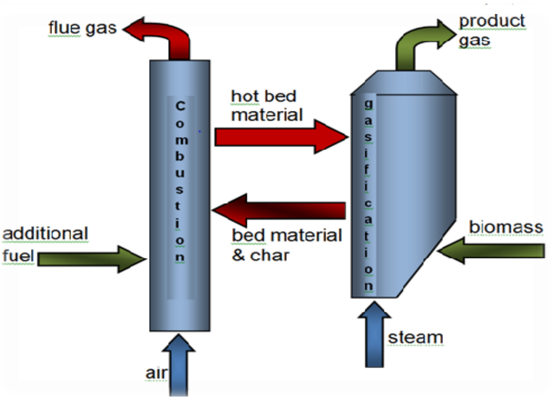

Figure 1: Principle of dual fluidized bed gasification technology.

The reactor is divided into two separate zones: combustion and gasification. The combustion zone is a circulating fluidized bed reactor. The fluidizing gas is air. In the combustion zone, inert bed materials such as olivine particles or quartz sand are heated by burning fuels. The heated bed material is then circulated to the gasification reactor. The purpose of the recirculation of bed material is to supply necessary heat for the endothermic gasification reaction in the gasification zone.

The gasification zone is a bubbling fluidized bed reactor for steam gasification of biomass. The fluidizing gas is a high temperature steam. Biomass feed to the gasification reactor is mixed with hot bed materials. The biomass in the reactor is dried and devitalized to produce volatile gases and solid char particles. The char particles further react with steam to produce a mixture of combustible gases in addition to some CO_2 and water vapour. The technology is developed by Vienna University of Technology in Austria. The technology is demonstrated as a successful story in the example of the biomass CHP plant in Güssing, Austria [6].

Despite the novelty of the technology, the efficiency of the technology needs to be increased in order to make it sustainable and competitive in the world energy market. It is believed that the thermo-chemical process inside the gasification rector is one of the major factors that can increase the performance of the reactor significantly. The thermo-chemical process inside the reactor depends on a number of operating parameters as well as the design of the reactor. Experimental study of the thermo-chemical behaviour has been difficult due to high operating temperature in addition to time consumption and material costs related to the requirements of constructing hot models and pilot plants. The design of the reactor needs to be changed in order to study feed location of bed material and biomass. Therefore, taking a benefit of rapidly growing computational prediction methods such as CPFD simulation is a fast and economic way to study and optimize the reactors. This work is focused on the analysis of thermochemical process in the gasification reactor and the effect of fluid-dynamic parameters on the process.

2 Gasification reactions

In the dual fluidized bed gasification system, the gasification reactor is regarded as the heart of the system. Fluid-dynamic properties and the thermo-chemical process in the gasification reactor are responsible for the overall efficiency of the reactor. The thermo-chemical process in the gasification reactor constitutes several reactions. Identification of all the reactions and their kinetics and simulating them are almost impossible [7]. However the processes can be virtually divided into a group of separate sub-process which constitutes the major global processes.

Devolatilization is the first step of the biomass gasification. First, the biomass is dried and then it undergoes the process of devolatilization. The process is endothermic. All necessary heat for the process is supplied by the hot bed materials which circulate between two zones of the reactor.

The quantity and quality of volatiles produced in this process significantly affect the overall gas composition of the final product gas. The heating value of the product gas depends on its composition.

The biomass investigated in this work is wood chips. The wood is assumed as a virtual chemical compound with the elemental analysis given in Table 1 [8].

Table 1: Elemental analysis of wood.

Elements	Wt.%
Carbon, C	48.6
Hydrogen, H	5.6
Oxygen, O	45.6
Nitrogen, N	0.2

The elements included in the table are only the major elements with significant weight fraction.

The ash content (composition of elements such as potassium, calcium, sodium, silicon, phosphorous and magnesium) in wood is less than 1% [9]. The nitrogen content of the wood is 0.2%. For the simplicity of modelling all these minor components are neglected. Finally, the process of devolatilization of the wood can be modelled as shown in Equation (1).

$$C_xH_yO_z = aCH_4 + bCO + dCO_2 + eH_2 + fC_xH_y + gC + hH_2O \qquad (1)$$

The kinetics of devolatilization is assumed as given by equation (2).

$$r_0 = 264000\ m_s\ \theta_f \exp\left(\frac{-12629}{T}\right) \qquad (2)$$

The kinetics of the conversion process depends on the structure of the biomass and the heat and mass transfer inside the biomass particles [10]. Temperature, pressure and heating rate are the main operating parameters.

The second step of the gasification process is the char gasification. The reaction of char particles with fluidizing steam is the major process of char conversion. Hence the name of the process is steam gasification. The char particles also react with the CO_2 and H_2 gases produced during devolatilization of the wood. The major global reaction and reaction kinetics are given in Table 2 [11, 12].

Char yield and char reactivity are important in determining the capacity of the gasification reactor [8]. Minimum residual char production and maximum reactivity of char makes the reactor more efficient.

The chemistry described in the Table 2 is specified as mass action kinetics [13]. The reactions are described by stoichiometric equations and their rates. The effect of particle concentration on the reaction rate will be included within the reaction coefficient k. During the overall process of gasification, the biomass particles are heated from just above the ambient temperature up to the gasification reaction temperature (about 850°C) [14].

Besides the heterogeneous char gasification, the third step of the process is homogeneous gas-gas reaction. This step involves water-gas shift reaction and methanation. Starting with the devolatilization of wood, all the reactions are simulated individually in order to study their contribution to the whole biomass steam gasification process.

Table 2: Reaction kinetics used in the simulations.

Reactions	Reaction kinetics
Steam gasification $C+H_2O=H_2+CO$	$r_1 = 2.7\times10^7 m_s\, P^{0.73}\theta_f \exp\left(\frac{-26506}{T}\right)[H_2O]$
Carbon-dioxide gasification $C+CO_2=2CO$	$r_2 = 1.12\times10^8 m_s\, P^{0.31}\theta_f \exp\left(\frac{-29518}{T}\right)[CO_2]$
Methanation $0.5C+H_2=0.5CH_4$	$r_3 = 1.368\times10^{-3} m_s T \exp\left(\frac{-8078}{T}-7.087\right)[H_2]$
Water- gas shift reaction $CO+H_2O=CO_2+H_2$	$r_4 = 7.68\times10^{10} m_s T \exp\left(\frac{-36640}{T}\right)[CO]^{0.5}[H_2O]$
Methane reforming $CH_4+H_2O=CO+3H_2$	$r_5 = 3.0\times10^5 T \exp\left(\frac{-15042}{T}\right)[CH_4][H_2O]$

3 Model description

There is an increasing application of Computational Fluid Dynamics (CFD) modelling approach in the prediction of gas-solid multiphase flow. Eulerian-Eulerian and Eulerian-Langrangian are the two approaches commonly used in the CFD modelling. The difference between the two approaches lies in the modelling of gas-solid interaction.

In the Eulerian-Eulerian approach, the solid particles are considered as continuous phase interpenetrating and interacting with the gas phase. Both the fluid and solid are averaged by a statistical procedure. The averaging procedure creates many unclosed terms [7]. In order to close the terms, constitutive equations are required for particle phase as well as the particle gas interactions. These constitutive equations are derived from the kinetic theory of granular flow [15]. There are mainly two short-comings related to this approach. The closure models describing the mass, momentum and energy transfer between multiple continuous phases are complicated and not universally valid [16]. Separate closure models are valid only for mono-dispersed particles which makes it almost impossible to solve the multiphase flow with a wide range of particle sizes [7].

Eulerian-Langrangian approach tracks individual particles in time and space. The equations of mass, energy and motion are solved for individual particles. The approach offers the most accurate description of the particle motion (translational, rotational and particle-particle collision), chemical reaction and heat-mass transfer between the dispersed phase and the gas phase at the individual particle scale.

There are quite a lot of publications describing inert particle simulations using DEM model but only few describing particle systems involving heat and mass transfer and chemical reactions. In thermal reacting flows, the size of the particles changes due to devolatilization and gasification. Moreover rates of reactions and fluid temperatures depend on the solid surface areas, types of solid materials and discrete solid temperatures [7].

The CPFD numerical methodology incorporates the multi-phase particle in cell (MP-PIC) method for calculating dense particle flows. The CPFD method is a hybrid numerical method, where the fluid phase is solved using Eulerian computational grid and the solids are modeled using Langrangian computational particles. In MP-PIC, an isotropic particle stress gradient is added to the equation of motion of the particles. This addition enables the method to calculated flows of particles with any volume fraction from the dilute to the closed packed limits [17, 18].

In order to apply CPFD methodology for heat transfer and chemistry with solid material pyrolysis, an enthalpy equation is solved to calculate flows with large chemistry-induced temperature variations. The bed in the gasifier has a complex gas and solid flow patterns that help determine the gas-solid and gas-gas chemical conversion rates [7].

The CPFD methodology solves the fluid and particle equations in three dimensions. The fluid dynamics is described by averaged Navier-Stokes equations with strong coupling to the particle phase.

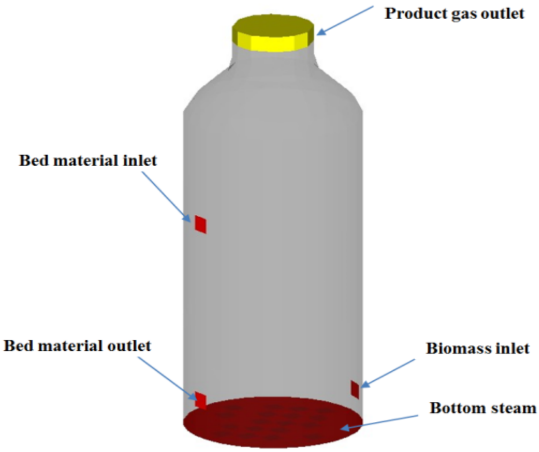

Figure 2: Model of gasification reactor.

The CPFD numerical methodology has been applied in this work. The aim of this work is to study the thermo-chemical process in the gasification zone. The reactor is modelled as bubbling fluidized bed reactor. The combustion zone is replaced by input and output of bed material to the gasification reactor as shown is Figure 2. The simulation parameters and boundary conditions applied in the simulations are presented in Table 3.

Table 3: Parameters used in the simulations.

Parameter	Unit	Value	Parameter	Unit	Value
Bottom steam feed rate	kg/h	112	Biomass feed rate	kg/h	112
Steam feed temperature	K	1073	Biomass inlet temperature	K	400
Fluidization velocity	m/s	0.64	Bed material circulation rate	kg/h	5980
Reaction temperature	K	1100 - 1130	Bed material inlet temperature	K	1150
Reactor diameter	m	0.55	Reactor height	m	2
Initial bed height	m	0.60	Wood feed position from the bottom of the reactor	m	0.15

4 Results and discussion

A series of simulations have been performed for the individual reactions occurring in the gasification reactor. The reaction sequences involved in the separate simulations are presented in Table 3.

Table 4: Reaction sequences involved in the simulations.

SN	Reactions
1	Volatilization
2	Volatilization + steam gasification
3	Volatilization + CO_2 gasification
4	Volatilization + methanation
5	Volatilization + water gas shift reaction
6	Volatilization + methane reforming
7	Total reactions

The sequences are further used as reaction sequence number 1, 2, 3, 4, 5, 6 and 7 for the description of the simulations.

The initial step of the simulation is volatilization of biomass which is the preliminary step for the rest of global reactions. Each of the reactions is simulated for the identical operating conditions and parameters. The simulations were run for 300s of real time. The volume percent of accumulated product gases are monitored during the simulation. The results of the simulation for reaction sequence 7 are used to calculate the product gas volume percent in dry basis. The volume percentages of the gases are compared with real data from the biomass gasification plant in Güssing, Austria. The results show a reasonable agreement between simulation and plant data.

During the simulation time, the accumulated quantities of gas species leaving the reactor are monitored. The accumulated gas compositions for each of the reactions are compared in Fig. 4. The reaction sequence is the same as given in Table 3. The simulation sequence 1 represents the volatilization of wood chips.

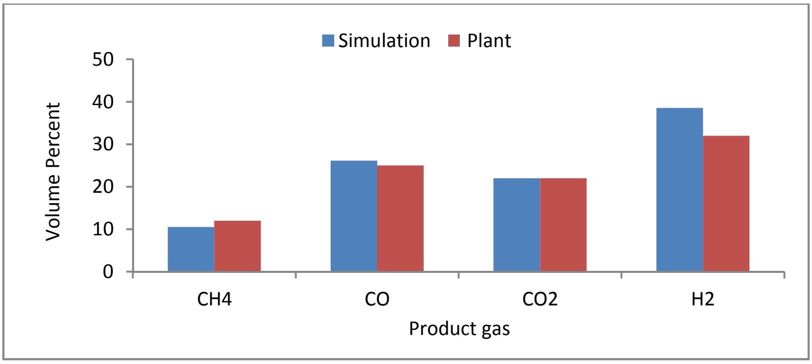

Fig. 3: Comparison of gas volume fraction of simulation with plant data

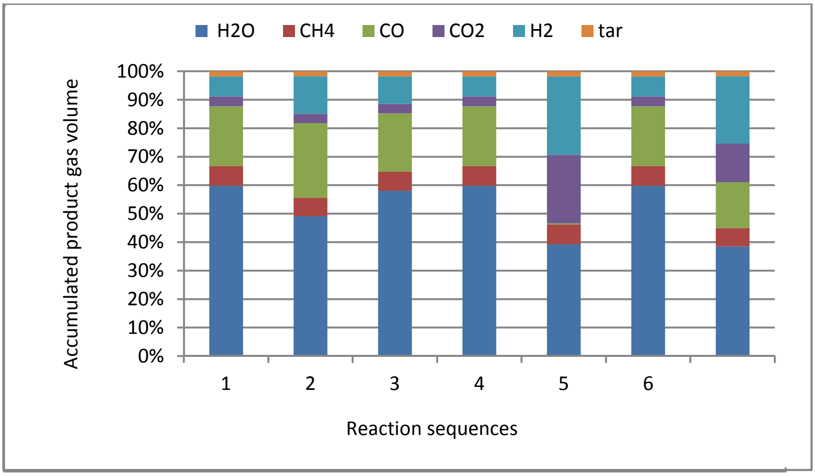

Figure 4: Accumulated volume percent of gas composition.

The steam to fuel ratio for the simulation is 1 and this ratio is one of the important parameters of the steam gasification process. Insufficient amount of steam in the reactor will have a negative effect on the product gas composition. Excess steam into the reactor makes excess amount of steam in the product gas. On the other hand, steam acts as fluidizing gas and the flow behavior and fluidization properties depend on the steam flow rate. Figure 4 shows that the maximum percent of steam occurs in the product gas in the stage of volatilization. The significant decrease in the steam indicates the steam consumption in the simulation sequences 2, 5 which are the steam gasification and water-gas shift reaction. Only small amount of steam is used for CO_2 gasification. The major part of methane is formed during the volatilization of the biomass.

Most of the CO gas is produced during volatilization and steam gasification reaction and a significant part is consumed during water gas shift reaction contributing to increase the content of H_2 and CO_2. The volatilization, steam gasification and water-gas shift reactions are responsible for further hydrogen formation. A significant percentage of the hydrogen is formed during the water-gas shift reaction. The amount of hydrocarbons as tar does not change since their reactions are not considered in the model.

The contours of particle volume fraction of wood and char are presented in Figure 5 and Figure 6 respectively. The contours are snap shots at the simulation time of 300s.

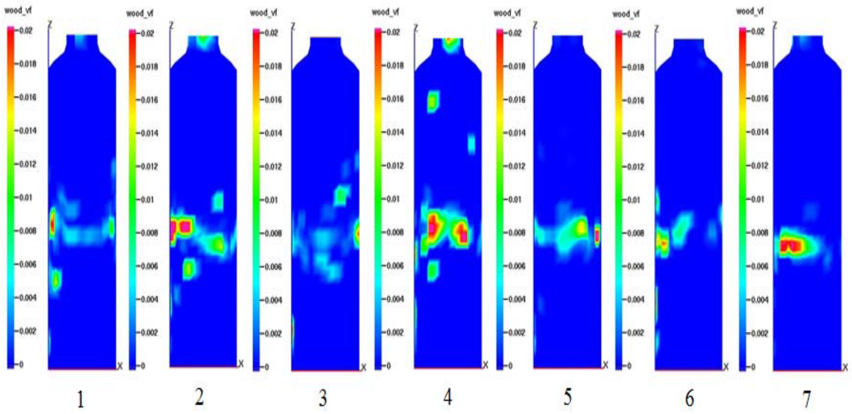

Figure 5: Contours of wood particle volume fraction at simulation time 300s.

Important information of the behavior of the reacting solid particles can be found from the contours of their volume fraction. The first obvious information is the major part of unreacted wood particles is floating on the top of the dense bed. The bed material and wood particles does not seem to be well mixed as required by the properties of fluidized bed system. The steam, biomass and bed material feeding velocities, biomass and bed material feeding positions, gas particle densities and reactor geometry are some of the parameters that can be optimized to get the desired mixing. The contours of char volume fraction shown in Figure 6 are different for the different reactions. The similarity between them is that the char particles are mainly located on the top of the bed.

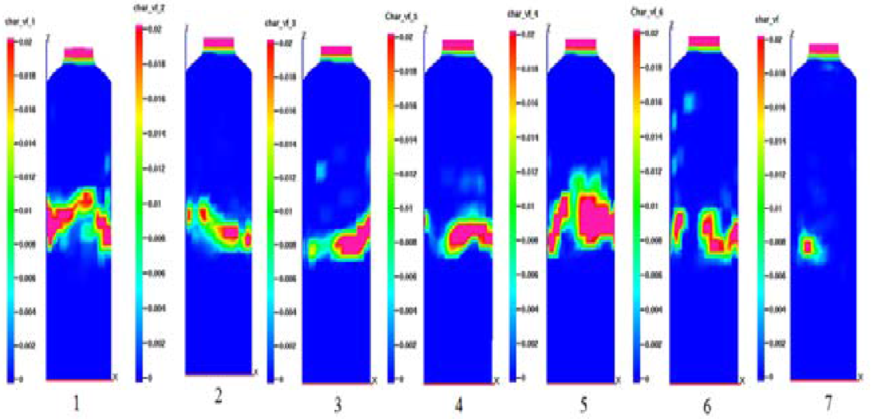

Figure 6: Contours of char particle volume fractions at simulation time of 300s.

Reaction sequence 1 is only volatilization and no char conversion is taken place. Consequently the volume fraction of char is high in this case. The high char particle volume fraction on reactions sequence 5 and 6 indicate low char conversion. The char particle volume fraction on steam gasification (sequence 2) is less than that of CO_2 gasification and methanation (sequence 3 and 4) indicating that the steam gasification reaction is responsible for more char conversion. The total reaction (sequence 7) shows that the maximum conversion of char is obtained when all the reactions are included.

The contours of char particles in all reactions show the accumulation of the particles on the top of the bed indicating the insufficient mixing between char and bed materials. The exact experimental evidence of bed material and wood/char mixing phenomenon in reacting flow is not found easily in the published literatures. Consequently, the result of the work also indicates the need of further investigation of mixing and segregation of particles in fluidized bed reactors.

5 Conclusion

A series of simulations have been performed to investigate the individual reactions involved in biomass steam gasification in a dual circulating fluidized bed gasification reactor. The reactions such as steam gasification, CO_2 gasification, methanation, water-gas shift reaction and methane reforming reactions are simulated along with the volatilization of biomass. The simulation parameters such as biomass and bed material circulation rates, bottom steam feed rate, fluidization velocity and reaction temperature are kept constant for all reactions. The contribution of the different reactions on the production of combustible gases (H_2, CO and CH_4) has been studied. The reactions do not affect significantly the production of CH_4. The gas CH_4 is mainly produced during devolatilization of the biomass. Steam gasification contributes to significant formation of CO and H_2 components of the product gas. The water-gas shift reaction contributes to significant consumption of CO forming more H_2. Steam gasification and water-gas shift reactions are the major contributors to the formation of more hydrogen component in product gas.

References

[1] Diego, L.F., *et al.*, *Modeling of the Devolatilization of Nonspherical Wet Pine Wood Particles in Fluidized beds.* Industrial & Engineering Chemistry Research, 2002. **41**: pp. 3642-3650.

[2] Di Blasi, C., *Modeling chemical and physical processes of wood and biomass pyrolysis.* Progress in Energy and Combustion Science, 2008. **34**(1): pp. 47-90.

[3] Di Blasi, C., *et al.*, *Product Distribution from Pyrolysis of Wood and Agricultural Residues.* Industrial & Engineering Chemistry Research, 1999. **38**(6): pp. 2216-2224.

[4] Bolhar-Nordenkampf, M. and H. Hofbauer. *Gasification Demonstration Plants in Austria.* in *IV. International Slovak Biomass Forum*. 2004. Bratislava.

[5] Demitbas, A., *Biomass resource facilities and biomass conversion processing for fuels and chemicals.* Energy Conversion and Management, 2001. **42**: pp. 1357-1378.

[6] Hofbauer, H., R. Rauch, and K. Bosch. *Biomass CHP Plant Gussing - A Success Story*. in *Expert Meeting on Pyrolysis and Gasification of Biomass and Waste*. 2002. Strasbourg, France.

[7] Snider, D.M., S.M. Clark, and PP.J. O'Rourke, *Eulerian–Lagrangian method for three-dimensional thermal reacting flow with application to coal gasifiers.* Chemical Engineering Science, 2011. **66**(6): pp. 1285-1295.

[8] Zanzi, R., K. Sjostrom, and E. Bjornbom, *Rapid pyrolysis of agriculatural residues at high temperature.* Biomass and Bioenergy, 2002. **23**: pp. 357-366.

[9] Di Blasi, C., *et al.*, *Product Distrubution from Pyrolysis of Wood and Agricultural Residues.* Industrial & Engineering Chemistry Research, 1999. **38**: pp. 2216-2224.

[10] Gaston, K.R., *et al.*, *Biomass Pyrolysis and Gasification of Varying Particle Sizes in a Fluidized-Bed Reactor.* Energy & Fuels, 2011. **25**: pp. 3747-3757.

[11] Umeki, K., *et al.*, *High temperature steam-only gasification of woody biomass.* Applied Energy, 2010. **87**(3): pp. 791-798.

[12] Xie, J., *et al.* , *Eulerian–Lagrangian method for three-dimensional simulation of fluidized bed coal gasification.* Advanced Powder Technology, 2013. **24**(1): pp. 382-392.

[13] Kee, S.B., M.E. Coltrin, and P. Glarborg, *Chemically Reacting Flow*, ed. John Wiley and Sons. 2003, Hoboken, NJ.

[14] Jand, N. and P.U. Foscolo, *Decomposition of Wood Particles in Fluidized beds*. Industrial & Engineering Chemistry Research, 2005. **44**: pp. 5079-5089.

[15] Gidaspow, D., *Multiphase Flow and Fluidization Continuum and Kinetic Theory Description*. 1994, Boston: Academic Press.

[16] Gerber, S., M. Oeermann, and F. Behrendt. *An Euler-Langrange modeling approach for the simulation of wood gasification in fluidized beds*. in *9th International Conference on Circulating Fluidized beds*. 2008. Hamburg.

[17] Andrews, M.J. and P.J. O'Rourke, *The multiphase particle-in-cell (MP-PIC) method for dense particle flow.* International Journal of Multiphase Flow, 1996. **22**: pp. 379-402.

[18] Snider, D.M., *An Incompressible Three-Dimensional Multiphase Particle-in-Cell Model for Dense Particle Flows.* Journal of Computational Physics, 2001. **170**(2): pp. 523-549.

Paper G

Heat transfer optimization in a fluidized bed biomass gasification reactor

This paper is published in WIT Transaction on Engineering Sciences, Vol. 83, pp 169-178, 2014, WIT press. ISSN 1743-3533. Doi: 10.2495/HT140161.

Heat transfer optimization in a fluidized bed biomass gasification reactor

R. K. Thapa & B. M. Halvorsen
Department of Process, Energy and Environmental Technology, Telemark University College, Norway

Abstract

A Computational Particle Fluid Dynamic (CPFD) model has been developed for the heat transfer optimization in a fluidized bed biomass gasification reactor with gasification reaction kinetics. The parameters investigated were bed material circulation rate, bed material inlet and outlet temperature, steam feed temperature and fluidizing velocity of steam. A series of simulations were performed for each of the parameters. Commercial CPFD software Barracuda was used for the simulations. The result of the simulations are used to propose optimal parameters for heat supply in the gasification reactor.

Keywords: heat transfer, fluidized bed reactors, CPFD, Eulerian-Lagrangian approach, reaction kinetics, biomass gasification.

1 Introduction

Biomass is the oldest source of energy known to the world. The renewable source of energy is neutral to CO_2 and has less emission of sulphur and nitrogen compounds in comparison to fossil fuel [1]. In conventional power plants, biomass is combusted to produce steam. The steam is then used in steam cycle for power production. The overall efficiencies of those power plants are relatively low compared to the plants based on gasification of biomass. During the past two decades many research studies have been focused on the gasification of biomass. The technology allows producing a mixture of combustible gases instead of burning it directly to produce heat. The mixture of combustible gases can be used in gas turbines or engines to produce electric power and heat. The gas can also be further processed for the production of liquid and gaseous biofuels [2].

© 2014 WIT Press
www.witpress.com, ISSN 1743-3533 (on-line)
doi:10.2495/HT140161

There are various types of technology for biomass gasification. One of them is a dual circulating fluidized bed gasification system. The technology was developed by Vienna University of Technology [3, 4]. The fundamental principal of the gasification process is shown in Figure 1. The dual fluidized bed gasification system can be divided into two parts: gasification reactor and combustion reactor. The gasification part is a bubbling fluidized bed reactor where bed materials such as sand or olivine are fluidized by high temperature steam. Biomass feed to the reactor is mixed with the bed material and the steam. The biomass undergoes an endothermic gasification reaction to produce a mixture of combustible (CO, CH_4, H_2) and non-combustible (CO_2 and H_2O) gases. The heat required for the endothermic gasification reaction is supplied by fluidizing steam and the hot bed material supplied to the reactor from the combustion part of the system.

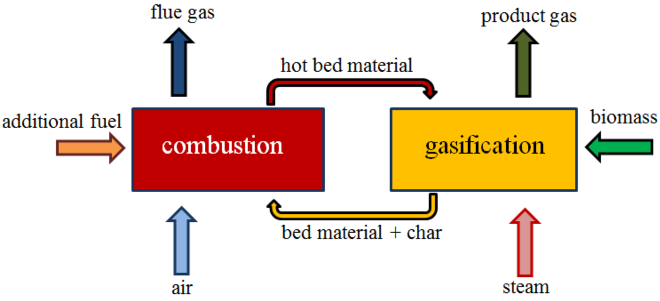

Figure 1: Principal of dual fluidized bed gasification process.

The combustion part is a circulating fluidized bed which is fluidized by ambient air. The purpose of the combustion reactor is to heat inert bed material. The heated bed material is circulated to the gasification reactor [5, 6].

The product gas quality and quantity depends on the endothermic gasification reaction occurring in the reactor. The endothermic reaction is dependent on the uniform and optimized heat transfer to the reactor. There is a great importance of heat transfer optimization in order to insure effective and efficient performance of fluidized bed gasification reactor. The optimization depends on factors as bed material circulation, steam feed rates and feed temperatures.

2 Computational model

A three dimensional computational model for dual fluidized bed gasification system has been developed. The model calculates gas-solid reacting flow and heat transfer using commercial Computational Particle Fluid Dynamic (CPFD) software Barracuda VR. 15. The details of the CPFD modelling approach can be found in publications [7, 8]. In the model, the combustion part is replaced by inlet and outlet of the hot bed material as boundary conditions. The computational model of the reactor is shown in Figure 2.

Heat supply to the reactor is accomplished through the boundaries of bottom steam and bed material inlet. Heat transfer to the reactor should ensure sufficient heat necessary for the endothermic gasification reaction. Excess heat reduces the performance of the reactor. Moreover, the heat transfer should be uniform in order to have a uniform gas composition and high quality product gas for the further use. The optimization of the heat transfer has the objective of finding the best thermo-chemical and fluid dynamic parameters in order to maintain uniform and appropriate heat supply for endothermic gasification reaction in the reactor.

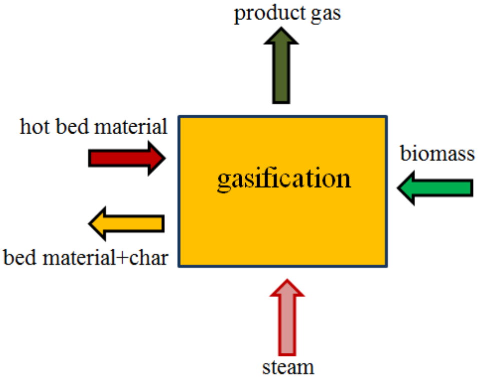

Figure 2: Computational model of the reactor.

The model considers analysis of the energy balance in the reactor. Energy is entered to the reactor in the form of biomass, hot bed material and bottom steam. Energy outlet from the reactor is in the form of a mixture of bed material with some unreacted char particles leaving at the dense bed and product gas leaving at the top of the reactor. The optimization of heat transfer should ensure maximum energy outlet in the form of product gas and minimizing the energy outlet in the form of bed material with char particles. The objective is to find the optimum fluid dynamic and thermo-chemical parameters which insure maximum conversion of input energy to the energy of product gas.

The energy of the product gas constitutes the sum of heating values of combustible gases, enthalpy of formation and sensible enthalpy of all component of product gas. The term ‘total product gas energy’ is further used to indicate the sum of energy

The energy conversion in the form of product gas, the composition and flow rates are analysed using the gasification reaction and the kinetics presented in Table 1 [9–11].

The thermo-chemical and fluid dynamic parameters studied are bed material circulation rate, bed material feed temperature, steam feed rate and steam feed temperature. Energy conversion and product gas composition as a function of these parameters need to be analysed in order to optimize them. Some of the constant parameters used in the model are given in Table 2.

Table 1: Reaction kinetics used in the simulations.

Reactions	Reaction kinetics
Steam gasification $C+H_2O=H_2+CO$	$r_1=2.7\times10^7 m_s\,P^{0.73}\theta_f\,\exp\left(\frac{-26506}{T}\right)[H_2O]$
Carbon-dioxide gasification $C+CO_2=2CO$	$r_2=1.12\times10^8 m_s\,P^{0.31}\theta_f\,\exp\left(\frac{-29518}{T}\right)[CO_2]$
Methanation $0.5C+H_2=0.5CH_4$	$r_3=1.368\times10^{-3} m_s T\exp\left(\frac{-8078}{T}-7.087\right)[H_2]$
Water- gas shift reaction $CO+H_2O=CO_2+H_2$	$r_4=7.68\times10^{10} m_s\,T\exp\left(\frac{-36640}{T}\right)[CO]^{0.5}[H_2O]$
Methane reforming $CH_4+H_2O=CO+3H_2$	$r_5=3.0\times10^5\,T\exp\left(\frac{-15042}{T}\right)[CH_4][H_2O]$

Table 2: Some constant parameters used in the model.

Parameter	Unit	Value	Parameter	Unit	Value
Biomass inlet temperature	K	300	Biomass feed rate	kg/s	0.125
Reactor diameter	m	0.55	Reactor height	m	2.00
Initial bed height	m	0.25	Wood feed position from the bottom of the reactor	m	0.15
Bed material feed position	m	0.50	Initial bed mass	kg	105

3 Results and discussion

Four series of simulations have been performed to investigate the energy flow behaviour in the reactor. The energy flow in the form of heat is analysed varying four main parameters of the reactor which are responsible for the heat transfer. The parameters are bed material circulation rate, bed material temperature, steam flow rate and steam temperature. Energy flow into the reactor in the form of biomass is constant in all cases. The final result of the all energy input to the reactor is product gas from gasification of biomass. This means biomass energy, heat from hot bed material and the heat carried by high temperature steam are partially converted into the product gas total energy. The optimization of heat transfer to the reactor is important to get a high amount of energy converted to product gas.

The first series of simulation are run to determine the effect of bed material circulation rate on the energy conversion. This investigation is achieved by gradual increasing the bed material circulation rate while keeping other operating parameters constant. As expected, the total energy contained in the product gas leaving the reactor is increased with the increasing bed material circulation rate. The total energy of the product gas as a function of bed material to biomass ratio is shown in Figure 3. The figure shows the accumulated energy of product gas during 100s of simulation. This is the case for all simulations performed in this work. The bed material circulation rate is presented as ratio of bed material feed rate to biomass feed rate.

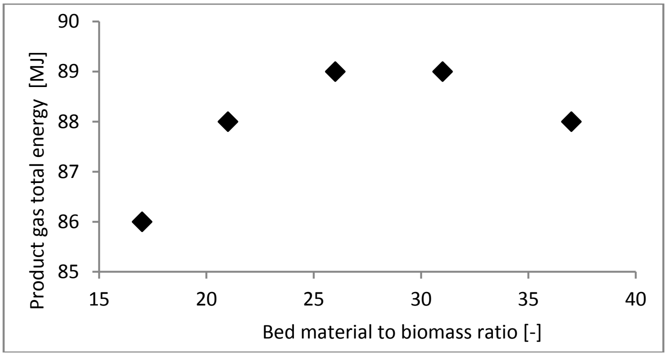

Figure 3: Product gas total energy as function of bed material to biomass ratio.

The product gas total energy reaches its maximum at the bed material to biomass ratio of 26 indicating on the optimum value of the bed material circulation rate about 26 times that of biomass. Above this value there is no reason to increase bed material circulation rate. A slight decrease in product gas energy is observed, indicating that excess bed material circulation can effect negatively in the energy conversion. However the reason for the decrease in total product gas energy is not clearly known and needs further investigation.

Figure 4(a) shows particle temperature distribution across the cross sectional area of the reactor. The char volume fraction distribution along the same cross sectional area is shown in Figure 4(b).

The particle temperature distribution in the Figures 4 a(1) to a(5) corresponds to the bed material to biomass feed ratio of 17 to 37 respectively (see Figure 3). The figures show that the particle temperature distribution over the cross sectional area of the reactor is not uniform. Particle temperature is higher close to the hot bed material inlet region whereas lower near to the bed material outlet region. Almost opposite can be seen in the Figures 4 b(1) to b(5) representing the char volume fraction. The char volume fraction is lower at the high particle temperature regions whereas the concentration is higher at the low particle temperature region. The lowest char volume fraction distribution is seen in Figure 4 b(3) which indicates the highest fraction of char conversion. The corresponding Figure 4a(3) shows much more uniform distribution of particle temperature. The Figures corresponds to the bed material to biomass feed ratio of 26 showing the optimum feed rate.

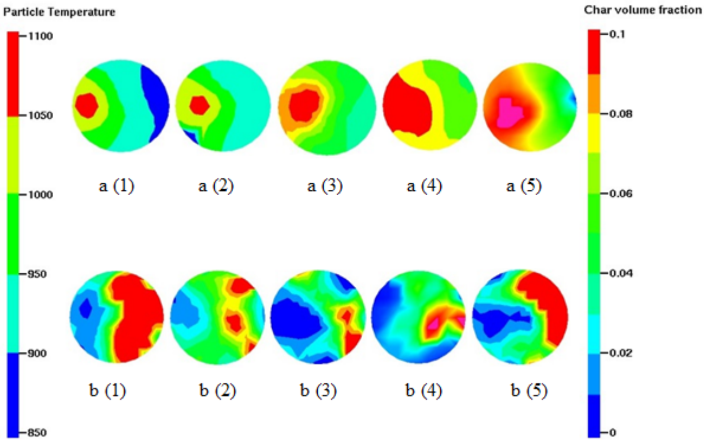

Figure 4: (a) Particle temperature variation along the cross section of the reactor at the height of 0.25m. (b) Volume fraction of the char particles at the same locations.

The optimum bed material circulation rate is further used for the second series of simulation. The simulations are run to investigate the effect of varying bed material feed temperature into the product gas total energy. Five sets of simulations are performed changing bed material temperature from 1123 K to 1223K with each interval of 25K. The results are shown in Figure 5.

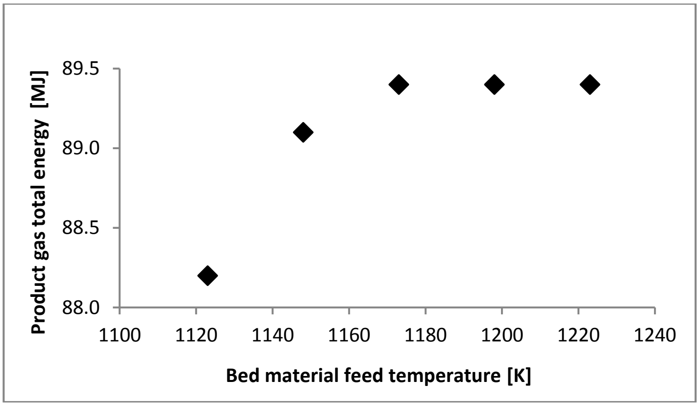

Figure 5: Product gas total energy as a function of bed material feed temperature.

The product gas energy is increasing with increasing bed material temperature for the first two series of the simulations. The product gas total energy is constant when the temperature reaches 1173K and remains unchanged for further increase in temperature. For the given bed material circulation rate, there is no use of increasing the temperature of the bed material.

The third series of simulation are run to investigate the effect of steam flow rate in the performance of the reactor. The optimized bed material flow rate and temperature from the first and second series of simulations are used in these simulations. In the reactor, the bed materials are olivine particles with mean particle size 530 µm. Approximate minimum fluidization velocity (u_{mf}) in the reactor is 0.18 m/s. The simulation is performed for the gas velocity of 1.5 u_{mf}, 2 u_{mf}, 2.5 u_{mf}, 3 u_{mf}, 3.5 u_{mf} and 4 u_{mf} which corresponds to each of the steam to biomass ratio from 0.15 to 0.40. The high temperature steam fed to the reactor through its bottom has two functions. First, it acts as a fluidizing gas. Second, the steam reacts with the other gas and solid components in the reactor to form some of the components of the product gas. The unreacted steam leaves together with the product gas from the top of the reactor. Increase in the steam to biomass ratio increases the steam flow rate as the biomass feed rate is constant. The increase in steam flow rate on the other hand increases energy input to the reactor. Moreover, if there are increasing un-reacted steam, it adds the product gas total energy. Therefore the result of this series of simulation is analysed in the form of change in product gas total energy as a function of steam to biomass ratio which is shown in Figure 6.

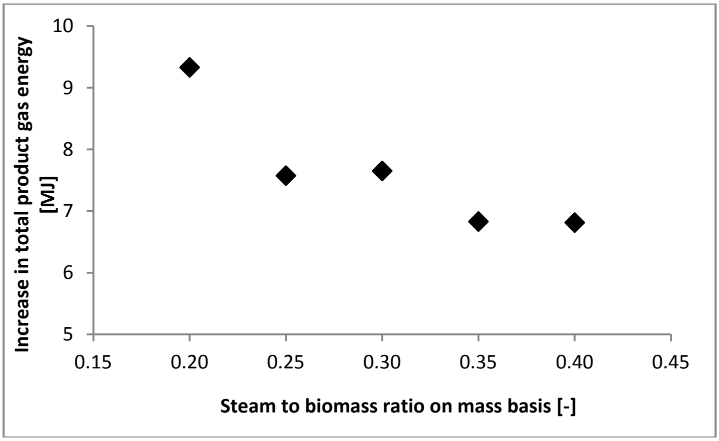

Figure 6: Increase in product gas total energy as a function of steam to biomass ratio.

From the result presented in the figure, the optimum value of the steam to biomass ratio is 0.2. Increase in steam to biomass ratio does not increase the product gas total energy. The figure also shows that the product gas total energy does not decrease linearly with the increase in steam to biomass ratio. In some interval, it is constant. Further investigations are necessary to figure out the reason of this behaviour.

The optimum values of bed material feed rate, bed material temperature and steam feed rate is now used in the fourth series of the simulation to investigate the performance of the reactor with increasing steam feed temperature. The product gas total energy as a function of bottom steam temperature is shown in Figure 7.

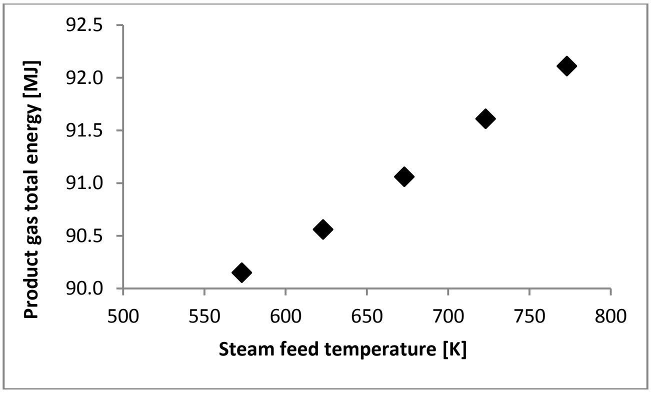

Figure 7: Product gas total energy as a function of steam feed temperature.

The results show that the product gas energy increase almost linearly with the increase in the steam feed temperature.

The temperature distribution of the fluid inside the reactor is shown in Figure 8. The figures represent the half part of the cross section of the reactor which covers dense bed and some freeboard part up to 1m height.

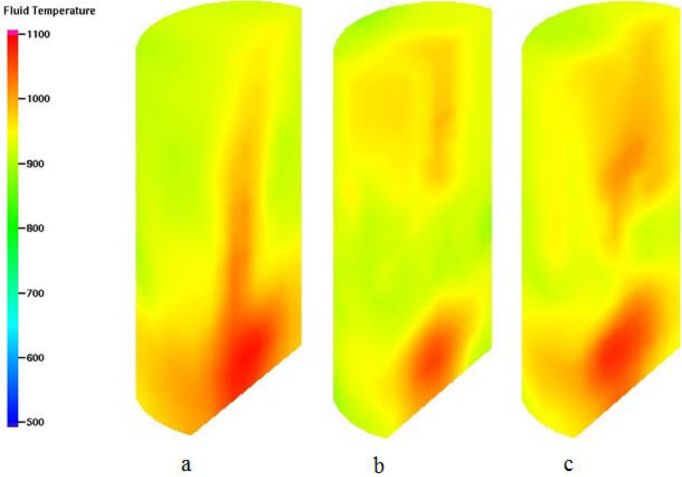

Figure 8: Contours of fluid temperature along the height of reactor.

Figure 8(a) represents the fluid temperature for the first and second series of simulations at bed material to biomass ratio of 26 and bed material temperature of 1173K. The steam to biomass ratio is 0.20. Figure 8(b) repeats the conditions of the Figure 8(a) with optimized steam to biomass ratio of 0.2. Figure 8(c) includes the conditions of the Figures 8(a) and 8(b) in additional to increased steam feed temperature of 773K. The figures show almost uniform fluid temperature in the reactor. However the Figure 8(b) shows most uniform fluid temperature having less spots indicating the area of high temperature concentration.

4 Conclusions

Four series of simulations are performed for optimization of heat transfer in the bubbling fluidized bed biomass gasification reactor. The parameters for optimization are bed material feed rate, bed material temperature, bottom steam feed rate and bottom steam feed temperature.

First series of simulation results shows that the bed material circulation rate is optimum when the ratio of bed material to biomass feed is about 26. Increasing this ratio does not increase the efficiency of the reactor. In the second series of simulations, the result indicates that the optimum temperature for the bed material feed is 1173K. Increasing the temperature further will not increase the energy conversion rate in the reactor.

The third series of simulation results shows that the optimum steam to biomass ratio is 0.2. More increase in steam to biomass ratio does not add the product gas total energy.

The fourth series of simulation have been performed to investigate the effect of bottom steam temperature on total product gas energy. The result shows that the energy of the product gas increases linearly with the increase in bottom steam temperature.

References

[1] Diego, L.F. *et al.*, *Modeling of the Devolatilization of Nonspherical Wet Pine Wood Particles in Fluidized beds.* Industrial & Engineering Chemistry Research, 2002. 41: p. 3642-3650.

[2] Demitbas, A., *Biomass resource facilities and biomass conversion processing for fuels and chemicals.* Energy Conversion and Management, 2001. 42: p. 1357-1378.

[3] Fercher, E., *et al. Two Years Experience With The Ficfb-Gasification Process*. in *10th European Conference and Technology Exhibition*. 1998. Wurzburg.

[4] Hofbauer, H., *et al. Six Years Experience With The Ficfb-Gasification Process*. in *12th European Conference and Technology Exhibition on Biomass, Energy, Industry and Climate Protection*. 2002. Amsterdam.

[5] Hofbauer, H., R. Rauch, and K. Bosch. *Biomass CHP Plant Gussing – A Success Story*. in *Expert Meeting on Pyrolysis and Gasification of Biomass and Waste*. 2002. Strasbourg, France.

[6] Marquard-Mollenstedt, T., *et al. NEW APPROACH FOR BIOMASS GASIFICATION TO HYDROGEN*. in *2nd World Conference and Technology Exhibition on Biomass for Energy, Industry and Climate Protection*. 2004. Rome, Italy.

[7] Snider, D. and S. Banerjee, *Heterogeneous gas chemistry in the CPFD Eulerian–Lagrangian numerical scheme (ozone decomposition).* Powder Technology, 2010. 199(1): p. 100-106.

[8] Boyalakuntla, D.S., *Simulation of Granular and Gas-Solid Flows Using Discrete Element Method*, in *Department of Mechanical Engineering*2003, Carnegie Mellon University. p. 74.

[9] Xie, J., *et al.*, *Eulerian–Lagrangian method for three-dimensional simulation of fluidized bed coal gasification.* Advanced Powder Technology, 2013. 24(1): p. 382-392.

[10] Xie, J., *et al.*, *Simulation on gasification of forestry residues in fluidized beds by Eulerian–Lagrangian approach.* Bioresource Technology, 2012. 121(0): p. 36-46.

[11] Umeki, K., *et al.*, *High temperature steam-only gasification of woody biomass.* Applied Energy, 2010. 87(3): p. 791-798.

Paper H

Circulating fluidized bed reactor: CPFD model validation and gas feed positions optimization

This paper is submitted to the international journal ‘Computers and Chemical Engineering’ and is under the review process.

Circulating fluidized bed reactor: CPFD model validation and gas feed position optimization

R.K. Thapa[1]*, A. Frohner[2], G. Tondl[2], C. Pfeifer[2] and B.M. Halvorsen[1]
1. Institute for Process, Energy and Environmental Technology, Telemark University College, 3901 Porsgrunn, Norway
2. University of Natural Resources and Life Sciences, Institute of Chemical and Energy Engineering, Muthgasse 107, A-1190 Vienna, Austria
*corresponding author: tel. +47 99485965, e-mail: rajan.k.thapa@hit.no
Kjølnes ring 56, PO BOX 203 N3901

Abstract

A 3D Computational Particle Fluid Dynamic (CPFD) model is validated against experimental measurements in a lab-scale cold flow model of a circulating fluidized bed (CFB). The model prediction of pressure along the riser and bed material circulation rates agree well experimental measurements. Primary and secondary air feed positons were simulated with varying feed positions along the height of the reactor in order to get optimum bed material circulation rate. The optimal ratio of height of primary and secondary air feed positions to the total height of the riser are 0.125 and 0.375 respectively. The model is simulated for high temperature conditions and for reacting flow including combustion reactions. At the high temperature and reaction conditions, the bed material circulation rate is decreased with corresponding decrease in pressure drop throughout the CFB for the given gas feed rate.

1 Introduction

Circulating fluidized bed reactors are widely used in various industrial applications including oxyfuel combustion, gasification and combustion of biomass or other carbonaceous feedstock. One of the applications of CFB in gasification processes is heating bed materials by combustion of fuels and then transport it to the gasification reactor (Pfeifer et al., 2009). Fluid dynamic properties of the reactor including gas-particle mixing and residence time depend on the gas velocity and particle circulation rate for a given bed inventory (Ludlow et al., 2008). Gas velocity and bed material circulation rate are major parameters determining the performance of the bed. The solid circulation rate is also crucial for reaction kinetics. The solid circulation rate determines the fluid - solid contact time, heat transfer and overall performance of the CFB as a rector (Roy et al., 2001). The solid circulation rate and solid distribution over the circulating system are determined by the fluid dynamics (Lei and Horio, 1998). In order to obtain proper distribution of the solids throughout the bed, proper pressure balance is required (Kaiser et al., 2001). Improvement of performance of CFB mainly needs optimum fluid dynamic properties of the bed. Many authors have studied the fluid dynamic behavior of CFB. Yerushalmi et al. have shown the transition between packed bed, bubbling bed, turbulent and fast fluidization regimes in the plot of bed voidage against superficial gas velocities (Yerushalmi et al., 1976). Flow regime maps of gas-solid flow are also developed plotting gas velocity against the solid flux (Leung, 1980). Takeuchi et al. performed experimental measurements to define the boundaries of fast fluidization (Takeuchi et al., 1986). Hirama et al. extended the flow diagram to transition from high velocity to low-velocity fluidization regimes (Hirama et al., 1992). Bi and Grace proposed unified flow regime diagram based on the experimental findings. They have shown relationship between flow regimes for both gas-solid fluidization and co-current upward transport (Grace, 1986, Bi et al., 1993, Bi and Grace, 1995). In the all of the mentioned studies, the experiments are carried out at the ambient conditions. One of the significant factors effecting overall fluid dynamic properties of the bed is the particle size distribution. The particle size distribution is not included in all above mentioned studies. When particles with larger size and lower density are mixed with the particles of smaller size and higher densities, the minimum fluidization velocity changes (Thapa et al., 2011). Change in minimum fluidization velocity effects in the transport velocity and fast fluidization velocity. High temperature gases have lower density and higher viscosity. Change in density and viscosity changes flow behavior in fluidized bed.

Therefore the study of fluid dynamics in CFB should include the particle size distribution and the effect of high temperature conditions. The gas solid flow without chemical reaction differs from the reacting flow. The significance of those differences is not studied yet. The fluid dynamic properties of the CFB used in gasification of biomass is complicated due to the gas feed positions at different levels of the reactor. Air is fed to the reactor as bottom air at the bottom of the riser and primary and secondary air are fed along the height of the rector (Kaushal et al., 2008a, Kaushal et al., 2008b). When the gas is fed at three position of the bed, the feed position itself is expected to affect strongly on the fluid dynamics of the bed and the bed material circulation rate.

Design, scaling, operation and improvements of the circulating fluidized bed reactors require good understanding of the fluid dynamic parameters effecting the performance (Gungor and Yildirim, 2013). Many of those parameters are studied through experimental investigations using laboratory models, pilot and demonstration plants. However not all parameters are easy to study using experimental methods. For example study of the effect of gas feed position needs different construction of design that could take enormous time and can be economically too costly. The facts indicates on the usefulness of the computational models to overcome those types of the challenges.

In order to overcome and/or substitute the experimental limitations, computer models have gained significant attention since early 1990s. Computer models make it possible to study the fluid dynamics without disturbing fluid flow field inside the reactor (Deen et al., 2007). The current work is therefore focused on a validation of CPFD (Computational Particle Fluid Dynamic) model against the experimental measurement in a cold model of CFB. The model is then used in further investigation of high temperature conditions as well as optimizing the feed positions of primary and secondary air.

2. Experimental Set-up

The experimental rig is located at University of Natural Resources and Life Sciences (BOKU), Vienna, Austria. The set up consists of a cold model of a circulating fluidized bed as shown in Figure 1. The model is made of a transparent Plexiglas which makes it easier to visualize the fluidization and circulation during the experiments. The model is wrapped with conductive wires to avoid electrostatic forces at the wall. The fluidizing gas used in the experiment is ambient air supplied from a compressor. The fluidizing gas is fed as bottom air, and primary air at two different stages of the reactor. The volume flow of primary and secondary air is measured through rotameters shown which is seen in Figure 1(a). The setup has 15 pressure tapping points which are connected to the pressure sensors. An industrial measurement and control system (B&R automation) is used to log the pressure data. The heights of pressure tapping points are shown in Table 1.

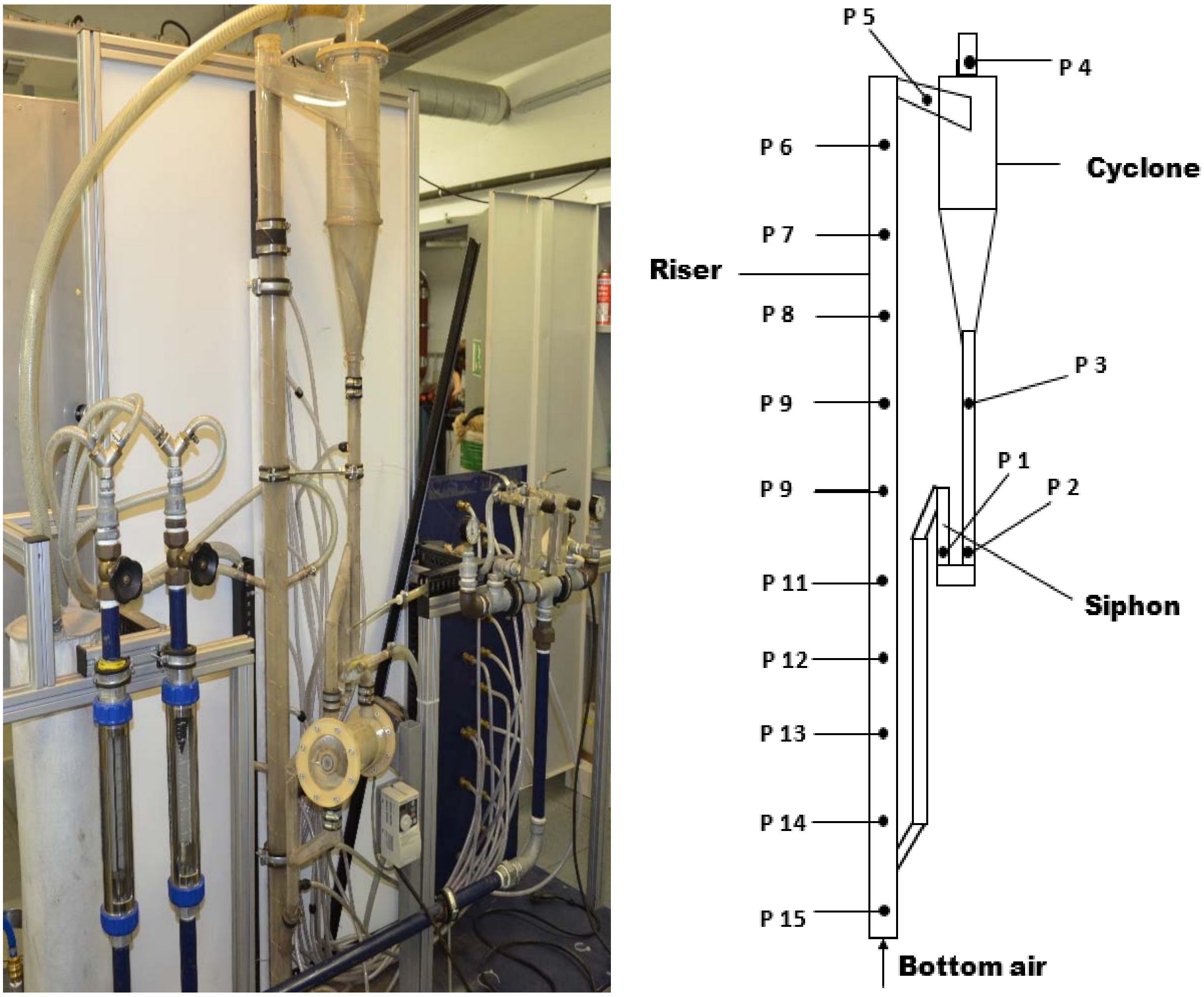

(a) (b)

Figure 1: (a) CFB cold model with air flow regulation and pressure measurement arrangements (b) pressure tapping points

Table 1: Height of the pressure tapping point

Labelling	Position	Height [mm]
P1	Siphon top	665
P2	Siphon top	665
P3	Down comer	1010
P4	Exit Filter	1685
P5	Intersection Precipator	1595
P6	Reactor	1535
P7	Reactor	1330
P8	Reactor	1170
P9	Reactor	1005
P10	Reactor	850
P11	Reactor	610
P12	Reactor	525
P13	Reactor	365
P14	Reactor	205
P15	Reactor	40
P16	Siphon bottom	425
P17	Siphon bottom	205

The siphon shown in Figure 1b, is also fluidized by air. The particles used in the experimental investigations are glass particles of density 2650 kg/m^3. The particle size distribution is presented in Figure 2.

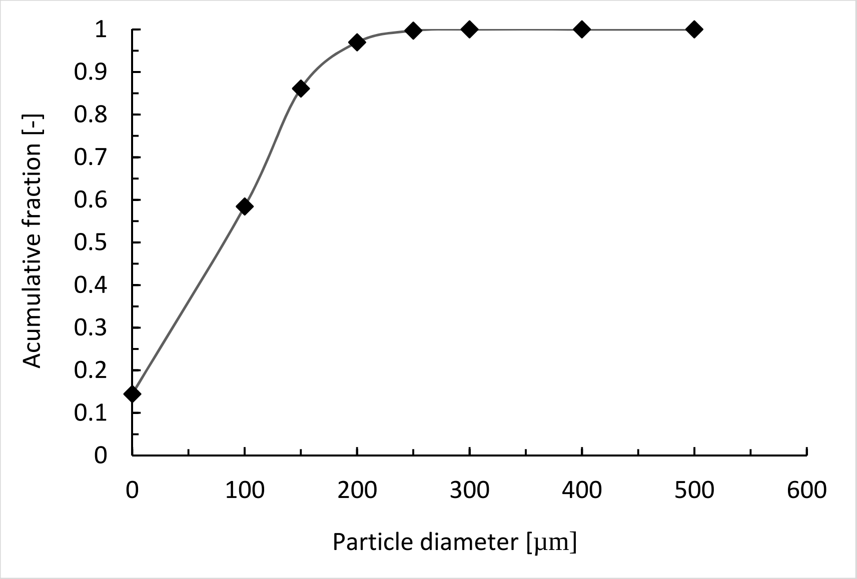

Figure 2: Particle size distribution

3. Computational model

Two different approaches are found in modeling of gas-solid flow; the Eulerian-Eulerian approach and the Eulerian-Lagrangian approach. The Eulerian-Eulerian approach treats both the gas and solid phase as interpenetrating continua. A kinetic theory similar to kinetic theory of gases is developed for the solid phase. This approach is widely used in CFD modeling. However, each particle size needs to be considered as a separate phase when the bed has particle size distribution. Separate continuity and momentum equations have to be solved for each size and type of particles (Gidaspow, 1994). Particle size distribution significantly influences the performance of fluidized bed reactors. In Eulerian-Lagrangian approach, solid phase is treated as discrete elements. The motion of individual particle is tracked using Newton's laws. The particle-particle, particle-wall and fluid-particle interactions forces are taken into account (Boyalakuntla, 2003).This approach simulates the gas-solid flow with a wide range of particle sizes (Cundall and Strack, 1979, Amsden et al., 1989) .

The computational particle fluid dynamics (CPFD) numerical method has been developed recently to supplement the conventional Eulerian-Eulerian and Eulerian-Lagrangian methods. The CPFD numerical method uses Eulerian-Lagrangian model for gas-solids flows. The Navies-Stokes equation is applied for fluid with strong coupling between the discrete particles. The particle momentum model is based on the multiphase particle-in-cell numerical description which is a Lagrangian description of particle motion described by ordinary differential equations with coupling to the fluid. Thus this numerical method can readily handle particle type and size distribution.

In the present CPFD numerical method, actual particles are grouped into computational particles each containing a number of particles with identical densities, volume and velocities located at a specific position. The computational particle is a numerical approximation similar to the numerical control volume where a spatial region has a single property for the fluid. With these computational particles, large commercial systems containing billions of particles can be analyzed using millions of computational particles (Chen et al., 2013).

3.1 Governing Equations

The fluid dynamic equations can be derived from kinetic theory for dilute gases or the continuum points of view. The volume averaged fluid mass and momentum equations for a continuum are:

$$\frac{\partial(\varepsilon_g\rho_g)}{\partial t} + \nabla\left(\varepsilon_g\rho_g\boldsymbol{u}_g\right) = 0 \qquad (5)$$

$$\frac{\partial\left(\varepsilon_g\rho_g\boldsymbol{u}_g\right)}{\partial t} + \nabla\left(\varepsilon_g\rho_g\boldsymbol{u}_g\boldsymbol{u}_g\right) = \nabla p - \boldsymbol{F} + \varepsilon_g\rho_g\boldsymbol{g} + \nabla\varepsilon_g\tau_g \qquad (6)$$

The particle acceleration is given by:

$$\frac{\partial u_p}{\partial t} = D_p\left(\boldsymbol{u}_g - \boldsymbol{u}_p\right) - \frac{1}{\rho_p}\nabla p + \boldsymbol{g} - \frac{1}{\varepsilon_s\rho_p}\nabla\tau_p \qquad (7)$$

The terms in the equation represent the acceleration due to aerodynamic drag, the pressure gradient, gravity and the gradient of the inter-particle normal stress τ_p .

The particle movement is given by

$$\frac{d\boldsymbol{x}_p}{dt} = \boldsymbol{u}_p \qquad (8)$$

The particle properties are mapped from the particle to the grid to get grid-based properties such as particle volume fraction at cell ξ,

$$\varepsilon_{p\xi} = \frac{1}{V_\xi}\sum_{1}^{N_p} V_p n_p S_{p\xi} \qquad (9)$$

The conservation equations are approximated using finite volumes with staggered scalar and momentum nodes. The implicit numerical integration of the particle velocity equation is given by:

$$u_p^{n-1} = \frac{u_p^n + \Delta t \cdot \left[D_p u_{g.p}^{n+1} - \frac{1}{\rho_p}\nabla p_p^{n+1} - \frac{1}{\rho_p \theta_p}\nabla \tau_p^{n+1} - g\right]}{1 + \nabla t \cdot D_p} \qquad (10)$$

where $u_{g.p}^{n+1}$ is the interpolated fluid velocity at the particle location, ∇p_p^{n+1} is the interpolated pressure gradient at the particle location and $\nabla \tau_p^{n+1}$ interpolated particle stress gradient at the particle location. The new particle location at the next time is then

$$\boldsymbol{x}_p^{n+1} = \boldsymbol{x}_p^n + u_p^{n+1}\Delta t \qquad (11)$$

The fluid momentum equation implicitly couples the fluid and the particles through the interphase momentum transfer. The interphase momentum transfer at momentum cell ξ is:

$$\boldsymbol{F}_\xi^{n+1} = \frac{1}{\Omega_\xi}\sum_p s\xi \left[D_p\left(u_{g.p}^{n+1} - u_p^{n+1}\right) - \frac{1}{\rho_p}\Delta u_p^{n+1}\right] \cdot n_p m_p \qquad (12)$$

The interphase drag function $D_p$is calculated using the drag model:

$$D_p = C_d \frac{3\rho_g \left|u_g - u_p\right|}{8\rho_p r_p} \qquad (13)$$

3.2 Drag model

In the CPFD software Barracuda the Wen-Yu model, Ergun model, Wen-Yu/Ergun model and Turton drag model are used for gas-solid homogeneous flows. The Wen-Yu drag model have been implemented in this work. More detailed information of the model is presented by Wen and Yu (Wen and Yu, 1966).

3.3 Solid stress model

Unlike the discrete element method (DEM) which calculates the particle-to-particle forces using a spring-damper model and direct particle contact, the CPFD codes models the collision forces on particles as a spatial gradient. The particle stress gradient which is difficult to calculate for each particle in a dense flow is calculated as a gradient on the Eulerian grid and is then interpolated to discrete particles. Therefore, solids loadings from dilute to dense (closed packed) can be modeled by the particle stress tensor formulation and interpolation. Particle to particle collision are modelled by the particle normal stress τ_p. The particle stress is derived from the particle volume fraction which in turn is calculated from the particle volume mapped to the grid. The particle normal stress model used here was developed by Harris and Crighton.

$$\tau_p = \frac{p_s \varepsilon_p^{\gamma}}{\max\left[\varepsilon_{cp} - \varepsilon_p \theta \left(1 - \varepsilon_p\right)\right]} \qquad (14)$$

The constant γ is recommended to be $2 < \gamma < 5$. The constant θ is a small number in the order of 10^{-7} to remove the singularity in close packing. The fluid density, velocity and pressure are coupled by a semi-implicit pressure equation. The momentum and pressure equations are solved with a conjugate gradient solver. A quasi-second order upwind scheme is used for the convection term (Chen et al., 2013).

4. Results and Discussion

Experiments were performed in the lab-scale cold flow model with varying bottom air flow rate. Pressure along the height of the riser that are measured via pressure tapping points are stored for further processing. Pressure monitors are set in the computational model at the same locations as in experimental measurements. The experimental pressure measurements compared with the computational prediction for two air feed rates are presented in Figure 3.

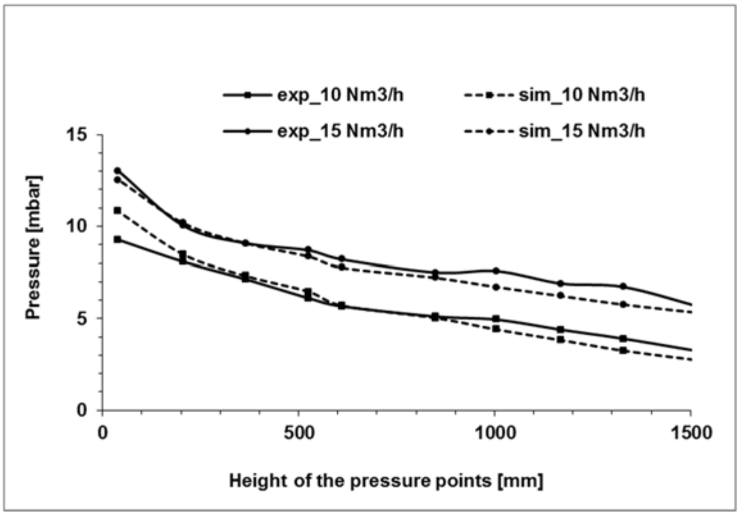

Figure 3: Pressure along the height of riser

The pressure is decreasing from bottom to top of the reactor. The computational pressure data deviate 0% to 20%. The maximum deviations are at the bottom and top of the reactor.

The particle height in the down comer above the siphon are measured for a given air feed rate. Then the siphon fluidizing air flow is stopped abruptly for a given time and then the height is measured again. The circulation rate per time (second/hour) is determined based on the difference of height of the bed material and the cross sectional area of the down-comer. Simulations were run for the same gas velocities with pressure monitors at the same heights along the riser as in the experimental set up. The flux plane assigned at the down-comer monitored the solid circulation rates. The simulation results are compared with the experimental measurements. The solid circulation rate at different bottom air feed rates is given in Figure 4. Experiments were carried out at air feed rate of 10, 15, 20 and 25 Nm^3/h and simulations were run with the corresponding air feed rates.

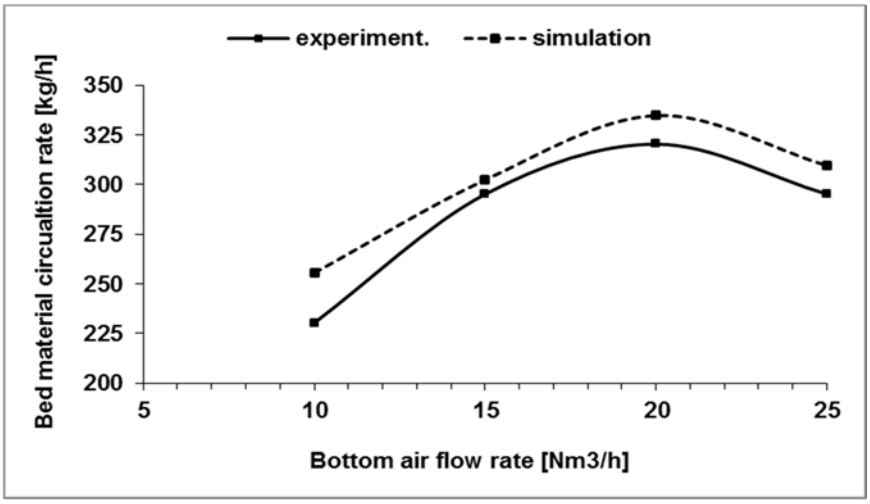

Figure 4: Solid circulation rate vs air feed rate

The deviation between experimental and computational results is from 2% to 10%. The maximum deviation is at the air flow rate of 10 Nm^3/h and minimum deviation at the air feed rate of 15 Nm^3/h. The highest solid circulation is achieved for bottom air feed rate of 20 Nm^3/h. When the air feed rate is further increased the circulation rate decreases.

The agreements of the pressure data and the solid circulation rates between the experimental and computational results give basis for using the CPFD model for further investigation of the fluid dynamics of the circulating fluidized bed. Therefore it is assumed that the further computational investigation of the CFB reactor without performing experimental measurements will give acceptable results.

Experimental investigation of the effect of primary and secondary air feed position can only be performed by reconstructing the rig which is time consuming and economically costly. Therefore, further investigations are continued only with the CPFD model. In the CPFD model, the primary air flow is introduced together with a constant bottom air feed rate. The bottom air feed rate is 15 Nm^3/h. Primary air feed rate is 5 Nm^3/h. The primary air feed position is varied from the height of 200 mm to 1200 mm from the bottom of the riser with the interval of 200 mm. For every primary air feed position, the total air feed rate in the simulation is constant, 20 Nm^3/h. The choice of the total air feed of 20 Nm^3/h is because the highest circulation rate is achieved at the feed rate as presented in Figure 4. The riser fluidization determines predominantly the circulation rate in the system. However, siphon fluidization needs to be adjusted for optimum operation (Xu and Gao, 2003). For the given flow the siphon air feed of 1 Nm^3/h gives a stable circulation through the siphon. Solid circulation rate as a function of the primary air feed position is shown in Figure 5. The solid circulation rate is decreasing with increasing height of primary air feed.

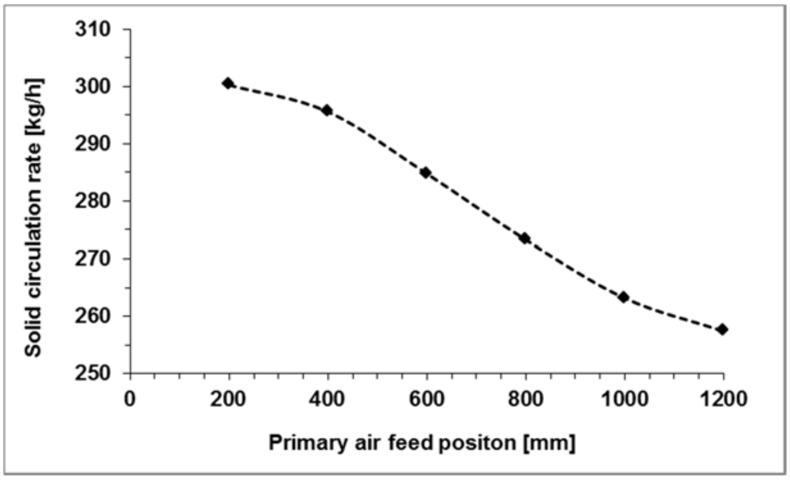

Figure 5: Solid circulation rate vs primary air feed position

The solid circulation rate for the feed of bottom air at the rate of 20 Nm^3/h is compared with the feed of air at two positions at total flow rate of 20 Nm^3/h. The rates are in Figure 5 and Figure 5. In Figure 4, the bed material circulation rate at the bottom air flow rate of 20 Nm^3/h is about 335 kg/h. Figure 6 shows that the maximum solid circulation rate is about 300 kg/h. When the gas feed positon is split into two, the solid circulation rate is decreased even though the total gas feed rate is the same. The solid circulation rate decreases with increased height of the feed position of primary air form the bottom of the reactor.

Different cross sectional particle volume fractions are presented in Figure 6. The first row represents the cross sectional volume fraction of particles when only the bottom air is fed to the riser. The cross sections are at the height of 200 mm to 1200 mm from the bottom with interval of 200 mm presented as column 1 to 6 respectively. The first three cross sections have higher particle concentration which indicates that the particle concentration is higher at the lower part of the riser than higher up. The solid concentration is higher near to the wall than in the center.

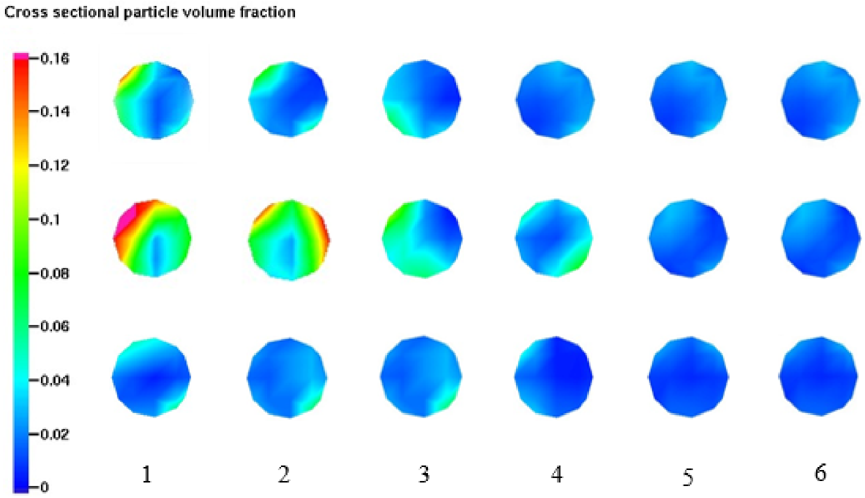

Figure 6: Cross sectional solid volume fractions

The second and third row present the solid volume fractions when primary air is introduced to the reactor in addition to constant feed of the bottom air. The second row presents the cross sectional solid volume fraction just below the primary air feed position and the third row present the solid volume fraction just above the primary air feed position. The first three columns show a large difference of cross sectional volume fractions below and above the primary air feed positions indicating that the introduction of primary air feed hinders the particle up flow. The primary air is introduced at the side of the reactor. The introduction of primary air feed resists to the particles that are moving upward which is known as 'cut off' or 'barrier' effect (Koksal and Hamdullahpur, 2004). This is the reason of decreasing solid circulation rate with introduction of primary air flow. When the air feed is located at much higher position as indicated by column 4, 5, 6 in the figure, the solid concentration is not effected significantly. It may be due the reason that the particle concentration are very low at the higher location of the riser.

The model is used to investigate how primary air feed rate effects on the bed material circulation rate. A series of simulations were run by gradually increasing the primary air feed rate. The set of simulations were repeated for the feed positions 200, 400 and 600 mm above the bottom air feed. Some of the results are presented in Figure 7.

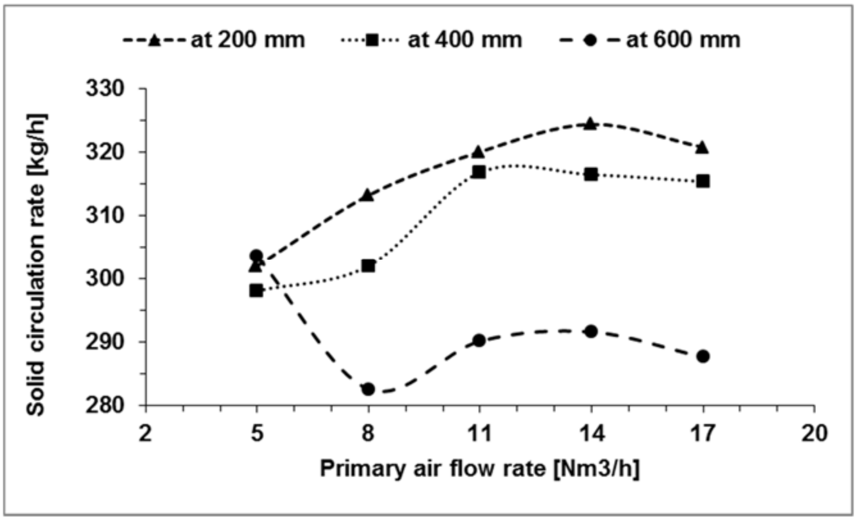

Figure: 7: Solid circulation rate vs primary air flow rate at various feed positons

The solid circulation rate is increasing with the primary air flow rate up to the feed positon of 400 mm. When the feed positions are higher, then the solid circulation rate falls down. Very high primary air feed positon is not suitable for the steady and maximized bed material circulation rate. The maximum solid circulation rate is achieved at the ratio of height of the feed positon to the total height of the reactor 0.125. The solid circulation rate is increasing with the primary air feed rate up to 14 Nm^3/h and then decreasing again.

Simulations were run to investigate the effect of secondary air flow position on bed material circulation rate. The bottom air feed is kept at 10Nm^3/h and the primary air feed is kept at the positon of 200 mm from the bottom with the feed rate of 14 Nm^3/h. These values are chosen because the combination gives the highest solid circulations rate. The secondary air flow rate is kept constant 5 Nm^3/h and the feed positions are 400 mm, 600 mm, 800 mm, 1000 mm and 1200 mm. The bed material circulation rate as a function of secondary air flow position along the height of the reactor is shown in Figure 8. The maximum solid circulation is achieved at the feed position at 600 mm from the bottom of the reactor. The ratio of the height of the feed position to the total height of the riser is 0.375.

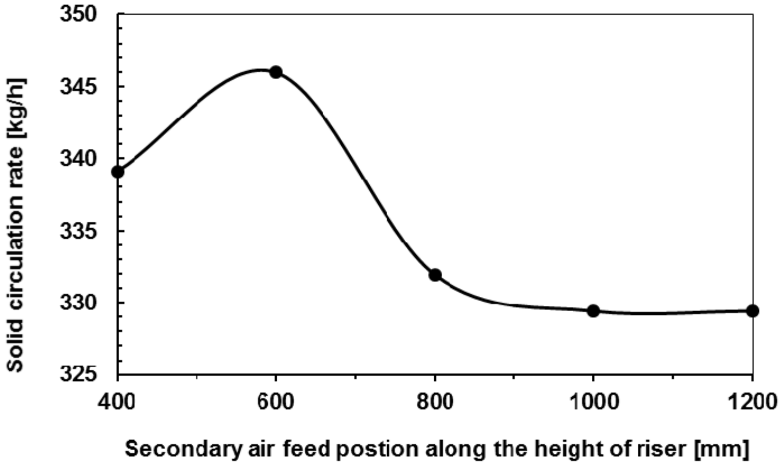

Figure 8: Solid circulation rate vs secondary air feed positon

A series of simulations were run to investigate the effect of increasing secondary air flow on the bed material circulation rate. The computational prediction shows that the bed material circulation rate is not effected significantly with the increasing secondary air feed rate.

The same feed rate of bottom air as in the experimental measurements was used in simulations with high temperature. Series of simulations were also run for the reacting flow including combustion of char particles. All the simulations were run with constant air flow rate of 10 Nm^3/h. The pressure along the riser and the solid circulation rate under these conditions are monitored and compared with results with the ambient conditions. In Figure 9 the solid volume fraction through the CFB is shown.

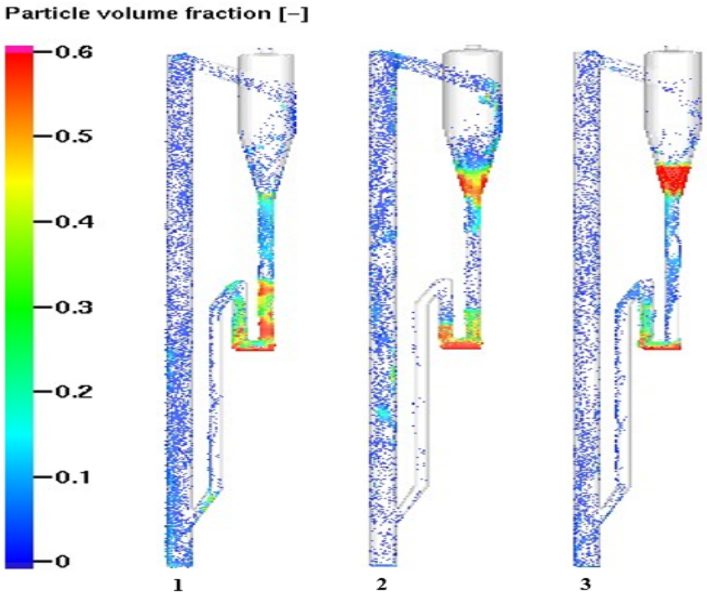

Figure 9: Solid volume fraction throughout the CFB

The contours presented in the figure are snap shoots at time 100s. The contours 1, 2 and 3 are for the ambient, high temperature and reacting flow respectively. The solid concentrations in the CFB are almost similar except for the high concentrations in the downcomer and cyclone separator in the case of flow at high temperature and flow with combustion reaction. The high concentration indicates that the siphon air flow rate needs to be increased. The contour of pressure for the corresponding simulations are shown in Figure 10. The pressure drop throughout the CFB is less for the high temperature and reacting flow case than for the bed at ambient conditions.

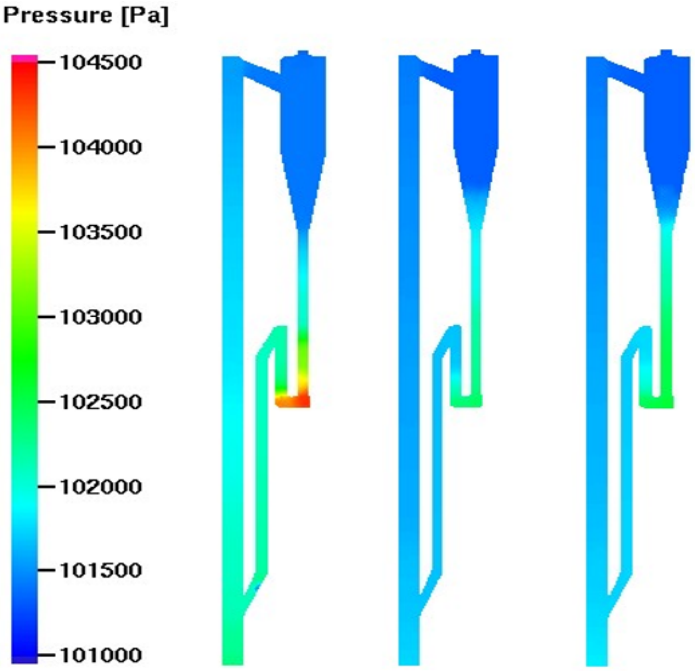

Figure 10: Contours of pressure in CFB

With the decreased pressure drop, the solid circulation rate is monitored with these conditions are less than with ambient conditions. The solid circulation rates are 254 kg/h, 198 kg/h and 210 kg/h for the ambient, high temperature and reacting flow conditions respectively.

The difference in the flow properties at ambient conditions and high temperature conditions are mainly due to the gas density and viscosity. At temperature 1173 K, the density of the air is decreased by four times and the viscosity is increased about two and a half time. Changes in density and viscosity changes the flow behavior. The particles used in the current work, have small diameter and consequently they do not need high gas velocity for fluidization. The particle Reynolds number is 3.4 which is within the viscous dominated flow (Gidaspow, 1994). Viscosity plays an important role in such flow and increase in the viscosity decreases the minimum fluidization and transport velocity of the particle. The increase in viscosity may also be one of the reasons for the pressure decrease and consequently the decrease of solid circulation rate.

5. Conclusions

A 3D CPFD (Computational Particle Fluid Dynamic) model of a circulating fluidized bed (CFB) is validated against the experimental measurements in a lab-scale cold model of CFB. The pressure drops monitored in the CPFD model at a number of locations along the height of the riser are compared with the corresponding experimental measurements. The deviations of pressure data are from 0% to 20%. The model is simulated to measure the solid circulation rate at a series of varying air feed rates. The deviation between computational prediction of solid circulation and corresponding experimental measurements at various locations of the bed are from 2% to 10%.

The CPFD model is used to investigate the optimum primary and secondary air feed positions for maximum circulation rate of bed material. The bed material circulation rate is maximum when the ratio of primary air feed position to the total height of the reactor is 0.125. The corresponding optimum ratio of secondary air feed position to total height of the reactor is 0.375. At a given feed rate, the bed material circulation is decreasing when air feed is spitted as bottom, primary and secondary air. The circulation rate is highest when the total air is fed as bottom air.

Further investigation using the CPFD model shows that the circulation rate of bed material is decreased at high temperature conditions and reacting flow conditions in comparison to the ambient conditions. The bed material circulation rates for ambient, high temperature and reacting flow conditions are 254 kg/h, 198 kg/h and 210 kg/h respectively.

5. References

AMSDEN, A. A., O'ROURKE, P. J. & BUTLER, T. D. 1989. A computer Porgram for Chemically Reactive Flows with Sprays. Los Alamos National Laboratory

BI, H. T. & GRACE, J. R. 1995. Flow regime diagrams for gas-solid fluidization and upward transport. *International Journal of Multiphase Flow,* 21**,** 1229-1236.

BI, H. T., GRACE, J. R. & ZHU, J. X. 1993. Types of choking in vertical pneumatic systems. *International Journal of Multiphase Flow,* 19**,** 1077-1092.

BOYALAKUNTLA, D. S. 2003. *Simulation of Granular and Gas-Solid Flows Using Discrete Element Method.* PhD, Carnegie Mellon University.

CHEN, C., WERTHER, J., HEINRICH, S., QI, H.-Y. & HARTGE, E.-U. 2013. CPFD simulation of circulating fluidized bed risers. *Powder Technology,* 235**,** 238-247.

CUNDALL, P. A. & STRACK, O. D. L. 1979. The discrete numerical model for granular assemblies. *Geotechnique,* 29**,** 47-65.

DEEN, N. G., VAN SINT ANNALAND, M., VAN DER HOEF, M. A. & KUIPERS, J. A. M. 2007. Review of discrete particle modeling of fluidized beds. *Chemical Engineering Science,* 62**,** 28-44.

GIDASPOW, D. 1994. *Multiphase Flow and Fluidization Continuum and Kinetic Theory Description,* Boston, Academic Press.

GRACE, J. R. 1986. Contacting models and behaviour classification of gas-solid and other two phase suspensions. *Can. J. Chem. Eng.,* 64**,** 353-363.

GUNGOR, A. & YILDIRIM, U. 2013. Two dimensional numerical computation of a circulating fluidized bed biomass gasifier. *Computers & Chemical Engineering,* 48**,** 234-250.

HIRAMA, T., TAKEUCHI, H. & CHIBA, T. 1992. Regime classification of macroscopic gas—solid flow in a circulating fluidized bed riser. *Powder Technology,* 70**,** 215-222.

KAISER, S., WEIGL, K., AICHERNIG, C., FRIEDL, A. & HOFBAUER, H. Simulation of a highly efficient dual fluidized bed gasification process. Third European Congress on Chemical Engineering 2001 Nuernberg.

KAUSHAL, P., PROLL, T. & HOFBAUER, H. 2008a. Model for biomass char combustion in the riser of a dual fluidized bed gasification unit: Part 1 - Model development and sensitivity analysis. *Fuel Processing Technology,* 89**,** 651-659.

KAUSHAL, P., PROLL, T. & HOFBAUER, H. 2008b. Model for biomass char combustion in the riser of a dual fluidized bed gasification unit: Part II - Model validation and parameter variation. *Fuel Processing Technology,* 89**,** 660-666.

KOKSAL, M. & HAMDULLAHPUR, F. 2004. Gas Mixing in Circulating Fluidized Beds with Secondary Air Injection. *Chemical Engineering Research and Design,* 82**,** 979-992.

LEI, H. & HORIO, M. 1998. A Comprehensive Pressure Balance Model of Circulating Fluidized Beds. *Journal of Chemical Engineering of Japan,* 31**,** 83-94.

LEUNG, L. S. 1980. Vertical pneumatic conveying: a flow regime diagram and a review of choking versus non-choking systems. *Powder Technology,* 25**,** 185-190.

LUDLOW, J. C., MONAZAM, E. R. & SHADLE, L. J. 2008. Improvement of continuous solid circulation rate measurement in a cold flow circulating fluidized bed. *Powder Technology,* 182**,** 379-387.

PFEIFER, C., PUCHNER, B. & HOFBAUER, H. 2009. Comparison of dual fluidized bed steam gasification of biomass with and without selective transport of CO2. *Chemical Engineering Science,* 64**,** 5073-5083.

ROY, S., KEMOUN, A., AL-DAHHAN, M. & DUDUKOVIC, M. P. 2001. A method for estimating the solids circulation rate in a closed-loop circulating fluidized bed. *Powder Technology,* 121**,** 213-222.

TAKEUCHI, H., HIRAMA, T., CHIBA, T., BISWAS, J. & LEUNG, L. S. 1986. A quantitative definition and flow regime diagram for fast fluidization. *Powder Technology,* 47**,** 195-199.

THAPA, R. K., RAUTENBACH, C. & HALVORSEN, B. M. Investigation of flow behavior in biomass gasfier using Electrical Capacitance Tomography (ECT) and pressure sensors. International Conference on Polygeneration Strategies (ICPS), 2011 Vienna. 97-106.

WEN, C. & YU, Y. 1966. Mechanics of fluidization. *Chemical Engineering Progress Symposium Series,* 62**,** 100-111.

XU, G. & GAO, S. 2003. Necessary parameters for specifying the hydrodynamics of circulating fluidized bed risers—a review and reiteration. *Powder Technology,* 137**,** 63-76.

YERUSHALMI, J., TURNER, D. H. & SQUIRES, A. M. 1976. The Fast Fluidized Bed. *Industrial & Engineering Chemistry Process Design and Development,* 15**,** 47-53.

Paper I

Flow Regime Identification in the Riser of a Dual Fluidized Bed Gasification Reactor

This paper is under the review process for publication in the international journal
‘Industrial Engineering & Chemistry Research’

Flow Regime Identification in the Riser of a Dual Fluidized Bed Gasification Reactor

Rajan K. Thapa[1], Christoph Pfeifer[2] & Britt M. Halvorsen[1]
1. Institute for Process, Energy and Environmental Technology, Telemark University College, Kjølnes ring 56, P.O. Box 203, N- 3901, Porsgrunn, Norway
2. University of Natural Resources and Life Sciences, Gregor-Mendel-Strasse 33, 1180, Vienna Austria
[*]Rajan K. Thapa, Telemark University College, Kjølnes ring 56, P.O. Box 203, N-3901, Porsgrunn, Norway
Email: rajan.k.thapa@hit.no
Tel: + 47 994 85 965

Abstract

A comprehensive 3D Computational Particle Fluid Dynamic (CPFD) model is prepared to study the gas-solid isothermal flow in a riser of a dual fluidized bed biomass gasification system. The fluidizing gas is air and the particles are olivine, char and their mixture. The isothermal temperature of the particle and fluid flow is maintained at 1300 K. Bubbling, turbulent and fast fluidization regimes in the reactor with their corresponding velocities are identified. The bed inventory emptying method is implemented to find the transport velocity. Average pressure drop and bed material influx and out-flux are monitored at a wide range of gas velocities to determine the stable flow regimes in the bed for solid transport. The fluidization properties of the bed of olivine particles differ from the bed of the mixture of olivine particles and char particles. Effects of bottom, primary and secondary air flows on the fluidization regime and particle transport rate have been investigated.

1. Introduction

Various thermo-chemical processes are used to extract energy from biomass. Gasification is one of them. The application of dual fluidized bed steam gasification system has increased during the past two decades [1-2]. The system consists of a dual fluidized bed reactor which is divided into two parts: gasification and combustion as shown in Figure 1. The gasification reactor or gasifier is a bubbling fluidized bed with high temperature steam as fluidizing gas. In this reactor, biomass is mixed with hot bed materials and steam to produce a mixture of combustible gases known as product gas. The major components of the product gas are methane, carbon-monoxide and hydrogen in addition to carbon dioxide and water vapor [3-6]. The gasification reactions are endothermic and need external heat which is supplied for the dual fluidized bed system by the combustion reactor.

In the combustion reactor, bed material is heated by burning residual char particles which are coming from the gasifier along with the bed materials. The combustion reactor is a circulating fluidized bed with air as fluidizing gas. The air also provides necessary oxygen for the combustion process. Air is supplied to the reactor at three positions: one at the bottom part of the reactor and two others are along the height of the reactor and they are called bottom, primary and secondary air respectively. The bottom air is supplied to maintain bubbling fluidization regime at the lower part of the reactor whereas the primary and the secondary air transport the bed materials from the combustion reactor to the gasification reactor.

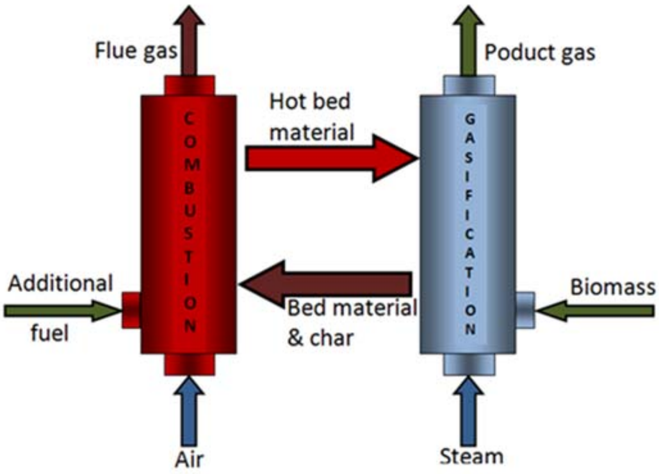

Figure 1.Principle of dual fluidized bed gasification system

The fluidization regime of the riser is complex because it maintains bubbling fluidization regime at the bottom part and fast fluidization regime at the higher part of the reactor. In some cases the flow regime at the highest part of the reactor can be even pneumatic transport regime depending upon the feed rate of secondary air.

The two most important parameters of the system, bed material temperature and its circulation rate, are affected by the air flow and fluidization regime. In the combustion riser the solid flux is usually high (about 120 kg/ (m^2 s)). This solid flux is maintained at steady state by fast fluidization or pneumatic conveying flow regimes [7]. The flow regime is dependent on particle size, density and composition as well as fluid properties such as density and viscosity. Different flow regimes provide different gas-solid mixing and chemical reaction rates [8]. Understanding the flow regime in the reactor is a key factor for successful design, scaling and optimization of the reactor.

The study of flow regime in a circulating fluidized bed has a long history with various proposed flow regime maps. Yerushalmi et al. have shown the transition between packed bed, bubbling bed, turbulent and fast fluidization regimes in the plot of bed voidage against superficial gas velocities [9]. Flow regime maps of gas-solid flow are also developed plotting gas velocity against the solid flux [10]. Takeuchi et al. performed experimental measurements to define the boundaries of fast fluidization [11]. Hirama et al. extended the flow diagram to transition from high velocity to low-velocity fluidization regimes [12]. Bi and Grace proposed unified flow regime diagram based on the experimental findings. They have shown relationship between flow regimes for both gas-solid fluidization and co-current upward transport [13-15]. All of those flow regime maps are proposed for the beds of similar particles and cannot be implemented for the combustion reactor in the gasification system due to the following reasons. They do not represent beds with binary mixture which is the case in this work; particle size distribution is not considered and experiments are carried out at ambient conditions without considering high temperature conditions. These factors significantly affect the flow properties and change the fluidization regime. For example the wider particle size distribution gives rise to smaller voids and earlier transition from bubbling to turbulent regime [16]. When particles with larger size and lower density are mixed with the particles of smaller size and higher densities, the minimum fluidization velocity changes [17]. Change in minimum fluidization velocity effects in the transport velocity and fast fluidization velocity. High temperature gases have lower density and higher viscosity. Change in density and viscosity changes flow behavior in fluidized bed.

The combustion reactor operates at high temperature. The particle temperature is about 950˚C and fluid temperature is even higher [18]. Understanding of flow regime requires measurements of pressure, temperature and solid volume fractions and solid flux. The measurements at high temperature need high safety consideration. In particular case, the measurements of solid volume fraction and solid flux are very difficult in the hot reactors. This may be the reason why the experimental investigations of the flow behavior of high temperature operated circulating fluidized beds are rare in publications [19]. Some authors scaled down the reactor to work at the ambient conditions [20-21]. They managed to overcome the high temperature problem. However, the precise scaling requires the particles with density more than 12000 kg/m^3 which are not easily found in the market. They had to rely on the available bronze particles of density about 9000 kg/m^3. The computational study of the flow regime helps to overcome both of the problems. It is possible to solve high temperature flow with wide range of particle size and gas properties using Computational Particle Fluid Dynamic (CPFD) models.

A 3D CPFD model is used to study the high temperature gas-particle flow regimes in a fluidized bed combustion reactor. The reactor in the 8 MW biomass gasification plant in Güssing, Austria is a reference for the current model. Particles and gas properties as well as the flow and geometric parameters are based on the plant data [22-23]. The model has two objectives: identification of parameters affecting the flow regime with special focus in more sensitive transitions and to investigate the effect of primary and secondary air feed rate on flow regimes and particle transport process.

2. Determination of fluidization velocities

The flow regimes in a fluidized bed reactor are packed bed, particulate fluidization, bubbling fluidization, slugging, turbulent fluidization, fast fluidization and pneumatic transport which occur at increasing gas velocities. Every regime fluidization regime is specified by a range of fluidization velocities. Air is fed at three positions in the combustion reactor which are known as bottom, primary and secondary air. Circulating fluidized beds of high solid flux (about 120 kg/ (m^2 s)) work at fast fluidization regime. However, the lower part of the combustion reactor in this work has to be maintained in bubbling fluidization regime. It is necessary to keep low air velocity (bubbling fluidization regime) at the bottom for preventing leakage of air to the gasification part through connecting chute. Leakage of the air from combustion reactor to gasification reactor is undesirable because it dilutes the product gas reducing the calorific value.

A detailed study of the fluidization velocities from minimum fluidization to pneumatic transport is necessary to establish a big picture of flow regimes in the reactor. The velocities are calculated using theoretical correlations. The theoretical calculations give an approximation for the CPFD model. Minimum fluidization velocity of the particles is calculated using Equation 1. The equation is derived from Ergun equation with gravity- equals - drag balance with Wen and Yu simplification [24-26].

$$u_{mf} = \frac{(\emptyset \cdot d_p)^2(\rho_p - \rho_g) \cdot g}{1650\mu} \qquad (1)$$

For Geldart B particles the bubbling velocity starts with the minimum fluidization velocity. The bed has aspect (H/D) ratio about 22 which is comparatively high. Slugging is possible in bed with aspect ratio greater than 2. Slugging produces a large pressure fluctuation in the bed resulting poor gas solid mixing which is undesirable. However, for the bed with large diameter (0.66m) with comparatively small particles of Geldart group B, it is more likely to transfer the fluidization regime from bubbling to turbulent [27]. A plot of pressure drop against the superficial gas velocity gives two distinct velocities U_c and U_k in turbulent regime. U_c corresponds to the bed operating condition when the bubble or slug reaches their maximum resulting large pressure drop [28]. Continuous increase in the gas velocity starts to break up bubbles resulting in smaller pressure fluctuation which makes the flow steady. The velocity in this state is U_k. The velocities are calculated using Equations 2 and 3 proposed by Horio [29]. Steady pressure fluctuation maintains the steady rate of particle transport which is important for the uniform heat transfer process in the gasification reactor.

$$(Re)_c = \frac{d_p\rho_g U_c}{\mu} = 0.936Ar^{0.472} \qquad (2)$$

$$(Re)_k = \frac{d_p\rho_g U_c}{\mu} = 1.46Ar^{0.472} \qquad (3)$$

Further increase in the gas velocity leads flow to fast fluidization. The velocity in this state is known as transport velocity. The velocity is calculated by Equation 4 [15].

$$U_{tr} = 1.53Ar^{0.5}\, for\; 2 < Ar < 4.10^{-5} \qquad (4)$$

The final transition is from fast fluidization to pneumatic transport. The transition velocity from fast fluidization to pneumatic transfer is known as chocking velocity.

The bubbling beds is characterized by a solid concentration about 0.45 - 0.25 whereas the turbulent bed is characterized by a solid concentration from 0.25 and lower [30]. The pneumatic transport regime occurs at the solid volume fraction less than 1%. Fast fluidization regime occurs when the solid volume fraction is 5 - 15% at the lower part and 1-5% at the upper part of the bed [31]. The theoretical gas velocities of the olivine and char particles are calculated and used as a starting value for the model simulation. At the same time the theoretical results are compared with computational prediction of the model.

3. Mathematical model:

Mainly two approaches are widely used in mathematical modeling of multiphase gas-particle flow. One of them is a continuum approach for both fluid and particles phases and another is a continuum approach for the fluid and Langrangian approach for particles. The continuum-continuum approach (Eulerian method) considers the particle flow as a pseudo fluid flow. Fluid and particles then become continuum. This assumption allows modelling of particle-particle stresses in dense particle flows using spatial gradients of particle volume fractions. However modeling of particle size distribution and composition (binary mixture of particles) complicates the continuum formulation because separate continuity and momentum equation must be solved for each size and type of particles. In the industrial applications of fluidized bed reactors, there are always particles with a wide range of size distributions.

Continuum approach for fluid phase and a Langrangian approach for the particle phase give solutions for overcoming the problems with particle size distributions [32]. But this approach has another problem with dense bed. In the bed with particle volume fractions above 5%, the particle-particle collision frequency is very high and cannot be realistically resolved by this approach. Computational Particle Fluid Dynamic (CPFD) numerical scheme has considered those shortcomings. It has combined Eulerian and Lagrangian method to solve the three dimensional gas-solid flow. Navier-Stocks equation is coupled with discrete particles to describe fluid flow [33]. The particle flow is described by the Particle-in-Cell (MP-PIC) numerical description. The MP-PIC numerical description is Langrangian description of particle motion governed by ordinary differential equations coupled with fluid [32, 34]. Instead of individual particles, the CPFD numerical scheme defines a numerical particle. The numerical particle is a group of particles having similar physical properties such as size and density. The numerical particle is a numerical approximation similar to the numerical control volume where a spatial region has a single property for the fluid. The numerical particles method is able to analyze large commercial system containing billions of particles converting them to millions of numerical particles.

3.1. Governing Equations

The fluid dynamic equations can be derived from kinetic theory for dilute gases or the continuum points of view. The volume averaged fluid mass and momentum equations for a continuum are

$$\frac{\partial(\varepsilon_g \rho_g)}{\partial t} + \nabla(\varepsilon_g \rho_g \boldsymbol{u}_g) = 0 \qquad (5)$$

$$\frac{\partial(\varepsilon_g \rho_g \boldsymbol{u}_g)}{\partial t} + \nabla(\varepsilon_g \rho_g \boldsymbol{u}_g \boldsymbol{u}_g) = \nabla p - \boldsymbol{F} + \varepsilon_g \rho_g \boldsymbol{g} + \nabla \varepsilon_g \tau_g \qquad (6)$$

The particle acceleration is given by

$$\frac{\partial u_p}{\partial t} = D_p(\boldsymbol{u}_g - \boldsymbol{u}_p) - \frac{1}{\rho_p}\nabla p + \boldsymbol{g} - \frac{1}{\varepsilon_s \rho_p}\nabla \tau_p \qquad (7)$$

The terms in the equation represent the acceleration due to aerodynamic drag, the pressure gradient, gravity and the gradient of the inter-particle normal stress τ_p.

The particle movement is given by

$$\frac{d\boldsymbol{x}_p}{dt} = \boldsymbol{u}_p \qquad (8)$$

The particle properties are mapped from the Eulerian grid to the particle locations. The particle properties are also then mapped from the particle to the grid to get grid-based properties such as particle volume fraction at cell ξ,

$$\varepsilon_{p\xi} = \frac{1}{V_\xi}\sum_{1}^{N_p} V_p n_p S_{p\xi} \qquad (9)$$

The conservation equations are approximated using finite volumes with staggered scalar and momentum nodes. The implicit numerical integration of the particle velocity equation is given by

$$u_p^{n-1} = \frac{u_p^n + \Delta t \cdot \left[D_p u_{g.p}^{n+1} - \frac{1}{\rho_p} \nabla p_p^{n+1} - \frac{1}{\rho_p \theta_p} \nabla \tau_p^{n+1} - g \right]}{1 + \nabla t \cdot D_p} \qquad (10)$$

where $u_{g.p}^{n+1}$ is the interpolated fluid velocity at the particle location, ∇p_p^{n+1} is the interpolated pressure gradient at the particle location and $\nabla \tau_p^{n+1}$ interpolated particle stress gradient at the particle location. The new particle location at the next time is then

$$\boldsymbol{x}_p^{n+1} = \boldsymbol{x}_p^n + u_p^{n+1} \Delta t \qquad (11)$$

The fluid momentum equation implicitly couples the fluid and the particles through the interphase momentum transfer. The interphase momentum transfer at momentum cell ξ is

$$\boldsymbol{F}_\xi^{n+1} = \frac{1}{\Omega_\xi} \sum_p s\xi \left[D_p \left(u_{g.p}^{n+1} - u_p^{n+1} \right) - \frac{1}{\rho_p} \Delta u_p^{n+1} \right] \cdot n_p m_p \qquad (12)$$

The interphase drag function $D_p$is calculated using the drag model

$$D_p = C_d \frac{3\rho_g |u_g - u_p|}{8 \rho_p r_p} \qquad (13)$$

3.2. Drag models

Among the drag models used in CPFD software Barracuda, the Wen-Yu model, Ergun model, Wen-Yu/Ergun model and Turton drag model are used for gas-solid homogeneous flows so their drag coefficient all increase with the solid concentration. Wen-Yu drag model have been implemented in this work. The details of the model is can be found in somewhere else [35].

3.3 Solid stress model

Unlike the discrete element method (DEM) which calculates the particle-to-particle forces using a spring-damper model and direct particle contact, the CPFD scheme models collision forces on particles as a spatial gradient. The particle stress gradient which is difficult to calculate for each particle in a dense flow is calculated as a gradient on the Eulerian grid and is then interpolated to discrete particles. Therefore, solids loadings from dilute to dense (closed packed) can be modeled by the particle stress tensor formulation and interpolation. Particle to particle collision are modelled by the particle normal stress τ_p. The particle stress is derived from the particle volume fraction which in turn is calculated from the particle volume mapped to the grid. The particle normal stress model used here was developed by Harris and Crighton.

$$\tau_p = \frac{p_s \varepsilon_p^\gamma}{\max[\varepsilon_{cp} - \varepsilon_p \theta (1 - \varepsilon_p)]} \qquad (14)$$

The constant γ is recommended to be$2 < \gamma < 5$. The constant θ is a small number in the order of 10^{-7} to remove the singularity in close packing. The fluid density, velocity and pressure are coupled by a semi-implicit pressure equation. The momentum and pressure equations are solved with a conjugate gradient solver. A quasi-second order upwind scheme is used for the convection term [36].

4. Model setup and parameters

The dimensions of the reactor are the same as the combustion reactor in the biomass gasification plant in Güssing, Austria. The basic dimensions are presented in Table 1.

Table 1: Reactor dimensions

Dimensions	Unit	Value
Diameter	m	0.66
Height	m	12
Primary air inlet	m	1
Secondary air inlet	m	1.5

The circulation system such as cyclone separator and downflow pipes are not involved. The aim is to study the flow only in the riser. The properties of gas and solid particles used in the model are presented in Table 2.

Table 2: Properties of solid and gases

Properties	Units	Value
Olivine particle size	µm	200-800
Olivine density	kg/m^3	2960
Char particles size	mm	0.5-5
Char density	kg/m^3	200
Air density	kg/m^3	0.27
Air temperature	K	1300
Air viscosity	Pa·s	$4.9 \cdot 10^{-5}$

5. Results and Discussions

The bed of three different particles olivine, char and mixture of olivine and char were fluidized at increasing superficial gas velocities. Pressure drops across the height of the bed are monitored and plotted against the wide range of the superficial gas velocities. The plot is presented in Figure 2. The minimum fluidization velocities of char and olivine particles have about the same value of 0.06 m/s. Theoretical calculation of the corresponding velocities are 0.053 and 0.058 m/s respectively. The reason of the deviations between the values is due the particle size distributions which are not possible to consider in theoretical calculations. When the olivine particles mixed with the char, the minimum fluidization velocity increased to 0.07 m/s. The char particle mixed with olivine is 1vol% which is the case in combustion riser in biomass gasification plant in Güssing, Austria.

The particles involved in this binary mixture have different size as well as density. The char particles have a significantly lower density (200 kg/m^3) in comparison to the olivine particles (2960 kg/m^3). The char particles have large range of size distribution (0.5mm-5mm) whereas the olivine particles have size distribution from 200µm to 800 µm.

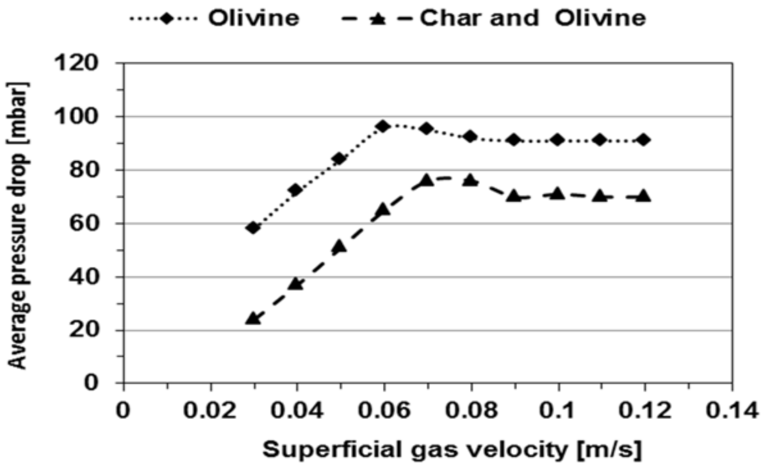

Figure 2. Determination of minimum fluidization velocity

It is believed that the bulk density and voidage are the main factors defining quality of fluidization. The minimum fluidization velocity decreases with increasing temperature in the bed. Minimum fluidization velocity of particles with wide range of size distribution varies with the fraction of coarse particles due to different inter-particle forces[37]. When coarse particles are added in a bed of comparatively fine particles, the voidage of the bed is increased significantly. The solid volume fractions of all particles (olivine, char and the mixture of olivine and char) at minimum fluidization conditions are monitored throughout the simulations and the corresponding void fractions are calculated. The void fraction of olivine, char and the mixture of olivine and char are 0.44, 0.45 and 0.52 respectively. The highest value of void fraction in the mixture is the main reason for increase in minimum fluidization velocity. This result reveals that the study of flow regimes of the combustion reactor without considering the presence of coarse char particles gives error.

The difference of minimum fluidization velocities between the bed of olivine particle and the bed of the mixture of olivine and char particles indicate that there should be the corresponding difference in transport velocities as well. A simple method was used to determine the transport velocities in which the bed inventory emptying time was monitored at different gas velocities as shown in Figure 3.

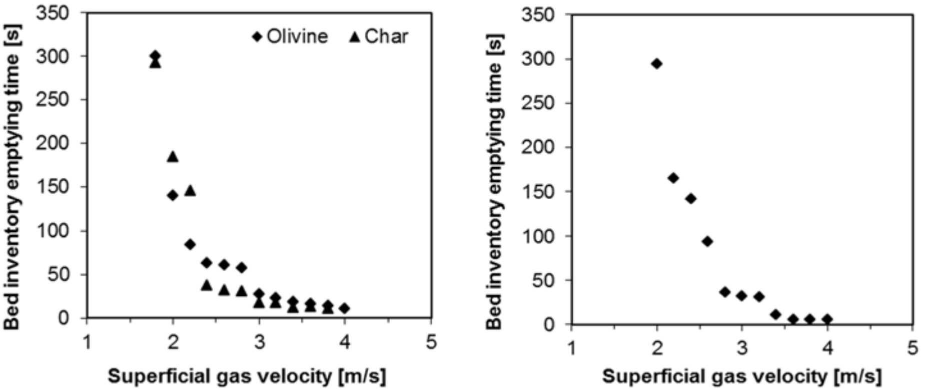

Figure 3: Determination of transport velocity (a) olivine and char particles separately (b) mixture of char and olivine

At the lower gas velocities, the bed inventory emptying time for the olivine and char particles is large. The time reduces significantly and remains almost unchanged at the gas velocities about 2.4 m/s. This is the beginning of fast fluidization and the corresponding velocities are transport velocities (Figure 3a). In the case of the mixture of olivine and char particles, the transport velocity is about 2.8 m/s as shown in Figure 3(b). The transport velocity is about 40 times the minimum fluidization velocity for all the particles showing that the transport velocity is dependent on the minimum fluidization velocity of the particles in the bed.

Further investigations were continued only for the bed with the mixture of char and olivine particles which is the case in the combustion reactor of the dual fluidized bed gasification system. A series of simulations were run to investigate average pressure drop across the bed for a constant solid influx at increasing superficial gas velocity. Individual simulations were run for each of the solid feed rate of 17, 51,…,189 kg/m^2. s. The average pressure drops on the bed were monitored at increasing dimensionless gas velocities from 9 u_{mf} to 58 u_{mf}. The dimensionless gas velocity is the ratio of superficial gas velocity to the minimum fluidization velocity.

The average pressure drop across the height depends on the solid influx (Figure 4). The average pressure drop is increases with increasing solid influx and also varies with increasing gas velocity up to certain value. First the average pressure drop increases continuously with increasing gas velocity and then gradually decreases after attaining a highest value.

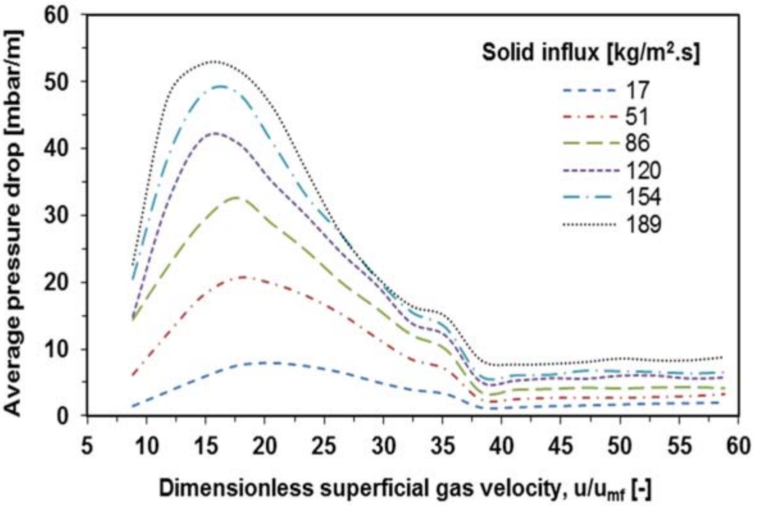

Figure 4. Average pressure drop vs gas velocity

The variation in average pressure drop continues up to the gas velocity of about 40 u_{mf} and then remains constant at the higher gas velocities. The velocity in this case is equal to the transport velocity. Above this gas velocity, there is no variation in pressure drop. The pressure drop remains constant for a given solid influx. The transport velocity is independent of solid influx.

The influence of the average pressure drop variation on the solid out-flux was also studied by monitoring the solid out-flux at the same solid influx and varying gas velocities which is presented in Figure 5.

The large variations in the average pressure drop are linked to the fluidization regime change in the bed from bubbling fluidization to turbulent. The large variation in the average pressure drop causes a large variation in solid out-fluxes within that range of gas velocity. The particle out-flux is greater than influx at the range of dimensionless superficial gas velocities from 15 to 35.

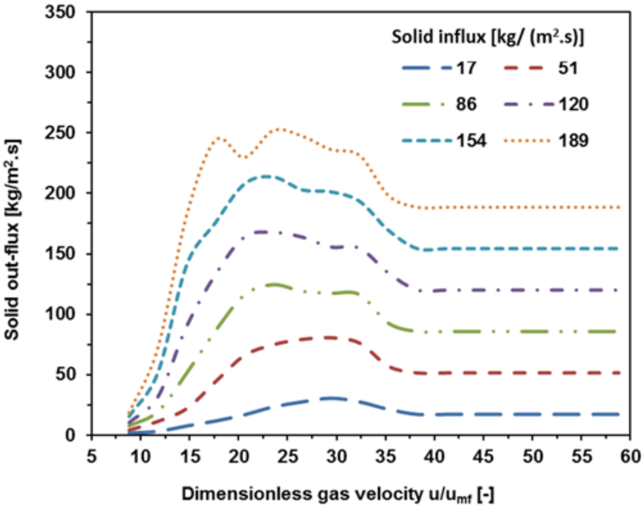

Figure 5. Solid out-flux vs gas velocity

This range of gas velocity should be avoided for a smooth and steady operation of the riser. The major function of the riser is not only the supply bed material but also maintain its constant feed rate. Even the upper part of the riser has fast fluidization regime, the lower part should be in the bubbling fluidization due to the process requirements. Therefore, particular attention should be given to avoid this velocity range in the combustion reactor.

In Figure 6, contours of particle volume fractions at increasing air velocities are presented. The particles here are the mixture of olivine and char. The contours are snapshot of the particle volume fraction. At the dimensionless superficial air velocity of 10 the particle volume fraction at the bottom of the reactor is significantly higher than the upper part. At the outlet the volume fraction is about 0.05% indicating the very low outflow rate of the particles. With increasing air velocity, the volume fraction at the bottom part decreases while at the upper part it increases.

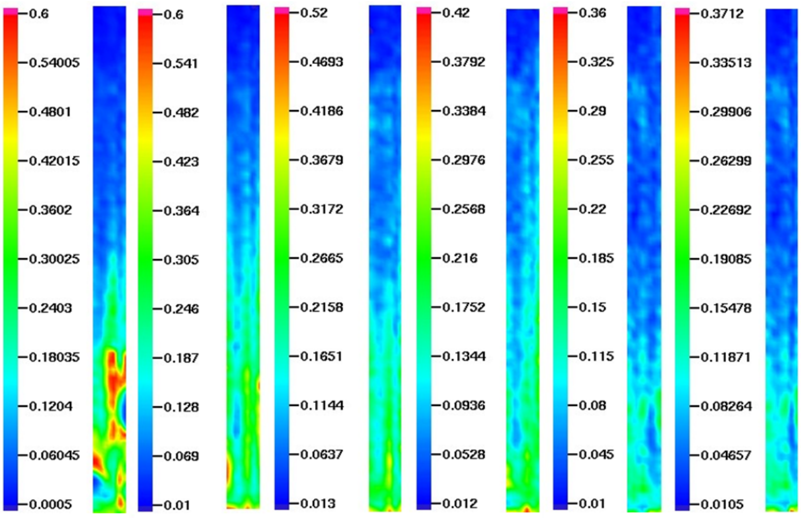

u/u_{mf} = 10 u/u_{mf} = 15 u/u_{mf} = 20 u/u_{mf} = 25 u/u_{mf} = 30 u/u_{mf} = 35

Figure 6. Contours of solid volume fraction vs superficial air velocity

The change in particle volume fractions at the lower and upper parts of the bed is significant at air velocity of 15, 20 and 25. However the particle volume fractions at the bottom and upper part of the bed is more uniform at dimensionless air velocity of 30 and it does not vary significantly with further increasing the air velocity. The results shows the particle volume fraction is about 36% at the dense part of the bed and about 10% at the upper part of the bed when the particle transport process becomes stable. Further increase in gas velocity reduces the difference of particle volume fraction at the upper and lower part of the bed.

The results of bubbling, turbulent and transport velocities are used to determine the wide operating range of primary and secondary air velocities in the reactor. The stability of the gas-solid flow in the bed is studied at the constant solid influx of 120 kg/(m^2s) (feed rate 35 kg/s). The feed rate is selected as in the Güssing plant.

Since the process requires the bottom part of the reactor to remain at bubbling fluidization regime, the velocity of the bottom air is fixed to 10 u_{mf}. Separate simulations were run for the increasing primary air while keeping the bottom air flow velocity and the bed material feed rate constant. The particle out flux was monitored with increasing primary gas flow. The result is presented in Figure 7.

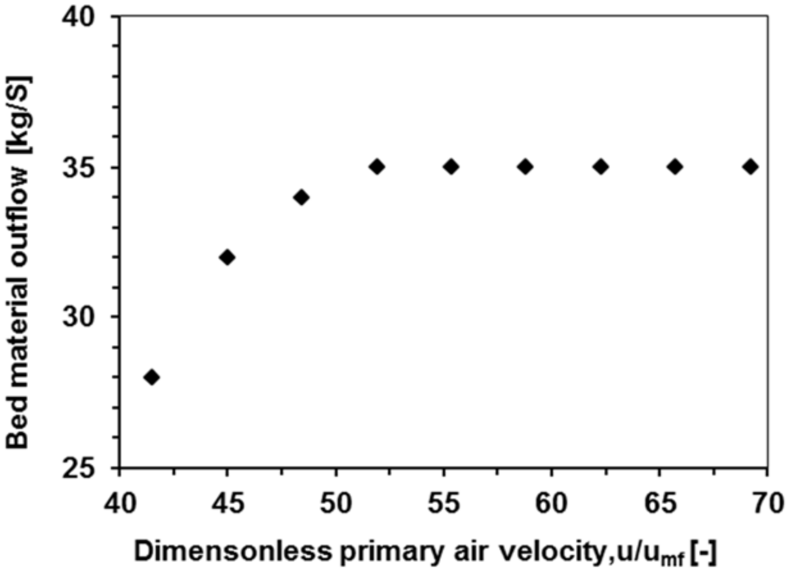

Figure 7. Bed material outflow vs air velocity

At the dimensionless gas velocity less than 48, the bed material outflow rate is less than the feed rate. When the primary air velocity reached the value of 48, the bed material inflow and outflow rate is equal. The bed material circulation rate is constant and steady with further increase in primary air velocity. The results show that much more gas feed is needed for the steady transport of particles when the gas feed stream is divided into the bottom air and the primary air. This experience is verified by cold flow model tests [20].

The bed inventories at increasing primary air velocities are presented in Figure 8.The results shown in the figure are recorded in 50 second of flow time.

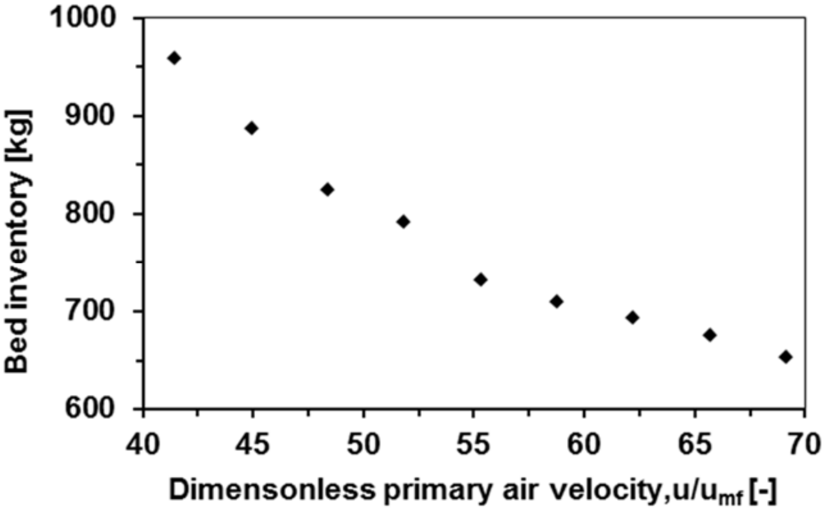

Figure 8. Bed inventory vs primary air velocity

The results show that the bed inventory decreases with increasing primary gas velocity.

A series of simulations was performed to investigate the effect of secondary air on the fluidization regime and particle transport process. In this case, the bottom air as well as primary air feed rate is kept constant in all simulations while increasing the feed rate of secondary air. The velocity of bottom and primary air are $10u_{mf}$ and 48 u_{mf} respectively. Simulation results show that the secondary air flow has no significant effect in the particle transport system as long as the feed rate for bottom and primary air are sufficient.

6. Conclusions

A series of simulation has been performed to identify the various flow regimes in the combustor of a dual fluidized bed gasification system. In addition investigation of the effect of bottom, primary and secondary air feed on the flow regime and particle transport process was carried out. Three groups of particles have been investigated: Olivine particles, char particles and the mixture of olivine and char particles. The minimum fluidization velocities of char particles, olivine particles and their mixture are 0.06 m/s,0.06 m/s and 0.07 m/s respectively with the corresponding transport velocities 2.4 m/s, 2.8 m/s. The minimum fluidization and transport velocities are found to increase when two particles of different sizes and densities are mixed.

Average pressure drops across the bed height were determined for the mixture of olivine and char particles at different particle feed rates. The pressure increases and then decreases before becoming stable at gas velocity about 40 u_{mf}. At this gas velocity, the solid out-flux also becomes constant. The optimum bottom air velocity is about 10 u_{mf} and the optimum velocity of the secondary air flow is above 48 u_{mf}. The result shows that the total gas feed rate has to be increased when the feed positions are split as bottom and primary air instead of single feed positon as bottom air. The bed inventory decreases with increasing primary air feed rate. There is no significant effect on the particle transport rate when secondary air is introduced to the bed as long as the bottom and the primary air feed rates are kept sufficient and constant.

7. Nomenclature

Ar = Archimedes number

D_p = Drag function at the particle location

d_p = particle diameter

$\mathbf{F}$ = rate of momentum exchange per volume between fluid and particle phases

g = acceleration due to gravity

N_p = numerical particles

n_p =number of numerical particles

p = fluid pressure

p_s = positive contact

Re = Reynolds number

$S_{p\xi}$ = interpolation operator

$\mathbf{u}_g$ = fluid velocity

u_{mf} = minimum fluidization velocity

$\mathbf{u}_p$ = particle velocity

U_{tr} =transport velocity

V_ξ = element volume

V_p = particle volume

ρ_p = particle density

ρ_g = fluid density

ε_{cp} = particle volume fraction at close packing limit

ε_g = fluid volume fraction

ε_p = particle volume fraction

τ_g = fluid stress tensor

τ_p = inter particle normal stress

μ = gas viscosity

ϕ = particle sphericity

ε_{cp} = particle volume fraction at close packing limit

8. References

(1) Bolhar-Nordenkampf, M.; Hofbauer, H. In *Gasification Demonstration Plant in Autria*, IV. International Slovak Biomass Forum, Bratislava, 2004.
(2) Fercher, E.; Hofbauer, H.; Fleck, T.; Rauch, R.; Veronik, G. In *Two Years Experience with the FICB-Gasification Process*, 10th European Conference and Technology Exhibition, Wurzburg, 1998.
(3) Hofbauer, H.; Rauch, R.; Bosch, K. In *Biomass CHP Plant Gussing - A Success Story*, Expert Meeting on Pyrolysis and Gasification of Biomass and Waste, Strasbourg, France, 2002.
(4) Hofbauer, H.; Rauch, R.; Loeffler, G.; Kaiser, S.; Fercher, E.; Tremmel, H. In *Six Year Experience with the FICB- Gasification Process*, 12th European Conference and Technology Exhibition on Biomass, Energy, Industry and Climate Protection, Amsterdam, 2002.
(5) Hofbauer, H.; Veronik, G.; Fleck, T.; Rauch, R., The FICFB Gasification Process. *Developments in thermochemical biomass conversion* **1997,** *2*, 1016-1025.
(6) Kern, S.; Pfeifer, C.; Hofbauer, H., Gasification of wood in a dual fluidized bed gasifier: Influence of fuel feeding on process performance. *Chem Eng Sci* **2013,** *90* (0), 284-298.
(7) Balasubramanian, N.; Srinivasakannan, C.; Ahmed Basha, C., Transition velocities in the riser of a circulating fluidized bed. *Advanced Powder Technology* **2005,** *16* (3), 247-260.
(8) Monazam, E. R.; Shadle, L. J.; Mei, J. S.; Spenik, J., Identification and characteristics of different flow regimes in a circulating fluidized bed. *Powder Technology* **2005,** *155* (1), 17-25.
(9) Yerushalmi, J.; Turner, D. H.; Squires, A. M., The Fast Fluidized Bed. *Industrial & Engineering Chemistry Process Design and Development* **1976,** *15* (1), 47-53.
(10) Leung, L. S., Vertical pneumatic conveying: a flow regime diagram and a review of choking versus non-choking systems. *Powder Technology* **1980,** *25* (2), 185-190.
(11) Takeuchi, H.; Hirama, T.; Chiba, T.; Biswas, J.; Leung, L. S., A quantitative definition and flow regime diagram for fast fluidization. *Powder Technology* **1986,** *47* (2), 195-199.
(12) Hirama, T.; Takeuchi, H.; Chiba, T., Regime classification of macroscopic gas—solid flow in a circulating fluidized bed riser. *Powder Technology* **1992,** *70* (3), 215-222.
(13) Grace, J. R., Contacting models and behaviour classification of gas-solid and other two phase suspensions. *Can. J. Chem. Eng.* **1986,** *64*, 353-363.
(14) Bi, H. T.; Grace, J. R.; Zhu, J. X., Types of choking in vertical pneumatic systems. *Int. J. Multiphase Flow* **1993,** *19* (6), 1077-1092.
(15) Bi, H. T.; Grace, J. R., Flow regime diagrams for gas-solid fluidization and upward transport. *International Journal of Multiphase Flow* **1995,** *21* (6), 1229-1236.
(16) Smolders, K.; Baeyens, J., Hydrodynamic modeling of circulating fluidized beds. *Advanced Powder Technology* **1998,** *9* (1), 17-38.
(17) Thapa, R. K.; Rautenbach, C.; Halvorsen, B. M. In *Investigation of flow behavior in biomass gasfier using Electrical Capacitance Tomography (ECT) and pressure sensors*, International Conference on Polygeneration Strategies (ICPS), Vienna, 2011; pp 97-106.
(18) Kaushal, P.; Pröll, T.; Hofbauer, H., Model for biomass char combustion in the riser of a dual fluidized bed gasification unit: Part II — Model validation and parameter variation. *Fuel Process Technol* **2008,** *89* (7), 660-666.
(19) Seo, M. W.; Goo, J. H.; Kim, S. D.; Lee, J. G.; Guahk, Y. T.; Rho, N. S.; Koo, G. H.; Lee, D. Y.; Cho, W. C.; Song, B. H., The transition velocities in a dual circulating fluidized bed reactor with variation of temperatures. *Powder Technology* **2014,** *264* (0), 583-591.
(20) Kreuzeder, A.; Pfeifer, C.; Hofbauer, H., Fluid-Dynamic Investigations in a Scaled Cold Model for a Dual Fluidized bed Biomass Steam Gasification Process: Solid Flux Measurements and Optimization of Cyclone. *Int J Chem React Eng* **2007,** *5*.
(21) Lim, M. T.; Pang, S.; Nijdam, J., Investigation of solids circulation in a cold model of a circulating fluidized bed. *Powder Technology* **2012,** *226* (0), 57-67.

(22) Kaushal, P.; Pröll, T.; Hofbauer, H., Model for biomass char combustion in the riser of a dual fluidized bed gasification unit: Part 1 — Model development and sensitivity analysis. *Fuel Process Technol* **2008,** *89* (7), 651-659.

(23) Kaushal, P.; Pröll, T.; Hofbauer, H., Model development and validation: Co-combustion of residual char, gases and volatile fuels in the fast fluidized combustion chamber of a dual fluidized bed biomass gasifier. *Fuel* **2007,** *86* (17–18), 2687-2695.

(24) Gidaspow, D., *Multiphase Flow and Fluidization Continuum and Kinetic Theory Description*. Academic Press: Boston, 1994.

(25) C.Y., W.; Y.H., Y., Mechanics of fluidization. *Chem Eng Prog Symp Ser* **1966b,** *62* (62), 100-111.

(26) C.Y., W.; Yu, Y. N., A generalized method for predicting the minimum fluidization velocity. *AIChE J.* **1966a,** *12*, 610-612.

(27) Yang, W. C., *A Hand Book of Fluidization and Fluid-Particle System*. MARCEL DEKKER, INC: New York, 2003.

(28) Bi, H. T.; Grace, J. R., Effect of measurement method on the velocities used to demarcate the onset of turbulent fluidization. *The Chemical Engineering Journal and the Biochemical Engineering Journal* **1995,** *57* (3), 261-271.

(29) Yerushalmi, H.; N.T., C., Further studies of the regimes of fluidization *Powder Technol.* **1979,** *24*, 187-205.

(30) Smolders, K.; Baeyens, J., Gas fluidized beds operating at high velocities: a critical review of occurring regimes. *Powder Technology* **2001,** *119* (2–3), 269-291.

(31) Kunnii, D.; Levenspiel, O., *Fluidization Engineering*. 2 ed.; Butterworth-Heinemann: USA, 1991.

(32) Snider, D. M., An Incompressible Three-Dimensional Multiphase Particle-in-Cell Model for Dense Particle Flows. *Journal of Computational Physics* **2001,** *170* (2), 523-549.

(33) Snider, D.; Banerjee, S., Heterogeneous gas chemistry in the CPFD Eulerian–Lagrangian numerical scheme (ozone decomposition). *Powder Technology* **2010,** *199* (1), 100-106.

(34) Andrews, M. J.; O'Rourke, P. J., The multiphase particle-in-cell (MP-PIC) method for dense particle flow. *International Journal of Multiphase Flow* **1996,** *22*, 379-402.

(35) Wen, C.; Yu, Y., Mechanics of fluidization. *Chemical Engineering Progress Symposium Series* **1966,** *62*, 100-111.

(36) Chen, C.; Werther, J.; Heinrich, S.; Qi, H.-Y.; Hartge, E.-U., CPFD simulation of circulating fluidized bed risers. *Powder Technology* **2013,** *235* (0), 238-247.

(37) Jiliang, M.; Xiaoping, C.; Daoyin, L., Minimum fluidization velocity of particles with wide size distribution at high temperatures. *Powder Technology* **2013,** *235* (0), 271-278.